

**Investigation of the Normal and Pathological
Development of the Macula of the Infant Human Eye
using High Resolution Optical Coherence Tomography
(OCT)**

Thesis submitted for the degree of

Doctor of Philosophy

at the University of Leicester

by

Helena Lee MB, BCH, MSc, FRCOphth

Department of Cardiovascular Sciences

Ophthalmology Group

University of Leicester

September 2014

Abstract

Investigation of the Normal and Pathological Development of the Macula of the Infant Human Eye using High Resolution Optical Coherence Tomography (OCT)

Helena Lee

The fovea is a specialised retinal area responsible for high spatial vision. Development of the fovea involves centrifugal migration of inner retinal layers (IRLs) away from the fovea and centripetal displacement of the cone photoreceptors into the fovea and is thought to be complete by 5 years of age. Current understanding of human foveal development is limited to studies of few histological specimens. The recent development of hand-held spectral domain optical coherence tomography (HH-SDOCT), can overcome this limitation by facilitating large scale in vivo imaging of the infant human retina, both in controls and in conditions such as achromatopsia and albinism, where foveal development is disrupted.

In this thesis, we optimise image acquisition and analysis with HH-SDOCT in young children with nystagmus. We show that HH-SDOCT is reliable in children with and without nystagmus, with an intraclass correlation coefficient of 0.96 for central macular thickness measurements. The non-linear developmental trajectories of each retinal layer modelled in a large cohort of 256 controls suggest that development continues until 12 years of age. A paradigm for the etiological diagnosis of nystagmus using OCT is presented.

We describe multiple abnormalities of retinal development in young children with achromatopsia and albinism, including delayed regression of the IRLs from the fovea, diminished elongation of the photoreceptor layers with age and a reduction in perifoveal retinal thickness. This results in significantly increased IRL and decreased photoreceptor thicknesses at the fovea in both conditions ($p < 0.05$). In contrast, the IRL thickness is significantly decreased at the perifovea in both achromatopsia and albinism ($p < 0.01$). There is evidence of postnatal development in the achromat and albino retina. In achromatopsia, disruption of photoreceptors is progressive with age. With gene therapy imminent, potentially earlier treatment of these conditions may normalise retinal development and optimise vision.

Acknowledgements

The author would like to thank her supervisors; Professor Irene Gottlob and Dr Frank Proudlock for giving her the opportunity to complete a PhD degree in their department at the University of Leicester. Professor Gottlob has been a wonderful and inspiring mentor throughout this degree. Dr Proudlock has been a huge source of encouragement and provided much valued support in data analysis, programming and statistical advice. This work would not have been possible without his assistance.

Many thanks to every member of the Ophthalmology group at the University of Leicester, in particular Mr Ravi Purohit, Mr Viral Sheth, Miss Mashal Bibi, Miss Gail Maconachie, Miss Rebecca McLean, Dr Aarti Patel, Dr Eleni Papageorgiou, Dr Anastasia Pilat and Dr Mervyn Thomas at the University of Leicester who provided much help and support and a great deal of assistance in the recruitment of participants, data collection and technical support for this project and the publications that have subsequently arisen from this.

I would also acknowledge all of my collaborators and the participants who took part in this study. None of this work would have been possible without their support.

I would like to thank my colleagues, friends and family for their patience and support throughout this PhD.

Table of Contents

Abstract	2
Acknowledgements	3
List of Tables	11
List of Figures	12
Abbreviations	16
Chapter 1	18
Introduction and Literature Review	18
1.1. What is Known about Foveal Development	19
1.11. The First Trimester (Weeks 1 to 12)	31
1.12. The Second Trimester (Weeks 13 to 26)	31
1.13. The Third Trimester (Weeks 27 to 40)	32
1.14. Birth to 6 Weeks Postnatally	34
1.15. 6 Weeks to 9 Months Postnatally	34
1.16. 12 Months to 45 Months Postnatally	35
1.17. 13 Years to Adulthood	35
1.18. Limitations of Previous Studies	36
1.2. Optical Coherence Tomography (OCT)	37
1.21. Anatomical Correlation of OCT Findings with Histology	40
1.22. OCT in Infants and Young Children	43
1.23. Optimisation of the Bioptigen™ Hand-Held Spectral Domain OCT	45
1.24. Axial Length	45
1.25. Refractive Error	47
1.26. Corneal Curvature	47

1.27. Astigmatism	47
1.28. OCT in Retinopathy of Prematurity (ROP)	49
1.28a OCT in Older Children with a History of ROP	49
1.28b OCT in Infants with ROP	50
1.29. OCT of Normal Foveal Morphology in Older Children	56
1.3. Infantile Nystagmus	58
1.31. Typical Foveal Hypoplasia	63
1.32. Atypical Foveal Hypoplasia	66
1.33. Retinal Dystrophies	69
1.34. Idiopathic Infantile Nystagmus	70
1.4. Development of Visual Acuity in Infants	71
1.5. Research Aims	73
1.51. General Context of Research Aims	73
1.52. Research Aims	74
1.53. Outline of Chapters	75
Chapter 2	76
General Methods	76
2.1. Subjects and Clinical Examination	77
2.11. Power Calculation	78
2.12. Assessment of Teller Visual Acuity	80
2.2. Optimisation of the Examination Environment	81
2.3. OCT Acquisition	84
2.31. OCT Scan Protocol	86
2.4. OCT Segmentation and Analysis	90

2.5. Difficulties Encountered	95
Chapter 3	97
Is Hand-Held Optical Coherence Tomography Reliable in Infants and Young Children with and without Nystagmus?	97
3.1. Introduction	98
3.2. Patients and Methods	99
3.3. Results	107
3.31. Segmentation Difficulties	107
3.32. Reproducibility of Retinal Measurements Between Scans	111
3.33. Inter-Eye Comparison of Nystagmus and Control Subjects	111
3.34. Bland-Altman Assessment	111
3.4. Discussion	115
Chapter 4	118
Normal Foveal Development: An In Vivo study using Optical Coherence Tomography	118
4.1. Introduction	119
4.2. Methods	120
4.21. Participants	120
4.22. Optical Coherence Tomography	121
4.23. Statistics and Modelling	121
4.3. Results	123
4.31. General Outline of Foveal Development	123
4.32. Development of the Inner Retinal Layers	130
4.33. Development of the Outer Retinal Layers	134

4.34. Correlations with Visual Acuity	138
4.4. Discussion	139
Chapter 5	142
Potential of Hand-Held Optical Coherence Tomography to Determine Aetiology of Infantile Nystagmus in Children based on Foveal Morphology	142
5.1. Introduction	143
5.2. Methods	144
5.21. Subjects and clinical examination	144
5.22. Hand-Held Spectral Domain Optical Coherence tomography (HH-SDOCT)	146
5.3. Results	149
5.31. Feasibility	149
5.32. Comparison of Both Eyes of Control Subjects and Patients	149
5.33. Controls	152
5.34. Patients with Typical Foveal Hypoplasia (Category 1)	152
5.35. Patients with Atypical Foveal Hypoplasia (Category 2)	155
5.36. Patients with Other Abnormal Foveal Morphology (Category 3)	157
5.37. Patients with Normal Foveal Morphology (Category 4)	160
5.38. Sensitivity, Specificity and Predictive Value of the OCT by Masked Reviewers	162
5.39. A Diagnostic Algorithm for Infantile Nystagmus Using OCT	165
5.4. Discussion	167
Chapter 6	173
Time Course of Changes in Retinal Development in Infants and Young Children with Achromatopsia	173
6.1. Introduction	174

6.2. Methods	175
6.21. Participants	175
6.23. Statistics and Modelling	178
6.3. Results	179
6.31. General Outline of Foveal Development and Morphology	179
6.32. Timing of Hypo-Reflective Zone Appearance and Ellipsoid Disruption	179
6.33. Overall Retinal, Inner and Outer Retinal Layer Thicknesses	187
6.34. Individual Retinal Layers	195
6.35. Correlation between Outer Retinal and Inner Retinal Layer Thicknesses	200
6.4. Discussion	201
6.41. The Contribution of Cone Photoreceptors to Normal Foveal Development	201
6.42. Remodelling of the Plexiform Layers in Achromatopsia	202
6.43. Residual Plasticity and Potential for Treatment in Achromatopsia	203
6.44. Conclusion	204
Chapter 7	205
Time Course of Changes in Retinal Development in Infants and Young Children with Albinism	205
7.1. Introduction	206
7.2. Methods	208
7.21. Participants	208
7.22. Optical Coherence Tomography	208
7.23. Statistics and Modelling	208
7.3. Results	210
7.31. General Outline of Foveal Development and Morphology	210

7.32. Overall Retinal, Inner and Outer Retinal Layer Thicknesses	217
7.33. Individual Retinal Layers	220
7.4. Discussion	225
7.41. Inner Retinal Layers in Albinism	225
7.42. Outer Retinal Layers in Albinism	226
7.43. A Retinal Origin for Chiasmal Misrouting?	227
7.44. Residual Plasticity and Potential for Treatment in Albinism	227
Chapter 8	229
Discussion and Conclusion	229
8.2 Future Research Questions	233
Appendices	235
Appendix 1	236
Supplementary Data for Chapter 4	236
Table 1: Demographics	237
Table 2: Birth Weights & Gestational Ages	238
Table 3: Presence of Photoreceptor Outer Segments	241
Table 4: Contact Cylinder Visibility	242
Table 5: Foveal Normative Data	243
Table 6: Parafoveal Normative Data	252
Table 7: Perifoveal Normative Data	262
Table 8: Ages at which Retinal Layer Development reaches Maturity	272
Supplementary Video 1 Legend: Foveal Development between Birth and Adulthood	274
Appendix 2	275
Supplementary Data for Chapter 5	275

Table 1: Demographics	276
Table 2: Clinical Characteristics (Typical Foveal Hypoplasia)	277
Table 3: Pigmentary Characteristics in Albinism	279
Table 4: Clinical Findings in Albinism	281
Table 5: Clinical Characteristics (Atypical Foveal Hypoplasia)	282
Table 6: Clinical Characteristics (Abnormal Macular Morphology)	284
Table 7: Clinical Characteristics (Normal Macular Morphology)	286
Appendix 3	288
Supplementary Data for Chapter 6	288
Marginal Effects of Achromatopsia on Retinal Layer Thickness Measurements	289
Appendix 4	293
Supplementary Data for Chapter 7	293
Table 1: Demographics	294
Table 2: Clinical Characteristics	295
Table 3: Summary of Foveal Hypoplasia Grading, VEP and Genetic Testing	299
Marginal Effects of Albinism on Retinal Layer Thickness Measurements	303
Bibliography	308

List of Tables

Table 1.1	Summary of the roles and mechanisms of action of the guidance molecules expressed during foveal development	26
Table 1.2	Standard reference table for axial length, refractive error, reference arm position, and A-scans per B-scan by age (Maldonado 2010)	48
Table 2.1	Summary of OCT scan protocols	86
Table 3.1	Summary of demographic data and diagnostic category of participants	99
Table 3.2	Reproducibility of first to second scan measurements taken from the same eye of each outer retinal layer in both control and nystagmus groups	103
Table 3.3	Reproducibility of first to second scan measurements taken from the same eye of each inner retinal layer in the nystagmus groups	105
Table 3.4	Summary of Bland-Altman plot for measurements of each retinal layer	113
Table 4.1	Summary of the first-order partial correlations conducted in order to explore the relationship between each retinal layer measurement and the development of Teller acuity while controlling for the effects of age	138
Table 5.1	Sensitivity, specificity and predictive value of the hand-held OCT in infants and young children with nystagmus	162
Table 5.2	Breakdown of the results of the masked analysis by category and by grader	163
Table 6.1	Clinical Characteristics of Achromatopsia Participants	176
Table 6.2	Summary of the Presence of a HRZ or ISE Disruption in Achromatopsia	184

List of Figures

Figure 1.1	An OCT image showing a cross section through a normal human fovea (Lee 2013)	20
Figure 1.2	Histological section through a normal adult human fovea (Provis 1998)	21
Figure 1.3	Merged confocal image from a Fd105 monkey fovea (Provis 2000) and a modified fundus camera image from the fovea of a human subject with albinism (Dubis 2012)	23
Figure 1.4	Histological sections of the central fovea illustrating the maturation of the human fovea (Hendrickson 1992)	29
Figure 1.5	Fluorescein angiogram of a 28 week old child illustrating the absence of the foveal avascular zone (Mintz-Hittner 1999)	33
Figure 1.6	Schematic illustrating the principles of time domain OCT (http://archive.nrc-cnrc.gc.ca/eng/projects/ibd/oct.html)	38
Figure 1.7	Comparison of a OCT image of a normal adult human fovea with a histological section (Vajozovic 2012)	42
Figure 1.8	Schematic illustrating the problems of incorrect reference arm length on OCT (Maldonado 2010)	46
Figure 1.9	Three-dimensional retinal thickness maps demonstrating the regional changes in premature human foveal development from 31 weeks to 43 weeks PMA (Maldonado 2011)	52
Figure 1.10	Examples of oedema affecting the inner nuclear layer in 2 premature infants (Maldonado 2011)	53
Figure 1.11	Comparison of SD-OCT scans taken of the fovea in a 31 weeks PMA premature infant and a 23 year old adult who was born at term (Maldonado 2011)	54
Figure 1.12	Examples of “pattern A” macular oedema and “pattern B” macular oedema (Vinekar 2011)	55
Figure 1.13	Example of crossed asymmetry on a VEP examination (http://webvision.med.utah.edu/book/electrophysiology/visual-and-auditory-anomalies-associated-with-albinism/)	60
Figure 1.14	Examples of retinal abnormalities detected on an ERG examination (Kumar 2010)	62

Figure 1.15	Scatterplot of OS length against BCVA (Mohammad 2011)	65
Figure 1.16	Sagittal, coronal and parasagittal MRI slices from a normalised control subject overlaid by an statistical parametric mapping (SPM) region from a voxel-based morphometry (VBM) analysis of 24 aniridia subjects against 72 controls (Free 2003)	68
Figure 2.1	Example of the environment used for OCT acquisition and the acquisition of an OCT scan in a child with nystagmus	82
Figure 2.2	The reference arm (black circle) on the hand-held OCT is adjusted to be shorter or longer depending on the amount of clipping observed on the imaging	85
Figure 2.3	Example of the flattening and segmentation process for a single central foveal B-scan using the Bioptigen Manual Layers Program Fovea Beta v2	92
Figure 2.4	Example of a portion of a text file obtained after segmentation of each retinal layer has been completed using the Bioptigen Manual Layers Program Fovea Beta v2	94
Figure 3.1	Optical coherence tomograms of 1 control subject and 1 nystagmus subject showing how segmentation of the borders of each of the retinal layers was achieved	101
Figure 3.2	Optical coherence tomograms of 2 nystagmus subjects and 2 control subjects	109
Figure 4.1	Examples of foveal tomograms from a range of ages illustrating the anatomy of the fovea and the main features of foveal development over time	123
Figure 4.2	Mean thickness of each retinal layer plotted using a 4th order polynomial fit for each of the 16 age groups which have been colour coded	125
Figure 4.3	Development trajectories for the inner retinal layers, outer retinal layers and total retinal thickness at the fovea and parafovea	128
Figure 4.4	Development trajectories for the inner retinal layers: RNFL, GCL, IPL, INL and OPL at the parafovea and perifovea	131

Figure 4.5	Percentage change in the thickness of the foveal, parafoveal and perifoveal inner retinal layers between birth and time of peak development at the fovea	132
Figure 4.6	Development trajectories for the ONL, IS, OS and RPE at the fovea, parafovea and perifovea	135
Figure 4.7	Percentage change in the thickness of the foveal, parafoveal and perifoveal outer retinal layers between birth and time of peak development at the fovea	137
Figure 5.1	Structural Grading of foveal hypoplasia based on different stages of arrested development	147
Figure 5.2	Examples of foveal OCTs in normal control infants and young children of different ages	150
Figure 5.3	Example of the identification of the central foveal B-scan in the right eye of a child with grade 3 foveal hypoplasia	153
Figure 5.4	Atypical foveal hypoplasia in 2 young achromatopsia patients	156
Figure 5.5	Atypical macular morphology in 2 patients with microcephaly and 2 patients with retinal dystrophy	158
Figure 5.6	Normal foveal structure in a patient with IIN (5.6A) and a patient with manifest latent nystagmus	161
Figure 5.7	Schematic diagram illustrating the categorisation of infantile nystagmus syndrome (INS) into 4 diagnostic categories on the basis of OCT findings	166
Figure 6.1	Features of foveal development and morphology in achromatopsia	180
Figure 6.2	Age-dependent appearance of the HRZ and ISE disruption in achromatopsia	182
Figure 6.3	Kaplan-Meier survival curve for the development of a HRZ with increasing age (months)	185
Figure 6.4	Kaplan-Meier survival curve for the development of ISE disruption with increasing age (months)	186
Figure 6.5	Mean differences in retinal layer thickness measurements between the achromatopsia and control groups	189
Figure 6.6	Differences in the rate of change in retinal layer thicknesses with age between the achromatopsia and control groups	191

Figure 6.7	Development trajectories for the inner retinal layers, outer retinal layers and total retinal thickness at the fovea, parafovea and perifovea	193
Figure 6.8	Development trajectories for the RNFL, GCL, IPL and OPL at the fovea, parafovea and perifovea	196
Figure 6.9	Development trajectories for the ONL, OPL, IS, OS and RPE at the fovea, parafovea and perifovea	198
Figure 7.1	Examples of foveal tomograms from 2 albinism participants illustrating the main features of foveal development over time in albinism	211
Figure 7.2	Mean differences in retinal layer thickness measurements between the albinism and control groups	213
Figure 7.3	Differences in the rate of change in retinal layer thicknesses with age between the albinism and control groups	215
Figure 7.4	Development trajectories for the inner retinal layers, outer retinal layers and total retinal thickness at the fovea, parafovea and perifovea	218
Figure 7.5	Development trajectories for the RNFL, GCL, IPL and OPL at the fovea, parafovea and perifovea	221
Figure 7.6	Development trajectories for the ONL, OPL, IS, OS and RPE at the fovea, parafovea and perifovea	223

Abbreviations

AAV	Adeno-Associated Virus	LCI	Lower Confidence Interval
ACHM	Achromatopsia	L-Dopa	Dihydroxyphenylalanine
ADRP	Autosomal Dominant Retinitis Pigmentosa	LE	Left Eye
AO	Adaptive Optics	logMAR	Logarithm of the Minimum Angle of Resolution
AO-FDOCT	Adaptive Optics Fourier Domain OCT	M	Male
BCVA	Best Corrected Visual Acuity	MAP	Microtubule Associated Protein
BE	Both Eyes	MRI	Magnetic Resonance Imaging
CC	Contact Cylinder	n	Sample Size
CCD	Charge Coupled Device	N	No
CD-31	Cluster of Differentiation 31 (also known as Platelet Endothelial Cell Adhesion Molecule-1)	No	Number of Participants
c-FLIP	cellular FLICE-Inhibitory Protein	NS	Not Significant
CI	Confidence Interval	NFL	Nerve Fibre Layer
CMT	Central Macular Thickness	NPPB	Natriuretic Peptide Precursor B
COST	Cone Outer Segment Tip	ON	Optic Nerve
CRD	Cone-Rod Dystrophies	ONH	Optic Nerve Hypoplasia
CSNB	Congenital Stationary Night Blindness	OA	Ocular Albinism
EDT	Electrodiagnostic Tests	OCA	Oculocutaneous Albinism
ELM	External Limiting Membrane	ONL	Outer Nuclear Layer
ERG	Electroretinogram	OCT	Optical Coherence Tomography
ERK	Extracellular Receptor Kinase	OPL	Outer Plexiform Layer
F	Female	ORL	Outer Retinal Layers
F & F	Fixing and Following	OS	Outer Segment of Photoreceptors
FADD	Fas-Associated Death Domain protein	PDE	Phosphodiesterase
FAZ	Foveal Avascular Zone	PEDF	Pigment Epithelium Derived Factor
Fd	Foetal Day	PMA	Post Menstrual Age
FD	Fourier Domain	PL	Preferential Looking
FD-OCT	Fourier Domain Optical Coherence Tomography	PSF	Point Spread Function
FGFR4	Fibroblast Growth Factor Receptor 4	PRL	Photoreceptor Layers
FH	Henle Fibre Layer	PSL	Photoreceptor Synapse Layer

FLICE	FADD-like interleukin-1beta-converting enzyme	RCD	Rod-Cone Dystrophies
FMNS	Fusion Maldevelopment Nystagmus Syndrome	RE	Right Eye
FP	Foveal to Parafoveal Ratio	RE	Refractive Error
FP-IRL	Foveal Parafoveal Ratio of the Inner Retinal Layers	RFI	Retinal Function Imager
FP-PRL	Foveal Parafoveal Ratio of the Photoreceptor Layers	RNFL	Retinal Nerve Fibre Layer
FWK	Foetal Week	ROP	Retinopathy of Prematurity
GA	Gestational Age	RP	Retinitis Pigmentosa
GCC	Ganglion Cell Complex	RPE	Retinal Pigment Epithelium
GCL	Ganglion Cell Layer	SD	Standard Deviation
GFAP	Glial Fibrillary Acidic Protein	SD-OCT	Spectral Domain Optical Coherence Tomography
GMP	Guanosine Monophosphate	SEM	Standard Error of the Mean
HFL	Henle Fibre Layer	SLOR	Scan Length On Retina
HH-SDOCT	Hand-Held Spectral Domain Optical Coherence Tomography	SPM	Statistical Parametric Mapping
HRZ	Hypo-reflective Zone	SS	Swept Source
IAD	Interocular Acuity Differences	SS-OCT	Swept Source Optical Coherence Tomography
ICC	Intraclass Correlation Coefficient	TD	Time Domain
ID	Identification	TD-OCT	Time Domain Optical Coherence Tomography
IIN	Idiopathic Infantile Nystagmus	TID	Iris Transillumination Defects
ILM	Inner Limiting Membrane	TRL	Total Retinal Layer
INS	Infantile Nystagmus Syndrome	UCI	Upper Confidence Interval
IPL	Inner Plexiform Layer	UHR	Ultra High Resolution
INL	Inner Nuclear Layer	VA	Visual Acuity
IOP	Intraocular Pressure	VEP	Visual Evoked Potentials
IRL	Inner Retinal Layers	VBM	Voxel Based Morphometry
IS	Inner Segment of Photoreceptors	VEGF	Vascular Endothelial Growth Factor
ISE	Ellipsoid Band	VEGFR-1	Vascular Endothelial Growth Factor Receptor-1
JNK	Jun Amino Terminal Kinase	Y	Yes

Chapter 1

Introduction and Literature Review

1.1. What is known about foveal development

1.2. Optical Coherence Tomography

1.3. Infantile Nystagmus

1.4. Development of Visual Acuity in Infants

1.5. Research Aims

1.1. What is Known about Foveal Development

The human fovea is an area of the central retina responsible for high spatial resolution and colour vision.¹ It plays an important role in human visual cortex development, regulating calcarine fissure symmetry² and cortical maps.³ It is characterised by an absence of retinal vasculature, a pit without overlying ganglion cell or inner retinal layers and a high density of elongated cone inner and outer segments. The absence of the inner retinal layers facilitates light transmission to the photoreceptors without interference.⁴ In the centre of the fovea (the foveola) only the photoreceptor layer remains and this consists of tightly packed, elongated cones and Müller cell processes.⁵

Rods are excluded from the foveola, forming a central rod-free zone where cone density reaches more than 200 000/mm², the highest in the retina.⁶ The normal structure of the human fovea on OCT imaging is shown in figure 1.1. A histological section from an adult human fovea is shown for comparison in figure 1.2.

Several hypotheses have been proposed with regards to the mechanism of development of the human fovea. These include:

1. The role of growth factors, guidance molecules and anti-angiogenic factors
2. The presence of the foveal avascular zone and its effect on altering the elasticity of the foveal region
3. The role of intraocular pressure in initiating foveal indentation
4. The mechanical contribution of growth induced stretch of the retina

It is likely that it is not just one of these mechanisms, but in fact a complex interaction between all of these mechanisms that establishes the development of the human fovea. The exact nature of this interaction remains to be determined.

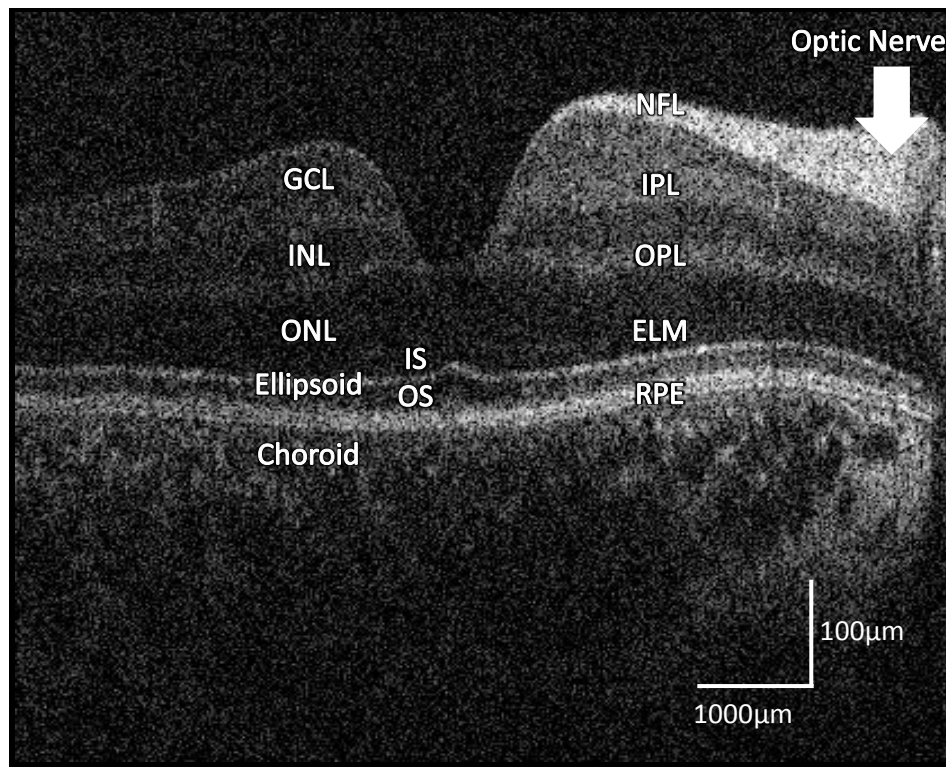


Figure 1.1: Optical Coherence Tomography (OCT) image showing a cross section of a normal human fovea at 35 months of age (modified from Lee et al 2013).⁷

The retina is composed of three layers of nerve cell bodies; the outer nuclear layer contains cell bodies of the rods and cones, the inner nuclear layer contains cell bodies of the bipolar, horizontal and amacrine cells and the ganglion cell layer contains cell bodies of ganglion cells and displaced amacrine cells. Separating these nerve cell layers are two layers of synapses; the outer plexiform layer where connections between the rods, cones, bipolar cells and horizontal cells occur and the inner plexiform layer where the bipolar cells connect to the ganglion cells. The inner retinal layers (NFL, GCL, IPL, INL, OPL) are absent in the central foveal pit, which facilitates light transmission to the photoreceptors.

NFL = nerve fibre layer; GCL = ganglion cell layer; IPL = inner plexiform layer; INL = inner nuclear layer; OPL = outer plexiform layer; ONL = outer nuclear layer; ELM = external limiting membrane; IS = inner segment of photoreceptors; OS = outer segment of photoreceptors; RPE = retinal pigment epithelium

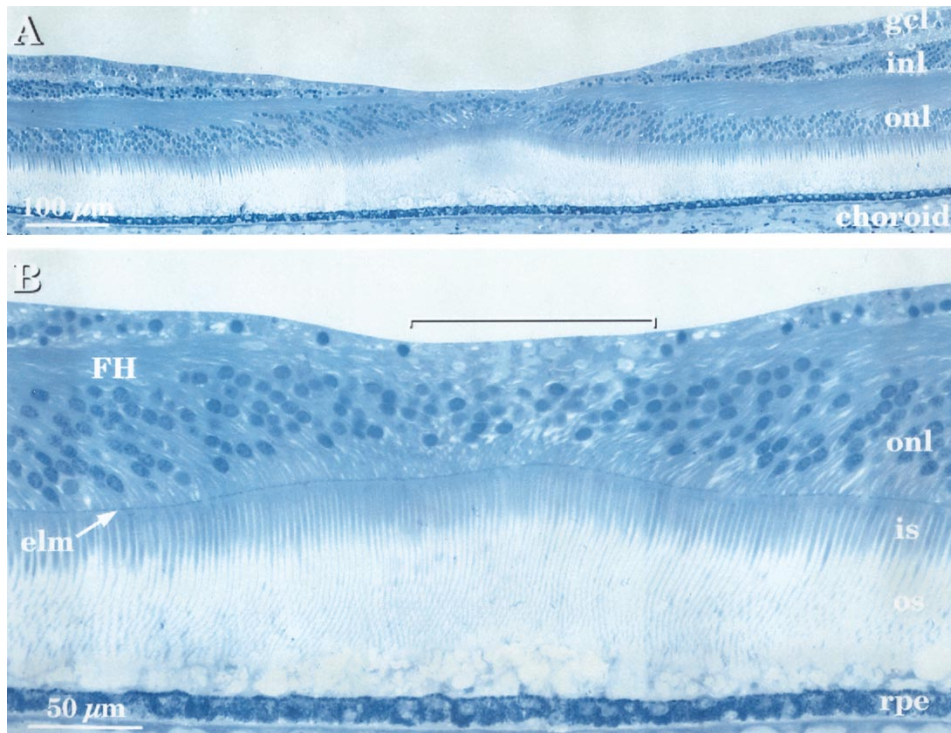


Figure 1.2: Histological section through a normal adult human fovea (taken from Provis et al. 1998).⁸

The nomenclature of the individual retinal layers on histology is comparable to that visualised with optical coherence tomography (OCT) (Figure 1.1). One key difference is that the Henle fibres that are visualised on histology between the OPL and ONL are hypo-reflective on conventional OCT and cannot be distinguished from the ONL. Therefore what is labelled as ONL on OCT also incorporates the Henle fibre layer.

NFL = nerve fibre layer; GCL = ganglion cell layer; IPL = inner plexiform layer; INL = inner nuclear layer; OPL = outer plexiform layer; FH= Henle Fibres; ONL = outer nuclear layer; ELM = external limiting membrane; IS = inner segment of photoreceptors; OS = outer segment of photoreceptors; RPE = retinal pigment epithelium

Macular development is a complex process, which requires the expression of several anti-angiogenic factors,^{5, 9-17} axon guidance genes and regulators of actin cytoskeleton and cell adhesion molecules.¹⁸⁻²⁰ These facilitate the formation of the foveal avascular zone and repels the ganglion cell axons away from the fovea into the arcuate bundles (Table 1.1).^{5, 15, 21, 22} A ring of parafoveal vasculature defines the central foveal avascular zone (FAZ) and the site of the future foveal pit.^{15, 23} Springer and Hendrickson^{23, 24} have developed a model of primate foveal development in which they suggest that the presence of a FAZ is a critical requirement for formation of the foveal pit (Figure 1.3).

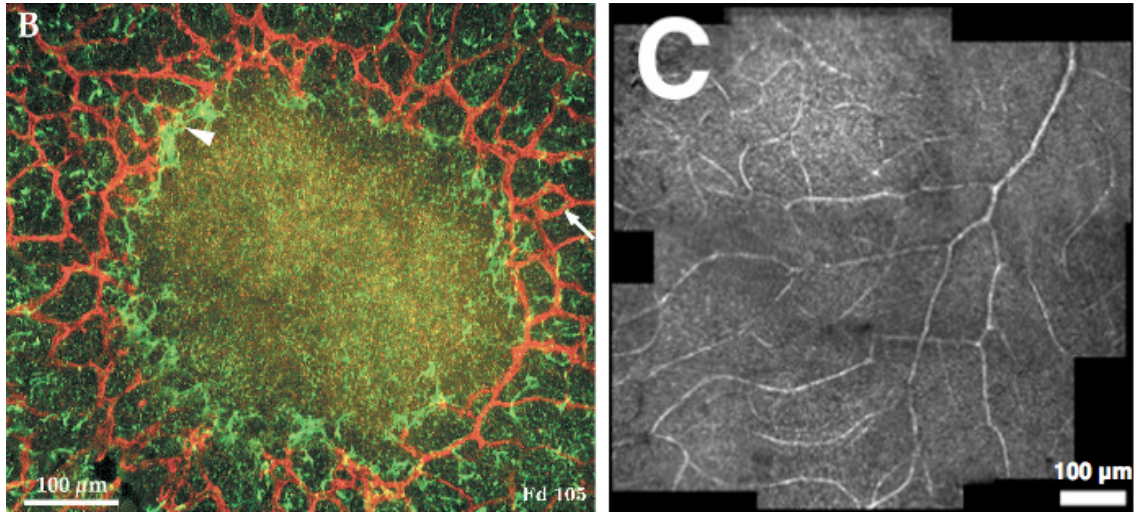


Figure 1.3: Merged confocal image (left) from a Fd105 monkey fovea (taken from Provis et al. 2000)¹⁵ and a modified fundus camera image (right) from the fovea of a human subject with albinism (taken from Dubis et al 2012).²⁵

In the merged confocal image on the left (figure 1.3), each retina has been double labeled to demonstrate blood vessels detected by CD31 (red) and GFAP staining in glia (green). The astrocytes and blood vessels in the ganglion cell layer plexus are surrounding the avascular developing foveal depression.

In the fundus image on the right (figure 1.3) a modified ophthalmoscope (the retinal function imager (RFI)) which uses an 840 nm wavelength to image the FAZ in a human subject with albinism known to have an absent foveal pit. There is an abnormal invasion of blood vessels into the FAZ.

Fd = foetal day; CD31 = cluster of differentiation-1; GFAP = glial fibrillary acidic protein; FAZ = foveal avascular zone

In humans, absence of an avascular area is associated with foveal hypoplasia (defined as the presence of the normally absent inner retinal layers at the fovea) (Figure 1.3).^{26, 27} Histological evidence from hypo-plastic human retinæ highlights the negative consequences of the absence of a normal FAZ on foveal development. The presence of abnormal blood vessels in the future foveal pit region are associated with a shallow, incomplete pit and decreased visual acuity.^{26, 28-31} Histological examination of two neonatal human anencephalic retinæ from one subject demonstrated the presence of abnormal blood vessels in the foveal region in one retina associated with failure of pit formation.²¹ In the second neonatal retina there was formation of a FAZ, which was associated with the presence of a shallow foveal pit.²¹

In the primate retina, it has been suggested that absence of blood vessels leads to a different elasticity in the foveal region as compared to the surrounding retina. This is thought to be sufficient to promote development of the foveal pit. The central retina changes tri-phasicly. It (i) increases in thickness prenatally, (ii) thins transiently after birth and then (iii) resumes thickening.²³ The onset of pit formation overlaps the late foetal quiescent phase (when the growth of the retina has paused), which suggests that intraocular pressure (IOP) is the major mechanical factor initiating pit formation. This is based on the assumption that blood vessels impart rigidity (i.e. reduced elasticity) to neural tissue.³² Initially, pit formation occurs passively by indentation of the avascular fovea (which is more pliable as a result of the absence of blood vessels and hence reduced elasticity than the surrounding vascularised retina) from intraocular pressure in utero. This is followed by a second active phase of growth-induced stretch that remodels the morphology of the fovea in the postpartum period.^{23, 33}

Consistent with IOP acting as the principal factor causing pit formation, the GCL is displaced first, followed in turn by the IPL, INL, and the OPL. Cone cell bodies appear to be resistant to this force. It has been postulated that a greater cohesiveness of the ONL could be caused by the tangential/lateral stiffness imparted by the zona adherens junctions between photoreceptors and Müller cells which form the outer limiting membrane.³⁴ In addition it has been shown that fibroblast growth factor receptor 4 (FGFR4) is expressed throughout the axon, soma and inner segment of the cone photoreceptor from very early development.³⁵ The expression of FGFR4 within

the outer limiting membrane neuronal cytoskeleton during pit formation and cone packing may further increase the cohesiveness and rigidity of the cone cell bodies so that they can resist the mechanical forces exerted by IOP pressure, but this needs to be further explored.

During the development of the central retina, the fovea consists of a rod-free zone that decreases in diameter as the cone inner segments become more slender, the outer segments elongate and the cones pack tightly together.^{36, 37} Cone elongation and packing are mainly postnatal events.³³ There is a 20 fold increase in cone density at the fovea. This occurs after all cones have been generated.³⁸ The cones could be drawn in to the foveal centre as a result of the forces generated by the interaction of pit formation and stretch of the central fovea.³⁹ A centrifugal displacement of inner retinal cells and a centripetal displacement of photoreceptors is postulated.^{5, 8, 36} It has been shown that the development is not completed until about 3-4 years of life, and the fovea is the last structure to become fully developed.³⁶

Table 1.1: Summary of the roles and mechanisms of action of the guidance molecules expressed during foveal development^{12-14, 17, 20, 40-42}

Factor	Role	Mechanism of Action
Pigment epithelium derived factor (PEDF)	Repels axons Anti-angiogenic	<ol style="list-style-type: none"> 1. Inhibition of VEGF action via the intracellular proteolysis of VEGFR-1 or inhibition of its phosphorylation 2. Stimulation of the Fas/Fas ligand-mediated apoptotic pathway which targets the endothelial cells of immature vessels 3. Down regulates the caspase-8 inhibitor c-FLIP (promoting apoptosis)
Natriuretic peptide precursor B (NPPB)	Anti-angiogenic	<ol style="list-style-type: none"> 1. Affects VEGF-induced angiogenesis by inhibiting certain signaling molecules such as ERK, JNK and p38 members of the MAP kinase family through stimulation of a cyclic GMP signaling cascade

Ephrin A6 & semaphorin axon guidance gene families	Repels axons Anti- angiogenic	<ol style="list-style-type: none"> 1. Known to have a repellent effect during vascular morphogenesis via interactions with integrins 2. Graded expression of genes involved in repellent signaling that is centered on the fovea during development retards the growth of vessels into the central region of the retina and contributes to definition of the foveal avascular area 3. Relative levels of ligand and receptor guide outgrowing axons
---	---	--

VEGF = vascular endothelial growth factor; VEGFR-1 = vascular endothelial growth factor receptor-1; c-FLIP = cellular FLICE-inhibitory protein; FLICE = FADD-like interleukin-1beta-converting enzyme; FADD = Fas-associated death domain protein; ERK = extracellular receptor kinase; JNK = Jun amino terminal kinase; MAP = microtubule associated protein; GMP = guanosine monophosphate

Knowledge of development of the normal central retina and foveal structure (particularly in the earliest stages of gestation) has depended heavily on anatomic studies of the simian retina sacrificed at various stages of gestation^{43, 44, 45} with very few histological studies of the infant human fovea (Figure 1.4).^{36, 37}

According to Hendrickson et al.³⁶ there are five parameters which indicate that the retina is reaching maturity:

1. Disappearance of the transient layer of Chievitz
2. Narrowing of the width of the rod-free zone in the central retina
3. Narrowing of the width of the individual foveal cones
4. Increasing length of the individual foveal cones
5. Increasing number and thickness of layers of nuclei within the fovea

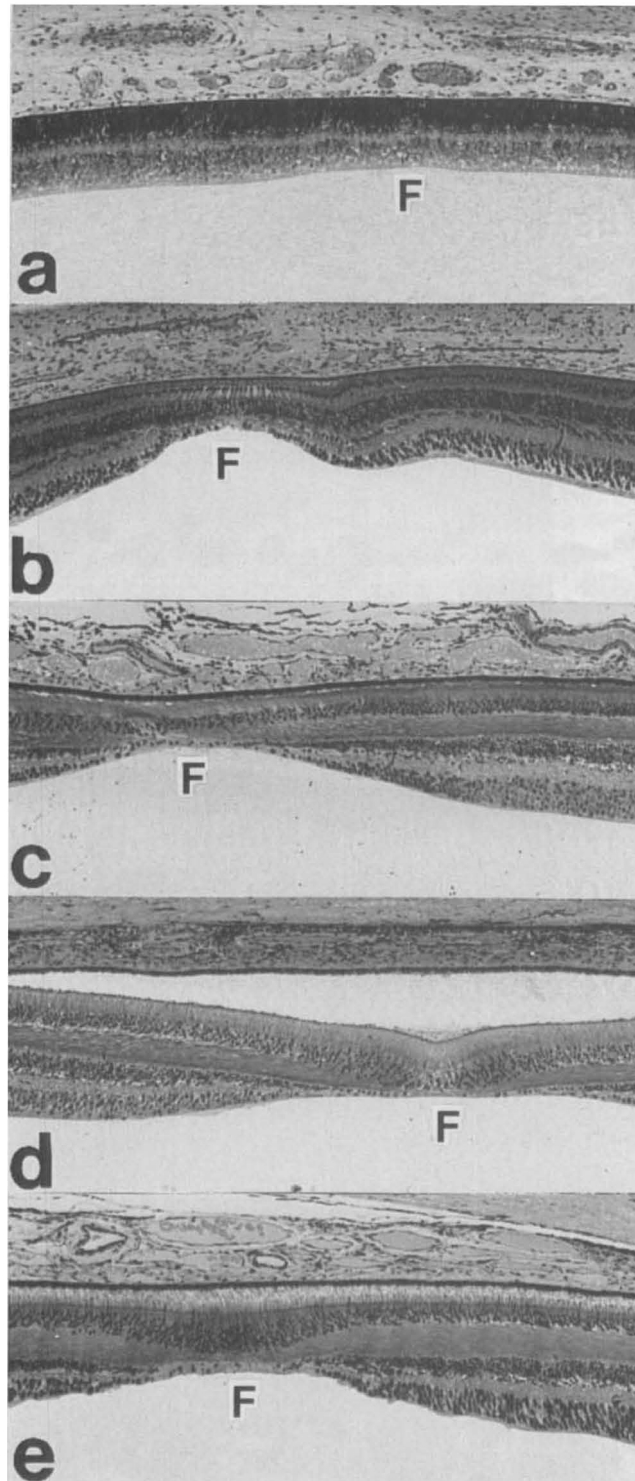


Figure 1.4: Histological sections of the central fovea illustrating the maturation of the human fovea (taken from Hendrickson et al. 1992).⁴⁵

(a) At foetal week 24; (b) At 5 days of age; (c) At 15 months of age; (d) At 45 months of age and (e) At 13 years of age. The images are orientated with the retinal pigment epithelium superiorly and foveal pit (marked with F on each image) inferiorly. The foveal pit is barely visible in the youngest specimen (a) and this becomes more prominent with maturity. This maturation due to a combination of processes including: migration of the inner retinal layers (nerve fibre layer, ganglion cell layer, inner plexiform layer, inner nuclear layer and outer plexiform layer) away from the fovea, migration of the photoreceptors into the fovea and elongation of the outer retinal layers (outer nuclear layer, inner segment of the photoreceptors and outer segment of the photoreceptors) over time.

1.11. The First Trimester (Weeks 1 to 12)

The earliest marker of the future location of the human fovea is indicated by a region which contains cones exclusively and is identifiable at 11 weeks gestational age (GA).⁴⁶ Cone nuclei in the foveal region reach a packing density of 14200 per mm².⁴⁷ Molecular analysis has indicated the presence of guidance molecules: pigment epithelium derived factor (PEDF); natriuretic peptide precursor B (NPPB), collagen type IV alpha2 and ephrin A6.^{9, 10} In monkeys an avascular area is defined by the ganglion cell plexus.¹⁵

1.12. The Second Trimester (Weeks 13 to 26)

At 14 weeks GA, the retinal vessels enter the developing human retina.⁵ The molecular barrier that is present at the fovea delays the growth of vessels into the central region of the retina.^{5, 15, 16} Pit development begins when the foveal avascular zone is formed at 24 weeks GA.^{5, 15, 21} Regulatory genes that are associated with axon guidance, regulation of the actin cytoskeleton and cell adhesion molecules are expressed.^{18, 19} These guidance factors repel ganglion cell axons away from the fovea into the arcuate axon bundles and optic nerve head between 8 and 25 weeks GA.²⁰ In addition it has been hypothesised that the presence of encircling blood vessels may provide a source of oxygen that acts as a trophic factor to induce inner retinal neurones to move peripherally out of the avascular zone. However this mechanism would not account for centripetal movements of the cones into the fovea.³⁵

The ganglion cell layer (GCL) and inner nuclear layer (INL) are differentiated at 15 weeks GA.⁴⁸ The neuronal circuitry is also established, with amacrine and bipolar cell synapses evident in the inner plexiform layer (IPL).⁴⁸ At 22 weeks of gestation, the fovea is comprised of a thin nerve fibre layer (NFL), five to seven layers of cells in the ganglion cell layer, a well-defined inner plexiform, inner nuclear and outer plexiform layers (OPL) and an outer nuclear layer (ONL) which contains exclusively cone nuclei.

36

The foveal cone mosaic is clearly differentiated with cone nuclei reaching a packing density of 38000 per mm² at 24 weeks.⁴⁷ The rod free zone measures between 1500 to 1800 μ m and the maximum rod density observed is 59200 per mm². Outside the

rod free zone the rods have become much more numerous so that at 2 mm from the fovea, the outer retinal layers are formed by a single layer of large cones and 3 to 4 layers of rod cell bodies. The rod cell bodies are added between the cone nuclei and pedicles, causing the cone axons to lengthen. The central cones are 6 to 8 μm wide with a large prominent nucleus. Foveal cones have a short, thick inner segment (IS) and very short outer segment (OS). At 1 to 2 mm from the fovea both rods and cone have a longer IS and OS in comparison to the central cones.^{36, 45, 49, 50} Foveal photoreceptors form synapses before mid-gestation with INL neurones.⁵¹ Photoreceptor axons are formed as a result of neuronal displacements in foveal development.^{36, 52, 53} As the INL neurones are displaced peripherally by pit formation, the photoreceptor axons elongate to keep contact. The sharper angle of the Henle Fibres (HF) (which consists of photoreceptor axons and Müller cells) around the pit reflects this growth.⁴⁴

1.13. The Third Trimester (Weeks 27 to 40)

The human retinal surface area increases rapidly from 3 months prenatal to birth.⁵⁴ The foveal avascular zone measures 500 μm in diameter at 35 weeks GA.⁵ There is some controversy with regards to the formation of the foveal avascular zone. One study using fluorescence angiography in human retina has reported “that the FAZ in developing humans is initially densely vascularised.”⁵⁵ (Figure 1.5) These authors propose that the FAZ develops by “apoptotic remodelling” after 36 weeks’ gestation.⁵⁶ In contrast to this Provis and colleagues⁸ have reported that in the human macula the vascular elements in temporal-superior and temporal-inferior retina are approaching, but have not yet reached, the incipient fovea at 22 weeks’ gestation. The presence of a FAZ at around 25 weeks’ gestation has been reported.⁵⁷ Thus, there is no evidence for vascularisation of the foveal region of human retina before 25 weeks’ gestation.

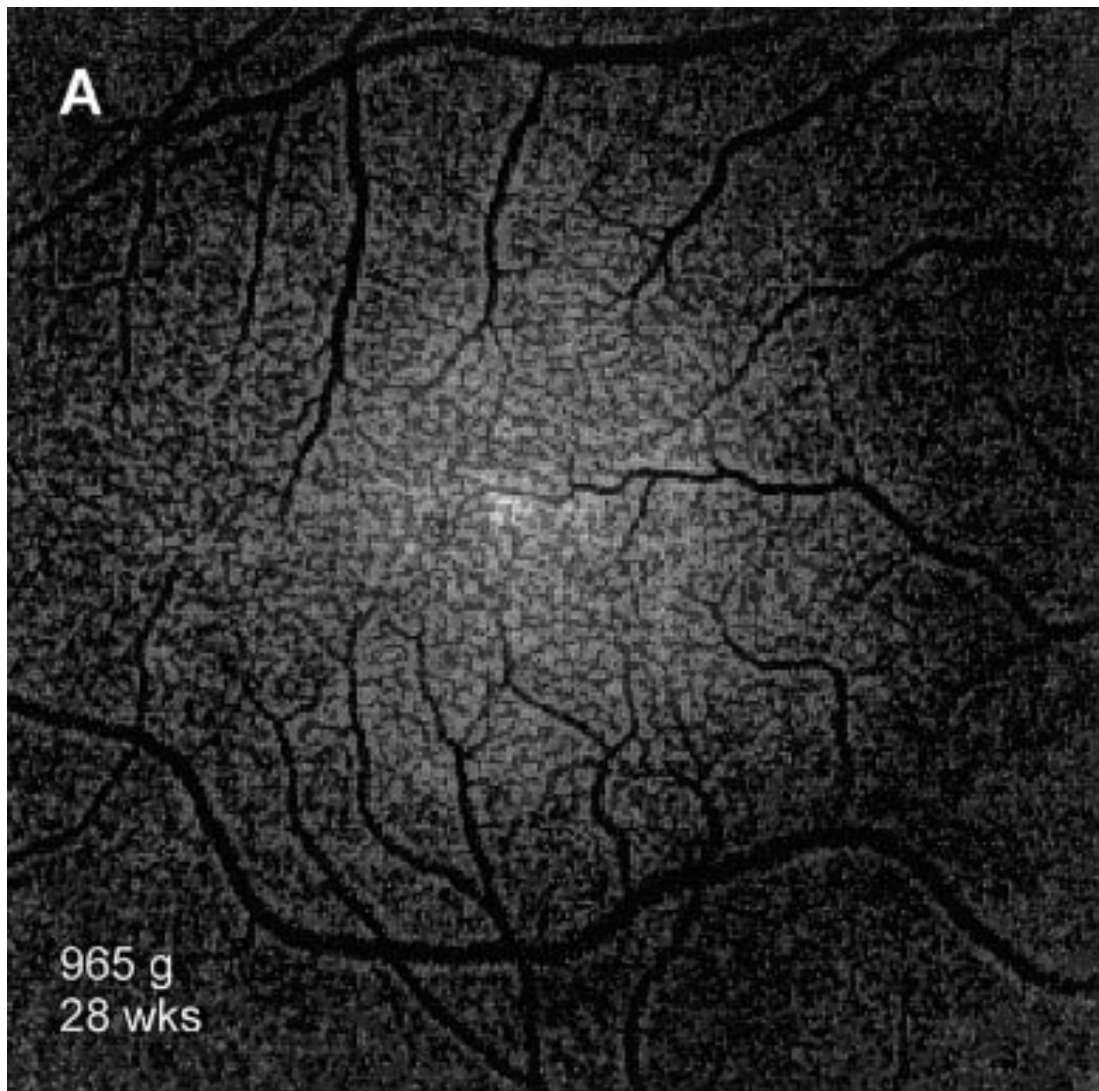


Figure 1.5: Fluorescein angiogram of a 28 week old child illustrating the absence of the foveal avascular zone (taken from Mintz-Hittner et al. 1999).⁵⁵

At 28 weeks a distinct foveal pit is formed with outward displacement of the GCL, IPL and INL.⁴⁷ This may be driven by relative hypoxia of the inner retinal layers at the fovea.⁵⁸ By the seventh month of gestation the inner nuclear layer becomes markedly thinner and the foveal pit appears more obvious. The INL becomes divided by a layer of pale fibres and/or cytoplasm which separates the innermost cell bodies from the remainder of the INL (Transient layer of Chievitz).³⁸ These consist mainly of Müller cell processes. The transient layer of Chievitz forms when pit formation reaches the INL. This layer represents a gap between the amacrine and bipolar cells. By 8 months two layers of cells remain in the GCL.³⁶

The rod free zone is narrower measuring 600 μm . The space between the external limiting membrane (ELM) and retinal pigment epithelium (RPE) is 12.5 μm at 800 μm from the pit centre and 20 μm at 2 mm.³⁷

1.14. Birth to 6 Weeks Postnatally

At birth the FAZ measures between 300 to 350 μm .⁵ The pit becomes deeper and wider with the INL, IPL and GCL only 1 to 2 cells deep.⁴⁷ The transient layer of Chievitz is still present in some retinae.^{36, 50} Between birth and 45 months of age the diameter of the cones continues to decrease.³⁶ The foveal cone diameter measures 7.5 μm at 5 days. Foveolar cone density is 18 cones/100 μm at 1 week postnatal. The space between the ELM and RPE measures 14 μm at the fovea, 20 μm at 1 mm and 30 μm at 2mm at 8 days of age.⁵⁹

1.15. 6 Weeks to 9 Months Postnatally

There is complete excavation of the inner retinal layers between 6 weeks and 9 months postnatally. In humans, the age at which this is complete is variable.^{36, 37, 50, 60} The youngest individual in which full excavation has been demonstrated on OCT was approximately 3 months of age.⁶⁰ The foveal pit continues to widen and the GCL, IPL and INL fuse into a single layer at the fovea.³⁷

In the monkey (*Macaca nemestrina*), there is initially a prenatal increase in pit depth, followed by a rapid postnatal decline in pit depth which occurs during the first 4 to 5 months (the equivalent human developmental time period of 16 to 20 months).^{33, 61}

There is a significant relationship between pit depth and foveolar cone density. Foveolar cone density approximately doubles when the pit depth changes from no depth to 88%, then cone density almost triples when the pit depth declines rapidly by 50%.³³ Studies in monkeys have also shown that the largest amount of cone packing does not occur until the pit reaches its maximum depth and retinal stretch starts to exert tensile forces.

In humans the foveal pit does not reach its maximum depth till late in the first year.^{37, 45} At 9 months the foveal cones are packed 2 to 4 nuclei deep and have a thin and long inner (IS) and outer segment (OS).³⁷

1.16. 12 Months to 45 Months Postnatally

The fovea is thought to reach maturity between 11 to 15 months of age and five years.^{36, 37, 50, 60} Provis et al.⁵ suggests that remodelling of the FAZ to adult dimensions (500 to 700 μm) is completed at about 15 months after birth.^{55, 62}

At 45 months of age, the rod free zone reaches adult dimensions, measuring 650 to 700 μm .³⁷ Foveolar cone diameter changes markedly from 7.5 μm at 5 days postnatal to 2 μm by 45 months.³⁷ At 13 months the foveal IS/OS are 36 μm long. Measures of foveola width and cone diameter have been reported to reach the adult stage of development at 45 months of age, but the two important visual factors of outer segment length and cone packing density are still only half of the adult values at 45 months of age.³⁷ The cone cell bodies are 8 cells deep and the cone density is 108400/mm². Pit remodelling may influence early phases of cone packing but the cause for doubling of density between 15 months and 3.8 years is not clear.³³ There may be a correlation with the expression of fibroblast growth factor.^{23, 35}

1.17. 13 Years to Adulthood

At 13 years, the fovea appears mature.⁴⁷ Cone cell bodies are up to 12 bodies deep. Foveal cone IS are 168-189 μm long and 3 μm wide throughout their length, while OS are 139-155 μm long. At 2 mm from the centre, OS are 40 μm long, almost 4 times shorter than foveal OS. In the adult a cone density of 208200/mm² has been reported.³⁷

1.18. Limitations of Previous Studies

These studies were performed using sub-micron resolution imaging and immunocytochemical labelling. However, serial sectioning is time-consuming, specimens are obtained at a single time point, the same tissue cannot be processed for a flat mount and serial sectioning, retinal detachment is a common fixation artefact, and more severe deformation of structures occurs in fixed sections. Measurements are affected by the rate of relative tissue shrinkage during processing and may not represent in vivo morphology. A significant portion of our histological knowledge of macular development is also heavily dependent on studies obtained from the simian retina, with much fewer samples of human retina available. All of these factors have limited the study of the 3-dimensional changes of the human macula, especially the photoreceptor layer. In addition many of these studies were limited by small sample sizes. The advent of high-speed, high-resolution retinal imaging allows investigation of the maturation of the central retina over time in humans in vivo on a much larger scale.

In this thesis, we will use OCT to explore in vivo human macular development on a much larger scale than was previously possible with histology.

1.2. Optical Coherence Tomography (OCT)

Optical coherence tomography (OCT) is a diagnostic imaging technique that provides cross-sectional images of human retinal morphology *in vivo*. Optical coherence tomography (OCT) is the optical analogue to ultrasonography and measures the echo time delay and magnitude of reflected or backscattered light using the principle of Michelson low-coherence interferometry. Cross-sectional images are obtained by measuring the backscattered light while scanning across multiple sites in a transverse fashion. Echoes from a single point on the retina represent an axial scan (A-scan), and optical cross-sections (B-scans) are obtained by directing the OCT beam in the transverse direction. The data obtained are displayed as false-colour or grey-scale images. The position of the reference mirror is altered in order to obtain reflected light from the retina at several different depths. OCT systems that rely on movements of a reference mirror in order to obtain direct measurements of the time delay and magnitude of the reflected light are known as time-domain OCT (Figure 1.6).⁶³

The use of a reference mirror imposes physical limitations on both the speed of acquisition and the resolution of imaging that can be obtained. These limits have been overcome by the incorporation of broadband light sources as part of modern OCT acquisition.^{64, 65} The frequency information produced is recorded using a charge-coupled device (CCD) camera, and a spectrometer.⁶⁶⁻⁶⁹ This frequency information then undergoes a mathematical transformation, known as Fourier transformation which converts the information obtained from a function of frequency into a function of time, in order to form the multiple intensity profiles (A-scans) that makes up an OCT scan.

Alternatively, in a technique known as swept-source OCT, frequency information can be obtained by sweeping a narrow-bandwidth source through a broad range of frequencies, and the frequency information obtained is recorded using a photodetector.^{65, 70-72}

Eye movements such as rapid micro-saccades, slow drift, and high-frequency, low-amplitude tremor take place while subjects are fixating in order to keep a target centred on the fovea.⁷³⁻⁷⁸ It is well known that these movements can create artefacts within OCT images by altering the intended location of a scan, and that such artefacts can affect quantitative measurements.⁷⁹⁻⁸¹

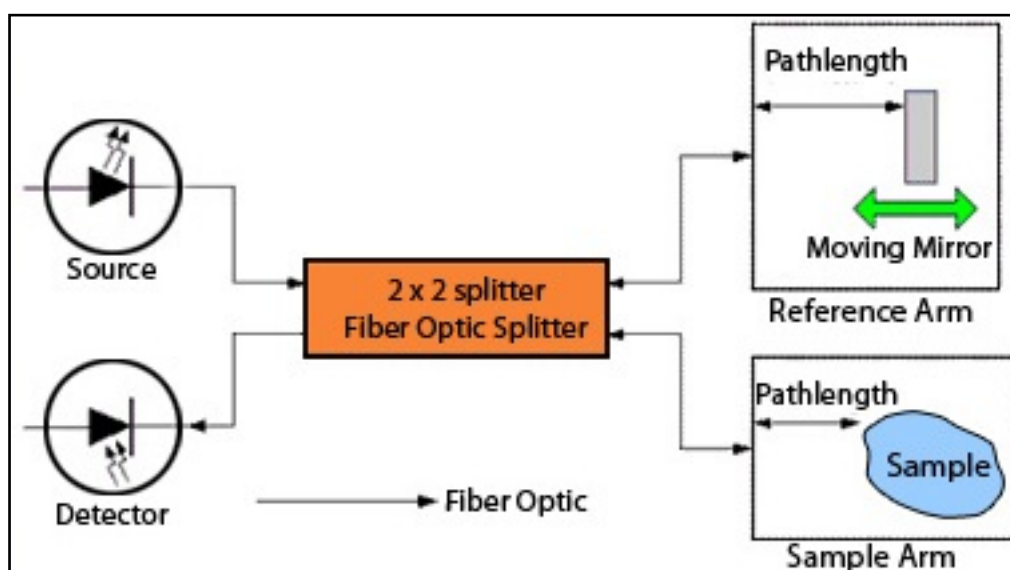


Figure 1.6: Schematic illustrating the principles of time domain OCT (taken from <http://archive.nrc-cnrc.gc.ca/eng/projects/ibd/oct.html>).⁸²

Light is transmitted via a splitter towards the sample and the reference arm. Light is reflected at each interface within the sample and from a moving mirror in the reference arm. The reflected light from the sample and reference arms generates interference patterns that are recorded by the detector.

Although numerous publications show the advantage of OCT ocular imaging in the adult,⁸³⁻⁸⁵ the higher speed of scanning is even more important in young children with limited attention spans and difficulty with sustained fixation. Until recently, infants and young children were deprived of this technology. A search of Pubmed (available at: <http://www.ncbi.nlm.nih.gov/pubmed/>) on September 7th, 2014 using the term: “ophthalmic optical coherence tomography”, found 11975 references. A search of Pubmed using the term: “ophthalmic optical coherence tomography in infants”, found only 148 references. The most likely reason for this is that conventionally OCT imaging is a chin rest system that requires good fixation and cooperation, thus limiting its use in infants and young children. A hand-held spectral-domain OCT (HH-SDOCT) has been

developed by Bioptigen™ and optimised with correction for lateral magnification in the paediatric population allowing visualisation of retinal and foveal development in vivo.^{49,}
⁸⁶ The lateral scales for OCT data were adjusted based on age-specific axial length estimates previously reported to facilitate comparisons at specific locations.

To use OCT quantitatively, a segmentation-based determination of the thicknesses of the different intraretinal layers is required. Segmentation is an important component of OCT data processing, in which different intraretinal layers are identified and separated from each other.

Segmentation in eyes with retinal pathologies has traditionally been difficult because these images often exhibit algorithm failure. Patel et al. found a high rate of segmentation errors in time-domain OCT retinal thickness measurements from patients with neovascular age-related macular degeneration.⁸⁷ Sadda et al. found errors in eyes with sub-retinal pathologies.⁸⁸ These findings are likely due to the segmentation algorithm's dependence on finding the boundary between the photoreceptor inner and outer segments, as this is often obscured by sub-retinal fluid or physically disrupted in patients with retinal pathology. The manual placement of boundaries was successfully used to obtain quantitative measurements,⁸⁹⁻⁹¹ but operator-dependence adds a layer of subjectivity to quantitative measurements.

1.21. Anatomical Correlation of OCT Findings with Histology

OCT images have been correlated with major histological findings at all several different ages, validating it as a reliable quantitative tool in assessing foveal morphology (Figure 1.7).⁹² It has been shown by both OCT imaging and histological studies, that preterm infants have a shallow foveal pit containing inner retinal layers and short, undeveloped foveal photoreceptors. At term there is movement of the inner retinal layers (IRL) away from the central fovea. Simultaneously, there is lengthening of the peripheral photoreceptors. The foveal IS and OS are initially shorter than the peripheral IS and OS for several weeks after birth. This difference disappears by 13 months. The Henle fibre layer (HFL) (which consists of photoreceptor axons and Müller cells) thickens on histology with maturity. However the HFL is normally not visible on OCT and appears as part of the ONL (Figures 1.1 & 1.2). The ONL/HFL on OCT also thickens by 13 months. At this stage, the cone cell bodies are greater than 6 cells deep. By 13 to 16 years the fovea reaches full maturation and has a full complement of OCT bands. The cone cell bodies are now greater than 10 cells deep and have now become thin, elongated and tightly packed.

The bands identified in the outer retina with OCT have been correlated anatomically with histology.⁹³ The OCT bands that have been attributed to the ELM (a linear confluence of Müller cell junctional complexes)⁹⁴ and the RPE are correct. These structures are represented by the first, innermost band and the fourth, outermost band respectively in the outer retina on OCT. The thinness of the histologic ELM is consistent with Müller cell junctional complexes of the ELM being the origin of the signal for Band 1, although it is possible that Müller cell microvilli could contribute to the width of the band.

The IS/OS aligns with the mitochondrial rich ellipsoid (ISE) region of the inner segments. The third band corresponds to an ensheathment of the cone outer segments by apical processes of the RPE in a structure known as the contact cylinder (CC). This was previously called Verhoeff's membrane and consists of junctional complexes between RPE cells.^{95, 96}

Another difference that should be noted between the nomenclature with histology and with OCT is that what is termed OPL. In classic histology the OPL

includes both the photoreceptor synapses and axons as they extend out from the foveal centre.⁹⁷ With OCT the photoreceptor axons are hypo-reflective and are indistinguishable from the photoreceptor nuclei and are therefore included with what is normally labeled as ONL with OCT. In addition the GCL and IPL layers (which are distinctly different on histology) have much less contrast with increasing age with OCT.⁹² The transient layer of Chievitz which is prominent around birth in the INL with histology, is hypo-reflective with OCT and cannot be distinguished from the INL.

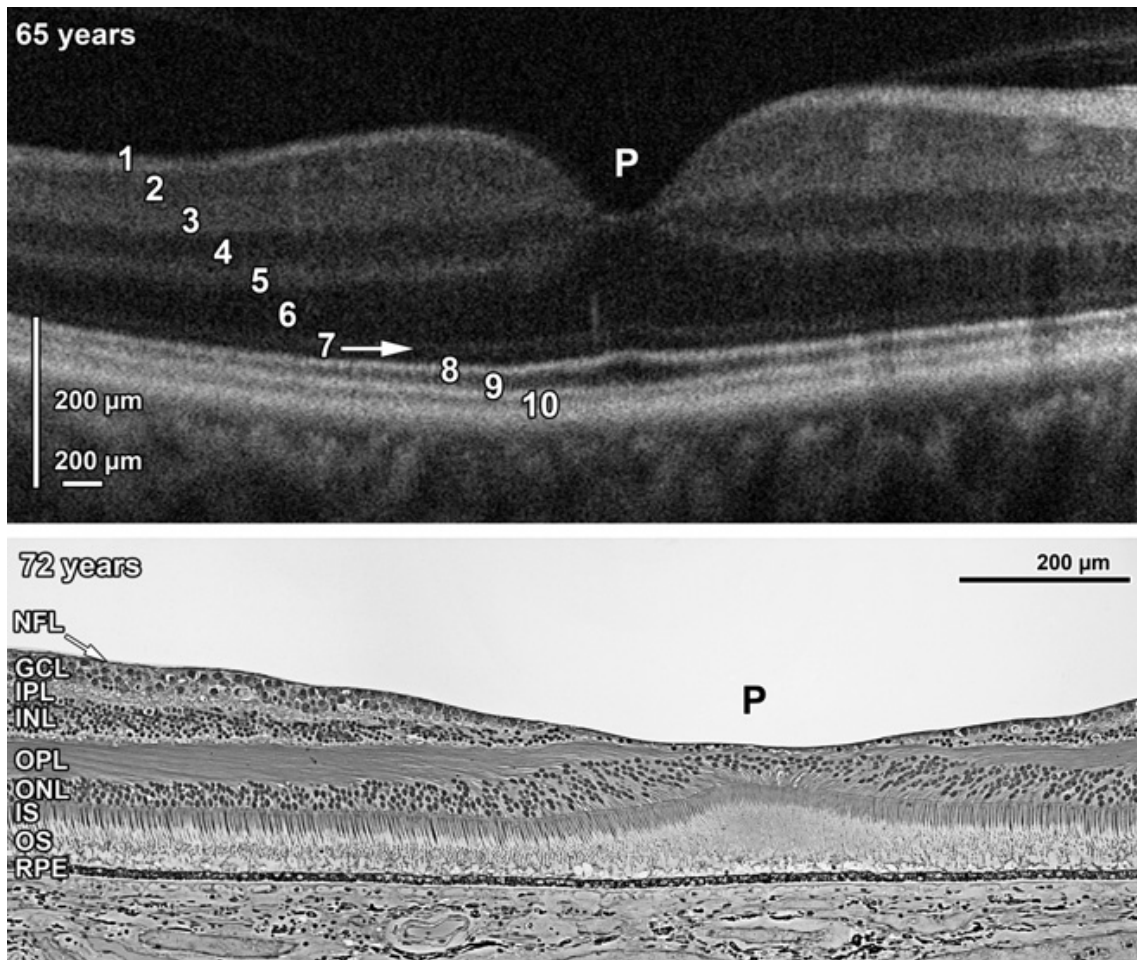


Figure 1.7: Comparison of an OCT image of a normal adult human fovea with a histological section (Taken from Vajzovic et al. 2012).⁹²

The SD-OCT bands are labelled 1-10 as follows: 1 = NFL; 2 = GCL; 3 = IPL; 4 = INL; 5 = OPL; 6 = ONL; 7 = ELM; 8 = photoreceptor inner segment ellipsoid (ISE); 9 = OS; 10 = RPE (split into two hyper-reflective bands).

SD-OCT = spectral domain optical coherence tomography; NFL= nerve fibre layer; GCL= ganglion cell layer; IPL= inner plexiform layer; INL= inner nuclear layer; OPL= outer plexiform layer; ONL= outer nuclear layer; ELM= external limiting membrane; IS= inner segment of the photoreceptors; ISE = photoreceptor inner segment ellipsoid; OS = outer segment of the photoreceptors; RPE= retinal pigment epithelium.

1.22. OCT in Infants and Young Children

Gerth et al.⁹⁸ tested the feasibility of a hand-held probe for Fourier-domain optical coherence tomography retinal imaging in infants and children. In that study, 30 children aged 7 months to 9.9 years were imaged; 10 with pathology and 20 without. The pathologies included maculopathy, retinal dystrophy, post traumatic choroidal neovascularization and Leber's congenital amaurosis with horizontal pendular nystagmus. All were successfully imaged. Dilating drops were used in 27 out of 30 patients. The remaining 3 were cooperative enough to obtain images without dilation. Examination under chloral hydrate sedation was used for 10 children aged 7 months to 3.7 years as part of standard-of-care diagnostic procedures. Children who could sit quietly were imaged with a chin rest with a mount for the scanner. The authors were successful in imaging children as young as 2.9 years with this approach. The remainder was asked to lie down on an examination stretcher.

In this study the authors report that the most challenging problem was the lack of an internal fixation target and the moving scanning line, which usually distracted the children from steady fixation. External fixation targets were successful in only a few cases. The localisation of the macular area was easier in conscious rather than in sedated children because of lack of simultaneous fundus viewing. It was also found that images obtained using the hand-held mode contained movement artefacts caused by the examiner and/or the child.

Scott et al.⁹⁹ successfully used the HH-SDOCT to evaluate 2 infants with shaken baby syndrome and felt that it was comparable with conventional chin-rest OCT. Rapid data acquisition limited motion artefact within the B-scan, although there was slight motion between B scans. The OCT images provided previously unseen details with regard to the morphologic features of retinal lesions in these infant eyes and influenced management.

Chavala et al.¹⁰⁰ examined 3 infants with ROP with the HH-SDOCT. Two were performed under sedation. They described pre-retinal structures, schisis, and retinal detachment found on OCT, but not on conventional clinical examination (portable slit lamp and indirect ophthalmoscope) in infants with ROP. The authors conclude that the

HH-SDOCT could affect future clinical decision-making if studies validate a management strategy based on findings from this imaging technique.

Chong et al.¹⁰¹ performed OCT on 3 groups of children; a control group of 4 children, 2 children with ocular albinism and 5 with suspected ocular albinism and 1 with oculocutaneous albinism. Two devices were used to carry out the imaging. This included a stationary spectral-domain OCT that was developed by the authors and the Bioptigen™ HH-SDOCT. In this study, a spectrum of foveal morphological abnormalities associated with albinism. The authors report that there are difficulties in using OCT technology to image children with known and suspected ocular albinism. This is due to movements on the part of the child, whether due to the nystagmus or shortened attention typical of young children.

In all these studies, limiting factors for imaging children were patient motion, poor fixation, patient position, and different optics compared with the adult eye. In paediatric patients, access to the eye may be limited by infant inattention and movement. Thus, it is critical to optimise scan quality in a short capture time.

In this thesis, we will investigate if the HH-SDOCT developed by Bioptigen™ can be used to produce reliable and repeatable retinal images in infants and young children.

We will also explore its diagnostic utility in investigating infants and young children with abnormalities of retinal development.

1.23. Optimisation of the Bioptigen™ Hand-Held Spectral Domain OCT

In a study by Maldonado et al.,⁸⁶ problems specific to imaging paediatric patients with HH-SDOCT were identified and technical corrections to solve these challenges were tested. In this paper four main issues with imaging the infant eye were identified:

1. Axial Length
2. Refractive Error
3. Corneal Curvature
4. Astigmatism

1.24. Axial Length

The axial length increases rapidly in the neonatal period growing 0.16 mm per week.¹⁰² This growth slows with age from approximately 1 mm/year during the first 2 years to 0.4 mm/ year from 2 to 5 years, and to 0.1 mm/year from 5 to 15 years. After age 15, no significant further growth occurs.^{102, 103}

Normally an OCT scan of the retina is obtained by pivoting the OCT beam in the plane of the patient's iris. In the shorter infant eye the OCT scanning pivot location is anterior to the iris plane. This results in clipping of the peripheral portion of the image by the iris (Figure 1.8). The shorter axial length in paediatric patients may be corrected for by shortening the OCT reference arm position such that the pivot point is positioned in the iris plane. Commercial OCT systems have a reference arm position pre-established by the manufacturer for a standard adult eye. This value needs to be adjusted by an age dependent corrective factor in children. The reference arm position is corrected in the HH-SDOCT system as follows:

$$\Delta \text{ in Reference Arm Position in mm} = \Delta \text{ in Axial length of the Eye in mm} \times n$$

where n is the index of refraction of the vitreous (1.334)

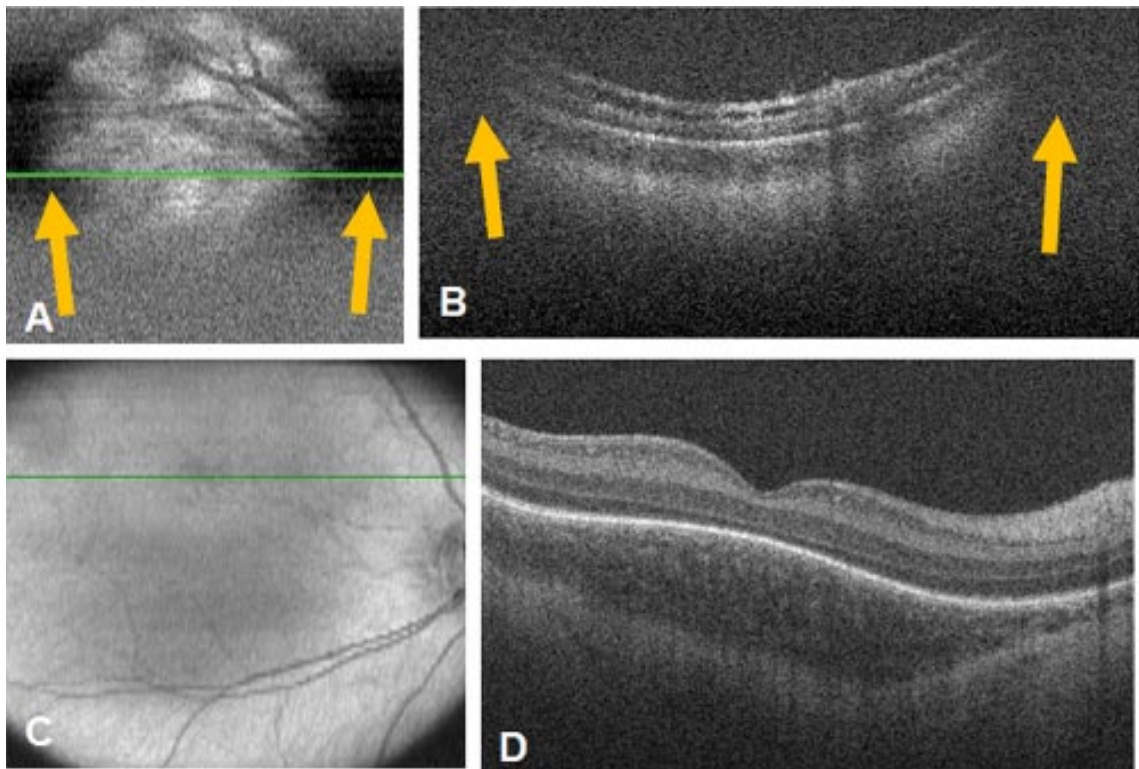


Figure 1.8: Schematic illustrating the problems of incorrect reference arm length on OCT (taken from Maldonado et al. 2010).⁸⁶

Examples of OCT images with vignetting from incorrect reference arm length (A & B). Clipping of the peripheral aspects of the images has occurred (yellow arrows). When the reference arm length is corrected for the shorter axial length of the infant eye, this clipping does not occur (C & D).

1.25. Refractive Error

Preterm infants are predominately myopic, with reported mean refractive error (RE) of -2.00 D at 32 weeks; -1.00 D at 30 to 35 weeks postmenstrual age (PMA) and -1.23 at 36 weeks.^{102, 103} There is a shift to hyperopia (mean RE of +2.12 D) by 52 weeks.¹⁰² From 36 weeks until the age of 6 years the mean refractive error reported is +0.5.¹⁰³ The focus of the hand-held probe has a range of -10 to +12 Diopters to allow for correction for refractive errors.

1.26. Corneal Curvature

The newborn cornea is generally steeper than the adult cornea, with a mean central corneal power of between 48 and 58.5 D, decreasing to mean adult values (43.5 D) by 3 months.¹⁰³⁻¹⁰⁸

1.27. Astigmatism

The newborn eye has greater astigmatism than the adult eye. The power and axis of infant astigmatism varies in the literature, but the condition also decreases by 50% at approximately 6 months of age.¹⁰⁵

Maldonado et al.⁸⁶ created a theoretical eye model for prematurely born neonates using data available in biometric studies of the infant eye and the optical formulas of Gullstrand and of Gross and West. In this model, the refractive indices of the media are assumed to be equal to those of the adult eye. Based on that analysis, age-specific considerations in the HH-SDOCT imaging protocol for young children were established. This included changing the reference arm position, focus, and scan settings based on age (Table 2).

Group Age	Refractive Error D	SD (D)	Axial Length (mm)	SD (mm)	Increase in Reference Arm† (Readout Units)	For a 10-mm (≈35 degree) Adult Scan Setting*				
						Scan Length on Retina (mm)	Scan Length on Retina (deg)	Number of A-scans per B-scans‡	Increment A-scans per Each 1 mm of Scan Length	Relative Scan Length to Adult Scan Length (%)
30–35 wk	–1	0.9	15.1	0.9	97	6.3	22	925	92	63
35–39 wk	0.3	1.6	16.1	0.6	86	6.7	23	986	99	67
39–41 wk	0.4	1.5	16.8	0.6	79	7.0	25	1029	103	70
0–1 mo	0.9	0.9	17.4	0.5	72	7.3	25	1066	107	73
1–2 mo	0.3	0.6	18.6	0.5	59	7.8	27	1139	114	78
2–6 mo	0.5	0.6	18.9	0.4	56	7.9	28	1158	116	79
6–12 mo	0.6	0.2	19.2	0.5	52	8.0	28	1176	118	80
12–18 mo	0.7	0.6	20.1	0.7	43	8.4	29	1231	123	84
18 mo–2 y	0.9	1.5	21.3	0.3	30	8.9	31	1305	130	89
2–3 y	1	1.1	21.8	0.1	24	9.1	32	1335	134	91
3–4 y	0.6	1.8	22.2	0.4	20	9.3	32	1360	136	93
4–5 y	–0.8	0.9	22.3	0.2	19	9.3	33	1366	137	93
5–9 y	–0.6	1	22.7	0.4	14	9.5	33	1390	139	95
10 y-adult	–0.5	1.5	24	0.7	0	10.0	35	1470	147	100
Axial myopia			26		–22	10.8	38	1593		

* Note that this would apply to an adult scan setting selected from any OCT system.
† A higher number equates with a shorter reference arm length on the system we used. To convert, we used manufacturer data (Bioptigen, Inc., Research Triangle Park, NC) of –10.86 readout units/mm of change in reference arm length. (Note that on the Bioptigen unit used in this study, the 10-mm adult scan appears as a 16-mm scan setting due to a manufacturer labeling error, as explained in Methods.)
‡ Presuming one wants 6.8 μm of separation between A-scans. This would be varied for a different A-scan density.

Table 1.2. Standard reference table for axial length, refractive error, reference arm position, and A-scans per B-scan by age, with an example of a 10-mm adult scan (taken from Maldonado et al. 2010).⁸⁶

The scan density (A-scans/B-scan) will also be greater in the shorter infant eye. If one wishes to perform paediatric imaging using the same scan density as in adults, paediatric scan settings need to be adapted and can be preset (using the established conversion table - Table 1.2) as follows:

$$\text{A-scans/B-scan} = (\text{Paediatric Axial Length in mm}/24 \text{ mm}) \times (\text{Scan Length mm}) \times \text{Selected number of A-scans per mm}$$

1.28. OCT in Retinopathy of Prematurity (ROP)

Although not the main theme of this thesis, much of the previously published HH-SDOCT work relates to infants and neonates with retinopathy of prematurity (ROP) and it is worth reviewing what this work has established with regards to premature foveal development. ROP is known to alter development of the central retina and, even if mild, may be associated with deficits in acuity and visual sensitivity.^{105, 109, 110} Studying the foveal architecture of ROP subjects using OCT may provide some helpful clues on what occurs during the course of a normal human foveal development.

Macular alterations are present in advanced ROP, and usually consist of temporal displacement or tractional retinal detachment.¹⁰⁵ In ROP, the presence of a line or a ridge in the peripheral retina may act as a barrier retarding peripheral migration of cells even in the posterior pole and thus delay macular development.

1.28a OCT in Older Children with a History of ROP

Akerblom et al.¹¹¹ examined the eyes of 65 prematurely born children aged 5-16 years with Stratus™ optical coherence tomography, and the results were compared with those of 55 children born at term.¹¹¹ Children with previous retinopathy of prematurity (ROP) had significantly thicker central maculae than those without it. This did not correlate with visual acuity or refraction. Gestational age at birth was the only risk factor identified for a thick central macula.

Ecsedy et al.¹¹² have described variations in the structure of the macula in formerly preterm children aged 7-14 when compared to age matched controls. In this prospective case control study using the Stratus™ time-domain OCT several groups were examined. Group 1 included 26 eyes of 13 patients who had ROP which was treated with laser. Group 2 included 17 eyes of 10 patients and had stage 1 or 2 ROP. Group 3 included 20 eyes of 10 patients without ROP. Group 4 consisted of age matched controls.

They found a significant increase in the mean central retinal thickness measured in all preterm children in comparison to their full term counterparts. In addition there was a significant increase in mean foveal thickness in children in whom ROP was treated with laser. In preterm children, the foveal area was larger. The depth of the fovea

was reduced as a result the presence of the normally absent inner retinal layers at the central foveal pit. In order to explain these differences, it is postulated that during the development of the fovea in preterm children, there is impairment of the normal migration of the inner retinal layers from the fovea and the centripetal migration of the cone photoreceptors in to the fovea. This hypothesis would be confirmed by a thicker measurement of the inner retinal layers and a thinner measurement of the outer retinal layers at the fovea. However, separate measurements of the inner and outer retinal layers were not carried out in this study.

Hammer et al.¹¹³ also reported similar findings using high-speed, high-resolution adaptive optics fourier-domain OCT videos in 5 subjects with a history of ROP (age 14–26 years). This was compared this to 5 age-matched control subjects. Foveal pit depth and volume form was calculated from three-dimensional (3-D) retinal maps and found to be wider and shallower in ROP than in control subjects. In this study, mean pit depth was defined from the base to the level at which the pit reaches a lateral radius of 728 μm . This was 121 μm in the control subjects compared to 53 μm in ROP. The thickness of retinal layers was measured manually. Intact, contiguous inner retinal layers overlay the fovea in 7 of 8 eyes measured in ROP subjects but were absent in the control subjects. Mean full retinal thickness at the fovea was greater in the subjects with ROP (279.0 μm vs. 190.2 μm). An avascular zone was not identified in 7 of the 8 subjects with ROP but was present all the control subjects.¹¹³

1.28b OCT in Infants with ROP

Lago et al.¹¹⁴ describe their findings in 13 eyes of 12 premature babies with retinopathy of prematurity using a Stratus™ time-domain OCT.¹¹⁴ Optical coherence tomography revealed a condensed retinal pigmented epithelial layer in the macular-foveal area shown by increased reflectivity. In these eyes the retinal layers were not well differentiated. A foveal depression was clearly evident in 23%.

Maldonado et al.⁴⁹ examined 31 prematurely born neonates aged between 31 and 41 weeks postmenstrual age and 9 full term control children and adults. In this study, central foveal thickness, foveal to parafoveal (FP) ratio (central foveal thickness divided

by thickness 1000 μm from the foveal centre), and 3-dimensional thickness maps were analysed.

They describe several signs of immaturity are in the neonates:

1. a shallow foveal pit
2. persistence of inner retinal layers (IRLs)
3. a thin photoreceptor layer (PRL)

Three-dimensional mapping showed displacement of retinal layers out of the foveal centre as the fovea matured and the progressive formation of the inner/outer segment band in the opposite direction (Figure 1.9). The FP-IRL ratios decreased from 0.46 in premature neonates to 0.05 in adults, as the IRL migrated before term and minimally after that. The FP-PRL ratios increased from 0.75 in premature neonates to 1.44 in adults, as the components of the PRL mature closer to term and into childhood (Figure 1.8). They also report the presence of cystoid macular oedema in 58% of premature neonates that appeared to affect inner foveal maturation (Figure 1.9).

Longitudinal imaging of 4 neonates without macular oedema demonstrated an age-dependent increase in PRL thickness at the fovea. This increase was most rapid after 38 weeks. Oedema was associated with a possible delay in maturation of IRLs, but no definite delay in photoreceptor development was identified.

Another feature of the immature retina in this study was the absence of a visible IS/OS and OS/RPE band on OCT examination. The IS/OS became visible in the perifovea with HH-SDOCT from 33 weeks PMA and was visible later in the central fovea at 43-48 weeks PMA. The OS/RPE band appeared to differentiate at the apical side of the RPE layer late in childhood, consistent with growth of apical microvilli of the RPE (Figure 1.10). It was not visible in any infants less than 10 years.

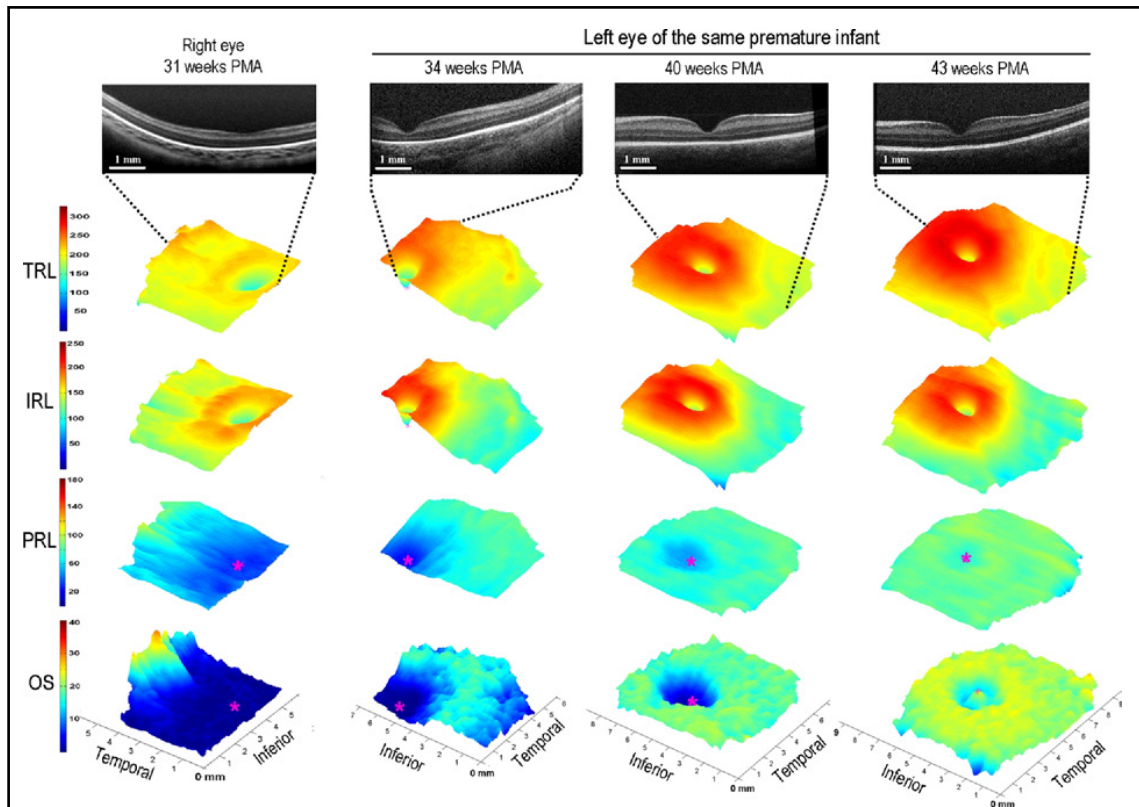


Figure 1.9: Three-dimensional retinal thickness maps demonstrating the regional changes in premature human foveal development from 31 weeks to 43 weeks PMA (Taken from Maldonado et al. 2011).⁴⁹

The total retinal thickness (TRL) increases in all areas, particularly in the parafoveal area. The inner retinal layers (IRL) undergo centrifugal displacement from a combination of pit size expansion and parafoveal ring thickening. The photoreceptor layer (PRL) undergoes centripetal migration, increasing in thickness at the foveal centre from a thin layer at 31 weeks to a focal point of thickness at the foveal centre at 43 weeks. The ring of photoreceptor outer segments (OS) surrounding the fovea increases in thickness over time.

TRL = total retinal layer; IRL = inner retinal layer; PRL = photoreceptor layer; OS = outer segment

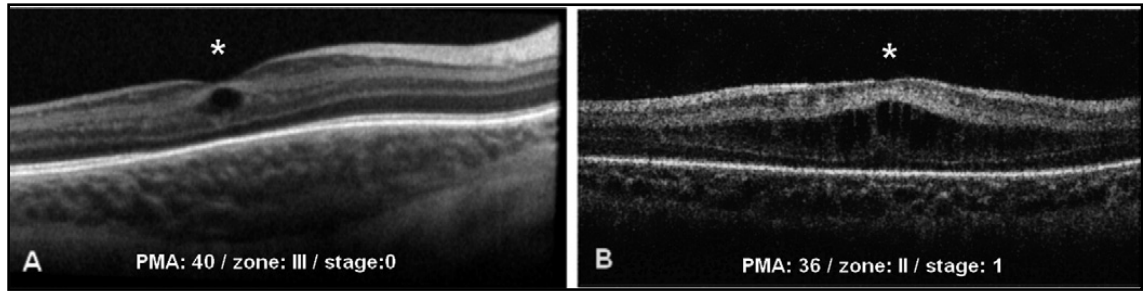


Figure 1.10: Examples of oedema affecting the inner nuclear layer in 2 premature infants (Taken from Maldonado et al. 2011).⁴⁹

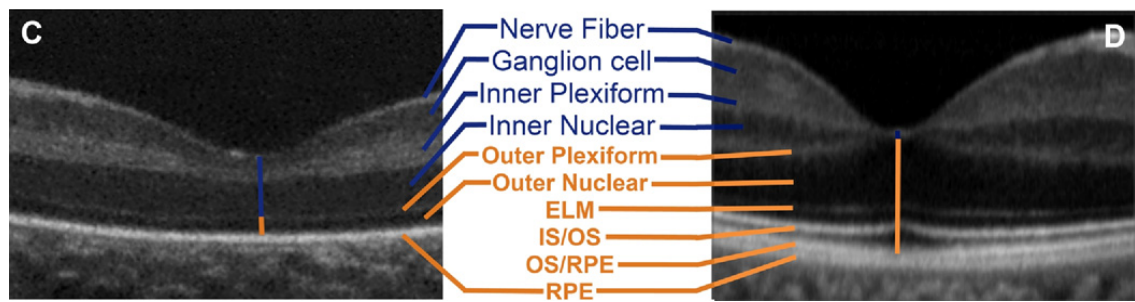


Figure 1.11: Comparison of SD-OCT scans taken of the fovea in a 31 weeks PMA premature infant (left) and a 23 year old adult who was born at term (right). (Taken from Maldonado et al. 2011).⁴⁹

The OS/RPE band is not visible in the infant. This band is clearly demarcated in the adult.

SD-OCT = spectral domain optical coherence tomography; PMA = post menstrual age; OS = outer segment of photoreceptors; RPE = retinal pigment epithelium

Vinekar et al.¹¹⁵ characterised the abnormal foveal changes that occur in ROP using a table-top Spectralis™ spectral-domain OCT which was modified to a hand-held model. They found that 23 of 79 eyes (29.1%) with stage 2 ROP showed abnormal foveal changes (macular oedema) with OCT examination, despite clinically normal foveae (Figure 1.12). Infants with stage 2 ROP had a significantly thicker central foveal thickness in comparison to normal controls ($p < 0.001$). The central foveal thickness 206.5 +/- 98.7 μm in stage 2 ROP eyes and 135.9 +/- 17.6 μm in control eyes. Nineteen of the 23 eyes had follow up imaging at 52 weeks' PMA, and all of them revealed normalisation of foveal contours.

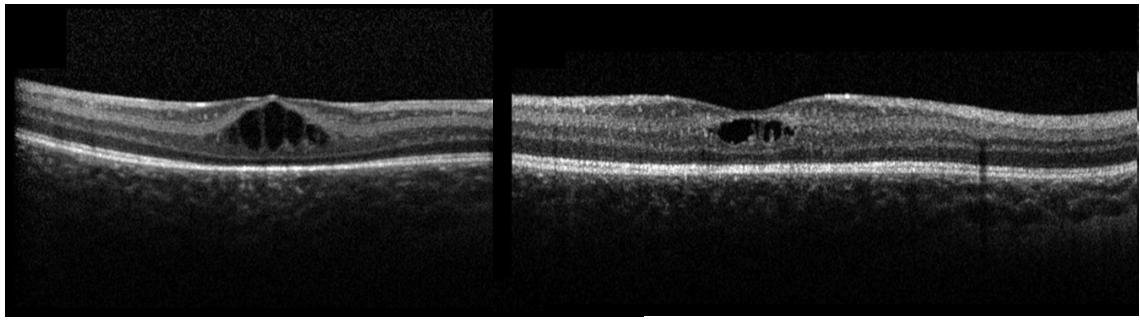


Figure 1.12: Examples of “pattern A” macular oedema (left) and “pattern B” macular oedema (right) (Taken from Vinekar et al. 2011).¹¹⁵

Two distinct patterns of macular oedema were observed in infants with retinopathy of prematurity: “pattern A,” which was characterised by dome-shaped foveal elevation and cystoid spaces with highly reflective intervening vertical septae, and “pattern B,” which was characterised by preservation of the foveal depression with fewer intraretinal cystoid spaces. These patterns were seen in 12 (52.2%) and 11 (47.8%) eyes, respectively.

In the absence of any obvious causes for the macular oedema, it is hypothesised that this “macular oedema” seen in eyes (29.1%) with more severe ROP could either be:

- (1) a response to biochemical modulators, including higher concentrations of vascular endothelial growth factors (VEGFs), which could play a role in increased vascular permeability leading to retinal oedema; or
- (2) could be caused by mechanical traction exerted on the macula.

1.29. OCT of Normal Foveal Morphology in Older Children

Analysis of tomograms obtained from older children that could cooperate with conventional OCT systems have established the possible effects of age, race, gender and axial length on OCT measurements obtained from children. El Dairi et al.¹¹⁶ described the optical coherence tomography findings in the eyes of 286 normal children aged 3 to 17 years, using the Status™ time-domain OCT. This study defined the normative paediatric values for OCT measurement and characterised the effect of age, race, axial length and spherical equivalent on macular thickness and volume, peripapillary RNFL thickness and optic nerve head morphology.

Results of this study showed that black children had smaller macular volume and foveal thickness, larger RNFL thickness and larger cup disc ratios compared with white children. Macular volume and average outer macular thickness correlated negatively with axial length in white children. Foveal thickness correlated positively with age in black children only.

Gupta et al.¹¹⁷ evaluated 32 eyes for macular thickness and 25 eyes for RNFL thickness in the paediatric population and compared the results to adult findings. The average foveal thickness for children was 221 µm vs 182 µm in adults. Children had slightly thicker maculae than adults; the RNFL thickness was comparable to adults.

The Sydney Childhood Eye Study examined 1765 6-year-old children from 34 randomly selected Sydney schools during 2003 and 2004 (78.9% response).¹¹⁸ Fast macular thickness scans were performed over a 6-mm diameter central retinal region with optical coherence tomography (Status™ time-domain OCT). The mean (SD) minimum foveal thickness was 161.1 (19.4) µm. The thickness of the central, inner, and outer macula was normally distributed, with means (SD) of 193.6 (17.9), 264.3 (15.2), and 236.9 (13.6) µm, respectively. Total macular volume was also normally distributed, with a mean (SD) of 6.9 (0.4) mm. The foveal minimum, central, and inner macula was generally significantly thicker in boys than in girls, and in white children than in East Asian children.

There is a shortfall in our existing knowledge of in vivo retinal development with regards to the age group in between the two age groups outlined above;

premature infants and older children. In this thesis, we will aim to bridge this gap by investigating retinal development in full term infants and young children aged between birth and 6 years of age.

We will also use the HH-SDOCT to explore retinal development in several conditions associated with infantile nystagmus (some of which are thought to affect retinal development) to provide further insights into retinal development in infants and young children.

1.3. Infantile Nystagmus

The key to understanding normal foveal development may lie in studying conditions in which there is abnormal foveal development. Infantile nystagmus syndrome (INS) encompasses several such conditions. INS is a rhythmic to and fro involuntary oscillation of the eyes with onset in early childhood. The prevalence of INS has been reported as 14.0 per 10000 population of which 17.9% are attributed to albinism, 13.6% to idiopathic (IIN) and 4.3% to latent nystagmus.¹¹⁹ INS can be subdivided based on aetiology into the following groups:¹²⁰

1. Albinism.
2. Idiopathic infantile nystagmus (IIN). This is also known as unassociated INS.
3. Latent or manifest latent nystagmus. This is also known as fusion maldevelopment nystagmus syndrome (FMNS).
4. Nystagmus associated with ocular disease. This includes retinal dystrophies such as achromatopsia and congenital stationary night blindness (CSNB) as well as other ocular conditions such as aniridia, congenital cataracts and optic nerve hypoplasia.
5. Spasmus nutans syndrome. This is a condition that involves rapid, uncontrolled eye movements associated with head bobbing.

The normal assessment of a patient with nystagmus involves recording a detailed history regarding onset, symptoms such as blurred or reduced vision, oscillopsia (the sensation that objects are moving around) and family history. Their vision is recorded monocularly and binocularly, both for distance and near.¹²¹ A full orthoptic assessment is performed detailing the presence of any squints, nystagmus form (amplitude, frequency, direction and conjugacy) and any associated head postures. A slit lamp examination is performed to check for the presence of iris transillumination defects (TID), which can suggest a diagnosis of albinism, iris abnormalities such as aniridia and cataract. A dilated retinal examination is normally performed to document if there are any optic nerve or retinal abnormalities such as optic nerve and foveal hypoplasia or abnormalities of pigmentation such as hypo-pigmentation in albinism.

Following this initial assessment a number of additional tests are performed in order to diagnose the aetiology. Eye movement recordings (EMR) are carried out in order to document the waveform. Electrodiagnostic tests (EDT) such as visual evoked potentials (VEP) and electroretinograms (ERG) are carried out. The VEP can diagnose albinism based on the presence of crossed asymmetry (Figure 1.12). The ERG can detect retinal abnormalities associated with conditions such as achromatopsia and congenital stationary night blindness (Figure 1.13).

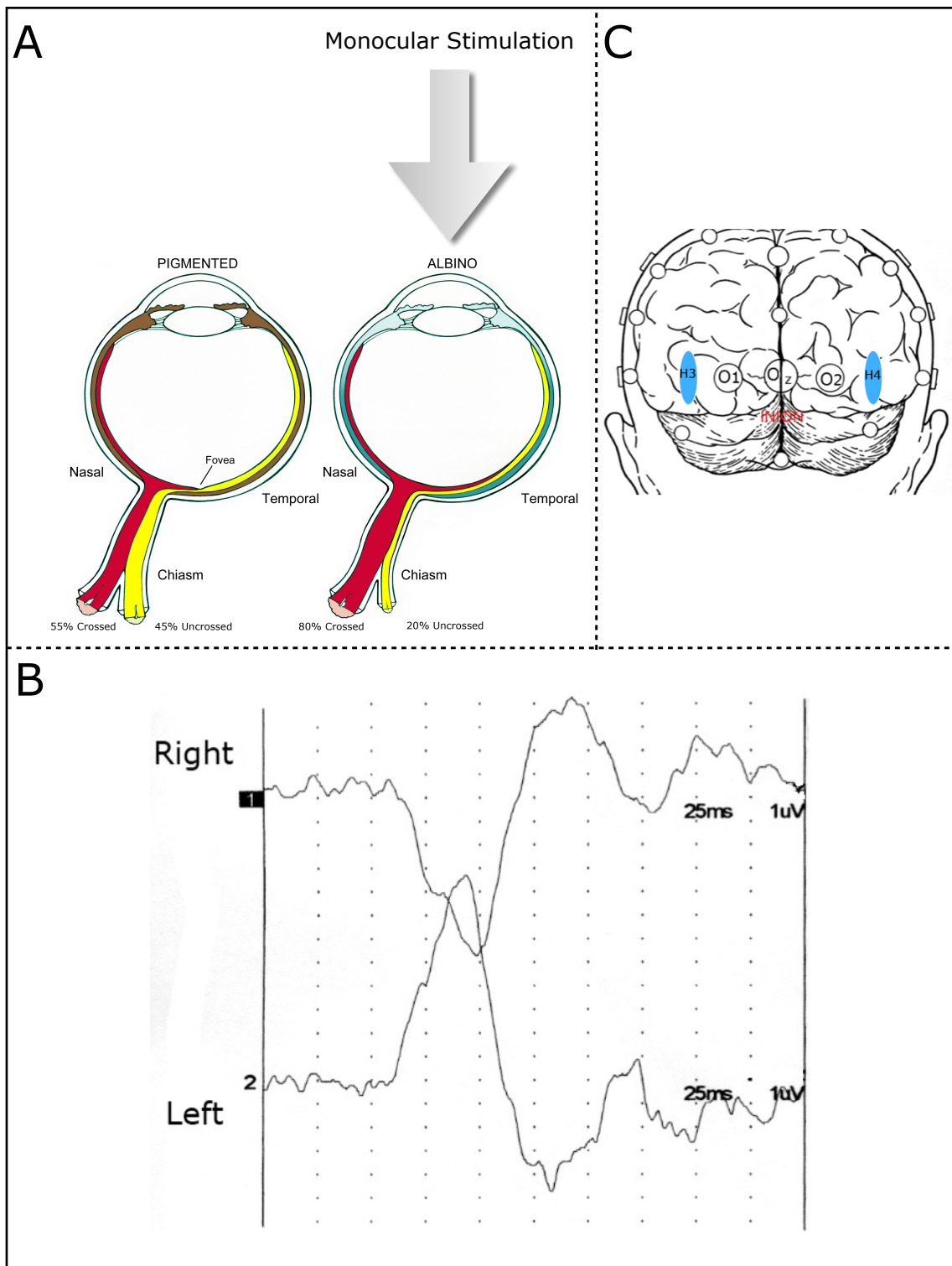


Figure 1.13: Example of crossed asymmetry in albinism on a VEP examination
 (Modified from <http://webvision.med.utah.edu/book/electrophysiology/visual-and-auditory-anomalies-associated-with-albinism/>).

Normally the right and left eyes have similar negative and positive deflections at the same time point on VEP recorded across the occipital scalp in response to monocular stimulation (i.e. they are symmetrical). In albinism, there is misrouting of the optic nerves (i.e. part of the temporal retina projects abnormally to the contralateral hemisphere) (A) and the deflections may occur in opposite directions in each eye at the same time point (i.e. they are asymmetrical) (B). This is most clearly seen when the inter hemisphere difference is calculated i.e. when the VEPs recorded from the left hemisphere are subtracted from those recorded from the right (Channel O1-O2 or Channel H3-H4) (C).

VEP = visual evoked potential

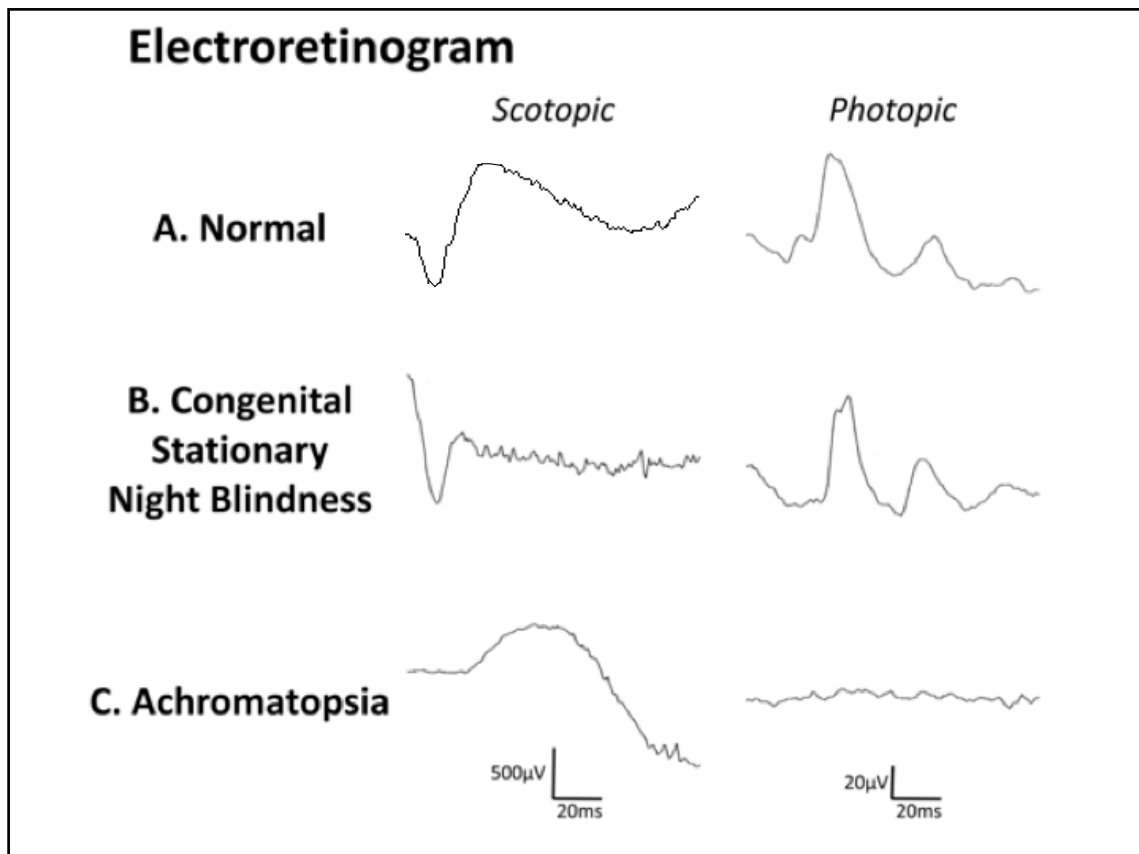


Figure 1.14: Examples of retinal abnormalities detected on an ERG examination (Taken from Kumar et al 2010).¹²²

Normally on ERG the eye has a positive response on scotopic (dark conditions) and photopic (light conditions) testing. In CSNB, the rod function is abnormal and this results in a negative deflection on scotopic testing. In achromatopsia, the cone function is abnormal and this results in a reduced or flat response on photopic testing.

ERG = electroretinogram; CSNB = congenital stationary night blindness

In older patients it has been shown that OCT is very helpful in determining foveal morphology in infantile nystagmus and hence differentiating the aetiology.¹²³⁻¹²⁹ Typical foveal hypoplasia is associated with albinism,^{127, 128} *PAX6* mutations¹²⁸ or isolated foveal hypoplasia;¹³⁰ atypical foveal hypoplasia with achromatopsia;¹²⁶ other foveal changes with retinal dystrophies¹³¹⁻¹³⁷ and normal foveal structure with idiopathic or manifest latent nystagmus.¹²⁴ It is thought that, in general, normal foveal development is arrested in individuals with albinism.¹³⁸ Examining foveal morphology in albinism and in other conditions associated with nystagmus may offer valuable insight into the process of normal and abnormal foveal development.

1.31. Typical Foveal Hypoplasia

Albinism is a group of congenital disorders in melanin biosynthesis that affects approximately 1 in 4000 people in the United Kingdom.¹¹⁹ Albinism is a disorder characterised by ocular and cutaneous hypo-pigmentation, reduced or absent foveal pit, nystagmus, iris transillumination, macular transparency, strabismus, refractive errors, and optic nerve misrouting.¹³⁹ Albinism can be divided broadly into 2 categories, oculocutaneous albinism (OCA) where there is a reduction or absence of melanin in the hair, skin, and eyes and ocular albinism (OA) where the melanin deficiency is limited mainly to the eyes.¹⁴⁰ Causative mutations in at least six genes including *TYR*, *OCA2*, *TYRP1*, *MATP* (*SLC45A2*), *SLC24A5* and *C10orf11* have been reported in OCA.^{140, 141} In addition a genetic locus for OCA5 has been mapped to the 4q24 chromosome.¹⁴¹ Several mutations in the *OAI* (*GPR143*) gene are associated with ocular albinism.¹⁴² There also a number of genes associated with syndromic forms of albinism such as Hermansky-Pudlak syndrome: *HPS1*, *AP3B1* (*HPS2*), *HPS3*, *HPS4*, *HPS5*, *HPS6*, *DTNBPI* (*HPS7*), *BLOC1S3* (*HPS8*), and *BLOC1S6* (*HPS9*) and Chediak-Higashi syndrome: *LYST*.^{143, 144}

OCT has been established in detecting the typical morphological pattern of foveal hypoplasia (typical foveal hypoplasia) associated with albinism in older children and adults.^{101, 123, 125, 127, 145-149} Mohammad et al.¹²⁷ performed high-resolution spectral-domain OCT imaging of the fovea in albinism. The thickness of each retinal layer at the fovea and foveal pit depth were quantified and compared with best-corrected visual

acuity (BCVA). Total photoreceptor layer thickness at the fovea was correlated highly to BCVA. Of all the layers at the fovea, the outer segment length was correlated most strongly to BCVA. There was no correlation between visual acuity and overall retinal thickness. The poor correlation between visual acuity and retinal thickness was due to increased thickness of the photoreceptor layers (for patients with better vision) being associated with a decreased thickness of the processing layers at the fovea (the nerve fibre, ganglion cell, inner plexiform, inner nuclear, and outer plexiform layers). This means that the overall retinal thickness and pit depth can mislead with regard to the degree of deficit in albinism. All processing layers are dramatically reduced in the normal fovea.

The *PAX6* gene is located on chromosome 11. Mutations in this gene may lead to a shortage of *PAX6* protein, which disrupts the formation of the eyes during embryonic development. Clinical features of *PAX6* mutations include iris hypoplasia, nystagmus, foveal hypoplasia, cataract, corneal anomalies and high refractive errors with morphological changes of the macula have been successfully identified on OCT.^{150, 151} The typical foveal hypoplasia is similar but usually less severe than that seen in albinism.¹²⁸

Patients with isolated foveal hypoplasia have typical foveal hypoplasia on OCT but no clinical or genetic signs of albinism or *PAX6* mutations.¹³⁰ Querques et al.¹⁵² describe the OCT findings in a single case of isolated foveal hypoplasia. Instead of excavation their patients showed a thickening of the fovea and absence of the regular foveal avascular zone similar to the macular anatomy in a 6-month human foetus. This suggests that there is an arrest in macular development with abnormal persistence of the early retinal structural

An OCT-based structural grading system for foveal hypoplasia has been developed. In this system, the stage of arrested foveal development provides a prognostic indicator for VA in a range of disorders associated with foveal hypoplasia.¹²⁸ In albinism the length of the photoreceptor outer segment is a strong predictor of VA.¹²⁷

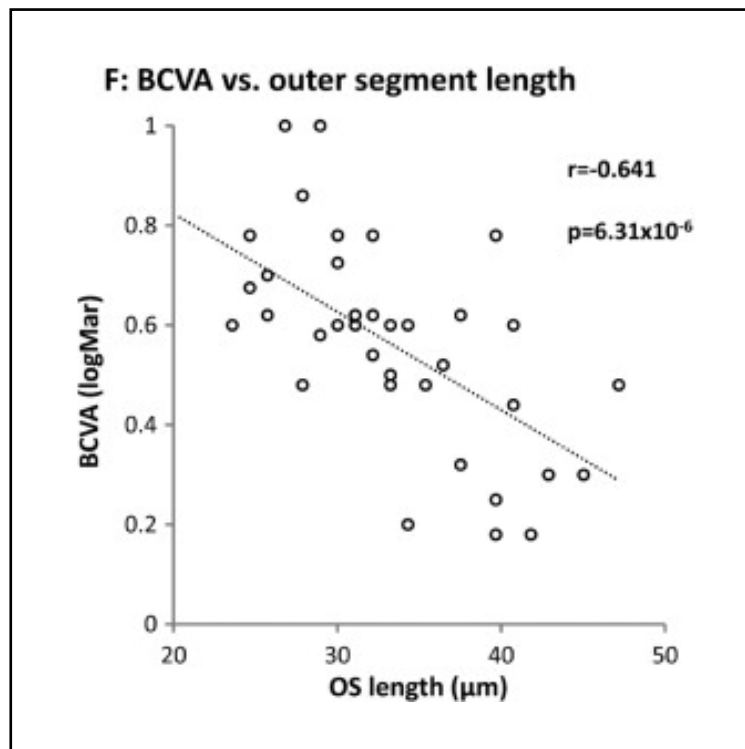


Figure 1.15: Scatterplot of OS length against BCVA (taken from Mohammad et al. 2011).¹²⁷

There is a linear relationship between the photoreceptor outer segment length and logMAR visual acuity. As the length of the OS increases, there is a corresponding increase in the best corrected logMAR visual acuity recorded.

OS = photoreceptor outer segment; BCVA = best corrected visual acuity

1.32. Atypical Foveal Hypoplasia

Achromatopsia (ACHM) is an autosomal recessive disorder which has a number of features including: infantile nystagmus, loss of colour discrimination, photophobia, and reduced visual acuity. It is a rare disorder with an estimated prevalence of 1 in 30000.¹⁵³ Mutations in *CNGA3*,¹⁵⁴ *CNGB3*,¹⁵⁵ *GNAT2*¹⁵⁶ and *PDE6H*¹⁵⁷ have been found. Their protein products are important for visual transduction and show expression restricted to cone inner and outer segments¹⁵³. Mutations in the *CNGA3*¹⁵⁴ linked to ACHM2 on chromosome 2q11 and *CNGB3*¹⁵⁵ linked to ACHM3 on chromosome 8q21 have been found found to be responsible by disrupting the function of the cGMP-gated channel in cone photoreceptors. The third mutation involving Cone Photoreceptor G-Protein α -Subunit Gene (*GNAT2*) which encodes the cone-specific α -subunit of transducin has been found to be involved in <2% of cases of achromatopsia.¹⁵⁶

With optical coherence tomography (OCT) in achromatopsia, there is atypical foveal hypoplasia consisting of continuous inner retinal layers in the macula region, evidence of inner segment/outer segment (IS/OS) junction disruption and the appearance of an evolving bubble (hypo-reflective zone (HRZ)) with cell loss in the cone photoreceptor layer^{128, 158-160} which has been noted to be present as early as 0.8 years of age.^{160, 161} This disorder was previously thought to be a static condition. However, more recent data suggests that it may be a progressive condition as longitudinal OCT examinations have demonstrated increasing changes with age, commencing with disruption of the IS/OS which eventually develops into the HRZ of progressively increasing size.^{126, 129, 162} The underlying pathology is uncertain, but may represent autolysis of the cone photoreceptor outer segments or impaired phagocytosis of the degenerating photoreceptor debris. This cascade of events is reported to have its onset predominantly in the second decade and showed a strong association with age thereafter. The end stage of this condition is characterised by atrophy of the retinal pigment epithelium (RPE).¹⁶⁰ With the imminent possibility of gene therapy for this condition, this work suggests that therapy would be most effective at an early age. Other findings on OCT include thinning of the outer nuclear layer (ONL), disruption of the cone outer segment tip (COST) reflectivity and a reduction in the intensity of the ellipsoid (ISE) band.^{126, 133, 162}

Abnormal development of the fovea in patients with known mutation in the *PAX6* gene has been related to a decrease in grey matter volume at the occipital cortex¹⁶³ and might be related to disruptions in visual pathways at the level of the optic chiasm (Figure 1.15).¹⁶⁴

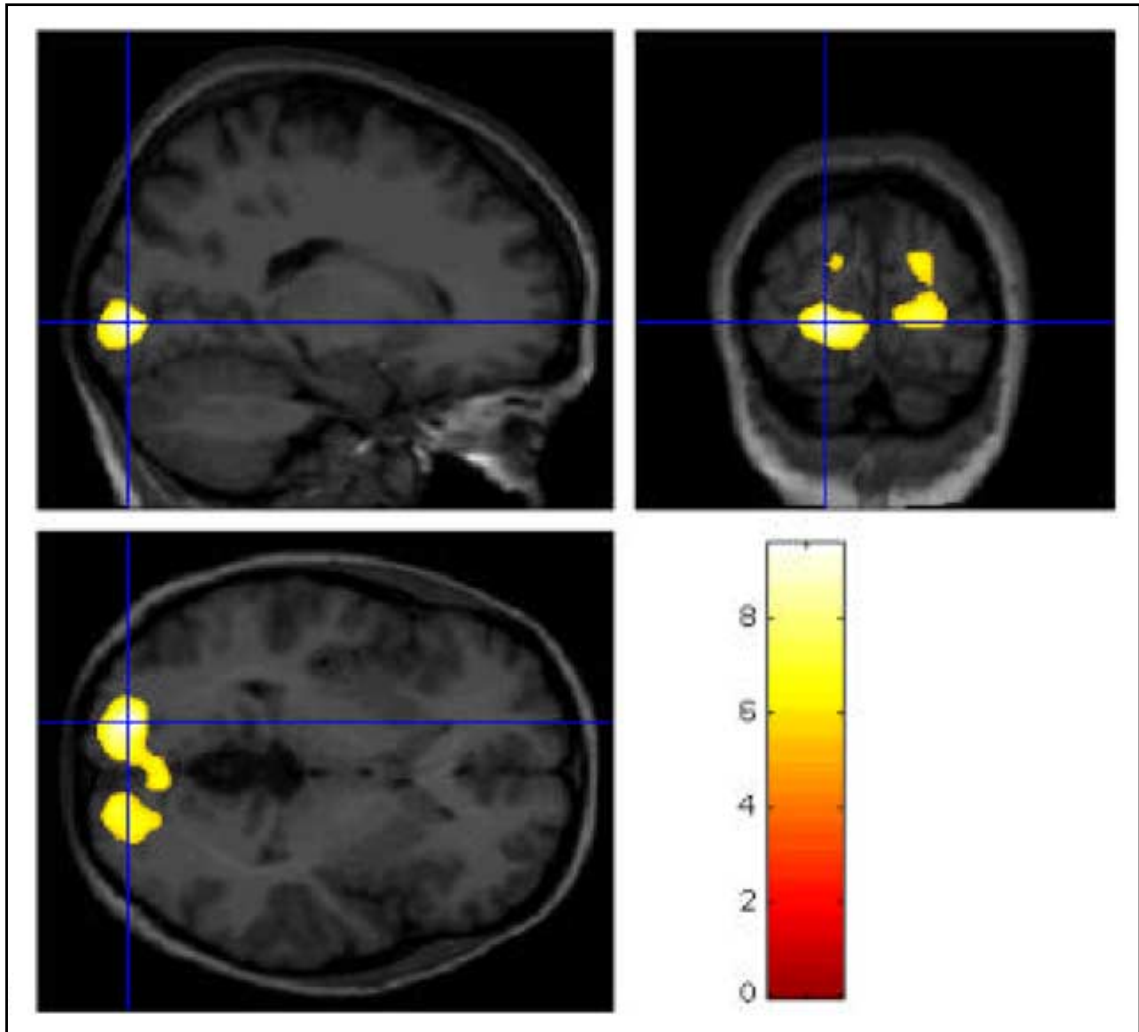


Figure 1.16: Sagittal, coronal and parasagittal MRI slices from a normalised control subject overlaid by an statistical parametric mapping (SPM) region from a voxel-based morphometry (VBM) analysis of 24 aniridia subjects against 72 controls (taken from Free et al. 2003).¹⁶³

The SPM data from the aniridia subjects have been overlaid on a normalised control subject. There is a reduction in grey matter concentration in the occipital lobes of aniridia subjects in comparison to controls.

MRI = magnetic resonance imaging; SPM = statistical parametric mapping; VBM = voxel-based morphometry

1.33. Retinal Dystrophies

OCT has also been used to characterise morphological features of retinal dystrophies. Lim et al.¹³² performed a pilot study with fourier-domain OCT of retinal dystrophy patients. Conditions included retinitis pigmentosa (RP), Stargardt disease and cone-rod dystrophy. They found that the macular and foveal outer retinal layers (ORL) was significantly different between the dystrophy and the controls. In patients with RP, ORL thickness profiles showed greatest thinning of the macular ORL versus foveal ORL. This is consistent with the peripheral pattern of field loss in the beginning which then progresses centrally in RP. The opposite occurs in Stargardt disease and cone rod dystrophy with greater thinning of the foveal ORL versus the macular ORL. This is also consistent with the early visual loss that occurs with these conditions. Similar findings in Stargardt disease was reported by Srinivasan et al 2006.¹³¹ The authors also note that the IS/OS is often obliterated in advanced case of retinal dystrophy.

Hood et al.¹³³ examined the extent of the cone contribution to the signal arising from the IS ellipsoid band (ISE band), previously known as the IS/OS border. Both rods and cones have been found to contribute to this band. This band is disrupted or missing in diseases that affect the outer retina and the cone contribution to this band can be extrapolated by examining patients with conditions that affect cone function. These include achromatopsia and cone dystrophy. There is a reduction in the intensity of the band in patients affected by these conditions when compared to healthy controls.

The prevalence of non-syndromic retinitis pigmentosa (RP) which is typically described as a rod-cone dystrophy (RCD) and cone-rod dystrophies (CRDs) are approximately 1/4,000¹⁶⁵ and 1/40,000¹⁶⁶, respectively. Both rod-cone dystrophies, including autosomal dominant retinitis pigmentosa (ADRP),^{131, 135} X-linked retinitis pigmentosa, RP-Recessive PDE 6B null mutation, Usher's syndrome,¹³⁶ Leber's congenital amaurosis¹³⁷ and cone or cone-rod dystrophies, including Stargardt disease,^{131, 132} progressive cone dystrophy,^{133, 134} cone dystrophy with supernormal rod electroretinogram have a number of features in common on OCT. These include:

1. Abnormal inner and outer retinal lamination
2. ONL thinning, disruption
3. Loss of the IS/OS junction
4. RPE complex abnormalities.

The presence of additional inner retinal layers corresponding to foveal hypoplasia has not been described in the retinal dystrophies.

1.34. Idiopathic Infantile Nystagmus

Clinical characteristics of idiopathic infantile nystagmus (IIN) include onset before 3 months of age, reduction in amplitude with age, increase in intensity with fixation, decrease in intensity on convergence and reduction of intensity in a certain direction of gaze (null zone). It is usually horizontal and conjugate.¹⁶⁷ Familial IIN is most commonly inherited in an X-linked mode caused by mutations on the *FRMD7* gene.¹⁶⁸ This gene plays a role in normal neuronal development. In addition it can be inherited in an autosomal dominant fashion with causative mutations found on chromosome 6p12 (*NYS2*), 7p11 (*NYS3*) and 13q (*NYS4*).¹⁶⁹⁻¹⁷¹

In comparison to this manifest latent nystagmus is typically associated with an infantile squint syndrome. It is horizontal and increases on monocular occlusion. The fast phase beats towards the fixing eye.¹⁷² Normal foveal morphology has been described in IIN and in manifest latent nystagmus (fusion maldevelopment syndrome).¹²⁴ Recently, preliminary reports have also described some individuals with *FRMD7* mutation that have foveal hypoplasia.¹⁷³

Measurements of the OS have been correlated with visual acuity in albinism. It is possible that measurements of the OS or other retinal layers may predict visual acuity in children. In this thesis, we will aim to correlate retinal layer thickness measurements with visual acuity in infants and young children.

1.4. Development of Visual Acuity in Infants

To date, there has been a paucity of work correlating the structural changes that occur during the course of normal foveal development with the increase in visual acuity that occurs as part of normal visual maturation in children. There are 3 main changes that are associated with improvement in visual acuity:¹⁷⁴

1. Development of the fovea
2. Myelination of the optic tract
3. Changes in the dorsal lateral geniculate nucleus and striate cortex

The histological development of the fovea has been described in detail (see section 1.1: What is known about foveal development).

Simultaneously with foveal development, myelination of the optic tract proceeds centrifugally towards the optic nerve.¹⁷⁵ Myelin is found in the optic tract at 32 weeks gestation and reaches the orbital section of the optic nerve at term. Myelination continues rapidly for the first two years of life and then more gradually afterwards.

In the dorsal lateral geniculate nucleus adult appearances of the parvocellular layers are reached by 12 months. The magnocellular layers reach adult appearances by 2 years.¹⁷⁶ The striate cortex has an initial increase in the population of spines and synaptic density for the first 8 months. Subsequently both the population of spines and synaptic density decrease, reaching adult levels by age eleven.¹⁷⁷

Grating acuity measured using preferential looking (PL) increases rapidly in the first 36 months of life. Mean monocular acuity has been consistently shown to increase from 0.5-1 cycles/degree to 25 cycles/degree from 4 weeks to 36 weeks of age. After this rapid increase there is a slower increase until 3 years of age.^{178, 179} In several studies, adult acuity levels (32 cycles/degree) are not reached until the age of five years.

179-181

In grating acuities an octave represents a doubling or halving of spatial frequency. There are discrepancies in the mean acuity values for different age groups ranging from 2.1 octaves to 3.3 octaves in the first year of life and from 1.1 octaves to 2.0 octaves in the older age groups.^{174, 179, 182} A 2 octave spread limits the clinical

application of this method. Testing interocular acuity differences (IAD) is a more specific indicator of a monocular acuity deficit. 95% of subjects have an IAD of less than or equal to one octave. An IAD of more than 0.5 octaves is abnormal.¹⁸³

Adult acuities are reached by 7 months if measured by pattern reversal visual evoked potentials (VEP) and by 8 months if measured by a sweep VEP technique.¹⁸⁴ VEP estimates are higher than PL acuity and appear to differ by as much as two to three octaves. This may be due to a number of factors:

1. Preferential looking (PL) vision is measured by looking at eye movements of the child and therefore demands active reaction of the child, requiring 70% correct responses in ensure that any positive responses that are obtained have not occurred by chance (See section 2.12: Assessment of Visual Acuity).
2. VEP stimuli measures foveal function, (which is normally responsible for fine detailed vision), while PL stimuli may stimulate extra-foveal regions (which are responsible for more gross navigational peripheral vision).
3. Both methods may provide information regarding different aspects of visual function, with the VEP indicating the level of foveal function and the PL vision indicating the level of extra foveal function.

There has been no previous work relating the normal age-related increase in visual acuity in infants and young children with retinal maturation. In this thesis, we will explore if there are any correlations between retinal development and visual maturation.

1.5. Research Aims

1.51. General Context of Research Aims

We have established that foveal development is a dynamic and complex process in which several hypothesis exist with regards to the mechanism underlying normal foveal development. This may be due to biochemical factors such as targeted expression of growth factors and guidance molecules, or mechanical factors such as the interaction of intraocular pressure and growth induced retinal stretch on the more elastic foveal avascular zone, or a combination of all of these. The exact role of each of these mechanisms remain to be clarified.

The time course of foveal development is also controversial, with the age at which this is thought to be completed varying from as young as 11 months to as old as five years. The development of visual acuity has yet to be correlated with the structural changes that occur as the fovea matures. This is due to several limiting factors such as the limits of histological examination, the relative paucity of human retinal specimens and generally small study numbers.

The advent of high speed HH-SDOCT now allows us to perform non-invasive detailed examination of the developing human fovea in vivo. Previous OCT studies in infants with ROP have established the value of examining pathological conditions for clues as to the mechanisms behind normal foveal development. Infantile nystagmus is an ideal condition in which abnormal foveal development can be studied, as it has several aetiologies in which foveal hypoplasia may occur, possibly via different mechanisms. In fact, it was in adults with a diagnosis of infantile nystagmus from albinism and *PAX6* mutation with typical foveal hypoplasia in whom the first structural visual prognostic indicators were found.¹²⁷ However, although OCT has established its role in the diagnosis of the aetiology of infantile nystagmus in adults, the reliability and the role of the HH-SDOCT in diagnosing infants and young children with nystagmus has yet to be established.

1.52. Research Aims

The aims of this work are:

1. To determine if the Bioptigen™ HH-SDOCT can obtain repeatable and reliable quantitative data in infants and young children both with and without nystagmus.
2. To define the normal pattern and time course of foveal development in infants and young children as measured using the Bioptigen™ HH-SDOCT, quantify the structural changes that are occurring and correlate these with the development of visual acuity.
3. To determine if OCT is a sensitive and specific method in determining the cause of infantile nystagmus in children.
4. To investigate the pattern and time course of foveal development in infants and young children with infantile nystagmus due to:
 - a. Achromatopsia
 - b. Albinism
5. To develop OCT based objective visual prognostic indicators in infants and young children both with and without nystagmus.

1.53. Outline of Chapters

A general overview of the methodology that was used to explore the research aims outlined above is provided in Chapter 2: “General Methods”. A more detailed description with regards to the specific methodology applied to each research aim are provided in the relevant chapter. Each chapter will commence with a brief overview of the research question, followed by methods, results and discussion/conclusion.

- **Aim 1** will be addressed in Chapter 3: “Is Hand-Held Optical Coherence Tomography Reliable in Infants and Young Children with and Without Nystagmus?”
- **Aims 2 & 5** will be addressed in Chapter 4: “Normal Foveal Development: An In Vivo Study using Optical Coherence Tomography”
- **Aim 3** will be addressed in Chapter 5: “Potential of Hand-Held Optical Coherence Tomography to Determine Aetiology of Infantile Nystagmus in Children based on Foveal Morphology”
- **Aim 4a** will be addressed in Chapter 6: “Retinal Development and Morphology in Achromatopsia”
- **Aims 4b & 5** will be addressed in Chapter 7: Retinal Development and Morphology in Albinism”

Chapter 8 will summarise the results of this thesis and discuss their overall implications.

Chapter 2

General Methods

2.1. Subjects and Clinical Examination

2.2. Optimisation of the Examination Environment

2.3. OCT Acquisition

2.4. OCT Segmentation and Analysis

2.1. Subjects and Clinical Examination

Foveal structures in healthy children and children with nystagmus were investigated over a period of 3 years using a mixed cross-sectional and longitudinal study design. We aimed to perform 3 repeated OCT measurements at different time points in 40 to 60 control subjects and 80 to 100 patients with infantile nystagmus of various aetiologies.

We aimed to obtain a minimum of 10 examinations from control participants and participants with nystagmus for each of the following age bands: 0-2 months; 3-5 months; 6-8 months; 9-11 months; 12-17 months; 18-23 months; 24-29 months; 30-35 months; 3rd year of life; 4th year of life; 5th year of life and 6th year of life. This would give a total of 120 examinations in each group. In addition, we planned to perform OCT examinations in a control group of 15 young adults (aged 18-27 years) as a comparison.

Healthy control participants and participants with nystagmus were recruited from outpatient clinics, wards and GP practices within the University Hospitals of Leicester NHS Trust and databases using a similar study design as in control subjects. We anticipated from preliminary work and our databases that half of the children with nystagmus would have albinism. At the time of submission of this thesis the following OCT examinations had been obtained:

- 534 mixed cross sectional and longitudinal OCT scans from 261 control participants
- 414 mixed cross sectional and longitudinal OCT scans from 101 patients with nystagmus including:
 - i. 219 OCT scans from 44 children with a diagnosis of albinism
 - ii. 41 OCT scans from 8 children with a diagnosis of achromatopsia
 - iii. 113 OCT scans from 37 children with a diagnosis of idiopathic infantile nystagmus
 - iv. 41 scans from 12 children with a diagnosis of retinal dystrophy

2.11. Power Calculation

As the cone outer segment length is the strongest predictor of VA in albinism,¹²⁸ the power calculation was based on identifying changes in OS length. In a previous study we have observed mean (\pm SD) OS lengths of 47.4 μ m (\pm 4.8 μ m) in controls and 33.4 μ m (\pm 6.6 μ m) in albinos. Based on these measurements, we calculated that a sample size of n=10 in each of the age bands outlined above will be sufficient to identify a difference in OS length of approximately 13% in healthy controls and 25% in albinos in comparison to older children and young adults (where α =0.05 and power = 90%). Data from histological studies^{36, 37} indicate that this is sufficiently powerful to demonstrate a significant difference in OS length in healthy controls between 15 months and 45 months of age and also between 45 months of age and adulthood.

All patients underwent ophthalmologic examination, which included slit-lamp examination where possible, determination of presence or absence of iris transillumination (TID) defects (also in parents if possible, as carriers of albinism frequently have iris transillumination^{185, 186}), presence and type of nystagmus, fundus examination and measurement of visual acuity. Visual acuity (VA) was assessed in younger infants and children by preferential looking using Teller acuity cards and/or crowded logMAR Kay Picture Tests if possible. In cooperative children, logMAR crowded optotypes (Glasgow Acuity Cards) were used to obtain VA. Electroretinograms (ERGs) and 5-channel VEPs (to detect increased optic nerve crossing in albinism) according to International Society for Clinical Electrophysiology of Vision (ISCEV) standards were obtained if possible.¹⁸⁷

- Albinism was diagnosed by the presence of crossed asymmetry on VEPs and clinical signs such as iris transillumination, fundus appearance, hair and skin pigmentation and/or genetic testing.
- Suspicion of *PAX6* associated disease was derived from iris abnormalities, atypical nystagmus with vertical component, dominant inheritance pattern in the family, normal VEP examination and/or genetic testing.
- Achromatopsia was diagnosed by extinguished or severely reduced photopic electroretinograms, photophobia, and typical small fast nystagmus Genetic testing for

all known achromatopsia gene mutations was also carried out in collaboration with Dr Susanne Kohl at the University of Tübingen.

- Rod-cone and cone-rod dystrophy were diagnosed based on clinical history, fundus examination and ERG findings.
- Idiopathic nystagmus was diagnosed with typical horizontal conjugate nystagmus which did not change upon covering one eye, if no abnormality other than nystagmus and squint was found and/or electrophysiology was within normal limits. Genetic testing for mutations in *FRMD7* was offered in all suspected cases of IIN.
- Manifest latent nystagmus was diagnosed if children had congenital squint syndrome, typical nystagmus which increased upon covering one eye and beating in the direction of the open or fixing eye and normal slit lamp and fundus examination.

The study adhered to the tenets of the Declaration of Helsinki and was approved by the Leicestershire, Northamptonshire & Rutland Research ethics committee. Informed consent was obtained from all parents/guardians of patients and control subjects participating in this study. Assent was obtained from all children that were capable of understanding this study. This applies to all subsequent work /studies described in this thesis.

2.12. Assessment of Teller Visual Acuity

Monocular occlusion was achieved with an adhesive eye patch. Older subjects who objected to the patch used a trial lens frame with an occlusive lens placed in front of one eye. Monocular acuity estimates were obtained with a two up and one down short staircase procedure.¹⁸³ Briefly in this procedure, the examiner who is initially masked to the grating position presents the card to the infant and judges the position of the gratings based on the response of the infant. If it is correct, the examiner rotates the card 180 degrees and represents it. If a second correct response was obtained, then the examiner proceeded to the next octave (i.e. a two card ascension), until an error occurs on either presentation. when an error occurred the examiner descended half an octave (i.e. a single card) and further trials are carried out in half octave steps until a positive score is obtained that is well above chance. Previously presented cards could be shown again as necessary in any order, at the discretion of the examiner. In terms of false positives, an acuity value lower than 95% prediction limit would be expected to occur in only 2.5% of children with normal eyes.¹⁸⁸ The cards were held vertically for children who had horizontal nystagmus.

2.2. Optimisation of the Examination Environment

The importance of a child friendly environment in maximising cooperation from infants and young children was highlighted. Lambert et al. 2013¹⁸⁹ performed an exploratory analysis of young children's (aged five to eight years) perspectives of what constitutes an ideal design for hospital built environments using an arts based participatory technique and semi-structured interviews. Three themes emerged from this work:

1. Personal space: Children valued having room space, privacy, noise control and control over lighting
2. Physical environment: The creative use of space, imaginative decoration and the use of naturalistic images to decorate their rooms was emphasised.
3. Access: It is important the environment is child and family friendly, with a sense of space that is smooth-flowing and is easy to navigate. The use of information and communications technology was also suggested.

Therefore the OCT was placed in a spacious room that would allow examinations in private, and allowed for the adjustment of lighting levels for the child's comfort. The room was decorated with images from familiar children's entertainment and television programs (Figure 2.1). Toys and children's reading materials were also readily available in the room. When possible, the children were familiarised with the OCT scanner and the room environment in advance.

In order to keep the children calm and cooperative for the OCT examination, a variety of techniques were employed. OCT scanning of young infants were most often successful when acquired while bottle or breast feeding. Older children responded well to age appropriate animated fixation targets that were employed using a portable laptop computer.

A



B



Figure 2.1: Example of the environment used for optical coherence tomography (OCT) acquisition and the acquisition of an OCT scan in a child with nystagmus.

- (A) The scan environment has been altered to make it more comfortable and less intimidating for children. Images from familiar children's entertainment programs have been placed on the surrounding walls, together with colourful fixation targets and toys.*
- (B) The optics of the scanner is contained within the hand piece, which is held in front of the eye being scanned. The information acquired is displayed and stored on the connected computer. The surrounding walls have being decorated with images from familiar children's entertainment media.*

2.3. OCT Acquisition

All OCTs were acquired using the Bioptigen™ hand held OCT which uses a wavelength of 840 nm and has a digital axial resolution of 2.4 μm per pixel. The position of the reference arm (Figure 2.2) was adjusted as previously described by Maldonado et al.⁸⁶ based on the age of the child prior to performing the OCT scan. At the start of imaging we checked for any OCT clipping (Figure 1.6).

Normally an OCT scan is obtained by pivoting the OCT beam in the plane of the iris. Clipping of the OCT scans occurs when the peripheral aspects of the tomogram are obstructed by the edge of the iris. This occurs in infants and young children because the axial length of the infant eye is smaller than in adults, resulting in anterior displacement of the pivoting position of the OCT beam. Therefore, the reference arm position of the HH-SDOCT needs to be altered in infants and young children to prevent clipping of the images.

If clipping was still observed after the reference arm position was adjusted for the age of the child, the scan response to a slight manual lateral movement of the hand-held probe was observed. If the reference arm position was too short, the clipping shadow moved in the same direction as the lateral probe movement and the reference arm position was increased. If it was too long, the shadow moved in the opposite direction to the probe movement and the reference arm position was shortened.



Figure 2.2: The reference arm (black circle) on the hand-held OCT is adjusted to be shorter or longer depending on the amount of clipping observed on the imaging.

2.31. OCT Scan Protocol

A 3-dimensional volumetric scan protocol to image both the fovea and optic nerve in one scan was selected. We found that the scan length should be ideally 10 mm to encompass the optic nerve and fovea in a single scan. This lengthens the time of acquisition so the vertical diameter was reduced to 5 mm to compensate. A scan protocol using a 6 mm x 6 mm framework makes the acquisition speed faster but sacrifices optic nerve detail. The angles, horizontal and vertical offsets were not altered. The A-scan/B-scan ratio should ideally be 1000, but by reducing this ratio, an increased speed of acquisition can be attained. The number of B-scans, frames/B-scan and inactive A-scans/B scans were not altered as it was anticipated that averaging would be very difficult as repeatedly scanning the same area may not be possible in patients with nystagmus. Five scan settings were set up in this protocol to balance speed in uncooperative patients with more detail in cooperative patients.

Table 2.1: Summary of Tested OCT scan protocols.

1. Fast Macula (1s)		
Parameter	Typical Setting	Test Settings
(Azimuth) Length	0.5-12 mm	6 mm
Width	0.5-12 mm	6 mm
Angle	0°-360°	0°
Horizontal Offset	0 mm	0 mm
Vertical Offset	0 mm	0 mm
Number of A-scans	200-5000 A-scans	600 A-scans
Number of B-scans	2-400 B-scans	60 B-scans
Frames/B-scan	1-10	1
Volumes	1-4	1
Inactive A-scans/B-scan	100-1024	N/A

2. Standard OCT with Optic Nerve		
Parameter	Typical Setting	Test Settings
(Azimuth) Length	0.5-12 mm	10 mm
Width	0.5-12 mm	5 mm
Angle	0°-360°	0°
Horizontal Offset	0 mm	0 mm
Vertical Offset	0 mm	0 mm
Number of A-scans	200-5000 A-scans	1000 A-scans
Number of B-scans	2-400 B-scans	100 B-scans
Frames/B-scan	1-10	1
Volumes	1-4	1
Inactive A-scans/B-scan	100-1024	N/A

3. Standard OCT		
Parameter	Typical Setting	Test Settings
(Azimuth) Length	0.5-12 mm	6 mm
Width	0.5-12 mm	6 mm
Angle	0°-360°	0°
Horizontal Offset	0 mm	0 mm
Vertical Offset	0 mm	0 mm
Number of A-scans	200-5000 A-scans	1000 A-scans
Number of B-scans	2-400 B-scans	100 B-scans
Frames/B-scan	1-10	1
Volumes	1-4	1
Inactive A-scans/B-scan	100-1024	N/A

4. Three-Dimensional (3-D) OCT		
Parameter	Typical Setting	Test Settings
(Azimuth) Length	0.5-12 mm	6 mm
Width	0.5-12 mm	6 mm
Angle	0°-360°	0°
Horizontal Offset	0 mm	0 mm
Vertical Offset	0 mm	0 mm
Number of A-scans	200-5000 A-scans	350 A-scans
Number of B-scans	2-400 B-scans	350 B-scans
Frames/B-scan	1-10	1
Volumes	1-4	1
Inactive A-scans/B-scan	100-1024	N/A

5. Fast Macula & Optic Nerve		
Parameter	Typical Setting	Test Settings
(Azimuth) Length	0.5-12 mm	10 mm
Width	0.5-12 mm	5 mm
Angle	0°-360°	0°
Horizontal Offset	0 mm	0 mm
Vertical Offset	0 mm	0 mm
Number of A-scans	200-5000 A-scans	500 A-scans
Number of B-scans	2-400 B-scans	100 B-scans
Frames/B-scan	1-10	1
Volumes	1-4	1
Inactive A-scans/B-scan	100-1024	N/A

After initial testing with the above protocols, it was clear that the most successful scan in terms of obtaining satisfactory image quality as well as speed was the fast macula and optic nerve scan protocol. Only this scan setting was used in the final imaging protocols for this study, with the aim of obtaining 3 repeatable scans on both eyes of each participant. With the limited cooperation and attention span of the paediatric patient, often only one good quality scan from each eye was possible to obtain.

2.4. OCT Segmentation and Analysis

The image files were exported as OCT files which could be opened by ImageJ software and subsequently converted to tiffs. There are extensive movement artefacts associated with the volumetric scans obtained with the OCT which makes reliable volumetric analysis extremely difficult. Therefore the individual B-scans that captured the central fovea were used when segmenting the individual retinal layers. Figure 5.3 (p 153) illustrates the type of movement artefacts that occur when imaging infants and young children with nystagmus.

A correction was applied to convert the ImageJ output from pixels to micrometers, based on the digital resolution of the system. Information obtained from Bioptigen™ indicated this correction is 2.4 µm per pixel. This correction is determined by the imaging depth of the system (3.4 mm), the number of pixels per line (1024 pixels) and the refractive index of the eye ($n = 1.38$).

In addition, we have to correct for the phenomenon of lateral magnification when analysing the OCT images. Variations in the optical system of the eye affect the magnification of retinal images. An inversely proportional relationship between the axial length of the eye and retinal image size has been described in time-domain OCT images.¹⁹⁰ As infants have a much shorter eye length in comparison to adults, this relationship is even more exaggerated. In order to calculate the correct scan length on the retina (SLOR), we used the following formula:

$$\text{SLOR} = (\text{Infant Eye Axial Length} / \text{Standard Adult Axial Length}) \times \text{System Scan Length}$$

This is best illustrated using an example showing how we analysed a point set at 1.0 mm from the fovea in a neonate and follow the changes at this point over time till adulthood (using a scan length of 10.0 mm throughout all examinations). When analysing the neonatal scan we would first need to calculate SLOR as above (assuming an axial length of 16.8 mm in the neonate and an axial length of 24.0 mm in the adult):

$$(16.8 \text{ mm} / 24.0 \text{ mm}) \times 10.0 \text{ mm} = 7.0 \text{ mm}$$

A 7.0 mm scan in this neonate is equivalent to a 10.0 mm scan in an adult due to lateral magnification.

Two customised ImageJ macros were used to segment the individual retinal layers. The first macro segmented the 10 retinal layers by placing a series of points at the fovea and at 1mm and 2mm nasal and temporal to the fovea (Figure 3.1). The X and Y coordinates of these points were subsequently exported as a text file and imported into Microsoft™ Excel where the measurements for each of the retinal layers at each of these locations were calculated. A second macro developed later on into the study, flattens the foveal B-scan, and segments each retinal layer in its entirety, by selecting multiple points on each retinal layer border, which are subsequently connected, and a curved line fitted using the ABSnake plugin (Figure 2.3) (available at: http://imagejdocu.tudor.lu/doku.php?id=plugin:segmentation:active_contour:start). The position of this line was then manually refined through adjustments of the position of selected points on this line where necessary. The X and Y coordinates of each pixel of the final segmented borders of each layer were exported as a text file (Figure 2.4), and imported into excel where the measurements of each layer were calculated. Statistical analysis was performed with SPSS™ software version 16.0 (SPSS™, Inc., Chicago, IL) and STATA™ software (Copyright 1996-2014, StataCorp). All analyses were considered significant at a probability value of $p < 0.05$.

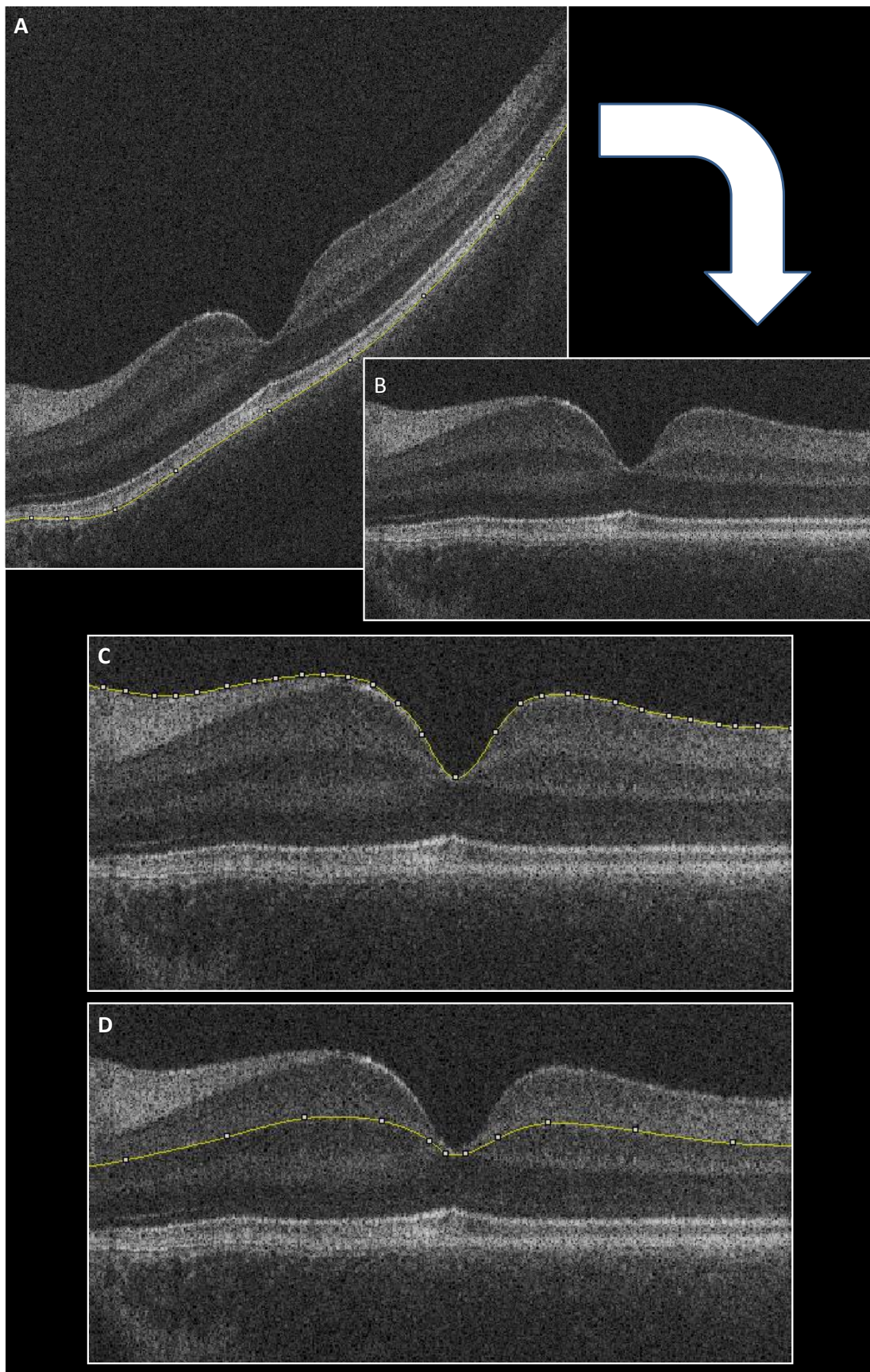


Figure 2.3: Example of the flattening and segmentation process for a single central foveal B-scan using the Bioptigen Manual Layers Program Fovea beta v2.

A series of points is placed along the bottom of the retinal pigment epithelium in the unprocessed B scan (A), which are subsequently joined and fitted with a spline using the ABSnake plug in. The entire scan is flattened relative to the RPE (B). This process is repeated for each border between each retinal layer. In this example the segmented ILM (C) and the segmented border between the IPL and INL (D) are shown.

RPE = retinal pigment epithelium; ILM = inner limiting membrane; IPL = inner plexiform layer; INL = inner nuclear layer

PATIENT PARAMETERS																	
Patient X OS2_L																	
gestational age (weeks) 226.11																	
axial length (mm) 19.27 ESTIMATED																	
correction factor 0.80																	
SCAN PARAMETERS																	
no Ascans 500																	
image width 10.0000																	
analysed image width 300																	
pixel height 2.4000																	
pixel width 16.0739																	
CUP PARAMETERS																	
foveal thickness (mm) 203																	
LAYERS																	
x_pixel	foveal	centre	ILM	RNFL	GCL	IPL	INL	OPL	ELM	ISOS	COST	ROST	upper RPE	RPE/Bruch's	CHOROID	upper EDEMA	lower EDE
-146.19	1	118.27	94.86	85.12	71.85	58.75	47.26	24.64	14.25	-7777.00	-7777.00	-7777.00	6.46	0.00	-7777.00	-7777.00	-7777.00
-145.19	1	118.63	95.06	85.31	71.87	58.74	47.29	24.64	14.31	-7777.00	-7777.00	-7777.00	6.51	0.00	-7777.00	-7777.00	-7777.00
-144.19	1	118.92	95.28	85.50	71.90	58.74	47.31	24.64	14.37	-7777.00	-7777.00	-7777.00	6.57	0.00	-7777.00	-7777.00	-7777.00
-143.19	1	119.19	95.50	85.68	71.92	58.74	47.34	24.65	14.43	-7777.00	-7777.00	-7777.00	6.62	0.00	-7777.00	-7777.00	-7777.00
-142.19	1	119.41	95.73	85.86	71.95	58.73	47.37	24.65	14.49	-7777.00	-7777.00	-7777.00	6.67	0.00	-7777.00	-7777.00	-7777.00
-141.19	1	119.61	95.97	86.05	71.98	58.72	47.39	24.65	14.55	-7777.00	-7777.00	-7777.00	6.71	0.00	-7777.00	-7777.00	-7777.00
-140.19	1	119.78	96.22	86.23	72.01	58.72	47.42	24.65	14.61	-7777.00	-7777.00	-7777.00	6.76	0.00	-7777.00	-7777.00	-7777.00
-139.19	1	119.93	96.48	86.41	72.05	58.71	47.44	24.65	14.66	-7777.00	-7777.00	-7777.00	6.81	0.00	-7777.00	-7777.00	-7777.00
-138.19	1	120.06	96.75	86.59	72.08	58.70	47.46	24.65	14.72	-7777.00	-7777.00	-7777.00	6.86	0.00	-7777.00	-7777.00	-7777.00
-137.19	1	120.17	97.03	86.76	72.12	58.69	47.49	24.65	14.77	-7777.00	-7777.00	-7777.00	6.90	0.00	-7777.00	-7777.00	-7777.00
-136.19	1	120.27	97.32	86.94	72.16	58.68	47.51	24.65	14.82	-7777.00	-7777.00	-7777.00	6.94	0.00	-7777.00	-7777.00	-7777.00
-135.19	1	120.36	97.63	87.11	72.20	58.67	47.53	24.65	14.87	-7777.00	-7777.00	-7777.00	6.99	0.00	-7777.00	-7777.00	-7777.00
-134.19	1	120.45	97.94	87.29	72.24	58.66	47.55	24.66	14.92	-7777.00	-7777.00	-7777.00	7.03	0.00	-7777.00	-7777.00	-7777.00
-133.19	1	120.54	98.27	87.46	72.29	58.65	47.57	24.66	14.97	-7777.00	-7777.00	-7777.00	7.07	0.00	-7777.00	-7777.00	-7777.00
-132.19	1	120.62	98.61	87.63	72.34	58.63	47.58	24.66	15.02	-7777.00	-7777.00	-7777.00	7.11	0.00	-7777.00	-7777.00	-7777.00
-131.19	1	120.72	98.96	87.80	72.39	58.62	47.60	24.66	15.07	-7777.00	-7777.00	-7777.00	7.15	0.00	-7777.00	-7777.00	-7777.00
-130.19	1	120.81	99.31	87.97	72.45	58.61	47.62	24.66	15.11	-7777.00	-7777.00	-7777.00	7.18	0.00	-7777.00	-7777.00	-7777.00
-129.19	1	120.92	99.68	88.13	72.50	58.60	47.63	24.66	15.16	-7777.00	-7777.00	-7777.00	7.22	0.00	-7777.00	-7777.00	-7777.00
-128.19	1	121.03	100.05	88.30	72.57	58.58	47.64	24.66	15.20	-7777.00	-7777.00	-7777.00	7.25	0.00	-7777.00	-7777.00	-7777.00
-127.19	1	121.15	100.44	88.46	72.63	58.57	47.65	24.66	15.24	-7777.00	-7777.00	-7777.00	7.28	0.00	-7777.00	-7777.00	-7777.00
-126.19	1	121.27	100.83	88.62	72.70	58.55	47.66	24.66	15.28	-7777.00	-7777.00	-7777.00	7.32	0.00	-7777.00	-7777.00	-7777.00
-125.19	1	121.39	101.23	88.78	72.77	58.54	47.67	24.66	15.31	-7777.00	-7777.00	-7777.00	7.35	0.00	-7777.00	-7777.00	-7777.00
-124.19	1	121.52	101.63	88.94	72.85	58.53	47.68	24.66	15.35	-7777.00	-7777.00	-7777.00	7.37	0.00	-7777.00	-7777.00	-7777.00
-123.19	1	121.66	102.04	89.10	72.93	58.51	47.68	24.66	15.38	-7777.00	-7777.00	-7777.00	7.40	0.00	-7777.00	-7777.00	-7777.00
-122.19	1	121.79	102.45	89.25	73.01	58.50	47.69	24.67	15.41	-7777.00	-7777.00	-7777.00	7.43	0.00	-7777.00	-7777.00	-7777.00
-121.19	1	121.93	102.87	89.41	73.10	58.48	47.69	24.67	15.44	-7777.00	-7777.00	-7777.00	7.45	0.00	-7777.00	-7777.00	-7777.00
-120.19	1	122.07	103.29	89.56	73.20	58.47	47.69	24.67	15.47	-7777.00	-7777.00	-7777.00	7.48	0.00	-7777.00	-7777.00	-7777.00
-119.19	1	122.21	103.72	89.70	73.30	58.45	47.69	24.67	15.49	-7777.00	-7777.00	-7777.00	7.50	0.00	-7777.00	-7777.00	-7777.00
-118.19	1	122.35	104.15	89.85	73.40	58.43	47.69	24.67	15.52	-7777.00	-7777.00	-7777.00	7.52	0.00	-7777.00	-7777.00	-7777.00
-117.19	1	122.49	104.58	89.99	73.51	58.42	47.68	24.67	15.54	-7777.00	-7777.00	-7777.00	7.53	0.00	-7777.00	-7777.00	-7777.00
-116.19	1	122.62	105.01	90.13	73.63	58.40	47.67	24.67	15.56	-7777.00	-7777.00	-7777.00	7.55	0.00	-7777.00	-7777.00	-7777.00
-115.19	1	122.75	105.44	90.27	73.74	58.39	47.67	24.67	15.57	-7777.00	-7777.00	-7777.00	7.57	0.00	-7777.00	-7777.00	-7777.00
-114.19	1	122.88	105.88	90.41	73.87	58.37	47.65	24.67	15.59	-7777.00	-7777.00	-7777.00	7.58	0.00	-7777.00	-7777.00	-7777.00
-113.19	1	123.01	106.32	90.54	74.00	58.36	47.64	24.67	15.60	-7777.00	-7777.00	-7777.00	7.59	0.00	-7777.00	-7777.00	-7777.00
-112.19	1	123.14	106.75	90.67	74.14	58.34	47.62	24.67	15.61	-7777.00	-7777.00	-7777.00	7.60	0.00	-7777.00	-7777.00	-7777.00
-111.19	1	123.26	107.19	90.79	74.28	58.32	47.60	24.67	15.62	-7777.00	-7777.00	-7777.00	7.61	0.00	-7777.00	-7777.00	-7777.00
-110.19	1	123.38	107.62	90.92	74.43	58.31	47.58	24.67	15.62	-7777.00	-7777.00	-7777.00	7.62	0.00	-7777.00	-7777.00	-7777.00
-109.19	1	123.50	108.05	91.03	74.58	58.29	47.55	24.67	15.62	-7777.00	-7777.00	-7777.00	7.63	0.00	-7777.00	-7777.00	-7777.00
-108.19	1	123.63	108.49	91.15	74.73	58.27	47.53	24.66	15.62	-7777.00	-7777.00	-7777.00	7.63	0.00	-7777.00	-7777.00	-7777.00
-107.19	1	123.75	108.92	91.26	74.89	58.26	47.50	24.66	15.62	-7777.00	-7777.00	-7777.00	7.64	0.00	-7777.00	-7777.00	-7777.00
-106.19	1	123.87	109.34	91.37	75.05	58.24	47.46	24.66	15.62	-7777.00	-7777.00	-7777.00	7.64	0.00	-7777.00	-7777.00	-7777.00
-105.19	1	123.99	109.77	91.47	75.21	58.23	47.43	24.66	15.61	-7777.00	-7777.00	-7777.00	7.64	0.00	-7777.00	-7777.00	-7777.00
-104.19	1	124.11	110.19	91.57	75.37	58.21	47.39	24.66	15.60	-7777.00	-7777.00	-7777.00	7.64	0.00	-7777.00	-7777.00	-7777.00
-103.19	1	124.24	110.62	91.67	75.53	58.19	47.35	24.66	15.59	-7777.00	-7777.00	-7777.00	7.64	0.00	-7777.00	-7777.00	-7777.00
-102.19	1	124.37	111.04	91.76	75.70	58.18	47.31	24.66	15.58	-7777.00	-7777.00	-7777.00	7.63	0.00	-7777.00	-7777.00	-7777.00
-101.19	1	124.49	111.46	91.85	75.86	58.16	47.26	24.66	15.56	-7777.00	-7777.00	-7777.00	7.63	0.00	-7777.00	-7777.00	-7777.00
-100.19	1	124.62	111.87	91.93	76.02	58.14	47.21	24.66	15.55	-7777.00	-7777.00	-7777.00	7.62	0.00	-7777.00	-7777.00	-7777.00
-99.19	1	124.76	112.29	92.02	76.18	58.13	47.16	24.65	15.53	-7777.00	-7777.00	-7777.00	7.62	0.00	-7777.00	-7777.00	-7777.00
-98.19	1	124.89	112.70	92.09	76.34	58.11	47.11	24.65	15.51	-7777.00	-7777.00	-7777.00	7.61	0.00	-7777.00	-7777.00	-7777.00
-97.19	1	125.03	113.11	92.16	76.50	58.09	47.06	24.65	15.49	-7777.00	-7777.00	-7777.00	7.60	0.00	-7777.00	-7777.00	-7777.00
-96.19	1	125.16	113.51	92.23	76.66	58.08	47.00	24.65	15.47	-7777.00	-7777.00	-7777.00	7.59	0.00	-7777.00	-7777.00	-7777.00
-95.19	1	125.29	113.92	92.30	76.81	58.06	46.95	24.65	15.45	-7777.00	-7777.00	-7777.00	7.58	0.00	-7777.00	-7777.00	-7777.00
-94.19	1	125.44	114.32	92.34	76.96	58.05	46.89	24.64	15.42	-7777.00	-7777.00	-7777.00	7.57	0.00	-7777.00	-7777.00	-7777.00
-93.19	1	125.57	114.71	92.39	77.11	58.03	46.82	24.64	15.40	-7777.00	-7777.00	-7777.00	7.56	0.00	-7777.00	-7777.00	-7777.00

2.5. Difficulties Encountered

1. The acquisition of repeated OCT examinations on infants and young children was often very difficult, due to short attention span and fatigue. This necessitated the incorporation of rest breaks, play time and feeding time into the examination visits. As it was apparent that in some cases it may only be possible to obtain a single OCT scan, we aimed to always scan the right eye first, followed by the left eye in order to maximise longitudinal data collection.
2. A large volume of OCT data was collected (approximately 1 terabyte every 6 months) during the course of this PhD. The management of the secure storage and back up of this data was a particular issue and necessitated documentation of all the OCT examinations obtained in an encrypted Microsoft™ Excel summary document as well as the backing up of the data to the University of Leicester's Research R: drive, which is a restricted access drive with automated backups.
3. The identification of the central foveal B-scan from the volumetric scans that were obtained (Figure 5.3) and subsequent manual segmentation of the 10 individual layers that make up the retina in the large dataset that was obtained in the control participants (total 534 examinations) was extremely time consuming and generated a large number of variables in the final analysis (Figures 2.3 & 3.1). For example, the analysis of the 534 mixed cross sectional and longitudinal examinations that were obtained in the control participants generated 1734 variables in the final analysis, which necessitated the maintenance of several Microsoft™ Excel documents and repeated checks of the data to ensure no errors had occurred during the transfer of the original segmentation results to the final templates for statistical analysis and modelling.
4. Finally modelling this data was complex as it consisted of non-linear growth curves that was unique for each retinal layer which varied depending on the retinal location. In order to describe these complex developmental trajectories, we needed to use a relatively new modelling technique known as fractional polynomial modelling (see section 4.23). In order to compare the developing retinae of controls

and participants with nystagmus, linear mixed models and generalised linear mixed models were used.

Chapter 3

Is Hand-Held Optical Coherence Tomography Reliable in Infants and Young Children with and without Nystagmus?

3.1. Introduction

3.2. Methods

3.3. Results

3.4. Conclusion

3.1. Introduction

In older patients with nystagmus, it has been shown that optical coherence tomography produces reliable retinal measurements and can differentiate albinism, changes in *PAX6* mutation and achromatopsia from idiopathic nystagmus by identifying typical or atypical foveal hypoplasia.^{126, 127, 191}

It has been reported that the images obtained using HH-SDOCT contain movement artefacts caused by the examiner and/or the child.⁹⁸ Also it is unclear if reliable measurements of the retinal layers from the central foveal B-scan can be obtained using the HH-SDOCT in infants and young children with and without nystagmus.

In this study we evaluated the reliability of the HH-SDOCT in assessing foveal morphology, in healthy children and in children with nystagmus (likely to be one of the most difficult pathologies to image), aged between birth and 6 years of age.

3.2. Patients and Methods

The cohort for this study included 49 children with nystagmus (mean age 43.83 months; standard deviation 24.1 months; range 1-82 months) and 48 control participants (mean age 43.02 months; standard deviation 24.7 months; range 0 to 83 months) in which a minimum of two separate successful OCT scans on at least one eye were obtained on the same day. The demographic data and diagnostic breakdown are summarised in Table 3.1.

Table 3.1: Summary of demographic data and diagnostic category of participants.

Category	Age Range (months)	Mean Age (months) (SD)	Gender		Eye Analysed	
			Male	Female	Right	Left
Control n = 48	0 to 83	43.83 (24.69)	n = 25	n = 23	n = 33	n = 15
Albinism n = 27	1 to 82	41.81 (22.93)	n = 17	n = 10	n = 20	n = 7
IIN n = 11	7 to 81	43.82 (28.06)	n = 10	n = 1	n = 6	n = 5
Achromatopsia n = 4	2 to 70	27.25 (30.02)	n = 2	n = 2	n = 1	n = 3
PAX6 mutations n = 3	48 to 76	59.67 (14.57)	n = 2	n = 1	n = 2	n = 1
Retinal Dystrophy n = 3	45 to 77	57.67 (17.01)	n = 2	n = 1	n = 3	-----
Latent Nystagmus n = 1	-----	36	n = 1	-----	n = 1	-----

n = sample size; *IIN* = idiopathic infantile nystagmus; *SD* = standard deviation

HH-SDOCT (Bioptigen™ Envisu system, Durham, NC, USA) was used to obtain a minimum of two separate volumetric scans (consisting of 100 B-scans and 500 A-scans per B-scan) on the same examination day of the foveal region. The acquisition speed for each B-scan was 5.8 milliseconds with an overall scan time of 2.9 seconds. This ensured that any motion artefact caused by nystagmus was minimal. All children were scanned in the outpatient clinic setting without sedation. A total of 166 scans in the nystagmus participants and 164 scans in the healthy controls were obtained. Repeat scans were obtained in at least one eye in all nystagmus subjects ($n = 49$) and all healthy controls ($n = 48$). Acquisition of an OCT scan was considered successful if the B-scan containing the foveal centre was captured together with a minimum of 5 uninterrupted B-scans (i.e. without refixations or blinks on either side of the central foveal B-scan). The retinal vasculature and optic nerve head were used to determine if refixations had taken place during the scan.

The acquired images were exported from the Bioptigen OCT software and imported into ImageJ software (available at: <http://rsbweb.nih.gov/ij/> Date accessed: May 11, 2012) where retinal layer segmentation was performed by manually identifying each layer at the fovea (Figure 3.1A and 3.1B). The fovea was identified by visual inspection of the B-scan images for the presence of a foveal depression, thinning of the inner retinal layers, doming of the outer nuclear layer and lengthening of the photoreceptor outer segments as described by Mohammad et al⁵. Measurements of each retinal layer were only performed if the borders between each adjacent retinal layers were visible. In cases where the border between adjacent retinal layers was not clear a combined measurement of the affected layers was taken (see first section of results).

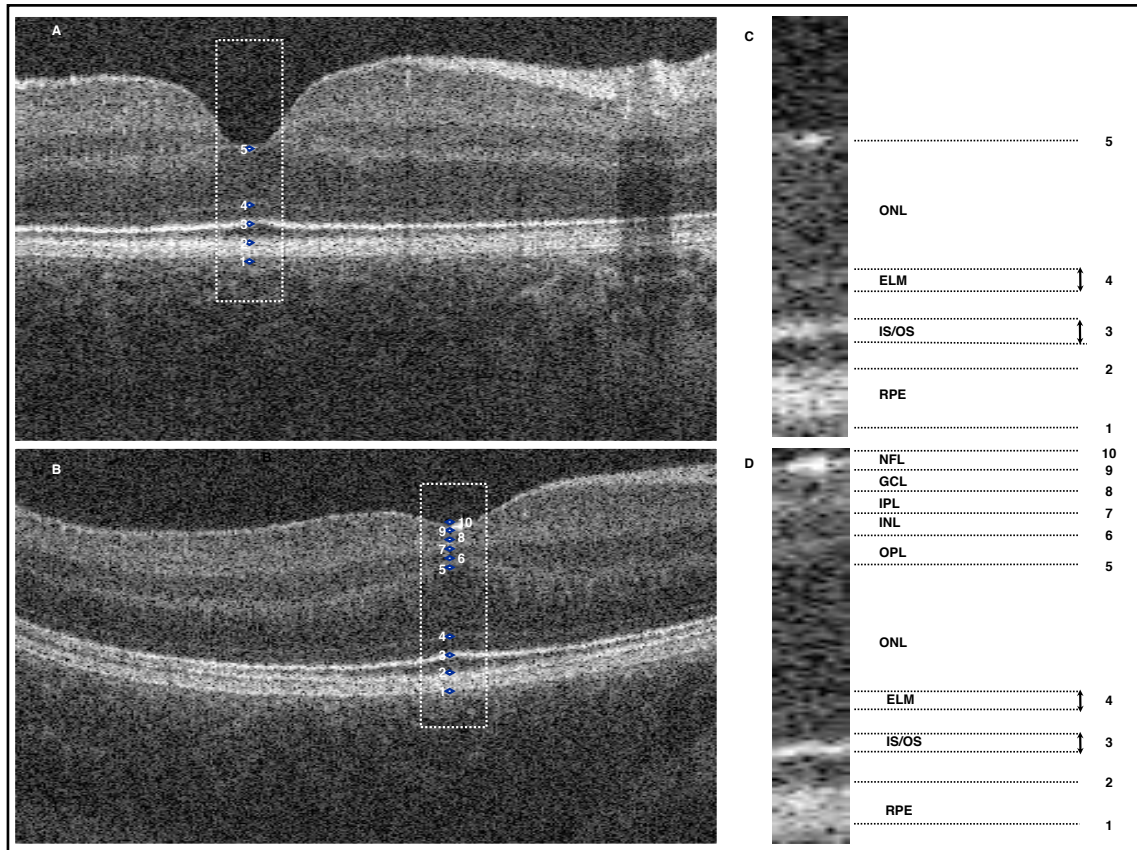


Figure 3.1: Optical coherence tomograms of 1 control subject (3.1A) and 1 nystagmus subject (3.1B) showing how segmentation of the borders of each of the retinal layers was achieved.

Figures 3.1C & 3.1D are magnified sections of the rectangular box areas that are outlined in figures 3.1A and 3.1B respectively. Segmentation of the foveal B scans was performed using ImageJ software which identifies ten points corresponding to the borders delineating each retinal layer (3.1C and 3.1D). These points represented: 1 to 2= RPE; 2 to 3= OS; 3= IS/OS junction; 3 to 4= IS; 4 ELM; 4 to 5= ONL, 5 to 6= OPL; 6 to 7= INL; 7 to 8= IPL; 8 to 9=GCL; 9 to 10= NFL.

NFL= nerve fiber layer; GCL= ganglion cell layer; IPL= inner plexiform layer; INL= inner nuclear layer; OPL= outer plexiform layer; ONL= outer nuclear layer; ELM= external limiting membrane; IS/OS= inner segment/outer segment junction (ellipsoid); RPE= retinal pigment epithelium.

We analysed: (1) the reproducibility of retinal layer measurements between separate scans of each participant; (2) the difference in reliability between scans obtained in children with nystagmus as compared to age-matched controls, and (3) the inter-eye agreement on scans obtained from the same subject. Reproducibility between scans was assessed by determining the intraclass correlation coefficient (ICC) and by Bland–Altman assessment. For the test-retest analysis, if repeat scans were present for both eyes only a single eye (the right eye) was analysed. If two repeated scans were available for only one eye this eye was chosen. A summary of the total number of right and left eyes analysed is provided in Table 3.1. If more than two scans were obtained the two highest quality scans were selected for analysis, with the highest quality scan analysed first so that any bias due to quality of the scan is shown by the test-retest analysis. As there is no automated quality index available for the HH-SDOCT we determined the quality of each scan based on the clarity of the borders of each retinal layer (Tables 3.2 and 3.3). In order to determine if there was a proportional bias present in interpreting higher quality scans as compared to lower quality scans, a linear regression procedure was performed, where we determined if the difference between measures is a function of the average of the measures. An independent-samples t-test was conducted to determine the effects of age on the reliability of the retinal measurements. All analyses were considered significant at a probability value of $p < 0.05$. Statistical analysis was performed with SPSS™ software version 16.0 (SPSS™, Inc., Chicago, IL).

Table 3.2: Reproducibility of first to second scan measurements taken from the same eye of each outer retinal layer in both control and nystagmus groups.

	Control (n=48 for ICC of repeated measures from one eye) (n=45 for ICC of inter-eye comparison)								Nystagmus (n=49 for ICC of repeated measures from one eye) (n=47 for ICC of inter-eye comparison)							
Retinal layer	Clear		Not Clear		Not Visible		Not Present		Clear		Not Clear		Not Visible		Not Present	
	ICC (n)	Inter-Eye (n)	ICC (n)	Inter-Eye (n)	ICC (n)	Inter-Eye (n)	ICC (n)	Inter-Eye (n)	ICC (n)	Inter-Eye (n)	ICC (n)	Inter-Eye (n)	ICC (n)	Inter-Eye (n)	ICC (n)	Inter-Eye (n)
CMT	0.960 (47)	0.947 (44)	— (1)	— (1)	— (0)	— (0)	— (0)	— (0)	0.966 (42)	0.987 (40)	0.982 (6)	0.341 (7)	— (1)	— (0)	— (0)	— (0)
ONL	0.887 (31)	0.820 (19)	0.928 (16)	0.808 (24)	— (1)	— (1)	— (0)	— (1)	0.932 (22)	0.877 (12)	0.858 (25)	873 (32)	— (2)	— (3)	— (0)	— (0)
IS	0.557 (33)	0.517 (25)	0.367 (12)	0.704 (17)	— (3)	— (3)	— (0)	— (0)	0.626 (20)	0.583 (12)	0.289 (18)	0.699 (22)	— (6)	— (8)	— (5)	— (5)
ONL and IS	0.931 (46)	0.897 (44)	— (2)	— (1)	— (0)	— (0)	— (0)	— (0)	0.931 (35)	0.878 (29)	0.633 (9)	0.911 (13)	— (2)	— (2)	— (3)	— (3)
OS	0.872 (38)	0.695 (36)	0.343 (8)	0.426 (8)	— (0)	— (0)	— (2)	— (1)	0.828 (33)	0.742 (26)	0.588 (9)	0.816 (12)	— (1)	— (3)	— (6)	— (6)
RPE	0.305 (39)	0.501 (36)	0.822 (9)	0.7 n = 9	— (0)	— (0)	— (0)	— (0)	0.671 (36)	0.624 (29)	0.687 (13)	0.560 (18)	— (0)	— (0)	— (0)	— (0)
OS and RPE	0.870 (48)	0.914 (45)	— (0)	— (0)	— (0)	— (0)	— (0)	— (0)	0.933 (49)	0.943 (47)	— (0)	— (0)	— (0)	— (0)	— (0)	— (0)

Clear = Borders of the retinal layer can be delineated accurately

Not Clear = Borders of the retinal layer are visible but indistinct making delineation inaccurate

Not Visible = Retinal layer is visible but the delineating borders are not visible

Not Present = Retinal layer is not present

The analysis was subdivided into groups based on the clarity of each retinal layer's borders on both scans. The measurements from both scans were then compared using intraclass correlation coefficients (ICC). The ICCs were only calculated where the number of eyes included in the group was greater than five. A similar comparison between the right and left eye measurements obtained from each participant was also performed (inter-eye correlation) and this is also shown for each retinal layer for both groups.

ICC = intraclass correlation coefficient; n = sample size; CMT = central macular thickness; ONL= outer nuclear layer; ELM= external limiting membrane; IS = inner segment segment of photoreceptor; OS = outer segment of photoreceptor; RPE = retinal pigment epithelium

Table 3.3: Reproducibility of first to second scan measurements taken from the same eye of each inner retinal layer in the nystagmus groups.

	Nystagmus (n=49 for ICC of repeated measures from one eye) (n=47 for ICC of inter-eye comparison)							
Retinal layer	Clear		Not Clear		Not Visible		Not Present	
	ICC (n)	Inter-Eye (n)	ICC (n)	Inter-Eye (n)	ICC (n)	Inter-Eye (n)	ICC (n)	Inter-Eye (n)
NFL	0.481 (24)	0.721 (20)	— (2)	0.369 (5)	— (1)	— (1)	— (22)	— (21)
GCL	0.623 (14)	0.750 (9)	-0.313 (12)	0.581 (14)	— (2)	— (3)	— (21)	— (21)
IPL	0.741 (16)	0.781 (10)	0.425 (13)	0.218 (15)	— (4)	— (6)	— (16)	— (16)
GCL and IPL	0.870 (24)	0.819 (19)	— (4)	0.833 (6)	— (3)	— (4)	— (18)	— (18)
INL	0.778 (23)	0.760 (18)	0.602 (5)	0.684 (6)	— (5)	— (7)	— (16)	— (16)
OPL	0.401 (21)	0.536 (13)	0.845 (7)	0.597 (10)	— (5)	— (8)	— (16)	— (16)

Clear = Borders of the retinal layer can be delineated accurately

Not Clear = Borders of the retinal layer are visible but indistinct making delineation inaccurate

Not Visible = Retinal layer is visible but the delineating borders are not visible

Not Present = Retinal layer is not present

The analysis was subdivided into groups based on the clarity of each retinal layer's borders on both scans. The measurements from both scans were then compared using intraclass correlation coefficients (ICC). The ICCs were only calculated where the number of eyes included in the group was greater than five. A similar comparison between the right and left eye measurements obtained from each participant was also performed (inter-eye correlation) and this is also shown for each retinal layer.

ICC = intraclass correlation coefficient; n = sample size; CMT = central macular thickness; NFL= nerve fiber layer; GCL= ganglion cell layer; IPL= inner plexiform layer; INL= inner nuclear layer; OPL= outer plexiform layer

3.3. Results

3.31. Segmentation Difficulties

There were several borders between retinal layers that were not easy to identify in a subset of participants. These were:

(i) The external limiting membrane (ELM), i.e. the border between the outer nuclear layer (ONL) and inner segment of the photoreceptors (IS), was difficult to identify clearly in 15 of 48 analysed eyes in control participants (31.2%). In 24 of 49 analysed eyes in participants with nystagmus (49%), the ELM was difficult to identify in the foveal area (Table 3.2 and figures 3.2C and 3.2D). Five of the 49 participants with nystagmus were achromats in whom the IS was disrupted by a hypo-reflective zone and therefore could not be analysed. The ELM appeared more difficult to identify in the younger participants in both groups. The mean age at which the ELM was clearly identified was 53.25 months and 45.61 months in the nystagmus and control groups respectively. In comparison to this, the mean age of the participants where the ELM was not visible was 23.17 months and 18.67 months in the nystagmus and control groups respectively. However the effect of age (calculated using an independent-samples t-test) was not significant in either the control participants or the nystagmus participants.

(ii) The border between the outer segment of the photoreceptors (OS) and the retinal pigment epithelium (RPE) although present on all scans was often indistinct preventing accurate demarcation (for example see magnified region of figure 3.2D). Consequently it was difficult to identify the border in 9 of 48 analysed eyes in control participants (18.8%) and in 13 of 49 analysed eyes in participants with nystagmus (26.5%) (Table 3.3). The mean age at which this border was clearly identified was 44.75 months and 49.26 months in the nystagmus and control groups, respectively. In comparison to this, the mean age of the participants where this border was not clear was 38.23 months and 20.33 months in the nystagmus and control groups, respectively. This border was significantly more difficult to delineate in the younger participants of the control group ($p < 0.05$). The effect of age did not reach significance in the nystagmus group.

(iii) In the case of foveal hypoplasia, in the nystagmus group, the border between the ganglion cell layer (GCL) and inner plexiform layer (IPL) could be difficult to identify.

The border was not clearly visible in 14 of the 28 participants (50%) with foveal hypoplasia, where these layers were present (Table 3.3) (Fig 3.2C and 3.2D). There was no significant age difference between any of the segmentation categories of this group. This border could be visualised clearly in 43.2% and 50% of the albinism and *PAX6* participants respectively. This was most difficult to identify in achromatopsia, with the border being clearly identified in only 25% of the achromatopsia participants.

We have provided measurements of the combined layers: IS-ONL; OS-RPE and GCL-IPL in tables 3.2 and 3.3 in order to take the difficulties with accurate segmentation of these borders into account.

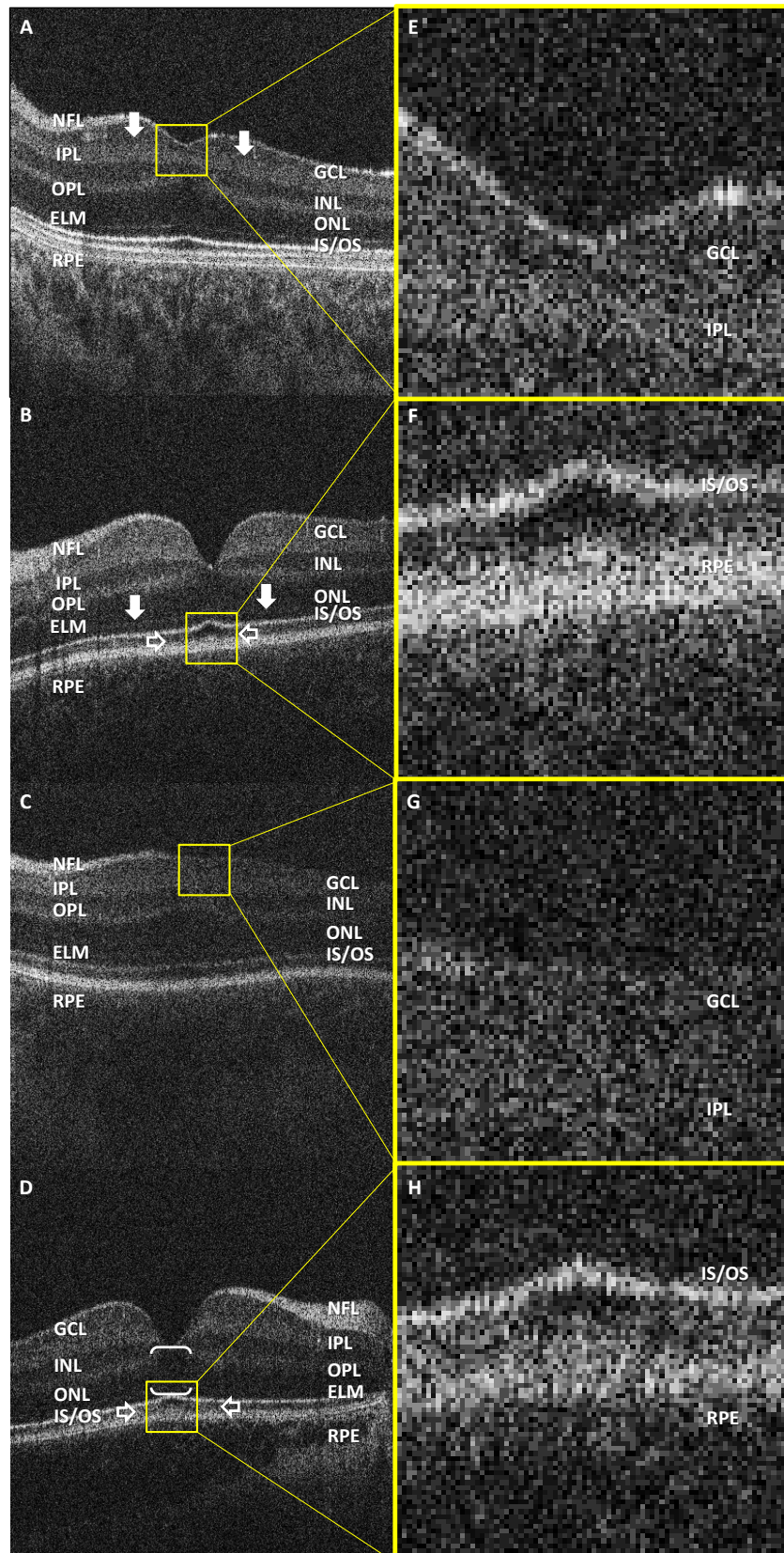


Figure 3.2: Optical coherence tomograms of 2 nystagmus subjects (3.2A and 3.2C) and 2 control subjects (3.2B and 3.2D).

Examples of the difficulties encountered in the segmentation of the retinal layers are shown. The border between the GCL and IPL (indicated by the arrows in Fig 3.2A) is often difficult to identify. If the border between these layers could not be delineated, then a combined measurement was taken from the GCL and IPL. A magnified section of the GCL and IPL in Fig 3.2B and 3.2D which is indicated by the yellow box is shown in Figs 3.2A and 3.2C. The ELM (indicated by the arrows in Fig 3.2B) is often difficult to delineate (Fig 3.2D). If the ELM could not be identified then a combined measurement was taken from the ONL and IS. The upper border of the RPE can be non-distinct (indicated by the open arrows in Fig 3.2D). If this occurred then a combined measurement was taken from the OS and RPE. A magnified section of the border between the OS and RPE as indicated by the yellow box in Fig 3.2B and 3.2D is shown in Fig 3.2F and 3.2H respectively.

NFL= nerve fiber layer; GCL= ganglion cell layer; IPL= inner plexiform layer; INL= inner nuclear layer; OPL= outer plexiform layer; ONL= outer nuclear layer; ELM= external limiting membrane; IS/OS= inner segment/outer segment junction; RPE= retinal pigment epithelium; ICC=intraclass correlation coefficient.

3.32. Reproducibility of Retinal Measurements Between Scans

Both the nystagmus and controls groups demonstrated excellent reproducibility between two examinations for central macular thickness (CMT) with ICCs greater than 0.96.

In general the outer retinal layers showed a good degree of reproducibility with ICCs of between 0.8 and 0.95 for the ONL, OS, combined ONL-IS and combined OS-RPE measurements in both the nystagmus group, and control group. The test-retest reliability of the other outer retinal layers: the IS and RPE when measured individually were not as consistent with ICCs of 0.626 and 0.671 respectively in the nystagmus group and 0.557 and 0.305 in the control group.

For the inner retinal layers which were present in the fovea in patients with foveal hypoplasia in the nystagmus group there was a good degree of reproducibility for the IPL, INL and combined GCL-IPL measurements with ICCs of 0.741, 0.778 and 0.870, respectively. The test-retest reliability of the other inner retinal layers; the nerve fibre layer (NFL); GCL and outer plexiform layer (OPL) was not as consistent with ICCs of 0.481, 0.623 and 0.401, respectively. The ICCs were comparable between both groups showing that there is no difference in the reliability of scans obtained in children with nystagmus as compared to age-matched healthy controls (Tables 3.2 and 3.3).

3.33. Inter-Eye Comparison of Nystagmus and Control Subjects

Scans of both eyes were compared in 47 of the nystagmus subjects and 45 of the control subjects. Both the nystagmus and controls groups showed a good degree of inter-eye agreement with ICCs greater than 0.94 for CMT (Tables 3.2 and 3.3 and Figure 3.1C).

3.34. Bland-Altman Assessment

A Bland-Altman assessment for agreement was used to compare the two separate measurements (Table 3.4). With the exception of the CMT and combined OS-RPE measurements in the control group and the INL, OPL and combined OS-RPE measurements in the nystagmus group, bias was not significantly different from zero in both groups for all retinal layer measurements.

There was a significant positive bias in the CMT and combined OS-RPE measurements in the control group with a biases of 0.291 ($p < 0.05$ and 0.484 ($p < 0.0001$) respectively, indicating a trend towards larger thickness measurements for these layers with better quality scans. There was also a significant positive bias in the OS and combined OS-RPE measurement in the nystagmus group with a bias of 0.402 ($p < 0.01$) and 0.647 ($p < 0.0001$) respectively, indicating a trend towards a larger thickness measurement for this layer with higher quality scans.

There was a significant negative bias in the measurements if the INL and OPL in the nystagmus group with biases of -0.615 ($p < 0.001$) and -0.609 ($p < 0.001$) respectively, indicating a trend towards smaller thickness measurements for these layers with higher quality scans.

The 95% limits of agreement that were established ranged from a minimum interval of -1.0 to 2.8 for the OS; a maximum interval of -3.2 to 3.4 for the ONL in the control group; a minimum interval of -1.7 to 2.2 for the RPE and a maximum interval of -6.7 to 5.4 for the combined ONL and IS measurement in the nystagmus group. The limits of agreement were narrower in control as compared to the patient group. The limits of agreement between patients and controls are of similar ranges and small enough for clinical tests.

Table 3.4: Summary of Bland-Altman plot for measurements of each retinal layer.

Control n = 48				Nystagmus n = 49			
Retinal Layer	Mean (µm) (SD)	95% Limits of agreement	Bias (p value)	Retinal Layer	Mean (µm) (SD)	95% Limits of agreement	Bias (p value)
CMT n = 48	192.100 (24.957)	-3.8 to 2.3	0.291* (<0.05)	CMT n = 48	240.908 (61.075)	-7.5 to 4.1	-0.066 (Ns)
NFL n = 1	-----	-----	-----	NFL n = 26	9.479 (3.962)	-4.9 to 0.2	0.058 (Ns)
GCL n = 1	-----	-----	-----	GCL n = 26	25.864 (8.288)	-4.3 to 6.4	0.092 (Ns)
IPL n = 4	-----	-----	-----	IPL n = 29	30.552 (9.455)	-4.6 to 4.2	0.139 (Ns)
GCL and IPL n = 1	-----	-----	-----	GCL and IPL n = 28	53.959 (20.355)	-6.4 to 4.4	0.290 (Ns)
INL n = 4	-----	-----	-----	INL n = 28	53.959 (20.355)	-6.2 to 4.4	-0.615*** (<0.001)
OPL n = 4	-----	-----	-----	OPL n = 28	18.893 (8.069)	-5.3 to 1.4	-0.609*** (<0.001)
ONL n = 47	96.049 (18.004)	-3.2 to 3.4	0.139 (Ns)	ONL n = 47	90.332 (22.557)	-5.2 to 3.8	0.080 (Ns)
IS n = 45	29.340 (5.234)	-3.5 to 0.8	-0.700 (Ns)	IS n = 38	26.871 (4.503)	-0.2 to 4.0	-0.830 (Ns)
ONL and IS n = 45	125.811 (20.261)	-3.9 to 2.6	0.196 (Ns)	ONL and IS n = 42	118.081 (22.498)	-6.7 to 5.4	0.060 (Ns)
OS n = 46	37.409 (8.031)	-1.0 to 2.8	0.089 (Ns)	OS n = 42	32.607 (7.664)	-1.3 to 3.5	0.402** (<0.01)
RPE n = 48	27.325 (5.091)	-0.9 to 2.9	0.210 (Ns)	RPE n = 49	25.753 (5.807)	-1.7 to 2.2	-0.117 (Ns)
OS and RPE n = 48	62.575 (13.377)	-2.5 to 3.1	0.484*** (<0.001)	OS and RPE n = 49	53.898 16.927	-2.9 to 2.1	0.647*** (<0.001)

The higher quality scan was always analysed first so that any bias due to image quality could be detected.

n = sample size; *CI* = confidence interval; *CMT* = central macular thickness; *NFL*= nerve fibre layer; *GCL*= ganglion cell layer; *IPL*= inner plexiform layer; *INL*= inner nuclear layer; *OPL*= outer plexiform layer; *ONL*= outer nuclear layer; *ELM*= external limiting membrane; *IS* = inner segment of photoreceptors; *OS* = outer segment of photoreceptors; *RPE*= retinal pigment epithelium; *SD* = standard deviation; *Ns* = not significant ($p > .05$), $*p < .05$, $**p < .01$, $***p < .001$, $****p < .0001$

3.4. Discussion

We have demonstrated for the first time that the HH-SDOCT produces reliable assessments of foveal morphology in young children with and without nystagmus. The ICCs for CMT were excellent with an ICC of 0.966 in the nystagmus group and 0.960 in the control group. These are only marginally lower than those obtained in adult patients with nystagmus (0.97) and adult controls (0.98).¹⁹¹ This should be expected as the inner limiting membrane (ILM) and Bruch's membrane exhibit the strongest signals on OCT. The ICCs for ONL and OS were also high with ICCs >0.8 in the nystagmus and in the control group, respectively. Reliable quantification of the OS is important clinically as this can potentially be used as an objective predictor of visual acuity.¹²⁷ Bland-Altman plots showed good agreement for both groups for intraretinal thickness measurements and the 95% limits of agreement were comparable to those reported in adults with and without nystagmus.¹⁹¹

We have also identified which retinal layers may be less reliable when quantified. This includes the GCL and OPL layers in the nystagmus group and the IS and RPE layers in both the nystagmus and control groups. The GCL and OPL layers have very similar reflectance profiles making their borders more difficult to delineate accurately. This leads to a poor signal-to-noise ratio when image quality is not of sufficient standard to allow accurate quantification of these layers.

Comparing the consistency of measurements based on whether the borders between individual layers are clear or not clear did improve the ICCs for the IS from 0.289 to 0.626 in the nystagmus group and from 0.367 to 0.557 in the control group. However the ICCs did not reach the same level of reliability as the other retinal layers such as ONL. Also comparing the consistency of measurements based on border clarity did not improve the ICCs for the OPL in the nystagmus group and the RPE in both the nystagmus and control groups. As these layers are much thinner than the other layers of the fovea their measurements are likely to be more sensitive to errors such as measurement error and quantisation effects. The ICCs obtained in this study were higher with the thicker retinal layers making this a plausible explanation.

One other explanation that would need to be considered is that in infants and young children the retinal layers are developing. It is possible that in the immature

retina, structures such as the ELM may not be visible until they have matured sufficiently. We observed a tendency towards more difficulties with segmentation of the ELM and the junction between the OS and RPE in the younger participants of both groups. This did not reach statistical significance for the ELM in both groups and for the junction between the OS and RPE in the nystagmus group. The effect of age (examined using an independent-samples t-test) did reach significance however, for the junction between the OS and RPE in the control group ($p < 0.05$).

We attempted to improve the reliability of measurements of these retinal layers, by performing combined measurements of the retinal layers where it was apparent that there were difficulties with delineating their borders. This affected the GCL-IPL layers; the ONL-IS layers and the OS-RPE layers. Assessment of these combined layers was consistent on test-retest analysis with ICCs of 0.870, 0.931 and 0.933, respectively, for the nystagmus group. The ICCs were 0.931 and 0.870 for the combined ONL-IS layer and combined OS-RPE layers, respectively, in the control group. This is a strategy that potentially could be used to improve reliability when using HH-SDOCT to quantify normal retinal development, identify retinal pathology and in developing objective OCT based predictors of visual acuity.

There was a trend towards a larger estimate of CMT measurements in the control group; OS measurement in the nystagmus group and combined OS and RPE measurements in both the nystagmus and control groups with higher quality images. This may be accounted for by the increased reflectance of the RPE border and IS/OS junction in the higher quality images, which make the RPE and OS appear thicker. The trend towards a larger estimate of measurement of the INL and OPL on lesser quality images may be explained by low reflectivity of the borders of these layers leading to an overestimation of thickness of these layers as their borders are not clearly delineated. The effects of image quality on the reliability of these measurements need to be taken into account if the HH-SDOCT is potentially going to be used in a clinically diagnostic and monitoring role in children with retinal conditions.

It has been previously shown that human foveal development as visualised by spectral-domain OCT correlates anatomically with histologic specimens.^{59, 92} Accurate assessment of foveal morphology is important as the HH-SDOCT will likely play an

increasingly important diagnostic and prognostic role in infants and young children with nystagmus and other eye diseases such as ROP and glaucoma. Reliability between measurements will allow accurate monitoring of both normal and abnormal foveal development.

In this study we have shown that the reliability of quantitative central macular thickness and photoreceptor outer segment length measurements using the HH-SDOCT in children are excellent and is comparable to adult OCT.¹⁹¹ An OCT-based structural grading system for foveal hypoplasia has been developed previously showing that the grade of arrested foveal development is correlated to VA in a range of disorders associated with foveal hypoplasia.¹²⁸ The reliability of the measurement of the length of the photoreceptor outer segment is important as this is a strong predictor of visual acuity in albinism¹²⁷ and potentially could help predict visual acuity in various other diseases. Our results provide an important basis for future use of OCT in infants and young children for research and clinical application. In future studies it would be important, for example, to analyse whether foveal morphology on OCT scans could be used to possibly predict visual acuity in preverbal children, especially as OS have been shown very reliable. Our results support that OCT can be used reliably clinically in young children, in diseases including foveal hypoplasia or can be used to monitor retinal dystrophies especially in view of imminent genetic therapy.

Chapter 4

Normal Foveal Development: An In Vivo study using Optical Coherence Tomography

4.1. Introduction

4.2. Methods

4.3. Results

4.4. Conclusion

4.1. Introduction

It was previously highlighted in section 1.1, that foveal development is a complex process, involving centrifugal displacement of the inner retinal layers away from the foveal centre and centripetal displacement of the cone photoreceptors into the foveal centre.^{5, 8, 36} The exact time course of foveal development is unclear with maturation reported to be completed between eleven months and five years of age^{36, 37, 50, 60} with current understanding limited to studies of few histological specimens.^{43, 45, 46, 59}

Hand-held spectral domain optical coherence tomography has the potential to overcome this limitation by allowing large scale, reliable and non-invasive in vivo imaging of the infant human retina at near microscopical (2.4 μm) level.^{49, 86, 192}

The aim of this study was to use the HH-SDOCT to systematically describe and quantify normal foveal development in full term infants and young children.

4.2. Methods

4.2.1. Participants

The cohort for this study included term 223 children with a mean age of 2.2 years (range 0-6.9 years) and 38 older children and adults with a mean age of 15 years (range 7.1-27 years). Term was defined as a gestational age between 37 and 42 weeks¹⁹³. Participants were excluded if they had any pre-existing ocular, neurological or metabolic abnormalities that may affect eye development, a refractive error of +4.00 diopters or greater in any axis, myopia of -3.00 diopters or greater in axis or anisometropia of 1.5 diopters or more. In addition there were 4 further participants recruited in whom cystoid macular oedema was identified on their initial scans. These scans were excluded from subsequent analysis. If tomograms were obtained of both the right and left eyes of a participant during a single visit, both eyes were included in the final models.

All participants underwent a full orthoptic and ophthalmologic examination, which included slit-lamp examination where possible, fundus examination and measurement of visual acuity. Visual acuity (VA) was assessed in younger infants and children by preferential looking using Teller acuity cards and/or crowded logMAR Kay Picture Tests if possible. In cooperative children, Teller acuity cards and/or logMAR crowded optotypes (Glasgow Acuity Cards) were used to obtain VA.

534 mixed cross sectional and longitudinal examinations were obtained. Participants were divided into sixteen age groups as follows:

<40 weeks GA n = 19	41-46 weeks GA n = 18	47-52 weeks GA n = 7	12-14 months GA n = 23
15-17 months GA n = 24	18-20 months GA n = 19	21-26 months GA n = 15	27-32 months GA n = 18
33-38 months GA n = 14	39-44 months GA n = 14	45-56 months GA n = 24	57-68 months GA n = 27
69-80 months GA n = 17	81-92 months GA n = 23	93-213 months GA n = 22	214-309 months GA (n = 16)

The demographic characteristics the participants in this study are provided in Tables 1 & 2 in Appendix 1.

4.22. Optical Coherence Tomography

HH-SDOCT (Biotigen Envisu™ system, Durham, NC, USA) was used to obtain a volumetric scan (consisting of 100 B-scans and 500 A-scans per B-scan) of the foveal region as previously described.¹⁹² The acquired images were exported from the Biotigen OCT software and imported into ImageJ software (available at: <http://rsbweb.nih.gov/ij/> Date accessed: May 11, 2012) where retinal layer segmentation was performed. The nomenclature used to label the segmented layers are based on previously established anatomical correlates with histology (Figure 1).^{93 94} If a border between two retinal layers could not be segmented reliably, then a combined measurement of the two layers was taken in order to optimise the reliability of the results obtained.¹⁹² This included the GCL and IPL which together make the ganglion cell complex (GCC); the ONL and inner segment of the photoreceptors (IS) which together make the ONL-IS complex and the outer segment of the photoreceptors (OS) and RPE which make the (OS-RPE complex). For the purposes of this study, the parafovea and perifovea were defined as the regions measured at 1000 μm and 2000 μm from the central fovea, respectively.

4.23. Statistics and Modelling

We calculated: (1) the mean thickness measurement, standard deviation and 95% confidence interval for each retinal layer in each of the 16 age groups; (2) the trajectory of development of each retinal layer over time, (3) the age at which the developmental trajectory for each retinal layer reaches the 95% confidence interval of the mean adult value and (4) the correlation between the thickness of each retinal layer and visual acuity. Developmental trajectories were mapped out by carrying out fractional polynomial modelling.¹⁹⁴ Fractional polynomial modelling is a very flexible method of modelling continuous, nonlinear data with skewed distributions. By choosing power transformations from the set $\{-2, -1, -0.5, 0, 0.5, 1, 2, 3\}$, where 0 denotes the log transformation fractional polynomial modelling can provide a range of shapes and curves that cannot be achieved using standard polynomials.

In order to determine the relationship between retinal layer thickness measurements and Teller visual acuity (measured in cycles per degree at 38 cm),

measurements from a single eye only from each examination visit was included in the analysis. If scans were available from both eyes from a single visit, then only the right eye measurements were included. First order partial correlation coefficients were calculated between each retinal layer and Teller visual acuity while controlling for age.

All analyses were considered significant at a type 1 probability value of $p < 0.05$. Statistical analysis was performed STATA™ software (Copyright 1996–2014, StataCorp).

4.3. Results

4.3.1. General Outline of Foveal Development

There is centrifugal migration of the inner retinal layers away from the central fovea. With increasing maturity, the foveal pit widens and the GCL, IPL and OPL fuse into a single thin layer (IRL) beneath the base of the central foveal pit. There is centripetal migration of the photoreceptors into the central fovea accompanied by concurrent elongation of these photoreceptors over time (Figure 4.1, Supplementary Video 1). At between 37-40 weeks gestational age (GA), the outer segments of the photoreceptors (OS) and ellipsoid (ISE) are absent in the central fovea in 62.1% of eyes (Figure 4.1). This decreases to 34.8% at 41-46 weeks GA. The OS are present in the central fovea in all eyes from 47 weeks GA (Table 3, Appendix 1). The appearance of the contact cylinder (Figure 1) of the photoreceptors becomes more obvious with increasing age. This structure is rarely identifiable in the youngest age groups but is almost always visible from 47 months GA (Table 4, Appendix 1). There is elongation of the outer retinal layers associated with an increase in the overall retinal thickness with increasing age (Figures 4.1 & 4.2).

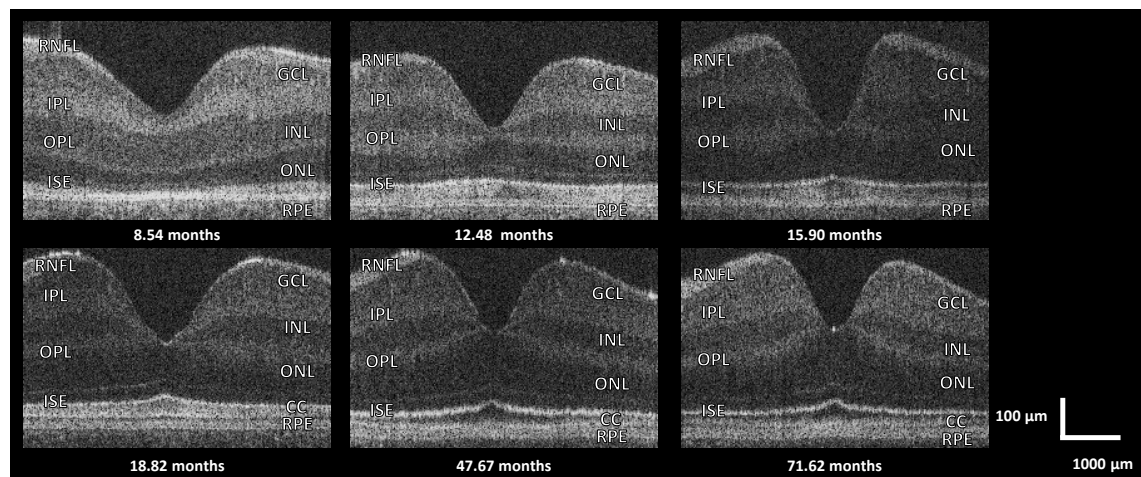


Figure 4.1: Examples of foveal tomograms from a range of ages illustrating the anatomy of the fovea and the main features of foveal development over time.

There is centrifugal migration of the inner retinal layers away from the central fovea, centripetal migration of the photoreceptors into the fovea and elongation of the photoreceptor layers over time.

RNFL = retinal nerve fibre layer; GCL = ganglion cell layer; IPL = inner plexiform layer; INL = inner nuclear layer; OPL = outer plexiform layer; ONL = outer nuclear layer; ELM = external limiting membrane; ISE = ellipsoid of the inner segment of the photoreceptor; CC = contact cylinder; RPE = retinal pigment epithelium

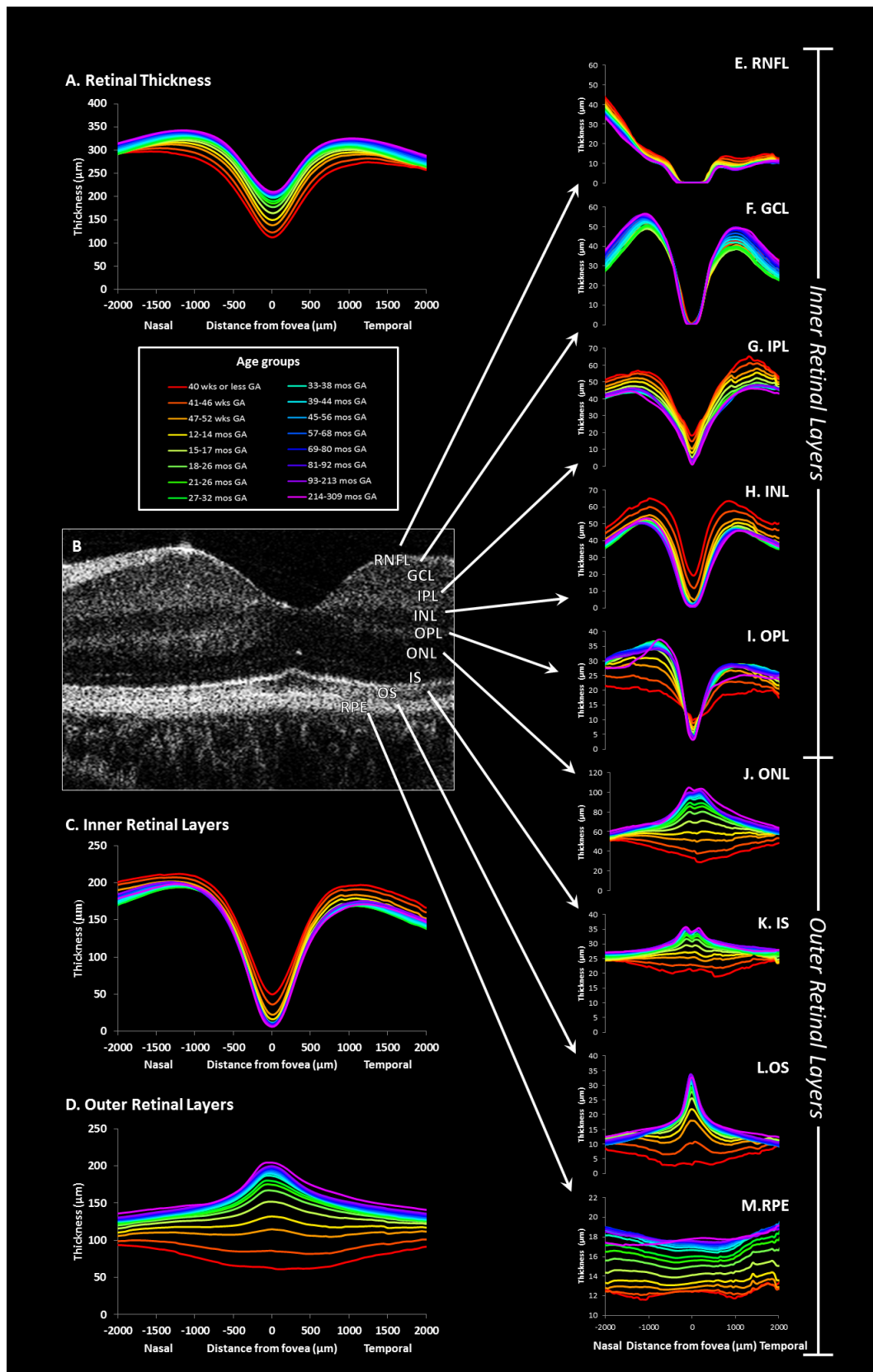


Figure 4.2: Mean thickness of each retinal layer plotted using a 4th order polynomial fit for each of the 16 age groups which have been colour coded.

The inner retinal layers include the RNFL, GCL, IPL, INL and OPL. The outer retinal layers include the ONL, IS, OS and RPE.

RNFL = retinal nerve fibre layer; GCL = ganglion cell layer; IPL = inner plexiform layer; INL = inner nuclear layer; OPL = outer plexiform layer; ONL = outer nuclear layer; IS = inner segment of the photoreceptor; OS = outer segment of the photoreceptor; RPE = retinal pigment epithelium; RT = retinal thickness

The central retinal thickness at the fovea (CMT) increases logarithmically between birth and 48.6 months gestational age (GA) by 62.4 % (Figures 4.2A & 4.3A). In contrast to this, there is a smaller 17% and 21% increase in the nasal and temporal parafoveal retinal thickness measurements, respectively, and a 6% and 13% increase in the nasal and temporal perifoveal measurements, respectively, by 48.6 months GA. The mean retinal thickness measurements for each age group at the fovea, parafovea and perifovea have been summarised in Tables 5, 6 & 7 in Appendix 1.

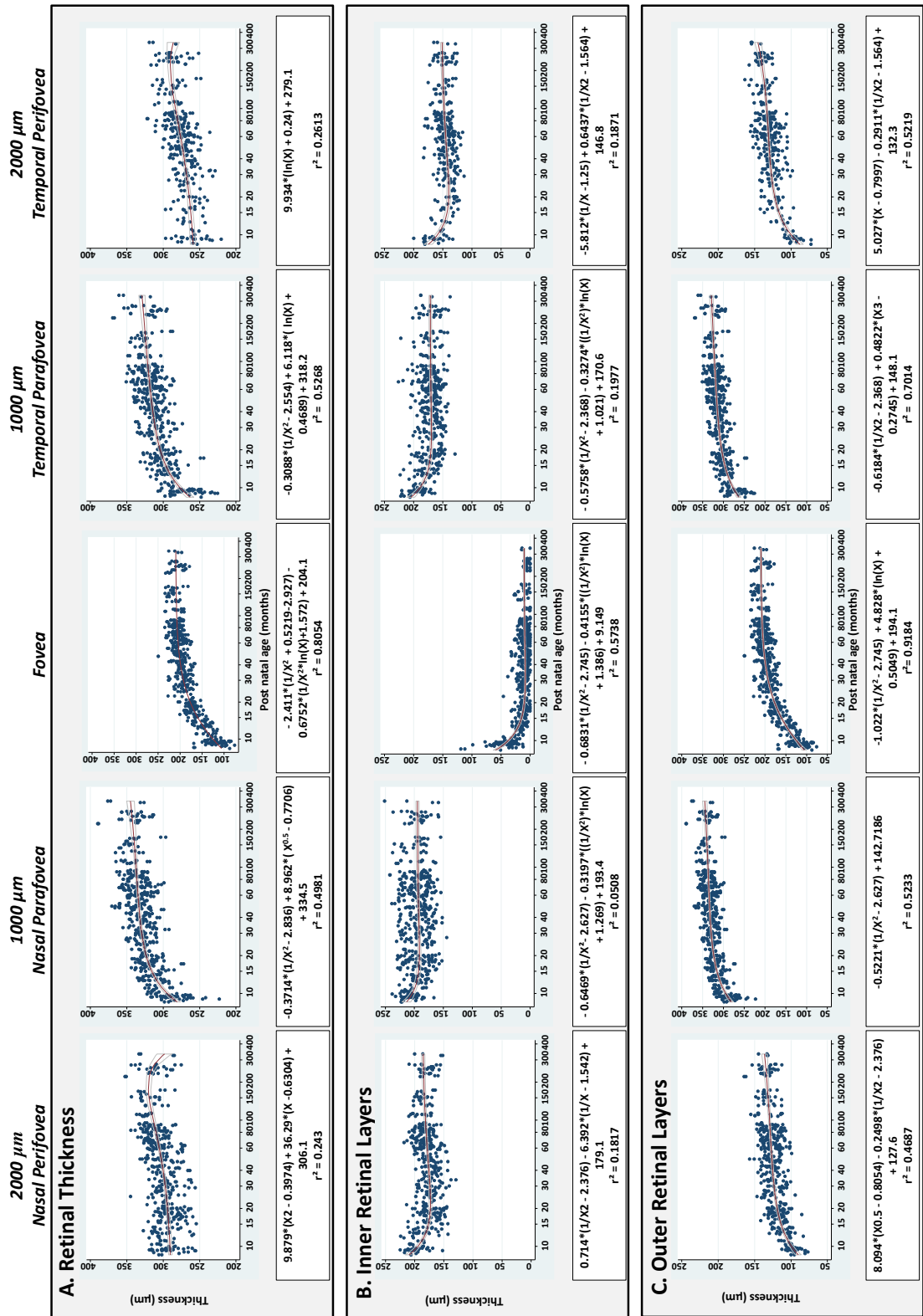


Figure 4.3: Development trajectories for the inner retinal layers, outer retinal layers and total retinal thickness at the fovea and parafovea.

The parafoveal and perifoveal measurements were taken at 1000 μm and 2000 μm nasal and temporal to the central fovea. The trajectories have been plotted over a time period spanning 8.4 through 333.9 months gestational age (GA). Each point represents a single value from each examination. The best fit curve line obtained with fractional polynomial regression analysis together with its 95% confidence interval is shown. The equation associated with the model is also given; where $X = \text{GA in months}/100$.

GA = gestational age; OCT = optical coherence tomography

4.32. Development of the Inner Retinal Layers

The foveal inner retina layers decrease in thickness with increasing age until adulthood (Figures 4.2C, 4.3B & 4.4). The GCL is visible at the fovea in the youngest age group (<40 weeks GA) only and has regressed from the fovea by 41-46 weeks GA. The inner plexiform layer (IPL), inner nuclear layer (INL) and outer plexiform layer (OPL) decrease in thickness exponentially during the immediate postpartum period. The IPL, INL and OPL decrease in thickness exponentially, completing their regression from the fovea by 18.7, 17.6 and 17.8 months GA, respectively (Figures 4.2G-I & 4.4). We calculated that regression of the inner retinal layers from the fovea is complete at 17.5 months GA (Table 8 in Appendix 1).

The developmental trajectories of the inner retinal layers at the parafovea and perifovea are more complex than directly at the fovea (Figures 4.4 & 4.5). The RNFL and IPL decrease exponentially in thickness until 31.4 months and 39 GA, respectively (Figures 4.4 & 4.5). The GCL and INL initially decrease in thickness until 17 months GA and then increase in thickness until 65.5 and 41.5 months GA, respectively (Figures 4.4 & 4.5). The OPL increases in thickness, peaking at 11.6 months GA (Figures 4.4 & 4.5).

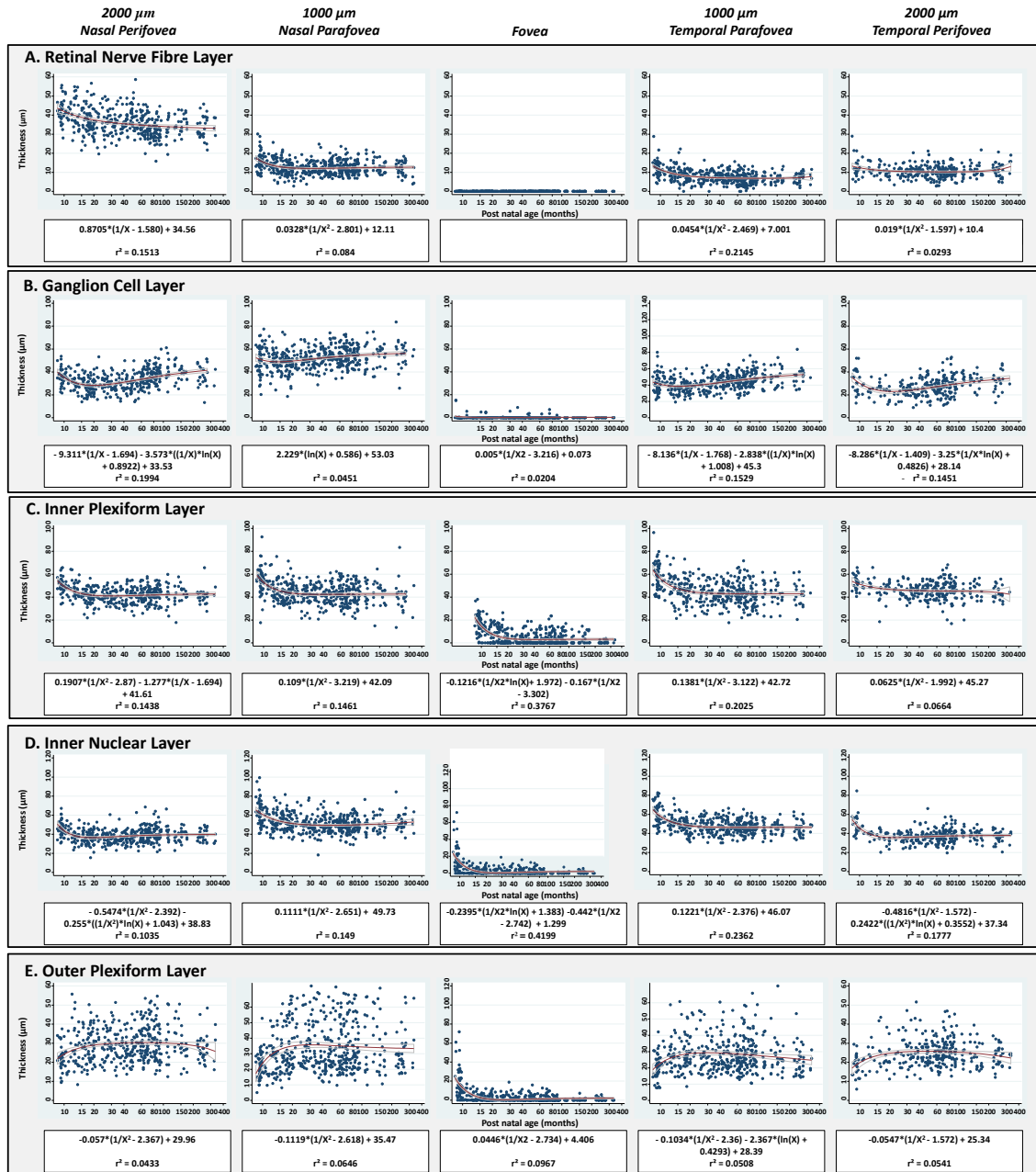


Figure 4.4: Development trajectories for the inner retinal layers: RNFL, GCL, IPL, INL and OPL at the parafovea and perifovea.

The parafoveal and perifoveal measurements were taken at 1000 μm and 2000 μm nasal and temporal to the central fovea. The trajectories have been plotted over a time period spanning 8.4 through 333.9 months GA. Each point represents a single value from each examination. The best fit curve line obtained with fractional polynomial regression analysis together with its 95% confidence interval is shown. The equation associated with the model is given, where $X = \text{GA in months}/100$.

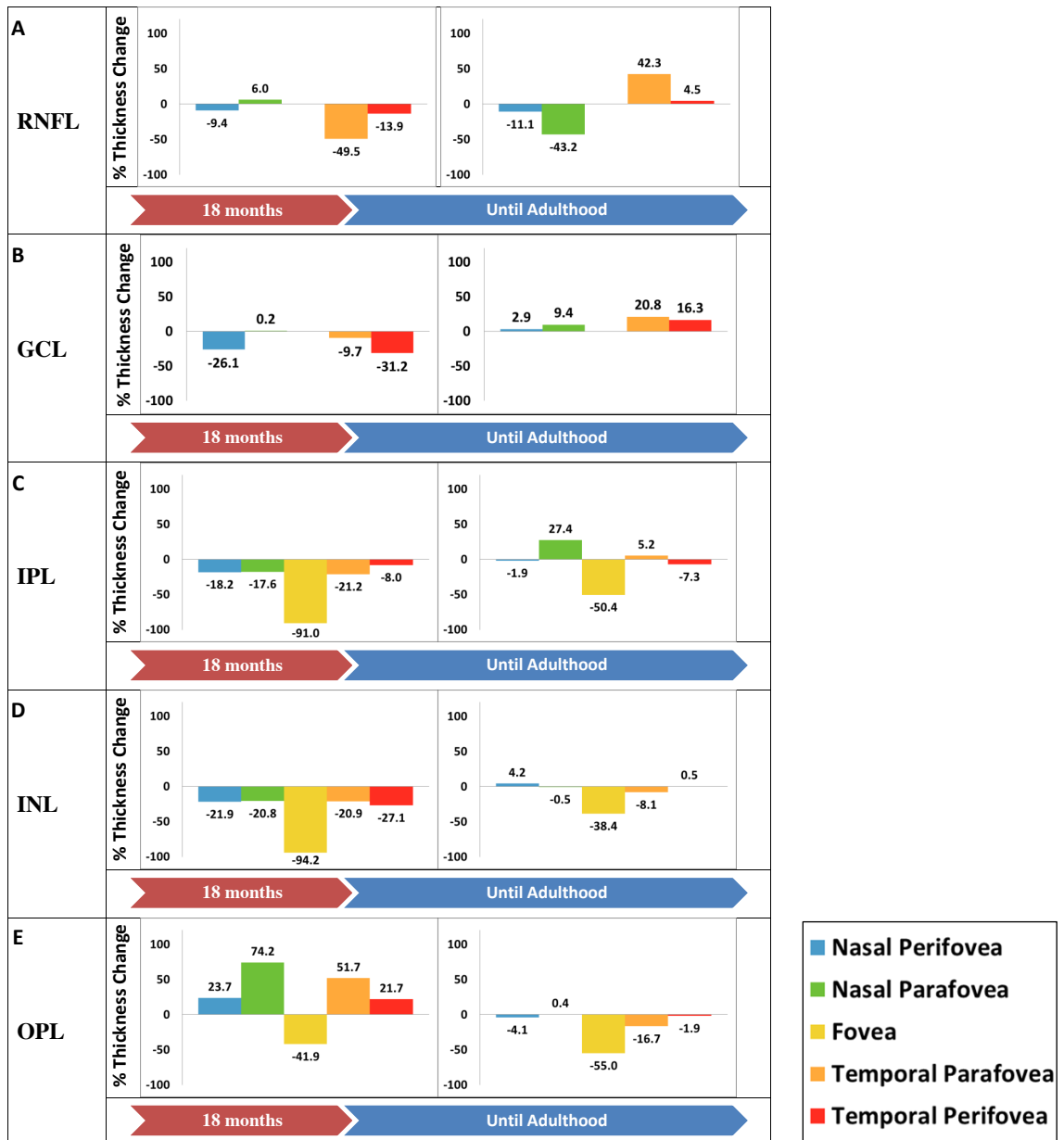


Figure 4.5: Percentage change in the mean thickness of the foveal, parafoveal and perifoveal inner retinal layers between birth and time of peak development at the fovea (red arrows).

The residual percentage difference between the retinal layer thickness at the time of peak development at the fovea and the mean adult thickness value is shown for comparison.

RNFL = retinal nerve fibre layer; GCL = ganglion cell layer; IPL = inner plexiform layer; INL = inner nuclear layer; OPL = outer plexiform layer

4.33. Development of the Outer Retinal Layers

The outer retinal layers at the fovea increase logarithmically by 185% between birth and 47 months GA, reaching maturity by 75 months GA (Figure 4.2D). The developmental trajectories for the outer retinal layers at the fovea, parafovea and perifovea are illustrated in Figure 4.6.

The outer nuclear layer (ONL), inner segment of the photoreceptors (IS) and outer segment of the photoreceptors (OS) thickness increases logarithmically at the fovea, between birth and 45.3, 26.9 and 32.4 months GA, respectively (Figure 4.6). The parafoveal and perifoveal ONL, IS and OS also increase in thickness exponentially initially and then increase more gradually until 128.4, 29.8 and 146 months GA, respectively (Figures 4.6 & 4.7). The most dramatic change occurs with respect to the OS of the cone photoreceptors, which increases in thickness at the fovea from 3.06 μm to 33.27 μm (987.3%) between birth and 45 months GA. Initially, the parafoveal and perifoveal photoreceptors are longer than the central photoreceptors. This difference disappears between 47-52 weeks gestational age.

The RPE rapidly increases in thickness at the fovea, parafovea and perifovea between birth and 54.4 months GA and then increase more slowly thereafter (Figures 4.6 & 4.7).

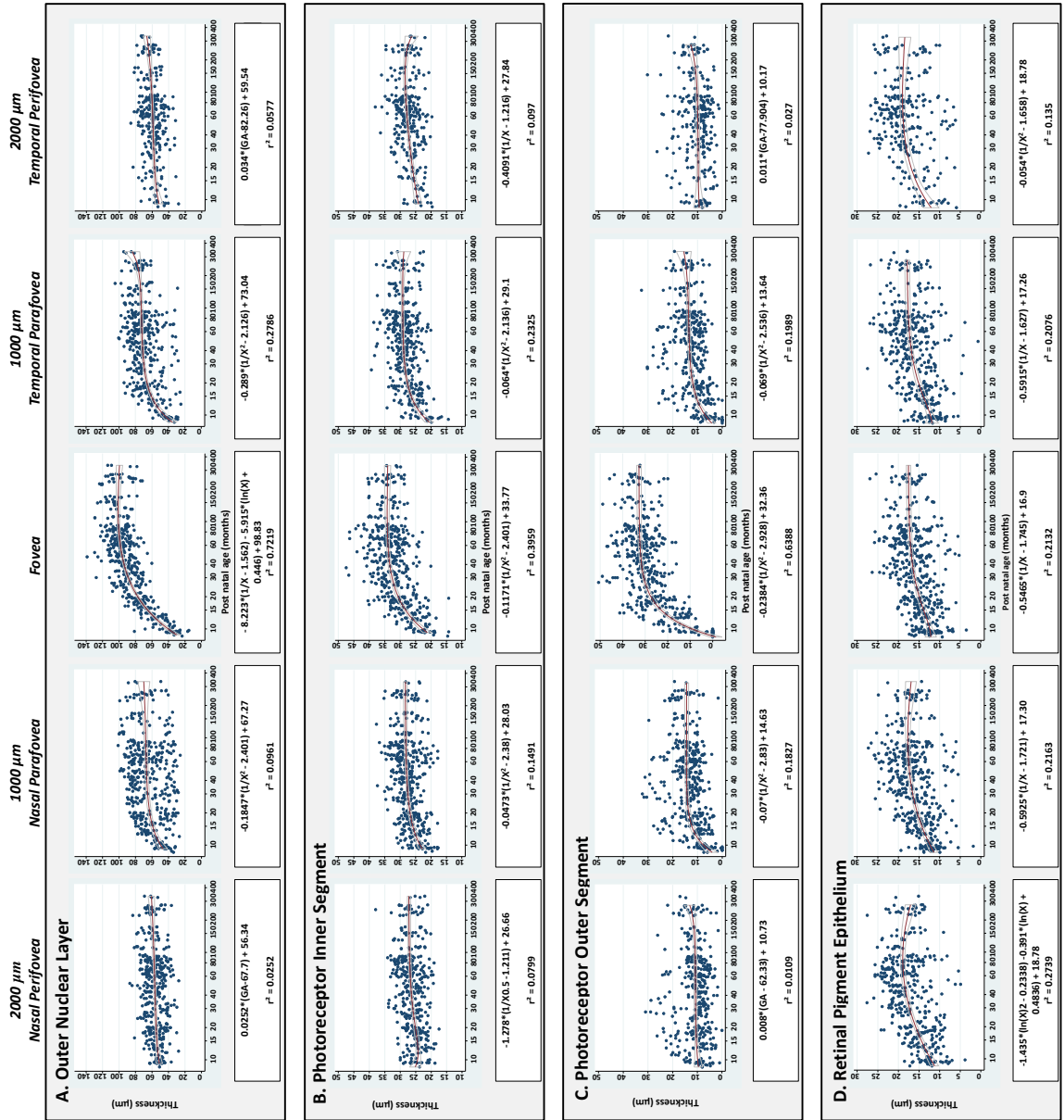


Figure 4.6: Development trajectories for the ONL, IS, OS and RPE at the fovea, parafovea and periphery.

The parafoveal and perifoveal measurements were taken at 1000 μm and 2000 μm nasal and temporal to the central fovea. The trajectories have been plotted over a time period spanning 8.4 through 333.9 months GA. Each point represents a single value from each examination. The best fit curve line obtained with fractional polynomial regression analysis together with its 95% confidence interval is shown. The equation associated with the model is given, where $X = GA$ in months/100.

ONL = outer nuclear layer; IS = inner segment of the photoreceptor; OS = outer segment of the photoreceptor; RPE = retinal pigment epithelium; GA = gestational age.

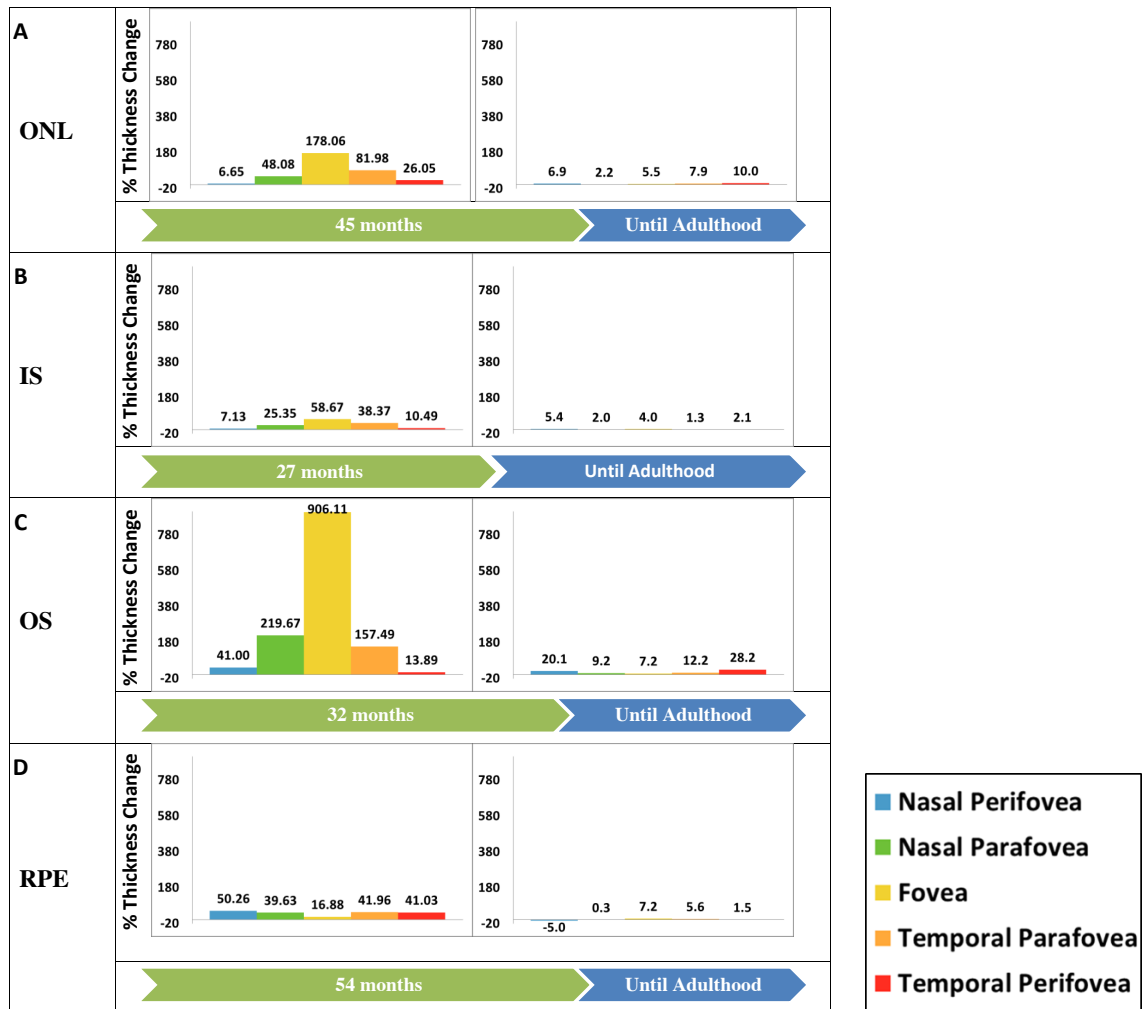


Figure 4.7: Percentage change in the mean thickness of the foveal, parafoveal and perifoveal outer retinal layers between birth and time of peak development at the fovea (green arrows).

The residual percentage difference between the retinal layer thickness at the time of peak development and the mean adult thickness value is shown for comparison.

RNFL = retinal nerve fibre layer; GCL = ganglion cell layer; IPL = inner plexiform layer; INL = inner nuclear layer; OPL = outer plexiform layer

4.34. Correlations with Visual Acuity

There was a weak negative correlation between the IRL thickness with VA, measured using Teller acuity cards (Teller acuity) ($r = -0.16$, $p < 0.05$). The ORLs and RT are strongly correlated with Teller acuity with $r = 0.54$ ($p < 0.0001$) and $r = 0.52$ ($p < 0.0001$) respectively. Each of the outer retinal layers measurements are significantly correlated with Teller acuity. This includes the ONL ($r = 0.51$, $p < 0.0001$); IS ($r = 0.29$, $p < 0.0001$); OS ($r = .22$, $p < 0.01$) and RPE ($r = 0.2$, $p < 0.001$) (Table 4.1).

Table 4.1: Summary of the first-order partial correlations conducted in order to explore the relationship between each retinal layer measurement and the development of Teller acuity while controlling for the effects of age.

	GCL	IPL	GCC	INL	OPL	ONL	IS	OS	RPE	IRLs	ORLs	RT
Teller Acuity	-0.02 <i>Ns</i>	-0.02 <i>Ns</i>	-0.74 <i>Ns</i>	-0.13 <i>Ns</i>	-0.04 <i>Ns</i>	0.52 ****	0.23 **	0.22 **	0.17 *	-0.16 *	0.47 ****	0.44 ****

N = 160 in all cases

*Ns = not significant ($p > 0.05$), * $p < 0.05$, ** $p < 0.01$, *** $p < 0.001$, **** $p < 0.0001$*

N = number of examinations where all retinal layers could be reliably segmented; GCL = ganglion cell layer; IPL = inner plexiform layer; GCC = ganglion cell complex; INL = inner nuclear layer; OPL = outer plexiform layer; ONL = outer nuclear layer; IS = inner segment of the photoreceptor; OS = outer segment of the photoreceptor; RPE = retinal pigment epithelium; GA = gestational age

4.4. Discussion

To our knowledge, this is the first large in vivo OCT study of normal term human foveal and visual development to be reported. We have confirmed that foveal development consists of the dual processes of centrifugal displacement of the inner retinal layers and a centripetal displacement of the outer retinal layers which occurs concurrently with elongation of the retinal layers. This has previously been outlined in detail in smaller scale histological and OCT studies.^{36, 49, 59} Previous studies have suggested that foveal development is completed at between 11-15 months of age and five years.^{37, 50, 59, 60} We have found in our study that the central foveal thickness reaches adult levels at 48.6 months GA. This does not suggest however that the individual developmental processes for each retinal layer at the fovea is complete at this age. In fact our study suggests that some changes may be continuing into adolescence.

The excavation of the inner retinal layers from the fovea has been reported to be complete at 6 weeks to 9 months postnatally.⁶⁰ Our study confirms that this process is complete at 18 months GA. The parafoveal and perifoveal pattern of development of the inner retinal layers is more complex and does not necessarily mimic what is occurring at the central fovea. With the exception of the GCL and OPL all of the parafoveal and perifoveal inner retinal layers decrease in thickness and then begin to level out from 18 months GA. If the hypothesis that mechanical stretch is the force that directs migration of the IRLs away from the fovea, then the effect of this would be then the effect of this would be greatest during the first two years of life, when the axial length (AL) of the eye reaches 90% of mean adult values when the increase in the axial length of the eye is at its greatest.^{33, 102, 103} Once the change in axial length plateaus, migration of the inner retinal layers would be expected to plateau around this age, which is what we observed in this study.

The parafoveal and perifoveal GCL and INL initially decrease in thickness until 17 months GA and then gradually increase in thickness until 65.5 and 41.5 months GA, respectively. The parafoveal and perifoveal OPL increases in thickness until it plateaus at 21.3 months GA. We postulate that what this pattern represents is the dual processes of migration of the inner retinal layers from the fovea as well as thickening of these retinal layers over time. In the case of the GCL and INL, the rate of increase in

thickness does not exceed migration until 18 months of age when thickening exceeds the rate of migration giving a net increase in the thickness of the GCL and INL in the parafovea and perifovea. The thickening of these layers then plateaus as maturity is reached. In the case of the OPL, the net increase in thickness of this layer always exceeds the rate of migration of the layer from the parafovea and perifovea, until it plateaus at 11.6 months GA.

We have demonstrated that the outer retinal layers increase in thickness exponentially until approximately 47 months GA followed by a gradual plateau. The ORL measurement reaches mean adult values by 69 months GA. Interestingly, however the ONL and OS appears to continue increasing in thickness into adolescence. This may be consistent with previous histological observations that the cone packing density at the fovea ($108400/\text{mm}^2$) have only reached half adult values at 45 months.³⁷ If the cone packing density at the fovea is continuing to increase into adolescence, then this may be reflected by the continuing increase in thickness of the OS and ONL layers on OCT into adolescence.

The visibility of the ISE band (previously termed the IS/OS band) at the central fovea on OCT is dependent on maturity. Although it is present histologically at 27 weeks post menstrual age (PMA) it has been reported not be visible in the central fovea on OCT until between 40 weeks and 43 weeks GA.^{49, 195} This is in contrast to histological findings, where the IS and OS can always be visualised at the fovea from birth in term infants. These IS and OS may be too short and immature in this age group to form a visible band on OCT.¹⁹⁵ We have shown in our study that the outer segment of the photoreceptors is frequently not identifiable in the central fovea on OCT in infants less than 46 weeks GA, but is always identifiable after 47 weeks GA.

The presence of the hyper reflective contact cylinder band (located between the ISE and RPE bands) on OCT is also a feature of foveal maturity. This structure was nearly always present after 45 months GA. This is consistent with previous work suggesting that this is identifiable on OCT at between 24 months and 5 years.¹⁹⁵ However this contrasts with reported findings in premature human foveal development, where this band was not found to be visible in any infants less than 10 years of age.⁴⁹ This suggests that perhaps development of the outer retinal layers may differ between

premature children and term children on OCT. Larger scale longitudinal OCT studies of premature foveal development would be needed in order to definitively answer this question.

We have shown that the RPE also increase in thickness until 57 months GA followed by a plateau. RPE thickening may be essential to normal visual development and retinal maturation as it is known that in macular dystrophies, there is atrophy of the RPE.¹⁹⁶

We have also been able to correlate grating visual acuity with the IRLs, ORLs, RT, ONL, IS, OS and RPE measurements. In the future it would be interesting to compare these correlations with those calculated in children with retinal pathology to see what effect the disease process has on the development of the retina and consequently, visual acuity. For example, it has previously been shown in adults with albinism that the length of the OS is strongly correlated with VA.¹²⁸

Although we have correlated several retinal layer measurements with the development of visual acuity, none of these can fully account for all of visual development. This is because other factors such as changes in the dorsal lateral geniculate nucleus and the striate cortex may be contributing to visual development.^{176, 177} Future studies may aim to define the exact contributions of retina and the cortex to overall visual development by monitoring both retinal, cortical and visual development simultaneously using OCT and magnetic resonance imaging.

To our knowledge, this is the first report of a large in vivo study of normal term human foveal development. Foveal development is a complex, nonlinear process which continues at least until 12 years of age, mimicking findings of longitudinal MRI brain development studies.¹⁹⁷ Visual functions such as hyper-acuity continue to develop until 21 years of age.¹⁹⁸ Although this has been attributed to refinement of neural circuitry at the cortical level, it is possible that ongoing retinal development is contributing. Our description of normal development will be helpful in detecting, monitoring and understanding retinal changes in pathology.

Chapter 5

Potential of Hand-Held Optical Coherence Tomography to Determine Aetiology of Infantile Nystagmus in Children based on Foveal Morphology

5.1. Introduction

5.2. Methods

5.3. Results

5.4. Conclusion

5.1. Introduction

Spectral-domain optical coherence tomography has revolutionised the investigation, diagnosis and management of many eye conditions over the past 10 years. Previously in section 1.2, the feasibility of the HH-SDOCT in identifying retinal morphology and abnormalities in infants and young children has been outlined. However very little work has been carried out on imaging young children with nystagmus. With gene therapy imminent for a number of paediatric retinal disorders¹⁹⁹⁻²⁰¹ associated with nystagmus it becomes important to investigate whether the HH-SDOCT is useful for diagnosis and monitoring of retinal abnormalities in these patients.

In older patients it has been shown that OCT is very helpful in determining foveal morphology in infantile nystagmus and hence differentiating the aetiology.¹²³⁻¹²⁹ This can be done based on the presence or absence of foveal hypoplasia; whether it is typical or atypical, or if there are other retinal abnormalities present (see section 1.3 Infantile Nystagmus).

In this study we investigated the feasibility and the clinical use of HH-SDOCT in children with nystagmus less than 6 years of age compared to age-matched healthy volunteers as it is known that the fovea continues to develop and mature at least until the age of four years.³⁶ Our aims were to develop an OCT based diagnostic algorithm for assessing infantile nystagmus and to determine the sensitivity and specificity of the HH-SDOCT in the classification of foveal abnormalities.

5.2. Methods

5.2.1. Subjects and clinical examination

The cohort for this study included 50 patients with nystagmus and 50 age-matched healthy controls. The mean age in the nystagmus group was 3.2 years (standard deviation; 2 years; range; 0-8 years), and in the control group was 3.2 years (standard deviation; 1.8 years; range; 0-8 years). All children were scanned in an outpatient clinic setting without sedation. The demographic data are summarised in Tables 1-7 in Appendix 2.

All patients underwent ophthalmologic examination, which included slit-lamp examination where possible, determination of presence or absence of iris transillumination (TID) defects (also in parents if possible, as carriers of albinism frequently have iris transillumination^{185 186}), presence and type of nystagmus, fundus examination and measurement of visual acuity. Visual acuity (VA) was assessed in younger infants and children by preferential looking using Teller acuity cards and/or crowded Logarithm of the Minimum Angle of Resolution (logMAR) Kay Picture Tests if possible. In cooperative children, logMAR crowded optotypes (Glasgow Acuity Cards) were used to obtain VA. Electroretinograms (ERGs) and 5-channel VEPs (to detect increased optic nerve crossing in albinism) according to International Society for Clinical Electrophysiology of Vision (ISCEV) standards were obtained if possible.¹⁸⁷

Albinism was diagnosed by abnormal decussation at the chiasm on VEPs and clinical signs such as iris transillumination, fundus appearance, hair and skin pigmentation and/or genetic testing. Where a diagnosis of albinism was suspected, genetic testing for mutations of the tyrosinase gene (*TYR*) was offered in all cases (tests for other genes was not available). Pigmentary characteristics of patients were classified using a modified Schmitz classification (Table 2 in Appendix 2). Suspicion of *PAX6* associated disease was derived from iris abnormalities, atypical nystagmus with vertical component, dominant inheritance pattern in the family and/or genetic testing. Achromatopsia was diagnosed by extinguished or severely reduced photopic electroretinograms, photophobia, typical small fast nystagmus and genetic testing for all known achromatopsia gene mutations. Rod-cone and cone-rod dystrophy were diagnosed based on clinical history and examination, and ERG findings. Idiopathic

nystagmus was diagnosed with typical horizontal conjugate nystagmus which did not change upon covering one eye, if no abnormality other than nystagmus and squint was found and/or electrophysiology was within normal limits. Genetic testing for mutations in *FRMD7* was offered in all suspected cases of IIN. Manifest latent nystagmus was diagnosed if children had congenital squint syndrome, typical nystagmus which increased upon covering one eye and beating in the direction of the open or fixing eye and normal slit lamp and fundus examination.

5.22. Hand-Held Spectral Domain Optical Coherence tomography (HH-SDOCT)

The retinae of the study subjects were scanned using a portable, hand-held, non-contact spectral domain optical coherence tomography device (Bioptigen™ Inc, Research Triangle Park, North Carolina, USA) as previously described.¹⁹² The acquired images were exported from the Bioptigen™ HH-SDOCT software and imported into ImageJ software (available at: <http://rsbweb.nih.gov/ij/>; Date accessed: May 11, 2012). The fovea was identified based on visual inspection of the scans for its characteristic features as described by Mohammad et al.¹²⁷ which includes the presence of: 1) foveal pit; 2) thinning of the inner retinal layers; 3) doming of the outer nuclear layer and 4) lengthening of the photoreceptor outer segments (Figure 3.1). Images of both eyes, where available were compared. OCT images were classified into one of the 4 following categories: 1) typical foveal hypoplasia (predicting albinism, *PAX6* mutations or isolated foveal hypoplasia); 2) atypical foveal hypoplasia (predicting achromatopsia); 3) other foveal changes (predicting retinal dystrophy); 4) normal fovea (predicting idiopathic or latent nystagmus), where:

Category 1: Typical foveal hypoplasia was graded as described by Thomas et al.¹²⁸ In grade 1, there is an absence of extrusion of the plexiform layers. In grade 2, there is an absence of the foveal pit. In grade 3, there is additional absence of outer segment (OS) lengthening. In grade 4, in addition to the features of grade 3 foveal hypoplasia, there is an absence of the ONL widening (Figure 4.1).

Category 2: Foveal hypoplasia was classified as atypical if there was in addition to abnormal inner retinal layers in the macular area (as described above for typical hypoplasia), IS/OS disruption or a hypo-reflective zone present in the foveal area.

Category 3: Other foveal changes that do not include the aforementioned features of foveal hypoplasia, were defined as the presence of a thinned ONL, loss of the IS/OS signal, thickened inner retinal layers and blurring of detectable boundaries between the thinned ONL and the thickened INL (abnormal lamination).

Category 4: Normal foveal morphology.

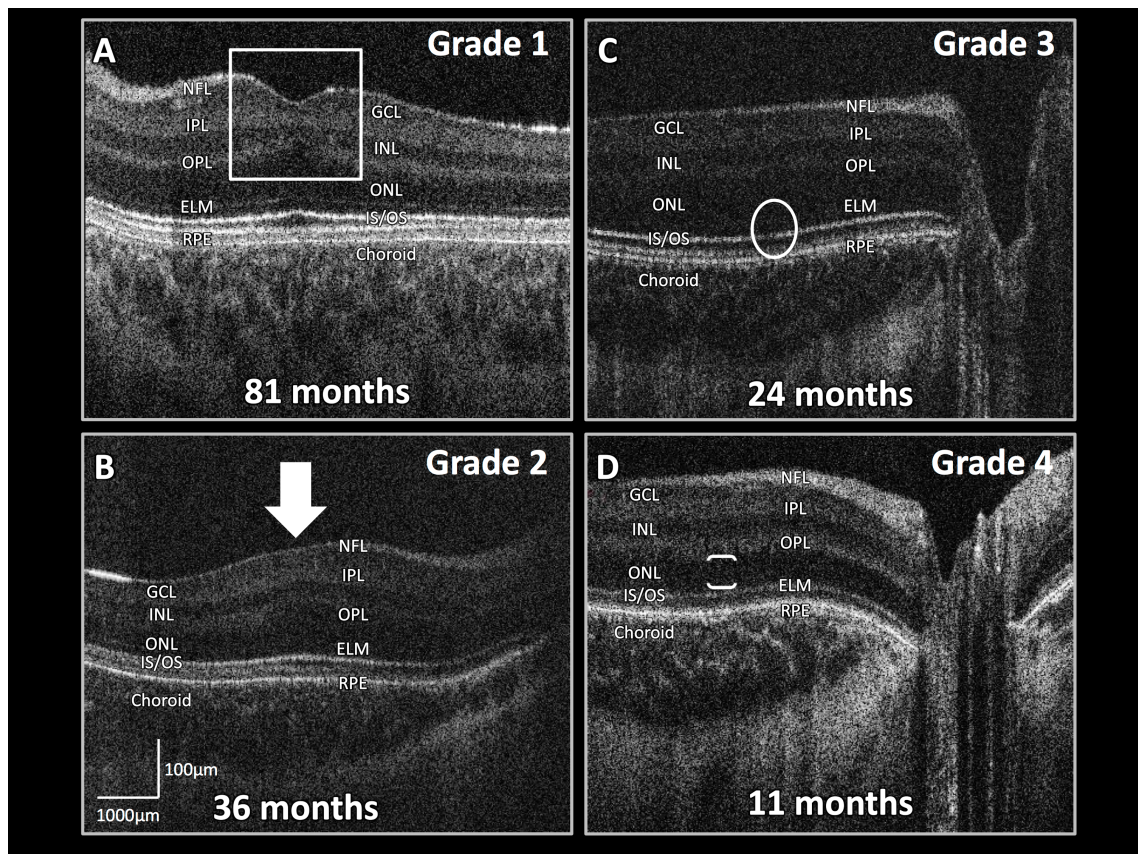


Figure 5.1: Structural Grading of foveal hypoplasia based on different stages of arrested development.

(5.1A). Grade 1 foveal hypoplasia. There is a continuation of the normally absent inner retinal layers including the NFL, GCL, IPL, INL and OPL at the fovea (white square). **(5.1B).** Grade 2 foveal hypoplasia. In addition to the continuation of the inner retinal layers, there is absence of the foveal pit (white block arrow). **(5.1C).** Grade 3 foveal hypoplasia. In addition to the features of grade 2 foveal hypoplasia, there is absence of lengthening of the outer segment of the cone photoreceptors (white oval). **(5.1D).** Grade 4 foveal hypoplasia. In addition to the features of grade 3 foveal hypoplasia there is absence of ONL widening as indicated by the brackets.

NFL= nerve fiber layer; GCL= ganglion cell layer; IPL= inner plexiform layer; INL= inner nuclear layer; OPL= outer plexiform layer; ONL= outer nuclear layer; ELM= external limiting membrane; IS/OS= inner segment/outer segment junction (ellipsoid); RPE= retinal pigment epithelium.

A OCT based diagnostic algorithm for infantile nystagmus was established using the classification as outlined above. The tomograms from each patient were compared to age-matched controls in order to ensure that described abnormalities were not due to incomplete maturation of foveal development. All control subjects that were recruited had equal vision in both eyes (where measurement was possible), no significant refractive error (defined as hyperopia of +4.0 D or greater in any axis, myopia of -3.0 D or greater in any axis or anisometropia of 1.5 D or more difference between corresponding axes in the two eyes), a normal orthoptic and ophthalmological examination and no known neurologic or metabolic conditions..

Sensitivity and specificity of predicting diagnosis by visual analysis of HH-SDOCT scans was calculated based on the classification of foveal abnormalities by three investigators not involved in clinical examinations in this study and masked to the clinical characteristics of patients (FAP (non-clinical lecturer), GM (research orthoptist) and AP (academic clinical fellow, second year of ophthalmology training)). The three investigators were asked to classify images into the same categories as specified above based on HH-SDOCT images only with no other knowledge of the patients. They were provided with randomised and anonymised scans from the nystagmus cohort. Each scan was paired with an age-matched control to allow comparisons. The instructions given to the three investigators for classification matched the descriptions for categories 1 to 4 as outlined above. The sensitivity, specificity, positive predictive value (PPV) of each OCT based predicted diagnostic category was calculated.

5.3. Results

5.31. Feasibility

There was initial failure to obtain scans in either eye in 3 (3/50) of the patients (47/50; 94% success rate). These patients were aged 12 months, 23 months and 24 months. We were successful in obtaining scans on one or both eyes on a subsequent day (100% success rate for imaging at least one eye). We successfully obtained scans in both eyes in 45 (45/50) of the patients and 45 (45/50) of the controls (90% success rate for both groups). All subjects were scanned without sedation. In 100% of controls and 98% of patients the scans were successfully obtained without mydriasis. One patient was scanned with mydriasis because she was already dilated during the clinical examination. Successful HH-SDOCT scans took between 2-5 minutes in cooperative children and up to 20 minutes in less cooperative children. Scanning was most difficult in children aged between 1 and 2 years.

5.32. Comparison of Both Eyes of Control Subjects and Patients

In all patients and normal subjects where scans were available for both eyes there was no inter eye difference in the configuration of the foveal tomograms. Some examples of foveal tomograms taken in children of different ages are shown in figure 5.2.

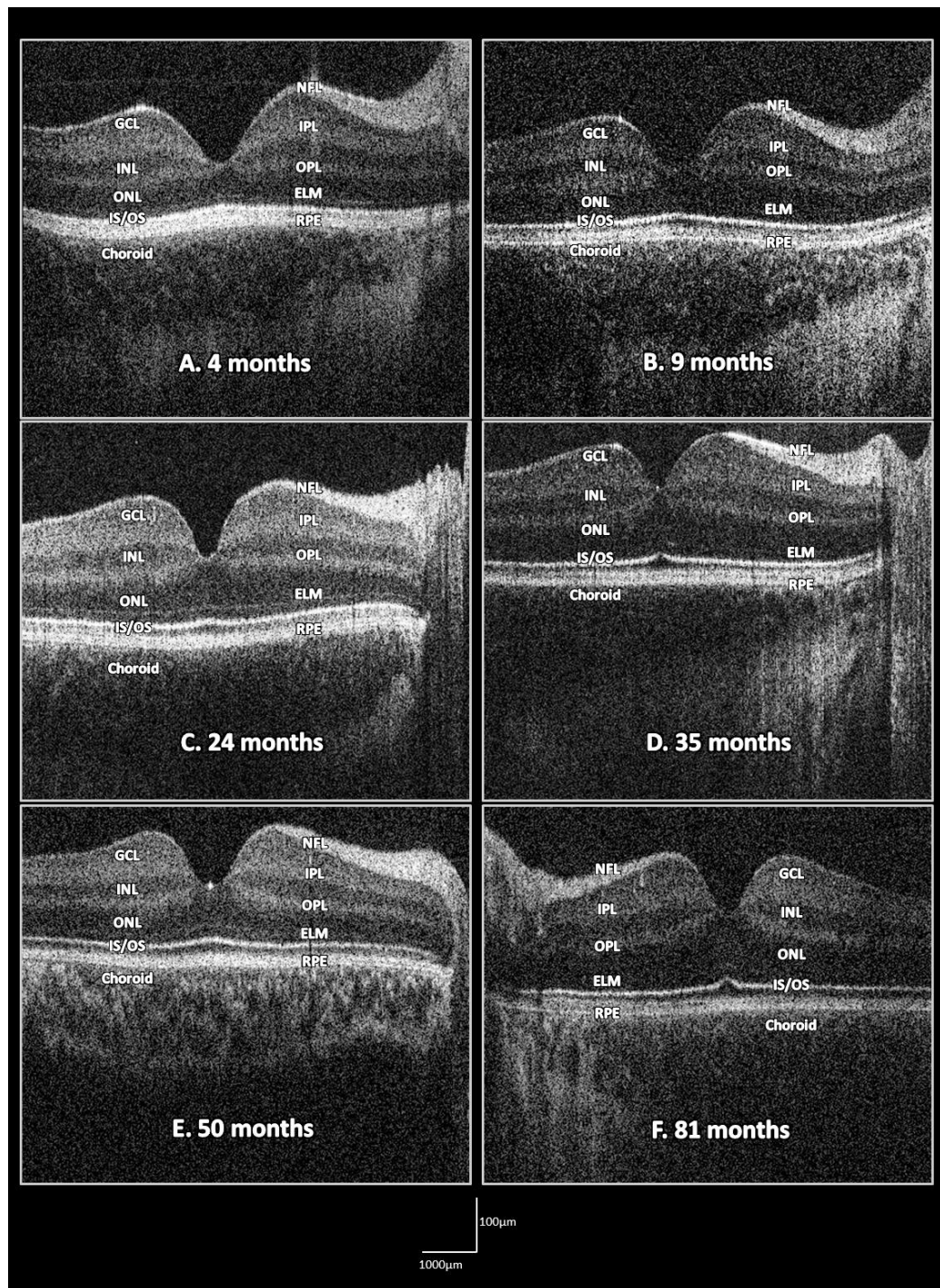


Figure 5.2: Examples of foveal OCTs in normal control infants and young children of different ages.

There is no evidence of foveal hypoplasia in any of these tomograms. The RPE is of normal calibre. The IS/OS junction is clearly present in the foveal and parafoveal areas. There is normal lamination of all the retinal layers. The length of the IS/OS as well as

the ONL appears to increase with age. There is also appears to be inter-subject variation in foveal morphology.

OCT = optical coherence tomography; NFL= nerve fiber layer; GCL= ganglion cell layer; IPL= inner plexiform layer; INL= inner nuclear layer; OPL= outer plexiform layer; ONL= outer nuclear layer; ELM= external limiting membrane; IS/OS= inner segment/outer segment junction (ellipsoid); RPE= retinal pigment epithelium.

5.33. Controls

None of the healthy control subjects had any evidence of foveal hypoplasia or other foveal abnormality as described in categories 2 and 3 above.

5.34. Patients with Typical Foveal Hypoplasia (Category 1)

Twenty-three (23/50) patients were identified with typical foveal hypoplasia (Table 5.1). Nine (9/23) patients had grade 1 foveal hypoplasia, five (5/23) had grade 2, four (4/23) had grade 3 and five (5/23) had grade 4. The clinical characteristics of these patients are summarised in Tables 2 & 3 in Appendix 2. Figure 5.1 shows examples of each of the grades of foveal hypoplasia. Figure 5.3 demonstrates an example of how the location of the fovea is confirmed in grade 3 foveal hypoplasia.

The final clinical diagnosis was albinism in 21 patients and *PAX6* mutations in 2 patients. Eighteen of the 21 (85%) albinism suspects had at least 2 clinical/VEP findings consistent with the diagnosis of albinism while three children had only one clinical finding (Table 5.4).

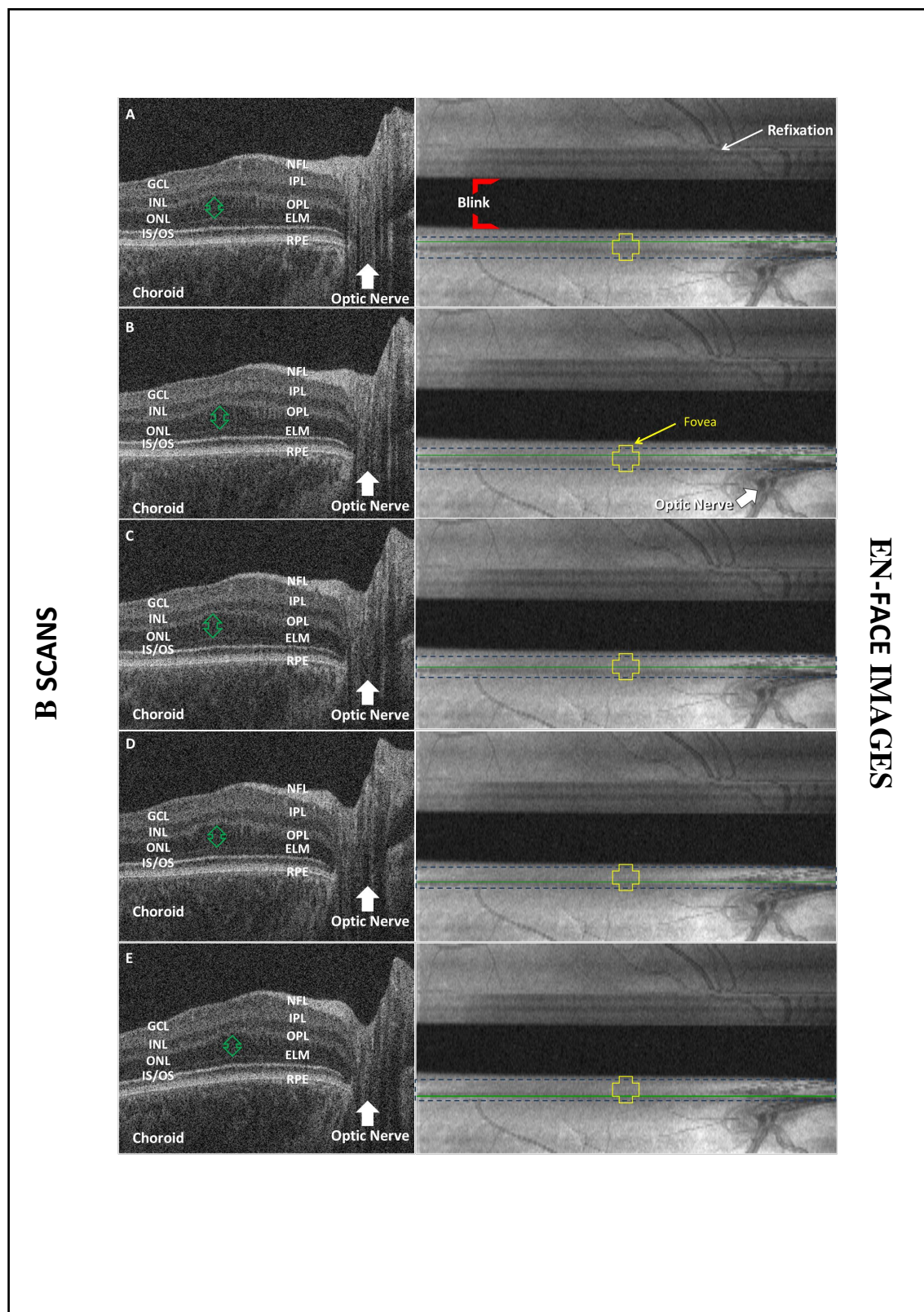


Figure 5.3: Example of the identification of the central foveal B-scan in the right eye of a child with grade 3 foveal hypoplasia.

The B-scan containing the foveal centre (5.3C) was captured together with a minimum of 5 uninterrupted B-scans superior and inferior to the central foveal B scan. The double-ended green arrow in each B-scan indicates the outer nuclear layer (ONL) thickness. The ONL is at its maximum thickness in 5.3C confirming that this is the location of the fovea. The two B-scans immediately superior (5.3A and 5.3B) and inferior (5.3D and 5.3E) to the central foveal B-scan are shown for comparison. The optic nerve is used as an anatomical landmark for orientation as the fovea is normally located temporal to the optic nerve. The location of each B-scan is outlined with a single green line on the corresponding en-face retinal image that was acquired. The yellow cross is marking the approximate position of the foveal centre on the en-face images. The fovea appears to be positioned slightly superior to the optic nerve due to the slightly tilted (clockwise) position of the probe during image acquisition. The blue rectangle is outlining the area where the 10 B-scans surrounding the central foveal B-scan were taken. The red brackets on the top scan indicate where a blink occurred and a white arrow indicates a refixations artefact.

NFL= nerve fiber layer; GCL= ganglion cell layer; IPL= inner plexiform layer; INL= inner nuclear layer; OPL= outer plexiform layer; ONL= outer nuclear layer; ELM= external limiting membrane; IS/OS= inner segment/outer segment junction (ellipsoid); RPE= retinal pigment epithelium.

5.35. Patients with Atypical Foveal Hypoplasia (Category 2)

Five patients were identified with atypical foveal hypoplasia on HH-SDOCT (Figure 5.4). The clinical characteristics of these patients are summarised in Table 5 in Appendix 2. All patients had evidence of foveal hypoplasia and abnormalities of the IS/OS junction (Figure 5.4A and 5.4B). In the youngest (2 months old) the IS/OS was abnormal in that it was non-distinct in comparison age-matched controls. Four of the patients had evidence of a hypo-reflective area disrupting the IS/OS (Figure 5.4B), which was larger in older children. A hypo-reflective zone was not seen in the youngest 2 month old child (Figure 5.4A).

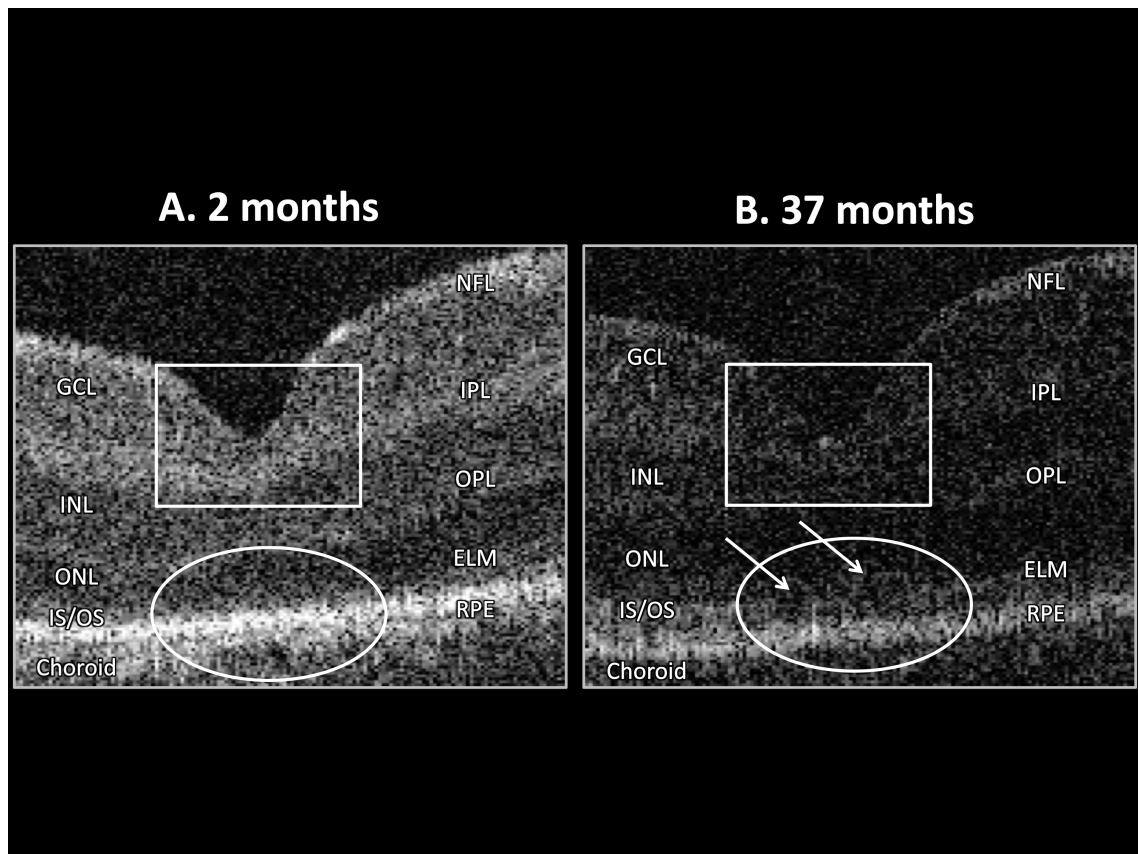


Figure 5.4: Atypical foveal hypoplasia in 2 young achromatopsia patients.

(5.4A). There is evidence of atypical foveal hypoplasia with continuation of inner retinal layers (white square) and interruption of the IS/OS junction (white oval) at the foveola. (5.4B). There is evidence of a punched out lesion (white arrows) representing a hypo-reflective zone at the foveola which is disrupting the normally contiguous IS/OS junction (white oval). In both patients there is absence of elongation of the outer segment of the cone photoreceptors. NFL= nerve fibre layer; GCL= ganglion cell layer; IPL= inner plexiform layer; INL= inner nuclear layer; OPL= outer plexiform layer; ONL= outer nuclear layer; ELM= external limiting membrane; IS/OS= inner segment/ outer segment junction (ellipsoid); RPE= retinal pigment epithelium.

5.36. Patients with Other Abnormal Foveal Morphology (Category 3)

Six patients had abnormal foveal morphology on HH-SDOCT (Table 5.1). The clinical characteristics of these patients have been summarised in Table 6 in Appendix 2. There was visible thinning of the RPE (Figure 5.5A, 5.5B, 5.5C and 5.5D) in comparison to age-matched controls. In addition a hyper-reflective area disrupting the IS/OS was evident at the fovea as well as abnormal lamination of the inner retinal layers (Figure 5.5B). Foveal hypoplasia was also identified in two cases (Figure 5.5A). The IS/OS band was less well developed and was not clearly evident beyond the foveola (Figure 5.5C and 5.5D). In each of these cases a rod-cone or cone-rod dystrophy was suspected.

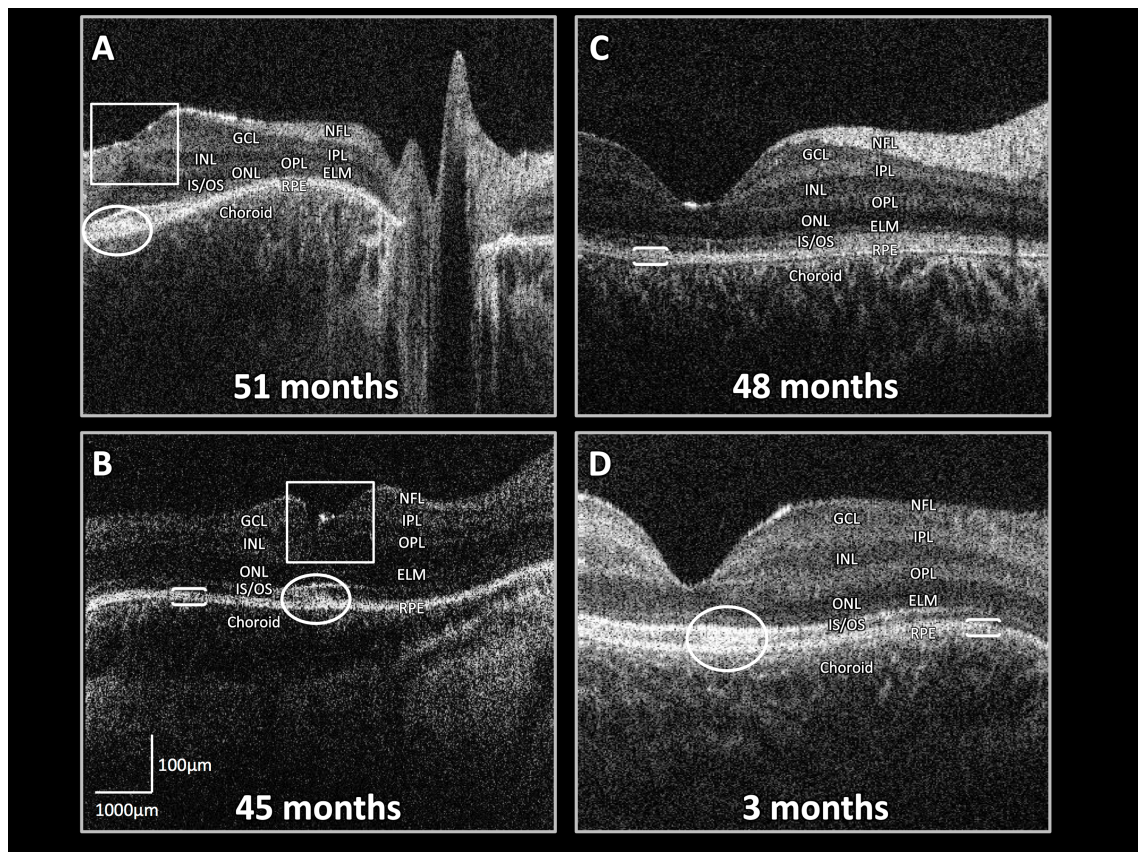


Figure 5.5: Atypical macular morphology in 2 patients with microcephaly (4.5A and 4.5B) and 2 patients with retinal dystrophy (4.5C and 4.5D).

(5.5A) and (5.5B). In both patients there is evidence of foveal hypoplasia (open squares). The RPE appears thinned and there is evidence of a hyper reflective zone disrupting the IS/OS at the fovea (white oval). The inner retinal layers have a mottled appearance disrupting the continuity of the inner plexiform/ganglion cell layers (open square). (5.5C). The RPE appears thinned (brackets) and the IS/OS band is not evident beyond the foveola. . There is evidence of a hyper reflective substance disrupting the IS/OS beyond the fovea (white oval)). (5.5D). The RPE appears thinned (open arrows). There is evidence of hyper-reflectivity present in the fovea affecting the IS/OS (white oval). In all cases the IS/OS is less well developed in comparison to equivalent age matched controls.

NFL= nerve fiber layer; GCL= ganglion cell layer; IPL= inner plexiform layer; INL= inner nuclear layer; OPL= outer plexiform layer; ONL= outer nuclear layer; ELM=

*external limiting membrane; IS/OS= inner segment/outer segment junction (ellipsoid);
RPE= retinal pigment epithelium.*

5.37. Patients with Normal Foveal Morphology (Category 4)

Sixteen patients with nystagmus had no evidence of either typical or atypical foveal hypoplasia or any other signs of abnormal foveal morphology (Table 5.1). The clinical characteristics of these patients are summarised in Table 7 in Appendix 2. None of these patients had any obvious differences in foveal morphology compared to controls (Figure 5.6). There was no evidence of foveal hypoplasia. The RPE was normal. The IS/OS was well developed in the foveal and parafoveal area. There was normal lamination of all the retinal layers. Twelve patients in this group were clinically diagnosed with idiopathic nystagmus (IIN) with typical horizontal nystagmus. The remaining four patients were diagnosed with manifest latent nystagmus (fusion maldevelopment syndrome) on the basis of ocular motility examination.

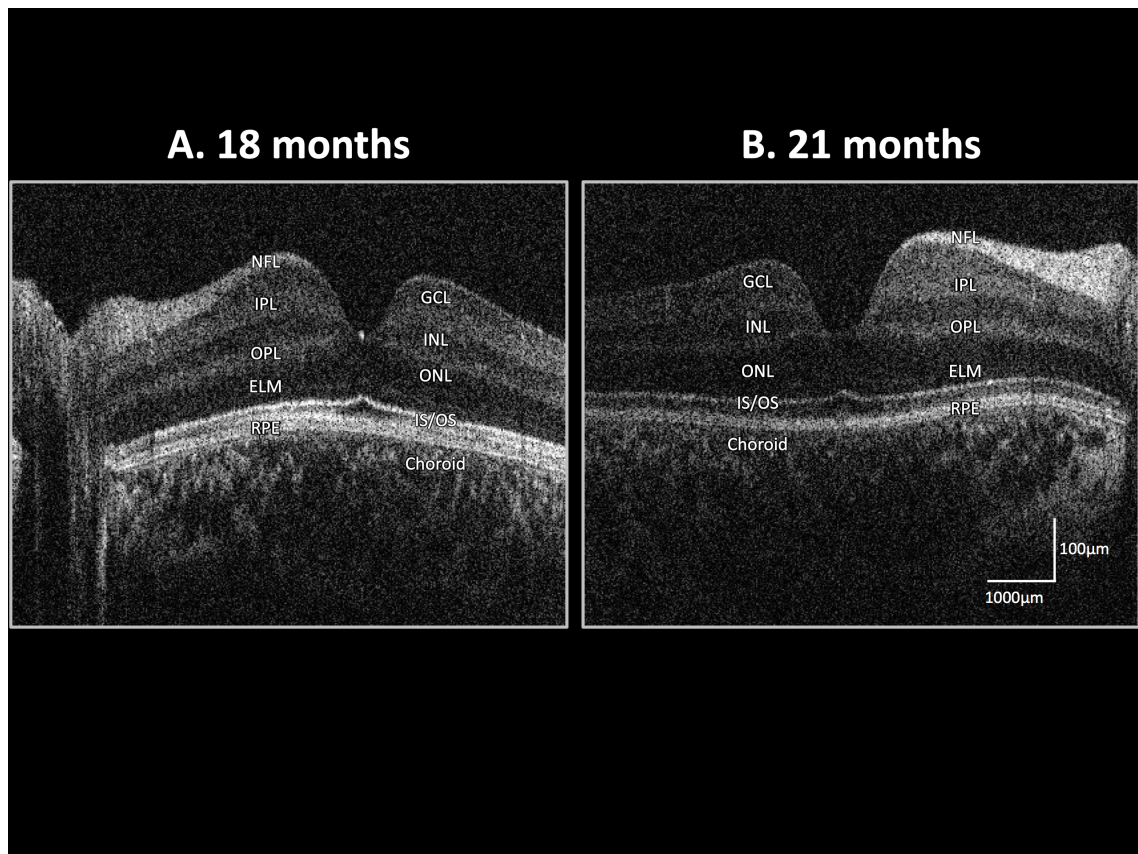


Figure 5.6: Normal foveal structure in a patient with IIN (5.6A) and a patient with manifest latent nystagmus (5.6B).

There is no evidence of foveal hypoplasia in either patient. The RPE is of normal calibre. The IS/OS is well developed in the foveal and parafoveal area. There is normal lamination of all the retinal layers.

NFL= nerve fiber layer; GCL= ganglion cell layer; IPL= inner plexiform layer; INL= inner nuclear layer; OPL= outer plexiform layer; ONL= outer nuclear layer; ELM= external limiting membrane; IS/OS= inner segment/outer segment junction; RPE= retinal pigment epithelium.

5.38. Sensitivity, Specificity and Predictive Value of the OCT by Masked Reviewers

Sensitivities of HH-SDOCT for classifying typical, atypical foveal hypoplasia, other abnormal foveal morphology and normal morphology were 92.8%, 86.7%, 41.1% and 88.4%, respectively, with specificities of 91.4%, 94.8%, 97.7% and 95.1%, respectively (Tables 5.1 & 5.2).

Table 5.1: Sensitivity, specificity and predictive value of the hand-held OCT in infants and young children with nystagmus

Category	Sensitivity	Specificity	PPV	NPV
Typical Foveal Hypoplasia	92.8%	91.4%	90.2%	93.6%
Atypical Foveal Hypoplasia	86.7%	94.8%	69.3%	98.4%
Other Abnormal Morphology	41.1%	97.7%	72.2%	92.5%
Normal Macular Morphology	88.4%	95.1%	89.1%	95.4%

PPV = positive predictive value; NPV - negative predictive value; OCT = optical coherence tomography

Table 5.2: Breakdown of the results of the masked analysis by category and by grader.

Category (n)	True Positive (n)	False Positive (n) Correct Scan Category (n)	False Negative (n) Incorrect Scan Category (n)	Uncertain (n)
Grader 1				
Foveal Hypoplasia (n=23)	n=22	n=1 Abnormal Morphology (n=1)	n=1 Abnormal Morphology (n=1)	n=0
Atypical Foveal Hypoplasia (n=5)	n=4	n=1 Abnormal Morphology (n=1)	n=1 Abnormal Morphology (n=1)	n=0
Abnormal Morphology (n=6)	n=2	n=2 Foveal Hypoplasia (n=1) Atypical Foveal Hypoplasia (n=1)	n=4 Foveal Hypoplasia (n=1) Atypical Foveal Hypoplasia (n=1) Normal (n=2)	n=0
Normal Morphology (n=16)	n=15	n=2 Abnormal Morphology (n=2)	n=0	n=1
Grader 2				
Foveal Hypoplasia (n=23)	n=19	n=5 Atypical Foveal Hypoplasia (n=1) Abnormal Morphology (n=1) Normal Morphology (n=3)	n=4 Atypical Foveal Hypoplasia (n=3) Abnormal Morphology (n=1)	n=0
Atypical Foveal Hypoplasia (n=5)	n=4	n=5 Foveal Hypoplasia (n=3) Abnormal Morphology (n=1) Normal Morphology (n=1)	n=1 Foveal Hypoplasia (n=1)	n=0
Abnormal Morphology (n=6)	n=2	n=1 Foveal Hypoplasia (n=1)	n=3 Foveal Hypoplasia (n=1) Atypical Foveal Hypoplasia (n=1) Normal Morphology (n=1)	n=1

Normal Morphology (n=16)	n=10	n=1 Abnormal Morphology (n=1)	n=4 Foveal Hypoplasia (n=3) Atypical Foveal Hypoplasia (n=1)	n=2
Grader 3				
Foveal Hypoplasia (n=23)	n=23	n=1 Normal Morphology (n=1)	n=0	n=0
Atypical Foveal Hypoplasia (n=5)	n=5	n=1 Abnormal Morphology (n=1)	n=0	n=0
Abnormal Morphology (n=6)	n=3	n=0	n=3 Atypical Foveal Hypoplasia (n=1) Normal Morphology (n=2)	n=0
Normal Morphology (n=16)	n=15	n=2 Abnormal Morphology (n=2)	n=1 Foveal Hypoplasia (n=1)	n=0

n = number of participants

5.39. A Diagnostic Algorithm for Infantile Nystagmus Using OCT

Figure 5.7 shows how infantile nystagmus syndrome (INS) can be separated into 4 diagnostic categories on the basis of OCT findings alone. If typical foveal hypoplasia is present, the diagnosis can be directed towards albinism, *PAX6* mutation or isolated foveal hypoplasia, and VEPs and genetic testing are the first line of investigation. However, work done by Thomas et al.¹⁷³ have demonstrated grade 1 foveal hypoplasia in some older patients with *FRMD7* mutation (idiopathic infantile nystagmus). Therefore, in the presence of grade 1 foveal hypoplasia with no evidence of crossed asymmetry on VEP and negative testing for *PAX6* mutations, genetic screening of *FRMD7* should be considered.

If atypical foveal hypoplasia is observed (foveal hypoplasia associated with disruption of the IS/OS) then the diagnosis of achromatopsia should be considered, where the most relevant investigations are ERG with/without genetic testing.

If other abnormal foveal morphology is seen, with or without signs of foveal hypoplasia, including abnormal inner retinal lamination and thinning of the RPE and a less well developed IS/OS junction, retinal dystrophy should be considered, and ERG with/without genetic testing being undertaken. In the absence of foveal hypoplasia, the presence of other aforementioned abnormalities of macular structure that may suggest a retinal dystrophy need to be further investigated with ERG with/without genetic testing, before diagnosing idiopathic infantile or manifest latent nystagmus.

Our study suggests that for typical idiopathic nystagmus with entirely normal foveal morphology, electrodiagnostic tests may not be necessary; they were normal in all our patients. Genetic screening of *FRMD7* should be considered. In patients with typical manifest latent nystagmus and congenital squint syndrome no further tests are necessary, with a normal fovea on OCT.

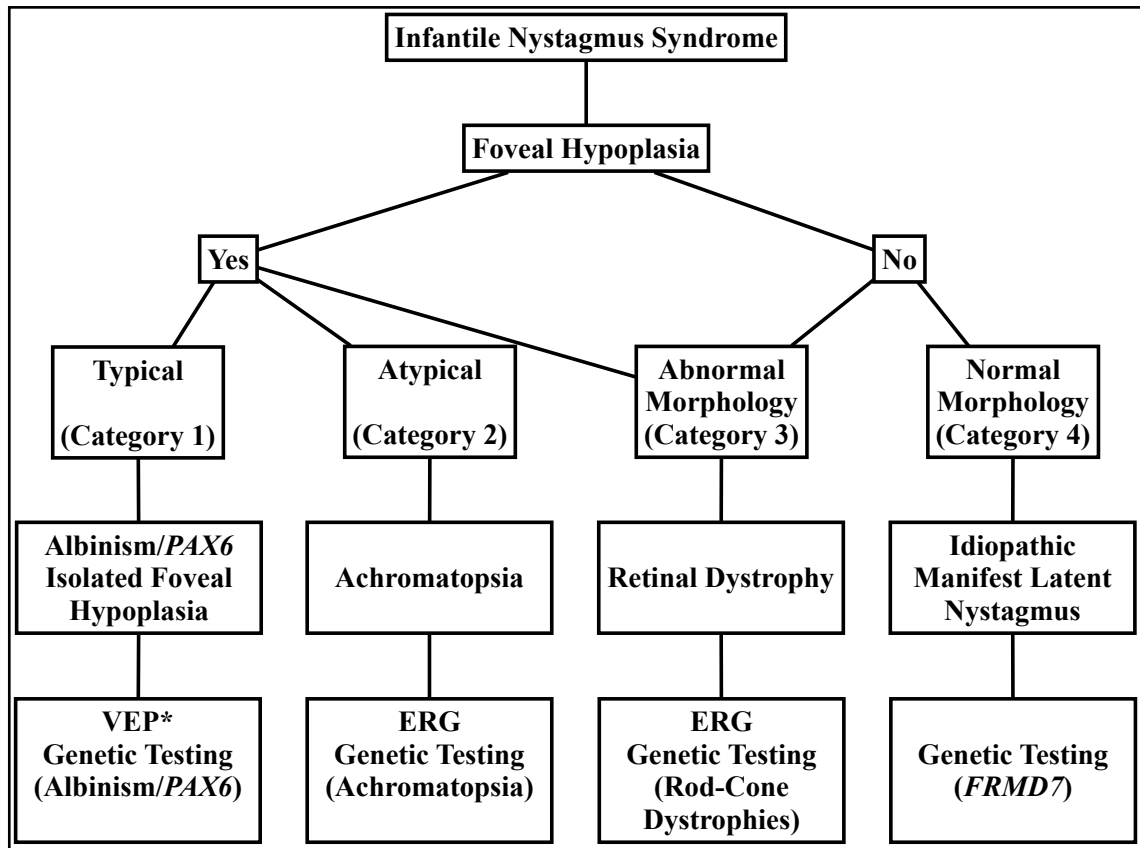


Figure 5.7: Schematic diagram illustrating the categorisation of infantile nystagmus syndrome (INS) into 4 diagnostic categories on the basis of OCT findings.

Depending on the presence or absence of foveal hypoplasia; or the presence or absence of other abnormal macular morphology, the aetiology of nystagmus can be predicted and diagnostic tests can be selected to confirm the diagnosis.

** In the presence of grade 1 foveal hypoplasia with no evidence of crossed asymmetry on VEP testing for mutations on the FRMD7 gene should be considered.*

OCT= optical coherence tomography; VEP = visual evoked potentials; ERG = electroretinogram

5.4. Discussion

Although OCT has been shown to be an important diagnostic adjunct for diagnosis and characterisation of retinal pathology associated with nystagmus in older children and adults,¹²³⁻¹²⁵ to date its use in children less than 6 years of age has been very limited. This paper has shown that the HH-SDOCT is highly sensitive and specific in classifying foveal abnormalities in infantile nystagmus. We have developed a simple algorithm which can direct further investigations and diagnosis in infants and young children between birth and 6 years of age.

In this paper we have reliably imaged infants with nystagmus as young as 2 months of age and have shown that using the HH-SDOCT as the first line of investigation in the diagnostic evaluation of infantile nystagmus is useful. The identification of the abnormalities such as foveal hypoplasia (without other changes of macular morphology that would indicate retinal dystrophy) on HH-SDOCT can eliminate the need for ERG testing as the differential diagnoses are albinism, *PAX6* mutation or isolated foveal hypoplasia. In these cases, we suggest VEP testing in the first instance to distinguish between albinism and *PAX6* mutation, followed by genetic screening for *PAX6* if the VEP is normal and does not demonstrate crossed asymmetry. In cases where there are several other clinical features such as characteristic hypopigmentation and iris TID consistent with albinism VEP may not be required as the presence of foveal hypoplasia on HH-SDOCT may be sufficient to confirm the diagnosis.

If atypical foveal hypoplasia or other abnormal foveal morphology such as abnormal lamination of the inner retinal layers or thinning of the RPE is identified on HH-SDOCT we suggest proceeding to ERG examination in order to confirm the diagnosis of achromatopsia or retinal dystrophy. With the exception of one child, all of the children with a confirmed diagnosis of achromatopsia in our study had the presence of the characteristic hypo-reflective sign and disruption of the IS/OS associated with this condition. These signs appear to be specific for achromatopsia and we would suggest that if they are clearly identified on OCT examination that ERG is not necessary and one can proceed directly to genetic screening. If there is any diagnostic ambiguity then ERG can help to clarify the diagnosis.

As all patients in our study with normal HH-SDOCT had normal ERG our results also indicate that if there are no abnormalities identified on HH-SDOCT further electrodiagnostic evaluation is not necessary especially if the clinical evaluation is consistent with a diagnosis of idiopathic or latent nystagmus. However, it would be prudent to test this hypothesis on a larger cohort.

Image acquisition in infants and young children using the HH-SDOCT was highly successful and very quick, taking between 2 to 5 minutes in cooperative children and up to 20 minutes in less cooperative children. Image acquisition from children aged between 1 and 2 years were the most challenging age group. Gerth et al⁹⁸ dilated the pupils in 27 of the 30 children that they imaged using the HH-SDOCT. In addition 10 of the children aged between 7 months and 3.7 years had their examinations under chloral hydrate sedation as part of their clinical assessment. We found that neither sedation nor mydriasis was necessary for obtaining high quality scans. As it is non-invasive and fast we are currently using HH-SDOCT for all children with nystagmus before they are seen in clinic.

We have shown that the HH-SDOCT can identify foveal hypoplasia in infants and young children with nystagmus. Out of 50 patients with nystagmus, 23 had typical foveal hypoplasia. 21 of these patients had a clinical diagnosis consistent with albinism. In the patients suspected to have albinism, 62% had reliable VEPs and demonstrated crossed asymmetry. It is known that the sensitivity of the flash VEP to detect crossed asymmetry decreases with younger age in particular in children less than 6 years of age with reported sensitivities ranging between 67% to 83%.²⁰²⁻²⁰⁴ Genetic screening for albinism also yields sensitivity results similar to VEPs. Sequencing of the known genes associated with oculocutaneous albinism detects mutations in 50%¹⁴⁰ to 70%²⁰⁵ of patients with albinism.

In comparison to VEPs and genetic testing the HH-SDOCT provides a sensitive, more rapid, well tolerated and less costly diagnosis in infants and young children with nystagmus. We have demonstrated high sensitivity and specificity for each of the diagnostic categories with the exception of other abnormal macular morphology. Although detection of other abnormal morphology was highly specific (97.7%), the

sensitivity rate was reduced (41.1%) in comparison to the other 3 groups which all had sensitivities above 86%.

The low sensitivity (41.1%) of the masked graders in correctly classifying the children with other abnormal morphology may be explained by the low numbers (6 patients) and non-homogeneity of the retinal findings in this group. The overlapping finding of foveal hypoplasia in two of the patients with microcephaly resulted in two of the graders classifying these patients into the foveal hypoplasia group. In two cases of rod-cone dystrophy, where the only finding was a subtle thinning of the retinal pigment epithelium, two of the graders classified these as normal. As age defined normal quantitative values for each retinal layer become available, one would expect this sensitivity to improve as this would allow clearer definition of inclusion guidelines for this category.

HH-SDOCT can diagnose typical foveal hypoplasia reliably (positive predictive value 90.2%) but does not distinguish albinism from *PAX6* or isolated foveal hypoplasia. In conjunction with other clinical signs such as typical hypo-pigmentation and iris transillumination defects, OCT can direct the diagnosis towards albinism at an early stage. This will become increasingly important in an era where gene therapy may become a potential treatment in albinism. It has been shown that intraocular administration of an adeno-associated virus (AAV)-based vector, encoding the human *TYR* gene in a mouse model of albinism resulted in ocular melanin accumulation. This prevented progressive photoreceptor degeneration as quantified on ERG analysis and resulted in restoration of retinal function.¹⁹⁹ The timing of such treatment may be crucial in the human infant eye, where it is known that the fovea continues to mature until at least the age of four years³⁶ with earlier treatment potentially facilitating foveal development and prevent/ameliorate photoreceptor loss. The HH-SDOCT will likely play a central role in the earlier identification of patients who may be suitable for enrolment to future trials.

We identified 5 children with atypical foveal hypoplasia. In all cases, a diagnosis of achromatopsia was confirmed on molecular analysis in addition to the typical clinical findings of photophobia and reduced or absent photopic responses on ERG. All of these children were below the age of 5 years. This included the youngest

achromat to be imaged using HH-SDOCT at the age of 2 months. Interestingly in this patient, the development of the IS/OS junction appears to be “immature” in comparison to a single age-matched control and she did not present with photophobia; a larger number of achromatopsia patients and controls are required to probe this further. It is possible that photophobia may develop later. We also noted that the disruption of the IS/OS was much milder in comparison to that reported in older children and adults, albeit in a limited number of cases; in keeping with progression seen in retinal imaging studies of achromatopsia.^{126, 129} Gene therapy trials are anticipated in achromatopsia. Cone rescue with gene therapy has recently been shown to be successful in a mouse model of *CNGA3* and *CNGB3*-achromatopsia.^{98, 199} The timing of such treatment may be important, as only the youngest animals had restoration of visual acuity,²⁰¹ although older mice also significantly responded.²⁰¹ Despite the inherent limitations of extrapolating from mouse to man, HH-SDOCT will likely have an important role in both the selection and monitoring of infants with achromatopsia in future gene replacement trials.

Different macular morphological abnormalities have been reported in other retinal dystrophies and degenerations.^{131-135, 137} Six children in our study were classified into this group. They had a wide variety of findings, which included abnormal RPE, poorly developed IS/OS junctions and abnormal lamination of the inner retinal layers. In four cases, reliable ERGs were obtained leading to a diagnosis of rod-cone or cone-rod retinal dystrophy on the basis of the electroretinograms. In the remaining two cases it was not possible to perform reliable ERGs due to poor cooperation. The HH-SDOCT played a central role in identifying morphological abnormalities of the fovea in these patients. Interestingly, 2 of these 6 patients had microcephaly with ERG evidence of generalised retinal dysfunction, and also had foveal hypoplasia; illustrating overlap between this OCT group and that of atypical foveal hypoplasia. To the best of our knowledge, foveal hypoplasia has only been previously described in retinal dystrophy in association with achromatopsia.

An interesting result in our study was also that patients with neurological syndromes such as microcephaly had foveal abnormalities consistent with retinal

dystrophy. Examination of further patients will be helpful to characterise the fovea in children with neurological syndromes.

To date no foveal morphological abnormalities have been reported in either idiopathic nystagmus or manifest latent nystagmus (fusion maldevelopment syndrome).¹²⁴ Sixteen of our patients fell into this category. Twelve had a diagnosis of idiopathic nystagmus. Four had been diagnosed with manifest latent nystagmus. The HH-SDOCT was successful in showing normal foveal structure and distinguishing these patients from those with other causes for their nystagmus associated with macular anomalies.

A limitation of this study is that we have not investigated whether the foveal thickness or individual layers such as the length of the OS were abnormal. However this was not the aim of this study which was to clinically grade foveal morphology in a clinically useful manner; this does not require quantitative analysis of retinal lamination. It is known that in infants and young children the fovea continues to develop with age and there is a broad spectrum of normal foveal structure.^{25, 36} Therefore it would be interesting to analyse all retinal layers of these patients in comparison to normative data of age-matched controls.

It is unclear whether the fovea continues to develop with age in children with typical foveal hypoplasia. Studies using preferential looking are controversial as one study showed visual development after birth which was at a lower level but parallel to normal children,²⁰⁶ while another study showed no progression in vision.²⁰⁷ Longitudinal OCT examination of patients with typical foveal hypoplasia could clarify whether a morphological development with age also occurs in these patients.

It would also be interesting to assess whether the HH-SDOCT can be used to accurately assess the peripapillary nerve fibre layer thickness in both normal children and children that may have abnormalities for example in vigabatrin toxicity or congenital glaucoma. As there is an inherent tendency towards foveal fixation when using the HH-SDOCT to acquire images this may prove to be more difficult.

This study has demonstrated excellent feasibility, sensitivity and specificity of using HH-SDOCT in imaging infants and young children with infantile nystagmus. By identifying diagnostic clues such as typical and atypical foveal hypoplasia, or the presence or absence of other foveal morphological abnormalities, further investigations

can be prioritised thereby resulting in a timelier definitive and more cost-effective underlying diagnosis. Furthermore, HH-SDOCT in young children with nystagmus will also become increasingly important with the onset of clinical trials, for diagnosis, patient selection and monitoring retinal changes following intervention.

Chapter 6

Time Course of Changes in Retinal Development in Infants and Young Children with Achromatopsia

6.1. Introduction

6.2. Methods

6.3. Results

6.4. Conclusion

6.1. Introduction

Achromatopsia (ACHM) is an autosomal recessive disorder associated with infantile nystagmus, loss of colour discrimination, photophobia, complete or incomplete loss of cone function with preservation of rod function on electroretinographic recordings (ERG), reduced retinal sensitivity on microperimetry, reduced visual acuity and typical OCT findings which have been outlined in section 1.32.

Normally, development of the retina involves migration of the inner retinal layers away from the foveal centre, migration of the cone photoreceptors into the foveal centre and elongation of the photoreceptors with age.^{5, 8, 36} It is not clear whether retinal development occurs in achromatopsia in a similar way. It is likely that the presence of normal functional cone photoreceptors are necessary for the development of a normal foveal pit and downstream intraretinal circuitry as has been shown in animal models of photoreceptor degeneration.²⁰⁸

Whether achromatopsia is a stationary or progressive condition is still the subject of ongoing debate. Recent work involving a large cross sectional group of 40 achromatopsia patients did not find a correlation between age and disruption of retinal structures on OCT and visual function. However, the authors did note an age related decline in retinal sensitivity on microperimetry.²⁰⁹

Previous studies have focused on imaging older children and adults with achromatopsia, with only one previous cross-sectional study describing a group of 9 infants and young children with achromatopsia.¹⁶¹ With gene therapy showing potential to cure this condition in animal models^{200, 201, 210-215} and treatment trials imminent in humans²¹⁶, it is important to develop a detailed understanding of the time course of retinal changes in achromatopsia, so that the timing of treatment can be optimised and reliable monitoring of the treatment can be carried out.

The aim of this study was to use HH-SDOCT to determine to what extent achromatopsia is progressive and whether it affects the developing retina in a group of infants and young children aged between birth and 6 years of age.

6.2. Methods

6.21. Participants

The cohort for this study included 8 children with a confirmed genetic diagnosis of achromatopsia and 45 normal age, gender and race matched controls. Six children had a mutation in the *CNGB3* gene. Two children had a mutation in the *CNGA3* gene. We obtained 41 mixed cross sectional and longitudinal examinations, which included 24 (58.5%) and 17 (41.5%) tomograms obtained from the right and left eyes, respectively, in the achromatopsia group. These were compared to 82 age, gender and race-matched control examinations at a 2:1 ratio, which included 48 (58.5%) and 34 (41.5%) tomograms obtained from the right and left eyes, respectively. The mean age at the time of examination was 3.3 years (range 0-8.3 years) for the achromatopsia group and 3.5 years (range 0-10.1 years) for the control group. If tomograms were obtained from both eyes at the same visit, both were included in the final analysis in order to increase the power of the study to detect intergroup differences and improve the precision of the calculated regression coefficients.

All participants underwent a full orthoptic and ophthalmologic examination, which included slit-lamp examination where possible, fundus examination and measurement of visual acuity. Visual acuity (VA) was assessed in younger infants and children by preferential looking using Teller acuity cards and/or crowded logMAR Kay Picture Tests if possible. In cooperative children, Teller acuity cards and/or logMAR crowded optotypes (Glasgow Acuity Cards) were used to obtain VA. The clinical characteristics of the achromatopsia participants are summarised in Table 6.1.

Table 6.1: Clinical Characteristics of Achromatopsia Participants

ID	Sex	Age at Each Visit (months)	BCVA (LogMAR)		Refraction		Genetic Diagnosis	ERG Δ	Foveal Hypoplasia Grade
			Right Eye	Left Eye	Right Eye	Left Eye			
1a	F	15.4	1.6	1.6	+7.50/-2.00@11	+6.00/-1.50@161	<i>CNGB3</i> 1148delC	Absent Cone Response	Atypical
2a	M	70.8	0.9	0.9	+4.00/-2.00@14	+4.00/-2.00@171	<i>CNGB3</i> 1148delC	Absent Cone Response	Atypical
		78.0	1.2	1.0	+4.00/-2.00@14	+4.00/-2.00@171			
3	M	22.8	0.9	0.9	+5.00	+5.00	<i>CNGA3</i> 661C>T 1768G>A	Severe Generalised Cone Dysfunction	Atypical
		28.5	1.2	1.2	+5.00	+5.00			
		40.0	0.4	0.4	+2.00/+1.50@90	+2.00/+1.50@90			
4	F	22.4	2.0	----	+4.50	----	<i>CNGB3</i> 1148delC	Unreliable	Atypical
		37.7	1.05	1.5	+1.75/-0.75@10	+0.75			
5b	M	37.4	0.9	0.9	+6.00/-5.00@175	+6.00	<i>CNGB3</i> 1148delC	Severe Generalised Cone Dysfunction	Atypical
		44.1	1.3	1.3	+6.00/-5.00@175	+6.00			
		50.2	1	1	+6.00/-5.00@175	+6.00			
		58.3	1	1	+6.00/-5.00@175	+6.00			
6b	F	2.4	1.5	1.5	+2.50/-5.00@180	+4.00/-0.75@180	<i>CNGB3</i> 1148delC	Severe Generalised Cone Dysfunction	Atypical
		6.3	1.5	1.5	+2.50/-5.00@180	+4.00/-0.75@180			
		9.0	1.3	1.3	+2.50/-5.00@180	+4.00/-0.75@180			
		15.2	1.3	1.3	+2.50/-5.00@180	+4.00/-0.75@180			
		23.3	1.3	1.3	+2.50/-5.00@180	+4.00/-0.75@180			
7	F	81.7	0.925	0.925	+4.25/-1.50@10	+4.50/-1.75@170	<i>CNGA3</i> 1641C>A	Severe Generalised Cone Dysfunction	Atypical
		93.8	0.65	0.85	+4.75/-1.75@10	+4.25/-2.00@170			
		98.7	0.8	0.725	+3.75/-2.25@12	+3.25/-1.75@170			
8	M	50.0	1.3	1.3	+3.75/-2.00@15	+4.25/-2.00@0	<i>CNGB3</i> 1148delC	----	Atypical

ID = identification number; M = male; F = female; BCVA = best corrected visual acuity; LogMAR = Logarithm of the Minimum Angle of Resolution; ERG = electroretinogram

Δ *Rod function was normal in all cases where an ERG result was reported*

a b *indicate sibling pairs*

---- *indicates not assessed or could not be performed*

6.22. Optical Coherence Tomography

HH-SDOCT (Biotigen™ Envisu system, Durham, NC, USA) was used to obtain a volumetric scan (consisting of 100 B-scans and 500 A-scans per B-scan) of the foveal region as previously described¹⁹². In all cases the OCT scan was obtained from the right eye first, followed by the left eye. The acquired images were exported from the Biotigen OCT software and imported into ImageJ software (available at: <http://rsbweb.nih.gov/ij/> Date accessed: May 11, 2012) where retinal layer segmentation was performed. The nomenclature used to label the segmented layers are based on previously established anatomical correlates with histology (Figure 1).^{93 94}

6.23. Statistics and Modelling

A linear mixed model, implemented in STATA™ software (Copyright 1996–2014, StataCorp), was used to analyse the differences between the achromatopsia and control groups with regards to the thickness measurements obtained for each retinal layer at the fovea, parafovea and perifovea. The model included fixed effects for diagnosis, age, eye and the interaction between diagnosis and age (diagnosis*age). Post-hoc estimates of the marginal effects of diagnosis on retinal layer thickness measurements were calculated for overall retinal thickness (RT), inner retinal layers (IRLs) and outer retinal layers (ORLs). The results of the marginal effects analysis are presented in Appendix 3.

A separate linear mixed model was constructed in order to identify if there is a correlation between the development of the photoreceptor layers and the inner retinal layer regression in achromatopsia. The model included an adjustment for age and eye.

The median time (including corresponding 95% confidence intervals (CI) to the the development of a hypo-reflective zone and ellipsoid disruption in achromatopsia was calculated through Kaplan-Meier survival analysis.

All analyses were considered significant at a type 1 probability value of $p < 0.05$. Statistical analysis was performed STATA™ software (Copyright 1996–2014, StataCorp).

6.3. Results

6.31. General Outline of Foveal Development and Morphology

In the normally developing fovea, there is centrifugal migration of the inner retinal layers (IRLs) away from the fovea. This leads to thinning of the retinal nerve fibre layer (RNFL), ganglion cell layer (GCL), inner plexiform layer (IPL), inner nuclear layer (INL) and outer plexiform layer (OPL) at the fovea. Conversely, there is centripetal migration of the photoreceptors into the fovea and increase in size of the photoreceptor layers with age (Figure 6.1 & 6.2). In achromatopsia, these processes are still occurring, albeit at an altered rate and magnitude in comparison to controls (Figures 6.5, 6.6 & 6.7).

In all of the participants with achromatopsia, there was evidence of foveal hypoplasia (presence of the normally absent IRLs at the fovea) at each visit on OCT examination. A HRZ was visible in 26 (63.4%) of the 41 achromatopsia tomograms examined (Figure 6.2, Table 6.2). The continuity of photoreceptor inner segment ellipsoid (ISE) band was disrupted in 29 (70.7%) of cases (Figure 6.2A). Of the 15 tomograms without evidence of a HRZ, 6 were attributed to a single patient (patient 7) with a *CNGA3* mutation. Two were attributed to the youngest achromat imaged in this study (patient 6), who was imaged at 2.4 months of age when the photoreceptor outer segment (OS) and ISE had not yet developed at the fovea (Figure 6.1A & Table 6.2). There was no evidence of foveal hypoplasia, ISE disruption or the presence of a HRZ in any of the control tomograms (Figure 6.1B).

6.32. Timing of Hypo-Reflective Zone Appearance and Ellipsoid Disruption

There is a visible delay in the migration of the photoreceptors into the central fovea in achromatopsia (Figure 6.1A). This is then followed by the appearance of a hypo-reflective zone (HRZ) which disrupts the normally continuous ellipsoid (ISE) band. This appears to be age-dependent (Figure 6.2). The youngest age at which the development of a HRZ with visible ISE disruption was observed was 6 months. The median time to development of a HRZ was 50.0 months (95% CI 32.8-67.1) (Figure 6.3). The median time to development of ISE disruption was 40.0 months (95% CI 27.7-52.3) (Figure 6.4).

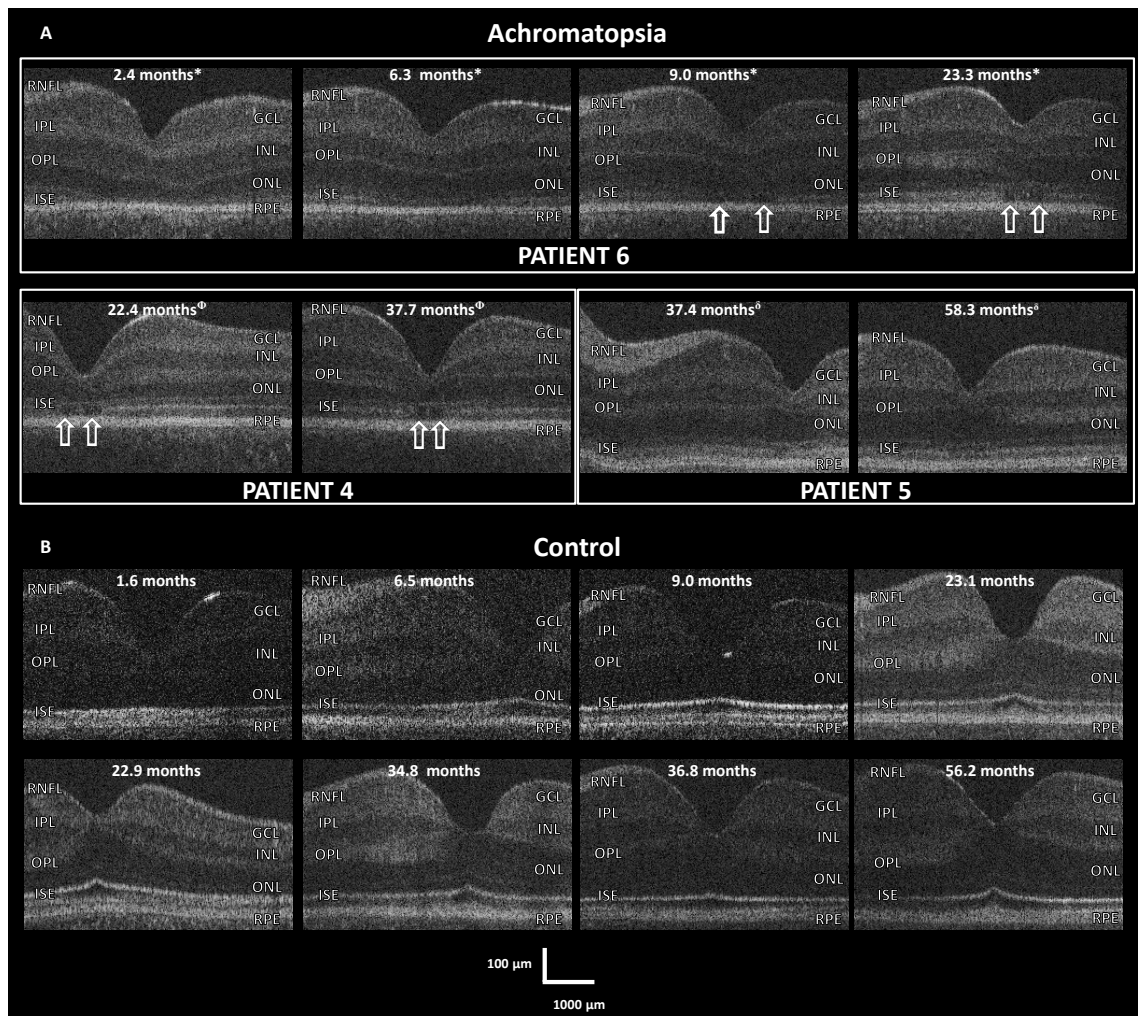


Figure 6.1: Features of foveal development and morphology in achromatopsia.

There is centrifugal migration of the inner retinal layers (IRLs) (which includes the RNFL, GCL, IPL, INL and OPL) away from the central fovea, centripetal migration of the photoreceptors into the fovea and growth of the photoreceptors with age in both the achromatopsia group (A) and the age-matched control group (B). The rate and extent to which this occurs in the achromatopsia group is reduced in comparison to the control group. Foveal hypoplasia (presence of the normally absent IRLs at the fovea) is evident in all of the tomograms taken from the achromatopsia group. In addition, there is evidence of an optically empty hypo-reflective zone (HRZ) (white arrows) appearing in several of the tomograms taken from the achromatopsia group which is disrupting the continuity of the photoreceptor inner segment ellipsoid (ISE) band.

**, Φ and δ indicate tomograms taken from the same patient at different time points*

RNFL = retinal nerve fibre layer; GCL = ganglion cell layer; IPL = inner plexiform layer; INL = inner nuclear layer; OPL = outer plexiform layer; ONL = outer nuclear layer; ELM = external limiting membrane; ISE = ellipsoid of the inner segment of the photoreceptor; RPE = retinal pigment epithelium; IRLs = inner retinal layers

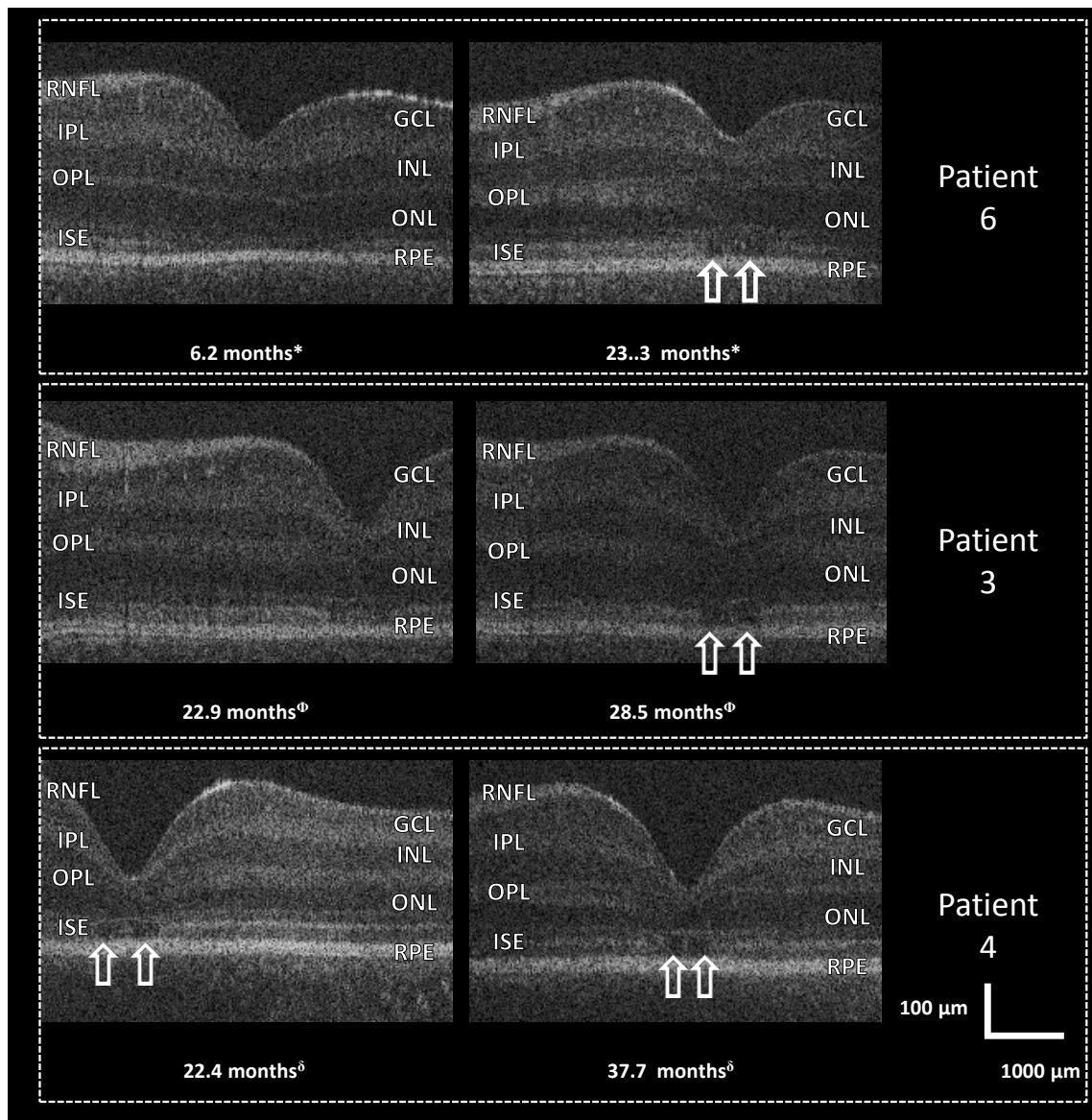


Figure 6.2: Age-dependent appearance of the HRZ and ISE disruption in achromatopsia.

Longitudinal tomograms have been taken of three achromats at two separate time points. There is evidence of an optically empty hypo-reflective zone (HRZ) (white arrows) which is disrupting the continuity of the photoreceptor inner segment ellipsoid (ISE) band. This is subtle in appearance at the younger ages and becomes much more obvious when the participants are older.

**, Φ and δ indicate tomograms taken from the same patient at different time points*

HRZ = hypo-reflective zone; RNFL = retinal nerve fibre layer; GCL = ganglion cell layer; IPL = inner plexiform layer; INL = inner nuclear layer; OPL = outer plexiform layer; ONL = outer nuclear layer; ELM = external limiting membrane; ISE = ellipsoid of the inner segment of the photoreceptor; RPE = retinal pigment epithelium; IRLs = inner retinal layers

Table 6.2: Summary of the Presence of a HRZ or ISE Disruption in Achromatopsia

Patient ID	Age at Each Visit (months)	ISE Disruption		Presence of HRZ	
		Right Eye	Left Eye	Right Eye	Left Eye
1a	15.4	Yes	Yes	Yes	Yes
2a	70.8	Yes	Yes	Yes	Yes
	78.0	Yes	Yes	Yes	Yes
3	22.8	Yes	Yes	Yes	Yes
	28.5	Yes	Yes	Yes	Yes
	40.0	Yes	Yes	Yes	Yes
4	22.4	Yes	NA	Yes	NA
	37.7	Yes	Yes	Yes	Yes
5b	37.4	Yes	Yes	No	No
	44.1	No	No	No	No
	50.2	No	No	No	No
	58.3	No	Yes	Yes	Yes
6b	2.4	----	----	No	No
	6.3	Yes	Yes	Yes	Yes
	9.0	Yes	Yes	Yes	----
	15.2	Yes	Yes	Yes	Yes
	23.3	Yes	Yes	Yes	Yes
7	81.7	No	No	No	No
	93.8	No	No	No	No
	98.7	No	No	No	No
8	50.0	No	No	Yes	Yes

ID = identification; ISE = Ellipsoid; HRZ = Hypo reflective zone; NA = Not Applicable

a b indicate sibling pairs

---- indicates could not be assessed

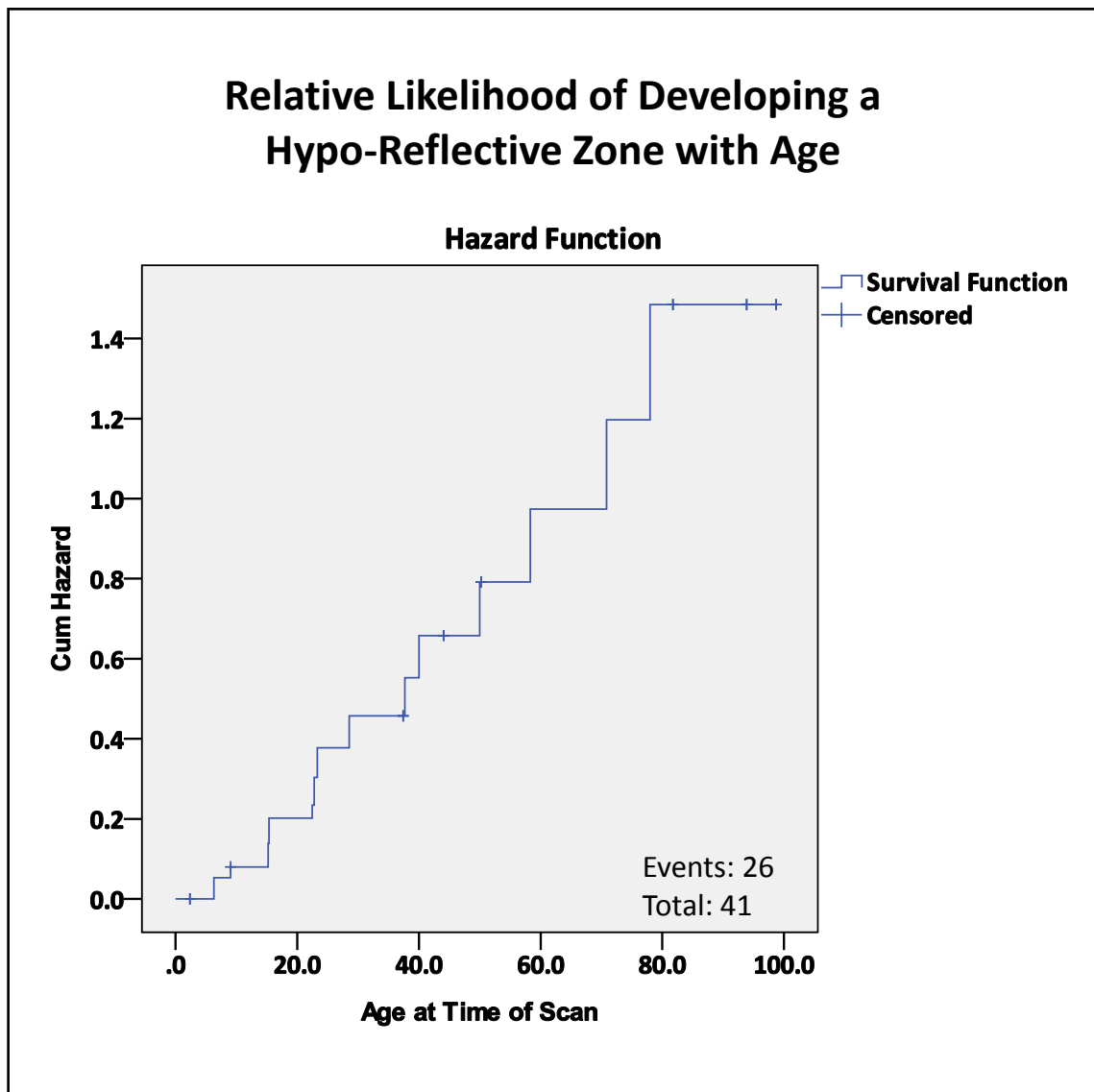


Figure 6.3: Kaplan-Meier survival curve for the development of a HRZ with increasing age (months).

The hazard function is describing the relative likelihood of a HRZ occurring at a particular age.

Cum = cumulative; HRZ = hypo-reflective zone

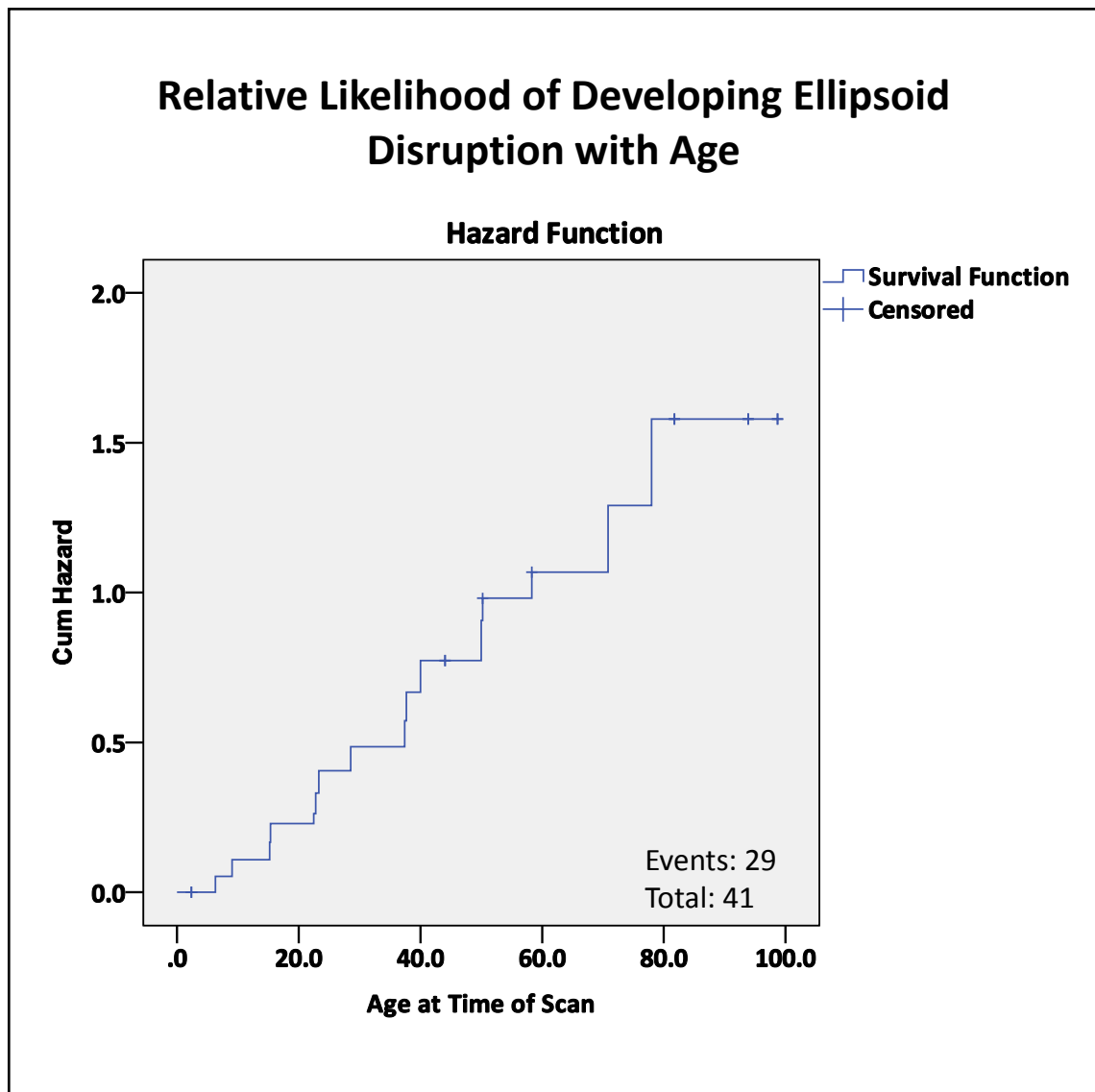


Figure 6.4: Kaplan-Meier survival curve for the development of ISE disruption with increasing age (months).

The hazard function is describing the relative likelihood of ISE disruption occurring at a particular age.

Cum = cumulative; ISE = ellipsoid band

6.33. Overall Retinal, Inner and Outer Retinal Layer Thicknesses

Figures 6.5 and 6.6 show z statistic scores across the retina for the terms in the statistical models. The overall differences in retinal layer thicknesses between achromats and controls (i.e. group term) are shown in figure 6.5, whereas differences in rate of change in retinal layer thicknesses with time are shown in figure 6.6 (interaction term between group and age). Positive scores indicate a higher value in achromats (i.e. thicker retinal layers in achromats for figure 6.2 and greater rate of change in achromats for figure 6.3). Z statistic ≤ -2 or ≥ 2 indicate statistical significance. Figures 6.5 and 6.6 represent the intercepts and slopes, respectively, in the best fit lines of the scatter plots of the change in retinal layers thicknesses with age shown in figures 6.7, 6.8 and 6.9.

Figures 6.5A indicates that the overall retinal thickness was greater in controls compared to achromats but that the differences were much more significant in the nasal and temporal parafovea ($p < 0.0001$). In general the rate of change in retinal thickness with age was similar in the two groups although the rate of change was slightly higher in controls in the parafovea with this reaching significant levels at locations 1500 μm nasally and temporally ($p < 0.01$) (Figures 6.6A).

The borderline significant differences observed between achromats and controls in retinal thickness at the fovea (Figure 6.5A) belie contrasting and radical patterns of underlying differences in the IRLs and ORLs observed at the fovea in the two groups (Figures 6.5B, 6.6B & central column of figures in 6.7).

In achromats the foveal IRLs are on average 5x the size of mean control values ($p < 0.0001$) whereas the ORLs are significantly smaller at only 0.6x the size of mean control values ($p < 0.0001$) (Figure 6.5B). Another contrasting pattern is the difference in the rate of change of the IRLs and ORLs with age (Figure 6.6B). The IRLs decrease in size with age in achromats in contrast to controls which show no change (difference in rate of change: $p < 0.05$). The ORLs increase with a similar rate of change in both achromats and controls (difference in rate of change: $p = 0.976$).

The pattern of differences in IRL and ORL between achromats and controls in the fovea are in contrast with the changes observed at the parafovea (Figures 6.5B, 6.6B and 6.7B & C). The IRLs are significantly thinner in achromats in the parafovea

compared to controls ($p < 0.01$), whereas the ORLs show no difference. Differences in the rate of change of the IRLs and ORLs outside the fovea are in general mild where the only differences observed are in the parafovea of the ORLs where a higher rate of thickening occurs in controls compared to achromats ($p < 0.05$).

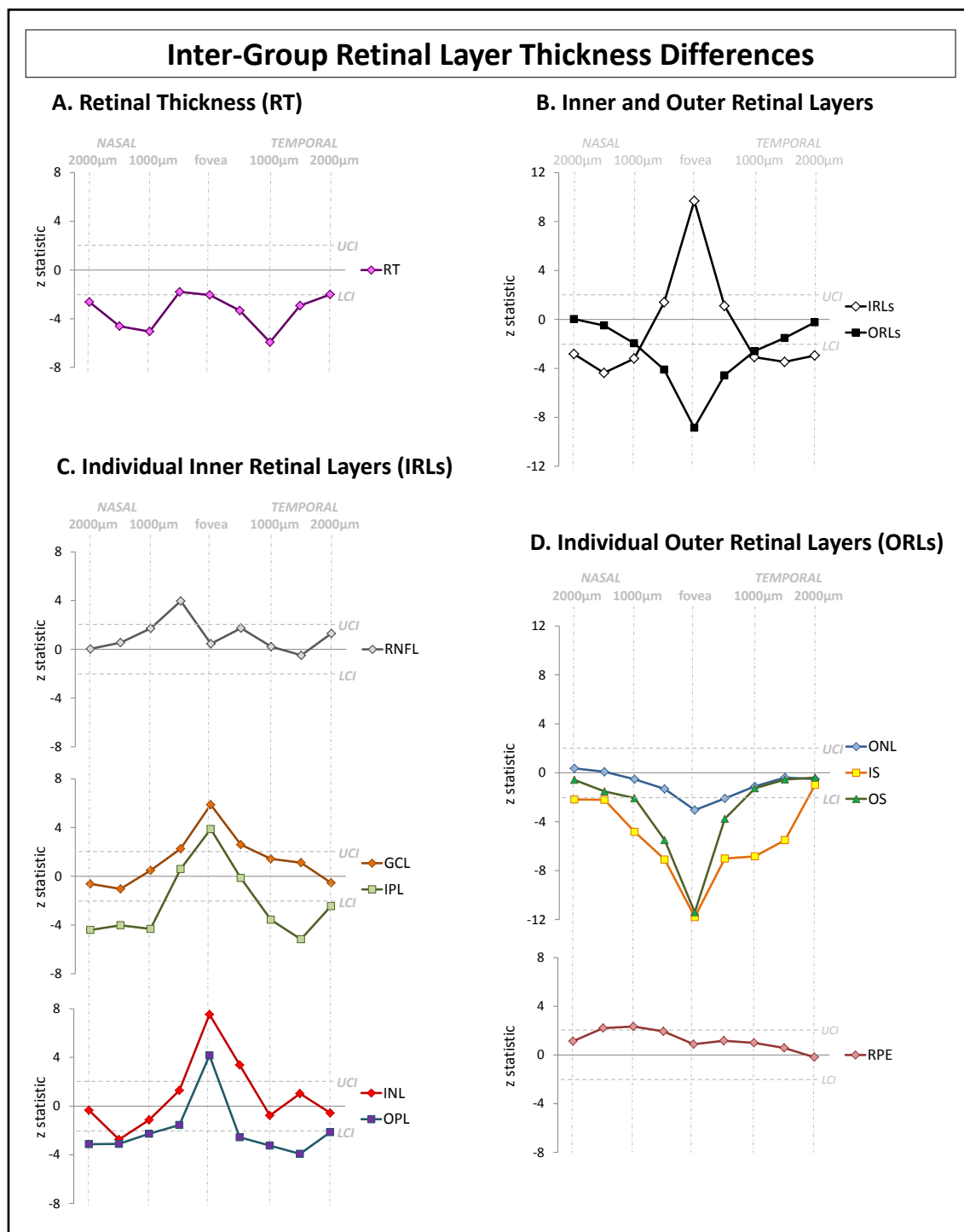


Figure 6.5: Mean differences in retinal layer thickness measurements between the achromatopsia and control groups.

Results are shown for (A) retinal thickness (RT), (B) inner (IRLs) and outer retinal layers (ORLs) as well as each individual retinal layer (C & D) at the fovea, parafovea

and perifovea. The parafoveal measurements were taken at 500 μm and 1000 μm nasal and temporal to the central fovea. The perifoveal measurements were taken at 1500 μm and 2000 μm nasal and temporal to the central fovea. Positive and negative z-scores indicate increased and decreased thickness measurements, respectively, in the achromats. Z statistic ≤ -2 or ≥ 2 indicate statistical significance (indicated by the two dotted lines).

RT = retinal thickness; IRLs = inner retinal layers; ORLs = outer retinal layers; RNFL = retinal nerve fibre layer; GCL = ganglion cell layer; IPL = inner plexiform layer; INL = inner nuclear layer; OPL = outer plexiform layer; ONL = outer nuclear layer; ELM = external limiting membrane; ISE = ellipsoid of the inner segment of the photoreceptor; RPE = retinal pigment epithelium

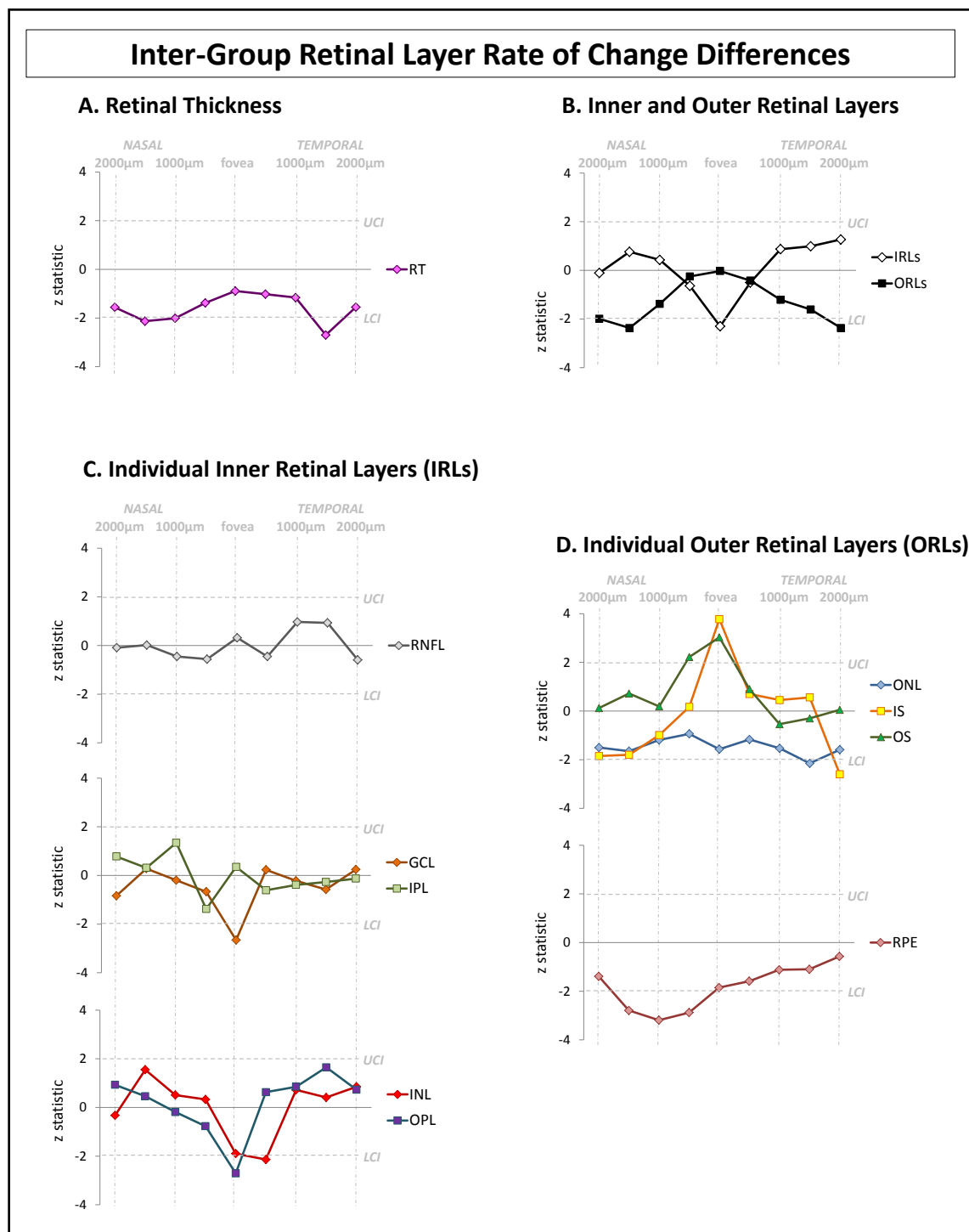
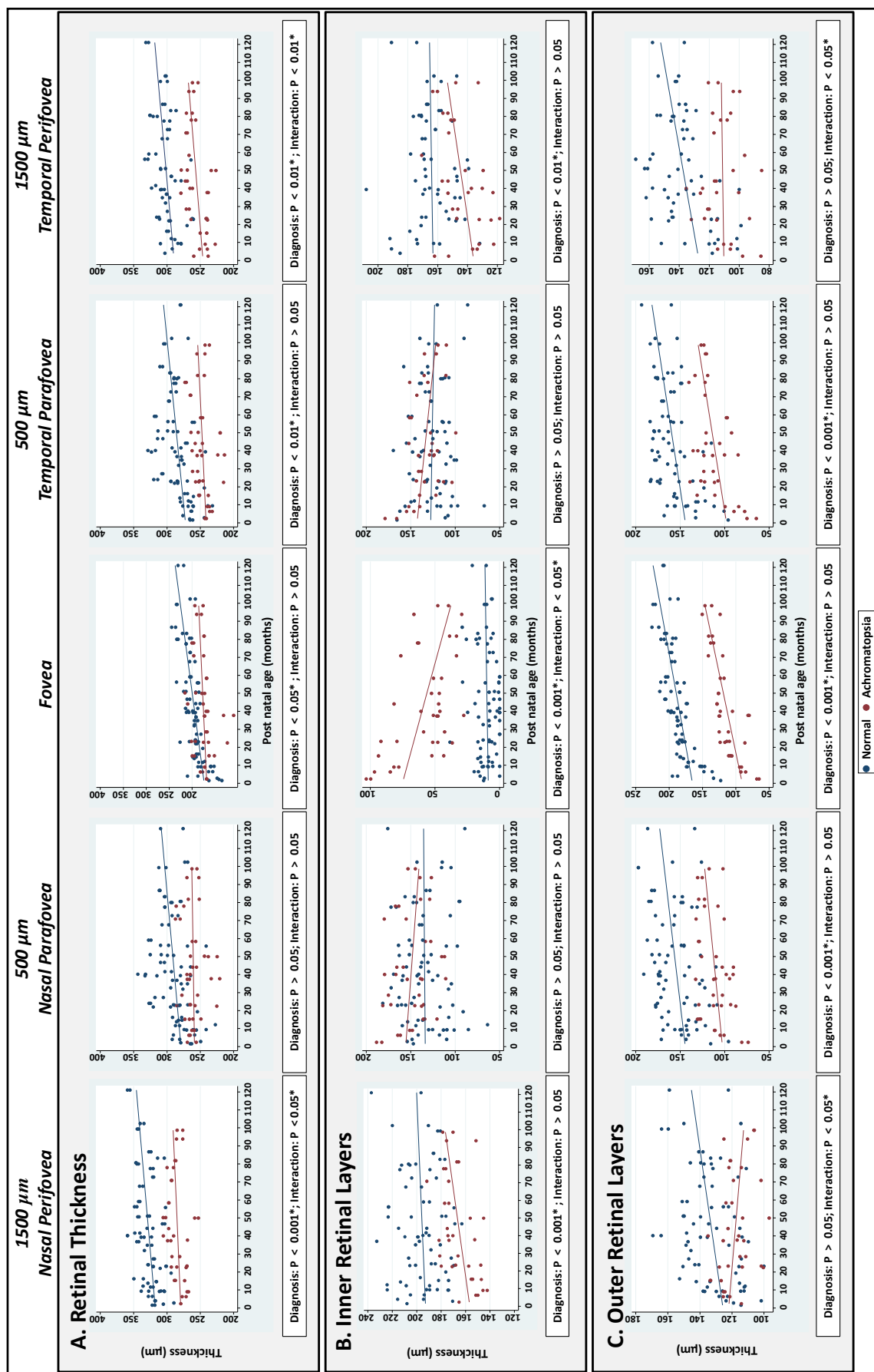


Figure 6.6: Differences in the rate of change in retinal layer thicknesses with age between the achromatopsia and control groups.

Results are shown for (A) retinal thickness (RT), (B) inner (IRLs) and outer retinal layers (ORLs) as well as each individual retinal layer (C & D) at the fovea, parafovea

and perifovea. The parafoveal measurements were taken at 500 μm and 1000 μm nasal and temporal to the central fovea. The perifoveal measurements were taken at 1500 μm and 2000 μm nasal and temporal to the central fovea. Positive z-scores indicate increased rate of change and negative z-score indicate decreased rate of change in achromatopsia. Z statistic ≤ -2 or ≥ 2 indicate statistical significance (indicated by the two dotted lines).

RT = retinal thickness; IRLs = inner retinal layers; ORLs = outer retinal layers; RNFL = retinal nerve fibre layer; GCL = ganglion cell layer; IPL = inner plexiform layer; INL = inner nuclear layer; OPL = outer plexiform layer; ONL = outer nuclear layer; ELM = external limiting membrane; ISE = ellipsoid of the inner segment of the photoreceptor; RPE = retinal pigment epithelium



● Normal ● Achromatopsia

Figure 6.7: Development trajectories for the inner retinal layers, outer retinal layers and total retinal thickness at the fovea, parafovea and perifovea.

*The trajectories have been plotted from between 0 to 120 months post natal age. Each point represents a single value from each OCT examination. The lines of best fit (trend lines) are shown in red and blue for the achromatopsia and control groups respectively. P values that were calculated from the linear mixed model analysis are provided with regards to the effects of diagnosis on the thickness measurements and the diagnosis*age interaction (difference between the slopes of the trend lines or rate of change in retinal layer thickness of each group).*

6.34. Individual Retinal Layers

Figures 6.5C and D show changes in mean thickness for individual retinal layers and figures 6.6C and D the rate of change with age, and hence indicate where the greatest changes are taking place to explain the patterns in IRLs and ORLs described. Scatter plots of changes in the thickness of each retinal layer with age are shown in figures 6.8 and 6.9 at the fovea and at positions 500 μm and 1500 μm nasally and temporally.

Figure 6.5C indicates that the dramatically thickened IRLs observed at the fovea for achromats are due to significantly increased thicknesses in all inner retinal layers except for the RNFL (i.e. GCL, IPL, INL and OPL, $p < 0.0001$). Figure 6.6C shows that the significant regression of the IRLs with time at the fovea seen in achromats is mainly due to changes in the GCL, INL and OPL. Figure 6.8 shows that this is because in controls these layers are almost completely regressed by the first few months of life but in achromats are slowly regressing. Interestingly the thinner parafoveal IRLs in achromats are due to changes specifically in the plexiform layers (the IPL and OPL, Figure 6.5C, $p < 0.05$).

Figure 6.5D shows that the profoundly thinner ORLs observed in the fovea for achromats compared to controls is due to highly significant changes in the IS ($p < 0.0001$) and OS layers ($p < 0.0001$) with milder but significant changes also observed in the ONL ($p < 0.01$). IS and OS measurements in achromats at the fovea show a bimodal distribution which matches the previous description of a punched out hypo-reflective zone in achromats where the IS and OS can no longer be measured. Differences in IS thickness between achromats and controls are apparent across the whole retina. A contrasting pattern of changes in the RPE appears to take place in the nasal retina where the RPE appears to get thinner with age in achromats and thicker with age in controls leading to a significant interaction term ($p < 0.01$) (see also figures 6.6D and 6.9D).

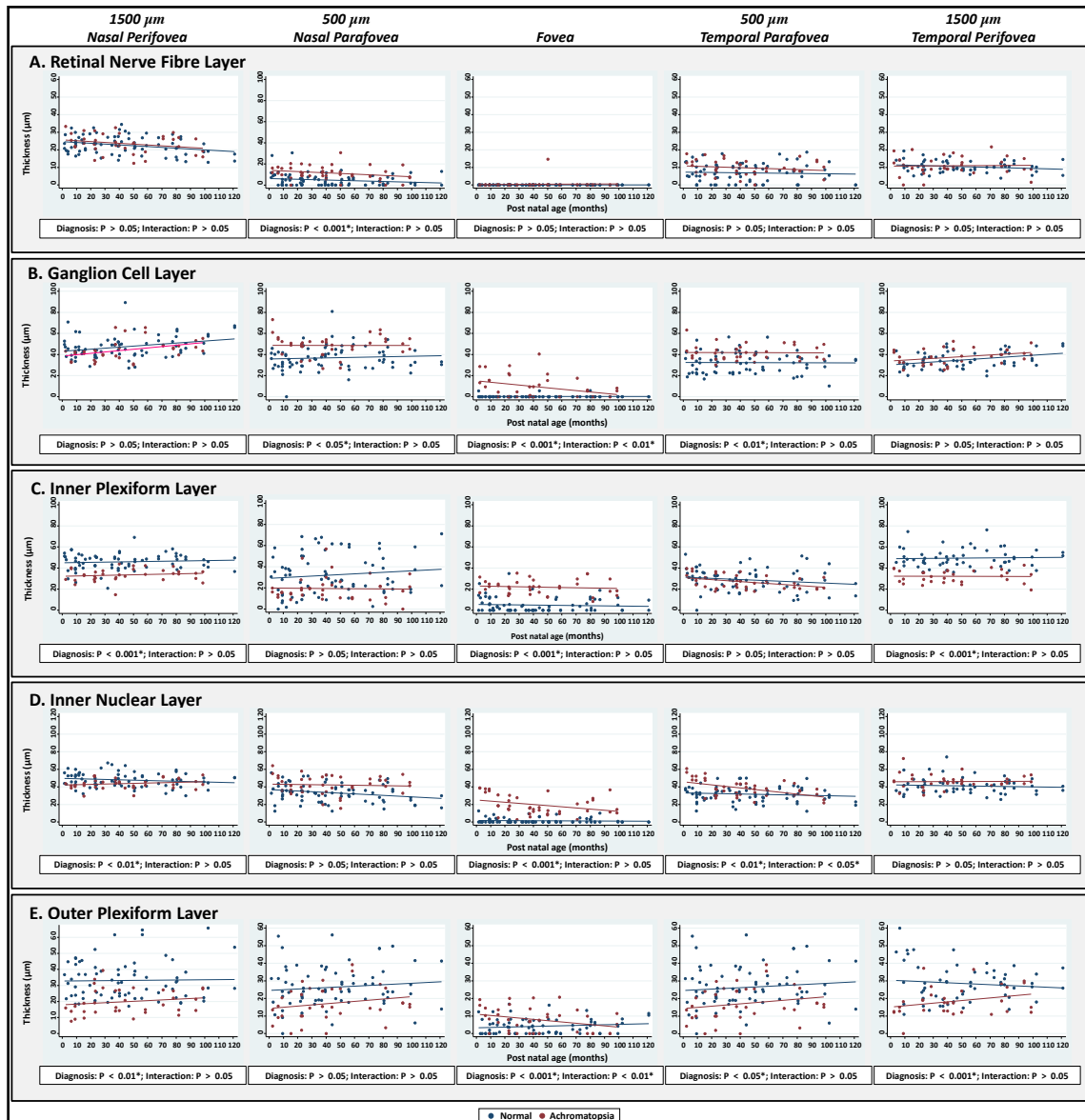


Figure 6.8: Development trajectories for the RNFL, GCL, IPL, INL and OPL at the fovea, parafovea and perifovea.

The trajectories have been plotted over a time period spanning 0 through 120 months post natal age. Each point represents a single value from each OCT examination. The lines of best fit (trend lines) are shown in red and blue for the achromatopsia and control groups respectively. P values that were calculated from the linear mixed model analysis are provided with regards to the effects of diagnosis on the thickness measurements and the diagnosis*age interaction (difference between the slopes of the trend lines or rate of change in retinal layer thickness of each group).

RNFL = retinal nerve fibre layer; GCL = ganglion cell layer; IPL = inner plexiform layer; INL = inner nuclear layer; OPL = outer plexiform layer

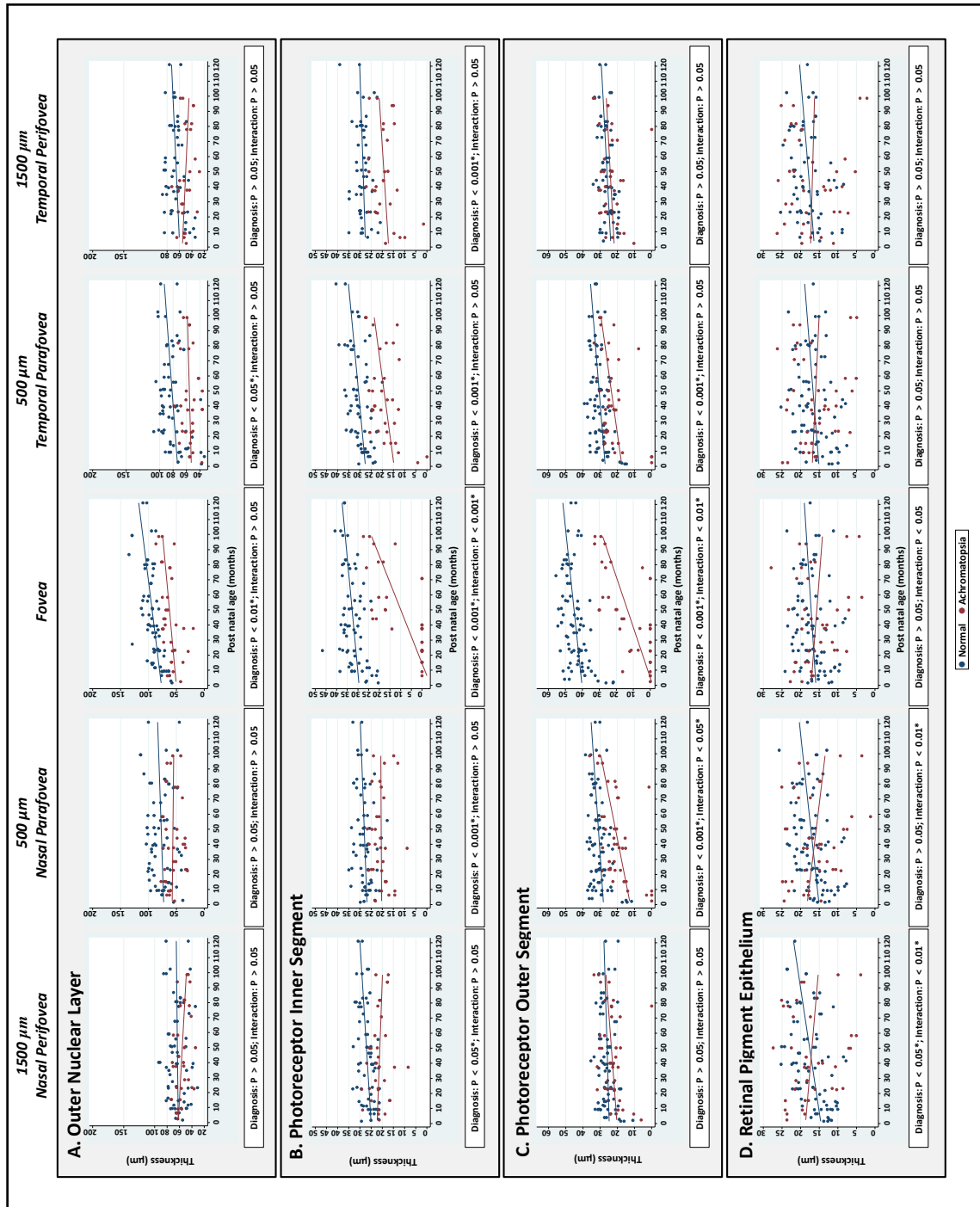


Figure 6.9: Development trajectories for the ONL, IS, OS and RPE at the fovea, parafovea and periphery.

The trajectories have been plotted over a time period spanning 0 through 120 months post natal age. Each point represents a single value from each OCT examination. The lines of best fit (trend lines) are shown in red and blue for the achromatopsia and

*control groups respectively. P values that were calculated from the linear mixed model analysis are provided with regards to the effects of diagnosis on the thickness measurements and the diagnosis*age interaction (difference between the slopes of the trend lines or rate of change in retinal layer thickness of each group).*

ONL = outer nuclear layer; IS = photoreceptor inner segment; OS = photoreceptor outer segment; RPE = retinal pigment epithelium

6.35. Correlation between Outer Retinal and Inner Retinal Layer Thicknesses

Mixed linear regression analysis showed a significant negative correlation between the thickness of the ORLs and the thickness of the IRLs at the fovea ($\beta = -0.53$, $p < 0.01$).

6.4. Discussion

This is the first study investigating foveal development in infants and young children with achromatopsia. It has been hypothesised that during normal foveal development, pit formation occurs passively by indentation of the avascular fovea from intraocular pressure in utero. This is followed by a second active phase of growth-induced stretch that remodels the morphology of the fovea in the postpartum period.^{23, 33} A centrifugal displacement of inner retinal cells away from the fovea and a centripetal displacement of the cone photoreceptors into the central fovea is postulated.^{5, 8, 36, 37} The majority of cone elongation and packing occurs postnatally.³³

6.41. The Contribution of Cone Photoreceptors to Normal Foveal Development

Achromatopsia offers a unique insight into the contribution of cone photoreceptors to the development of other foveal layers. Achromatopsia has been genetically well characterised. Mutations in *CNGA3*,¹⁵⁴ *CNGB3*,¹⁵⁵ *GNAT2*¹⁵⁶ and *PDE6H*¹⁵⁷ have been found. The protein products of these genes are important for visual transduction and show expression restricted to cone inner and outer segments.¹⁵³ Mutations in these genes cause achromatopsia by disrupting the function of the cGMP-gated channel in cone photoreceptors. The pathology appears to be localised to the cone photoreceptors in achromatopsia. Consequently, it is likely that any alterations that occur during the development of the retina in achromatopsia are secondary to the loss of the cone photoreceptor contribution to this process.

In this study we found that the centrifugal migration of the IRLs from the fovea is delayed in achromatopsia, resulting in foveal hypoplasia. However, after birth, the inner retinal layers continue to regress. Our data suggests that the presence of normal cone photoreceptors is a necessary prerequisite for the migration of the IRLs away from the fovea. We postulate that the normal elongation of the cone photoreceptors at the fovea also generates a mechanical or biochemical force that contributes to the displacement of the IRLs away from the fovea.

Consistent with this hypothesis, we found that the ORLs which includes the ONL, IS and OS are all significantly reduced in thickness at the fovea in achromatopsia

as compared to controls. There was a significant negative correlation between the size of the ORLs and the size of the IRLs at the fovea in achromatopsia. These findings of foveal hypoplasia and thinning of the ONL and photoreceptor layers have also been demonstrated in other high resolution OCT studies of achromatopsia carried out in older children and adults.^{126, 160}

It has previously been reported that there is a reduction in parafoveal and perifoveal retinal thicknesses in achromatopsia in comparison to age-matched controls.¹⁶⁰ Our results are consistent with these reports. During normal retinal development in infants and young children, foveal, parafoveal and perifoveal retinal thicknesses increase with age. The rate of thickening is reduced in achromatopsia in comparison to normal controls. This is attributable to reduced thickening of each of the outer retinal layers in achromatopsia.

6.42. Remodelling of the Plexiform Layers in Achromatopsia

There is a significant reduction in the thicknesses of both the inner and outer plexiform layers in achromatopsia. The lack of input from normal, functional cone photoreceptors alters the overall intraretinal connectivity and formation of synaptic connections (contained mainly in the plexiform layers) downstream from the photoreceptors. There is evidence for remodelling of the plexiform layers in several experimental animal models of photoreceptor degeneration. This includes the Royal College of Surgeons (RCS) rat and the CNGA3^{-/-} knockout mouse.²¹⁷⁻²¹⁹

The RCS rat has a recessive mutation in the gene coding for receptor tyrosine kinase, which results in a dysfunctional retinal pigment epithelium that cannot phagocytose photoreceptor debris leading to progressive photoreceptor loss.^{217, 218} Similar to achromatopsia, in this condition there is disruption of the outer segment (OS) of the photoreceptors, a decrease in the number of photoreceptors followed by the presence of a debris zone. The CNGA3^{-/-} knockout mouse lacks any cone mediated responses and undergoes progressive retinal degeneration.²¹⁹ Photoreceptor dysfunction in both the RCS rat and CNGA3^{-/-} knockout mouse models triggers remodelling and alterations in downstream intraretinal connectivity.²⁰⁸ This includes a reduction in the number of horizontal and bipolar cells and their synaptic connections with

photoreceptors over time; a loss of complexity in their dendritic processes and finally as the degeneration advances, an irregular extension of the cell processes into the photoreceptor debris zone and into the outer and inner nuclear layers. There is also sprouting of the horizontal cells processes into the inner plexiform layer (IPL) with loss of the normal stratification of the IPL. It is possible that a similar remodelling process is occurring in the IPL and OPL in human achromatopsia which may result in an overall reduction in the thickness of these layers on OCT examination.

6.43. Residual Plasticity and Potential for Treatment in Achromatopsia

This study has shown that there is continuing regression of the IRLs from the fovea and elongation of the perifoveal inner and outer plexiform layers after birth in achromatopsia. The ONL, IS and OS also continue to elongate after birth in achromatopsia. This suggests that there is residual plasticity in the developing retina of children with achromatopsia. Recent reports have shown that adenoassociated virus (AAV) gene therapy can successfully treat animal models of achromatopsia, with prevention of further photoreceptor degeneration and recovery of cone function demonstrated on ERG following treatment.^{201, 211, 220, 221} With the imminent possibility of gene therapy for this condition, these results suggests that therapy would be most effective at an earlier age, while the photoreceptors are still developing and before the remodelling of the plexiform layers results in a dysfunctional intraretinal circuitry that would be incapable of establishing new synaptic connections with the newly established cone photoreceptors.

An intact RPE is important for normal retinal function and has been shown to become atrophic in retinal dystrophies, including achromatopsia.^{160, 196} Consistent with this we have found that the thickness of the RPE decreases with age in children with achromatopsia.

We have observed the disruption of the ISE and the appearance of the HRZ occurring as early as 6 months of age, which is earlier than that previously reported.¹⁶⁰ We have also found a significant relationship between the development of these abnormalities with age, suggesting that achromatopsia is a progressive condition in

children. This finding is also consistent with previous reports suggesting that achromatopsia is a progressive condition in older children and adults.^{126, 160}

6.44. Conclusion

We have shown that the loss of normal functional cone photoreceptors has implications for normal foveal development, with consequences for all retinal layers. In addition to pathology of the outer retinal layers, we have shown that the inner retinal layers especially the plexiform layers are also affected by achromatopsia, most likely through remodelling of downstream intraretinal circuitry. We have demonstrated that achromatopsia is not a stationary condition in infants and young children, with evidence that disease processes such as ISE disruption and the appearance of the HRZ are more likely to occur with age. This suggests that early administration of gene therapy in achromatopsia may be beneficial in preventing any further damage to the underlying retinal architecture and facilitating normal retinal maturation in infants and young children.

Chapter 7

Time Course of Changes in Retinal Development in Infants and Young Children with Albinism

7.1. Introduction

7.2. Methods

7.3. Results

7.4. Conclusion

7.1. Introduction

Normal pigmentation of the eye is dependent upon the presence of a normal functioning tyrosinase enzyme,²²² which catalyses the conversion of DOPA to dopaquinone.^{223, 224} This is subsequently converted to phaeomelanin and eumelanin. Albinism is a group of congenital disorders of melanin biosynthesis (summarised in section 1.31), which disrupts this pathway and are characterised by cutaneous and/or ocular hypo-pigmentation, nystagmus, strabismus, refractive errors, foveal hypoplasia and optic nerve misrouting.^{119, 139} The clinical and genetic characteristics of albinism have been outlined in section 1.31.

Melanin has an important function in the eye, protecting the retina from light-damage and facilitating normal functioning and development of the photoreceptors.^{38, 225-228} Tyrosinase may also play an important role in guiding retinal ganglion cell migration from the retina to the visual cortex, which may be facilitated through its production of dopamine.²²⁹ Evidence for this is presented in work where the administration of dihydroxyphenylalanine (L-DOPA) to albino eyes in rats prevents the misrouting of the retinal ganglion cells that normally occurs in albinism.²³⁰ In addition, it has also been shown in mice that L-DOPA is abundantly expressed in the pigmented RPE during development after which it declines, suggesting that L-DOPA may have a central role in guiding normal retinal development and neural projections.²³¹

It is hypothesised that normal foveal development is arrested in individuals with albinism.^{138, 147} Pigment deficiency manifests in several ways during ocular development. This includes an abnormal division pattern of the retinal progenitor cells from the early stages,^{124, 232-234} an abnormal decussation of the ganglion cell axons^{233, 234} chiasmal misrouting²³⁵, an abnormal pattern of apoptosis and mitosis during post-natal development,^{233, 236, 237} and a reduction in the number of photoreceptors.^{232, 234, 238} This work is all based on animal or in vitro models with very little work done on in vivo retinal development in humans affected by albinism.

Subretinal administration of the tyrosinase gene using adenoassociated virus (AAV) vectors in a mouse model of oculocutaneous albinism type 1 (OCA1) results in intraocular melanin accumulation, prevents further photoreceptor degeneration and restores retinal function as measured on ERG.¹⁹⁹ Nitisinone is an inhibitor of 4-

hydroxyphenylpyruvate dioxygenase is an FDA approved drug used for the treatment of hereditary tyrosinemia type 1.²³⁹⁻²⁴² Administration of this drug in a mouse model of OCA-1B has been shown to elevate plasma tyrosine levels and increase oculocutaneous pigmentation, thus raising the possibility of this drug as a potential novel treatment in patients with OCA-1B.²⁴³

With these therapies potentially becoming available, it is important to develop a detailed understanding of in vivo human albino retinal development so that further therapeutic targets can be identified, the timing of treatment can be optimised and treatment outcomes can be objectively assessed. The aim of this study was to use OCT to determine to how albinism it affects the developing retina in a group of infants and young children aged between birth and 6 years of age.

7.2. Methods

7.21. Participants

The cohort for this study included 44 children with a confirmed diagnosis of albinism, based on the criteria outlined in section 2.1. The clinical and demographic characteristics of these participants are summarised in Tables 1, 2 & 3 in Appendix 4. We obtained 117 mixed cross sectional and longitudinal examinations (219 tomograms), which included 113 (51.6%) and 106 (48.4%) tomograms obtained from the right and left eyes, respectively, in the albinism group. These were compared to 223 control children that were previously described in chapter 4. The mean age at the time of examination was 3.0 years (range 0-7.2 years) for the albinism group and 2.2 years (range 0-6.9 years) for the control group.

All participants underwent a full orthoptic and ophthalmologic examination, which included slit-lamp examination where possible, fundus examination and measurement of visual acuity. Visual acuity (VA) was assessed in younger infants and children by preferential looking using Teller acuity cards and/or crowded logMAR Kay Picture Tests if possible. In cooperative children, Teller acuity cards and/or logMAR crowded optotypes (Glasgow Acuity Cards) were used to obtain VA.

7.22. Optical Coherence Tomography

HH-SDOCT (Bioptigen™ Envisu system, Durham, NC, USA) was used to obtain a volumetric scan (consisting of 100 B-scans and 500 A-scans per B-scan) of the foveal region as previously described¹⁹². The acquired images were exported from the Bioptigen OCT software and imported into ImageJ software (available at: <http://rsbweb.nih.gov/ij/> Date accessed: May 11, 2012) where retinal layer segmentation was performed. The nomenclature used to label the segmented layers are based on previously established anatomical correlates with histology^{93 94}.

7.23. Statistics and Modelling

A generalised linear mixed model, implemented in STATA™ software (Copyright 1996–2014, StataCorp), was used to analyse the differences between the albinism and control groups with regards to the thickness measurements obtained for

each retinal layer at the fovea, parafovea and perifovea using a pseudo-adaptive Gauss-Hermite quadrature rule. The model included effects for diagnosis, age, the interaction between diagnosis and age (diagnosis*age) and eye. Post-hoc estimates of the average marginal effects of diagnosis on retinal layer thickness measurements were calculated for overall retinal thickness (RT), inner retinal layers (IRLs) and outer retinal layers (ORLs). The results of the marginal effects analysis are presented in Appendix 4.

All analyses were considered significant at a type 1 probability value of $p < 0.05$. Statistical analysis was performed STATA™ software (Copyright 1996–2014, StataCorp).

7.3. Results

7.31. General Outline of Foveal Development and Morphology

In all of the participants with albinism, there was evidence of foveal hypoplasia (persistence of the normally absent inner retinal layers (IRLs)) at the fovea (Figure 7.1A). Ongoing foveal development with age is evident on the longitudinal OCT examinations obtained in the albinism group. There is a reduction in IRL thickness at the fovea, migration of the photoreceptors into the fovea and elongation of the photoreceptor layers with increasing age, although occurring at an altered rate and magnitude in comparison to the control group (Figures 7.1, 7.2 & 7.3).

Figures 7.2 and 7.3 show z statistic scores across the retina for the terms in the statistical models. The overall differences in retinal layer thicknesses between albinism and controls (i.e. group term) are shown in figure 7.2, whereas differences in rate of change in retinal layer thicknesses with time are shown in figure 7.3 (interaction term between group and age). Positive scores indicate a higher value in albinism (i.e. thicker retinal layers in albinism for figure 7.2 and greater rate of change in albinism for figure 7.3). Z statistic ≤ -2 or ≥ 2 indicate statistical significance. Scatter plots of the change in retinal layer thickness with age are presented in Figures 7.4, 7.5 and 7.6.

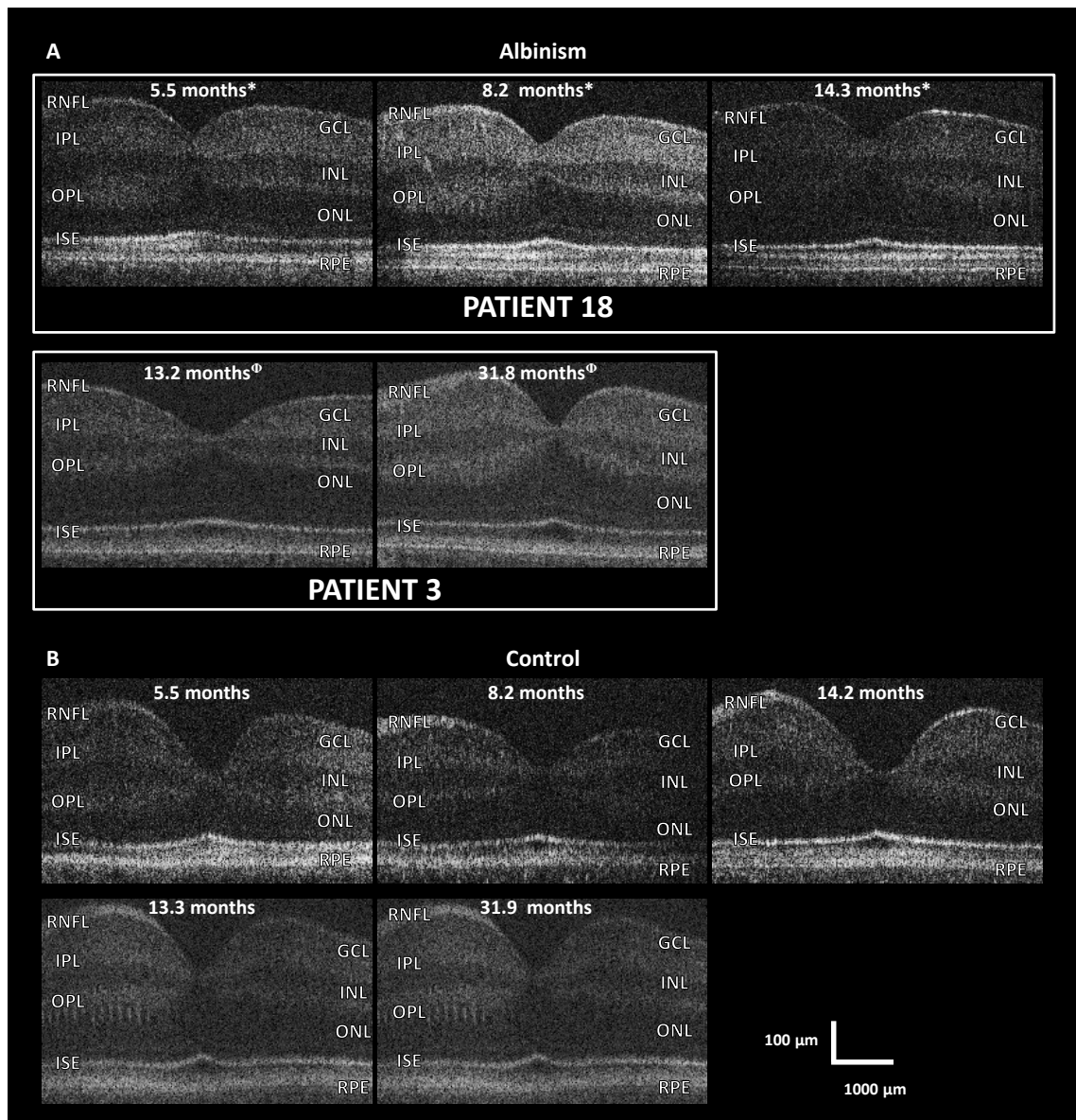


Figure 7.1. Examples of foveal tomograms from 2 albinism participants illustrating the main features of foveal development over time in albinism.

Foveal hypoplasia is evident in all of the tomograms taken from the albinism group (A). There is a reduction of the thickness of the inner retinal layers (IRLs) (which includes the RNFL, GCL, IPL, INL and OPL) with increasing age. This is in contrast to the control group where there are no IRLs visible at the fovea after the first few months of life (B). In both the albinism and control groups there is elongation of the outer retinal layers (ORLs) (which includes the ONL, IS and OS) with increasing age.

** and Φ indicate tomograms taken from the same patient at different time points*

RNFL = retinal nerve fibre layer; GCL = ganglion cell layer; IPL = inner plexiform layer; INL = inner nuclear layer; OPL = outer plexiform layer; ONL = outer nuclear layer; ELM = external limiting membrane; ISE = ellipsoid of the inner segment of the photoreceptor; RPE = retinal pigment epithelium; IRLs = inner retinal layers; ORLs = outer retinal layers; IS = inner segment of photoreceptors; OS = outer segment of photoreceptors

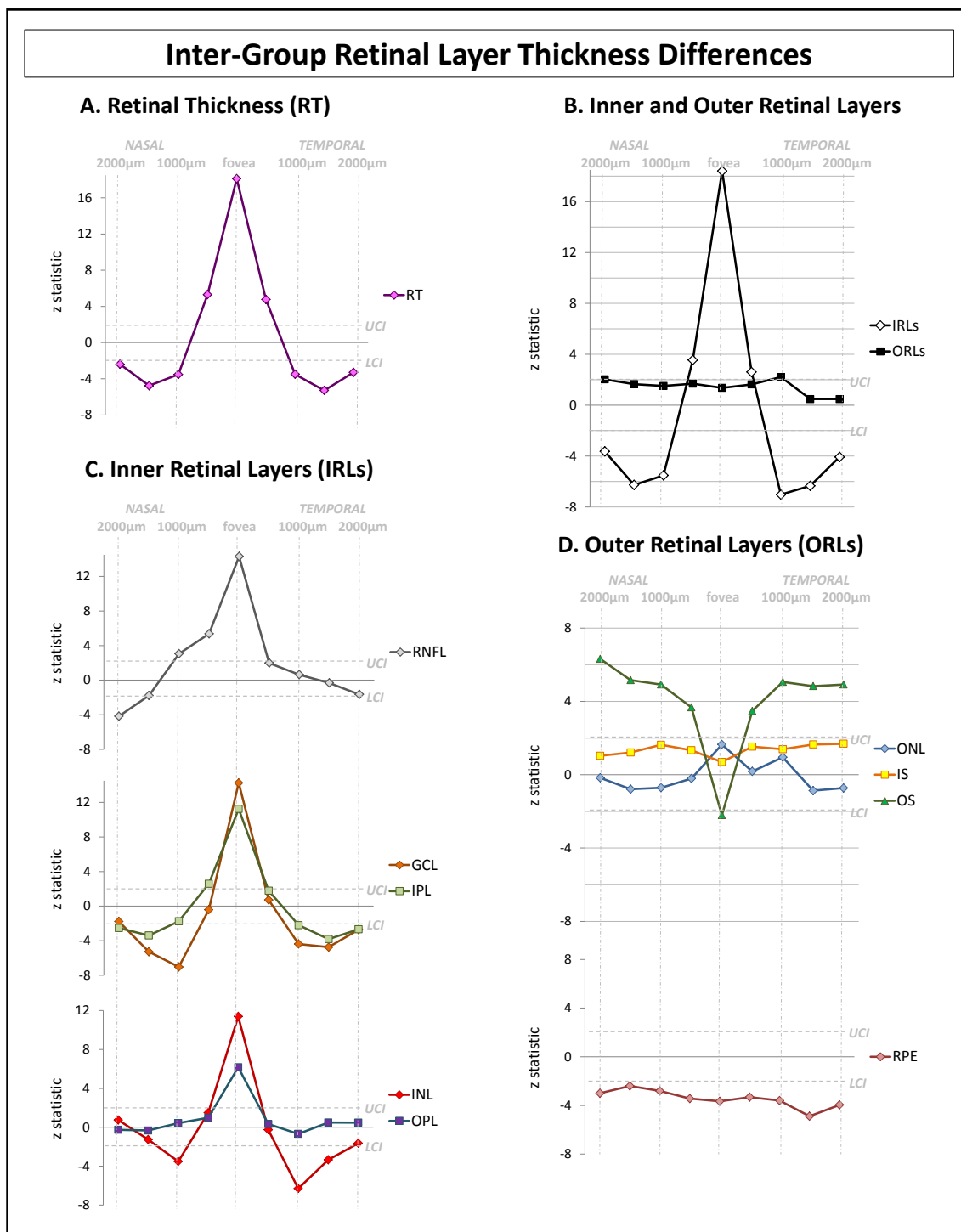


Figure 7.2. Mean differences in retinal layer thickness measurements between the albinism and control groups.

Results are shown for (A) retinal thickness (RT), (B) inner (IRLs) and outer retinal layers (ORLs) as well as each individual retinal layer (C & D) at the fovea, parafovea and perifovea. The parafoveal measurements were taken at 500 μm and 1000 μm nasal and temporal to the central fovea. The perifoveal measurements were taken at 1500 μm and 2000 μm nasal and temporal to the central fovea. Positive and negative z-score indicate increased and decreased thickness measurements, respectively, in the albinism group. Z statistic ≤ -2 or ≥ 2 indicate statistical significance (indicated by the two dotted lines).

RT = retinal thickness; IRLs = inner retinal layers; ORLs = outer retinal layers; RNFL = retinal nerve fibre layer; GCL = ganglion cell layer; IPL = inner plexiform layer; INL = inner nuclear layer; OPL = outer plexiform layer; ONL = outer nuclear layer; ELM = external limiting membrane; ISE = ellipsoid of the inner segment of the photoreceptor; RPE = retinal pigment epithelium

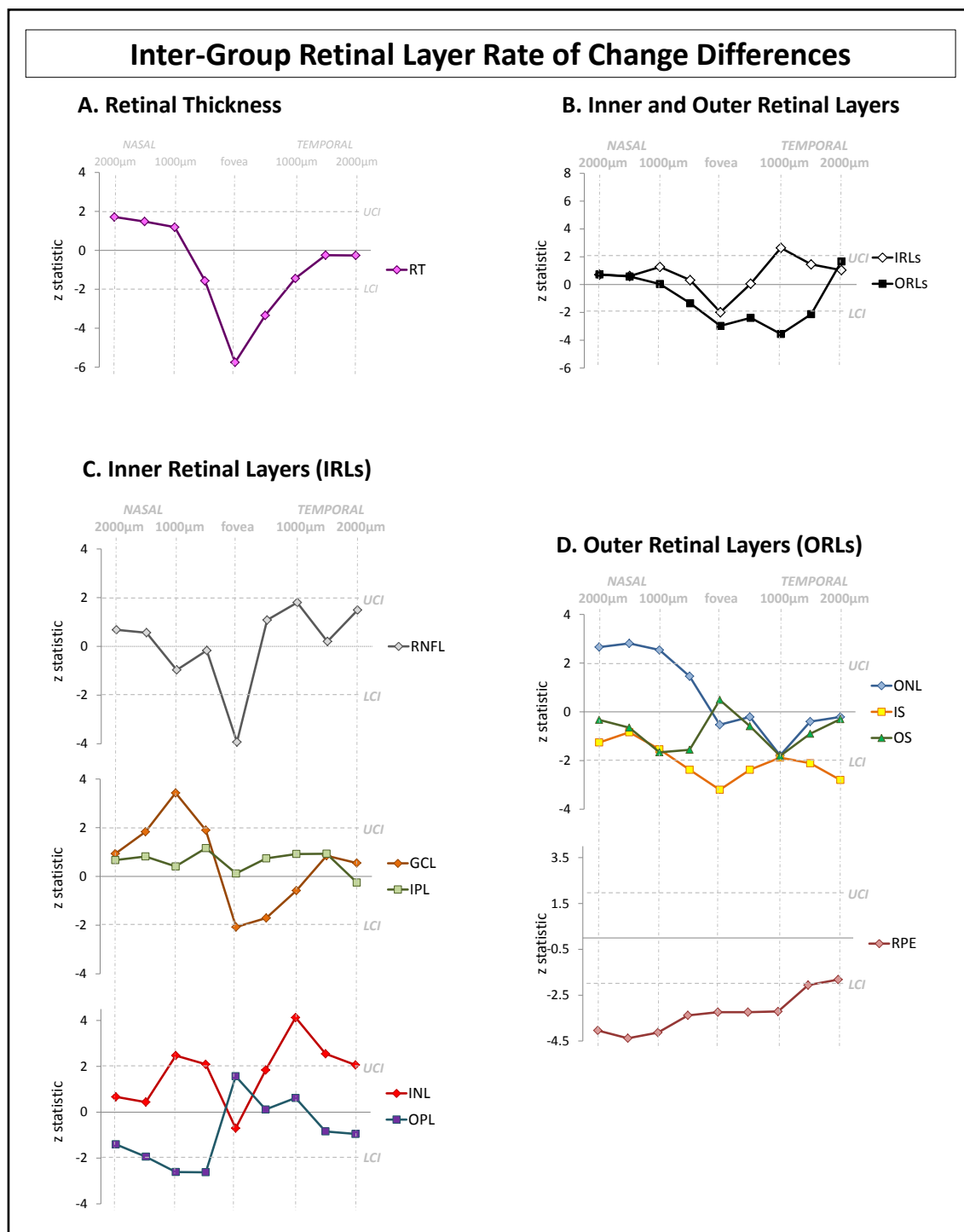


Figure 7.3. Differences in the rate of change in retinal layer thicknesses with age between the albinism and control groups.

Results are shown for (A) retinal thickness (RT), (B) inner (IRLs) and outer retinal layers (ORLs) as well as each individual retinal layer (C & D) at the fovea, parafovea and periphery. The parafoveal measurements were taken at 500 μm and 1000 μm nasal

and temporal to the central fovea. The perifoveal measurements were taken at 1500 μm and 2000 μm nasal and temporal to the central fovea. Positive z-scores indicate increased rate of change and negative z-score indicate decreased rate of change in achromatopsia. Z statistic ≤ -2 or ≥ 2 indicate statistical significance (indicated by the two dotted lines).

RT = retinal thickness; IRLs = inner retinal layers; ORLs = outer retinal layers; RNFL = retinal nerve fibre layer; GCL = ganglion cell layer; IPL = inner plexiform layer; INL = inner nuclear layer; OPL = outer plexiform layer; ONL = outer nuclear layer; ELM = external limiting membrane; ISE = ellipsoid of the inner segment of the photoreceptor; RPE = retinal pigment epithelium

7.32. Overall Retinal, Inner and Outer Retinal Layer Thicknesses

Figure 7.2A shows that the central macular thickness (CMT) at the fovea was significantly greater in albinism compared to controls ($p < 0.0001$). In contrast to this, the parafoveal and perifoveal retinal thicknesses are significantly decreased in albinism in comparison to controls ($p < 0.0001$). The rate of change with age was significantly higher in albinism for the CMT ($p < 0.0001$) but was similar in the two groups in the parafovea and perifovea (Figures 7.3A).

The significantly increased CMT observed between the albinism and control groups (Figure 7.2A) is mainly attributable to differences in the IRLs observed at the fovea in the two groups (Figures 7.2B, 7.3B & central column of figures in 7.4). In albinism the foveal IRLs are on average 6.3x the size of mean control values ($p < 0.0001$). There was no significant difference foveal ORL thickness between the albinism and control groups.

The difference in the rate of change of the foveal IRLs and ORLs with age is interesting (Figure 7.3B). The IRLs decrease in size with age in albinism in contrast to controls which show no change (difference in rate of change: $p < 0.05$). The ORLs increase in size in both groups but at a slower rate in albinism (difference in rate of change: $p < 0.01$).

The pattern of differences between albinism and controls in the foveal IRLs and ORLs are in contrast with the changes observed at the parafovea and perifovea (Figures 7.2B, 7.3B and 7.4B & C). The IRLs are significantly thinner in albinism in the parafovea and perifovea compared to controls ($p < 0.0001$). The thickness of the ORLs across the retina are similar between both groups. Differences in the rate of change of the IRLs and ORLs outside the fovea are in general mild. The only significant differences observed are in the temporal parafoveal ORLs which increase in thickness more slowly in albinism compared to controls ($p < 0.05$).

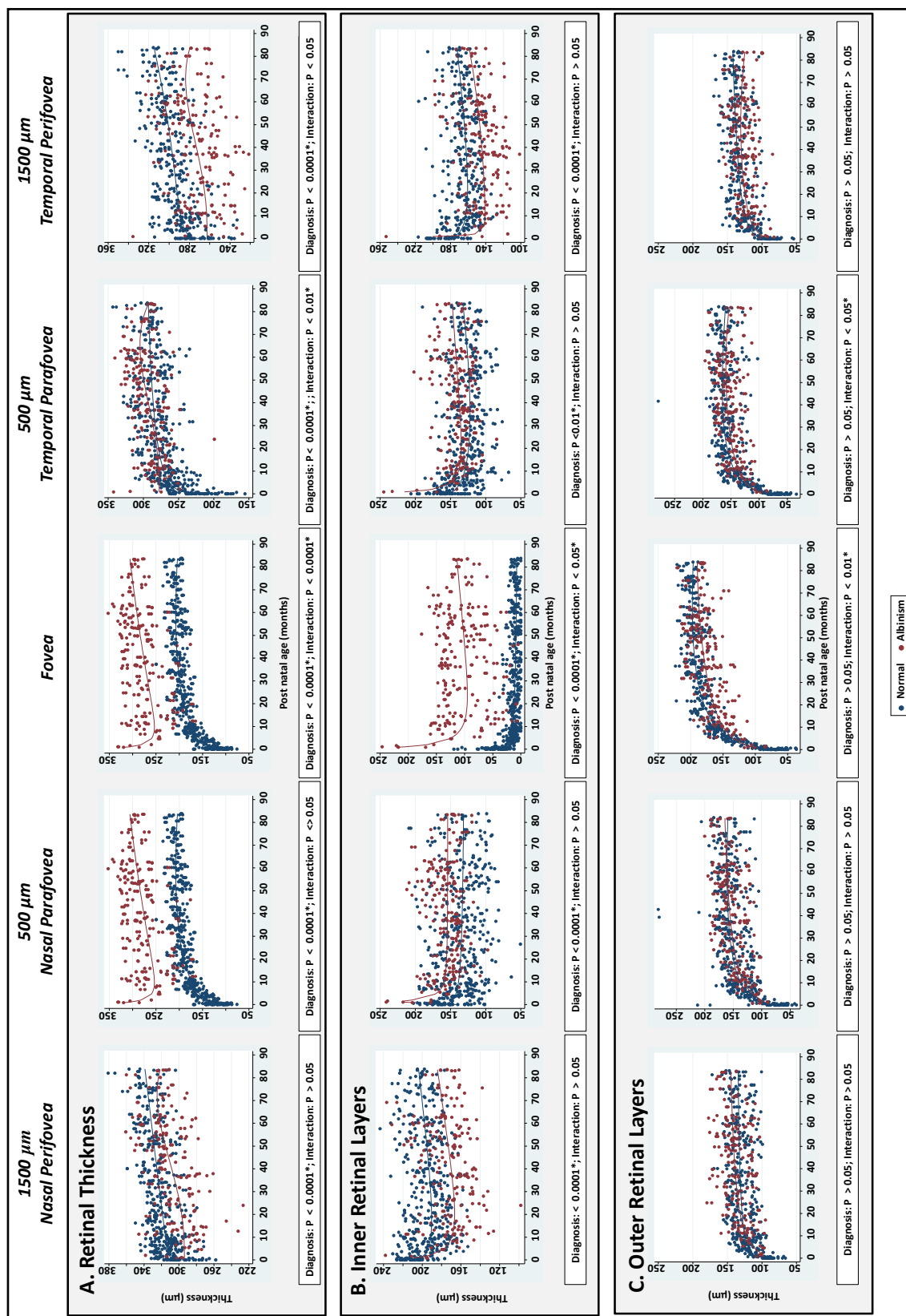


Figure 7.4. Development trajectories for the inner retinal layers, outer retinal layers and total retinal thickness at the fovea, parafovea and perifovea.

*The trajectories have been plotted over a time period spanning 0 through 90 months post natal age. Each point represents a single value from each OCT examination. The lines of best fit (trend lines) are shown in red and blue for the albinism and control groups respectively. P values that were calculated from the generalised linear mixed model analysis are provided with regards to the effects of diagnosis and the diagnosis*age interaction on each measurement.*

7.33. Individual Retinal Layers

Figures 7.2C and D show changes in mean thickness for individual retinal layers and figures 7.3C and D the rate of change with age, and hence indicate where the greatest changes are taking place to explain the patterns in IRLs and ORLs described. Scatter plots of changes in the thickness of each retinal layer with age are shown in figures 7.5 and 7.6 at the fovea and at positions 500 μm and 1500 μm nasally and temporally.

Figure 7.2C indicates that the dramatically thickened IRLs observed at the fovea for albinism are due to significantly increased thicknesses in all inner retinal layers ($p < 0.0001$). Figure 7.3C shows that the significant regression of the IRLs with time at the fovea seen in albinism are mainly due to changes in the RNFL ($p < 0.0001$) and GCL ($p < 0.05$). Figure 7.5 shows that this is because in controls the IRLs are almost completely regressed by the first few months of life but are only slowly regressing in albinism. The thinner parafoveal IRLs in albinism which is especially marked at 1500 μm from the fovea, is attributable to significantly decreased thicknesses in the GCL ($p < 0.0001$), IPL ($p < 0.0001$) and temporal INL ($p < 0.01$) (Figure 7.2C).

Figure 7.2D shows that although there was no significant difference in the thickness of ORLs observed across the retina between albinism and control groups that there are significant and interesting differences in the individual outer retinal layers. The foveal OS is significant decreased ($p < 0.05$) whereas the parafoveal OS is significantly increased in albinism in comparison to controls ($p < 0.0001$). The RPE is uniformly decreased in thickness across the retina in albinism ($p < 0.0001$). Figure 7.3D shows that the decreased rate of foveal and parafoveal ORL thickening in albinism is due mainly to changes in the foveal and parafoveal IS ($p < 0.01$) with smaller contributions from the ONL and OS layers. The rate of increase in RPE thickness with age across the retina is significantly reduced in albinism in comparison to the control groups ($p < 0.05$).

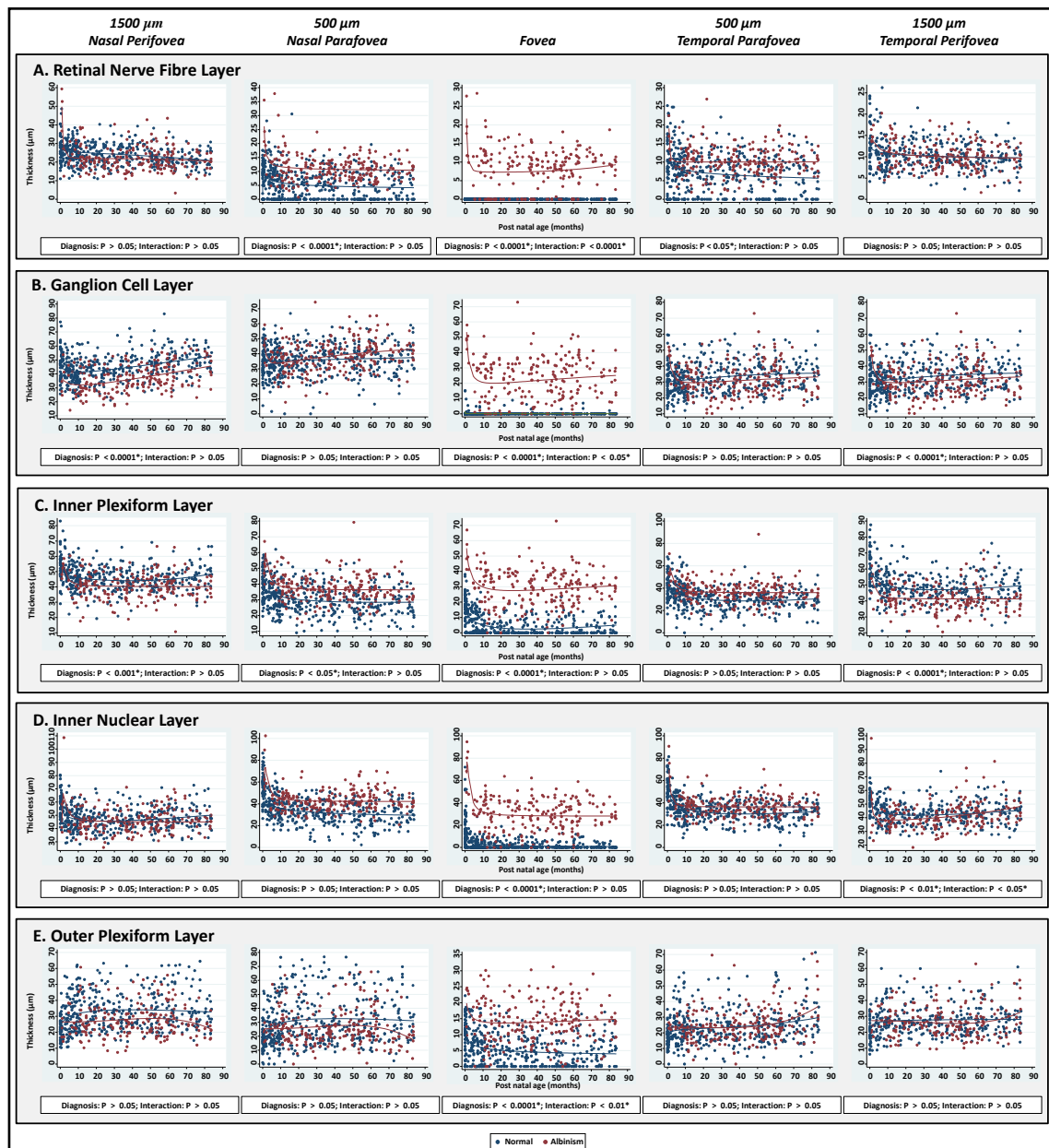


Figure 7.5. Development trajectories for the RNFL, GCL, IPL, INL and OPL at the fovea, parafovea and perifovea.

The trajectories have been plotted over a time period spanning 0 through 90 months post natal age. Each point represents a single value from each OCT examination. The lines of best fit (trend lines) are shown in red and blue for the albinism and control groups respectively. *P* values that were calculated from the generalised linear mixed model analysis are provided with regards to the effects of diagnosis and the diagnosis*age interaction on each measurement.

RNFL = retinal nerve fibre layer; GCL = ganglion cell layer; IPL = inner plexiform layer; INL = inner nuclear layer; OPL = outer plexiform layer

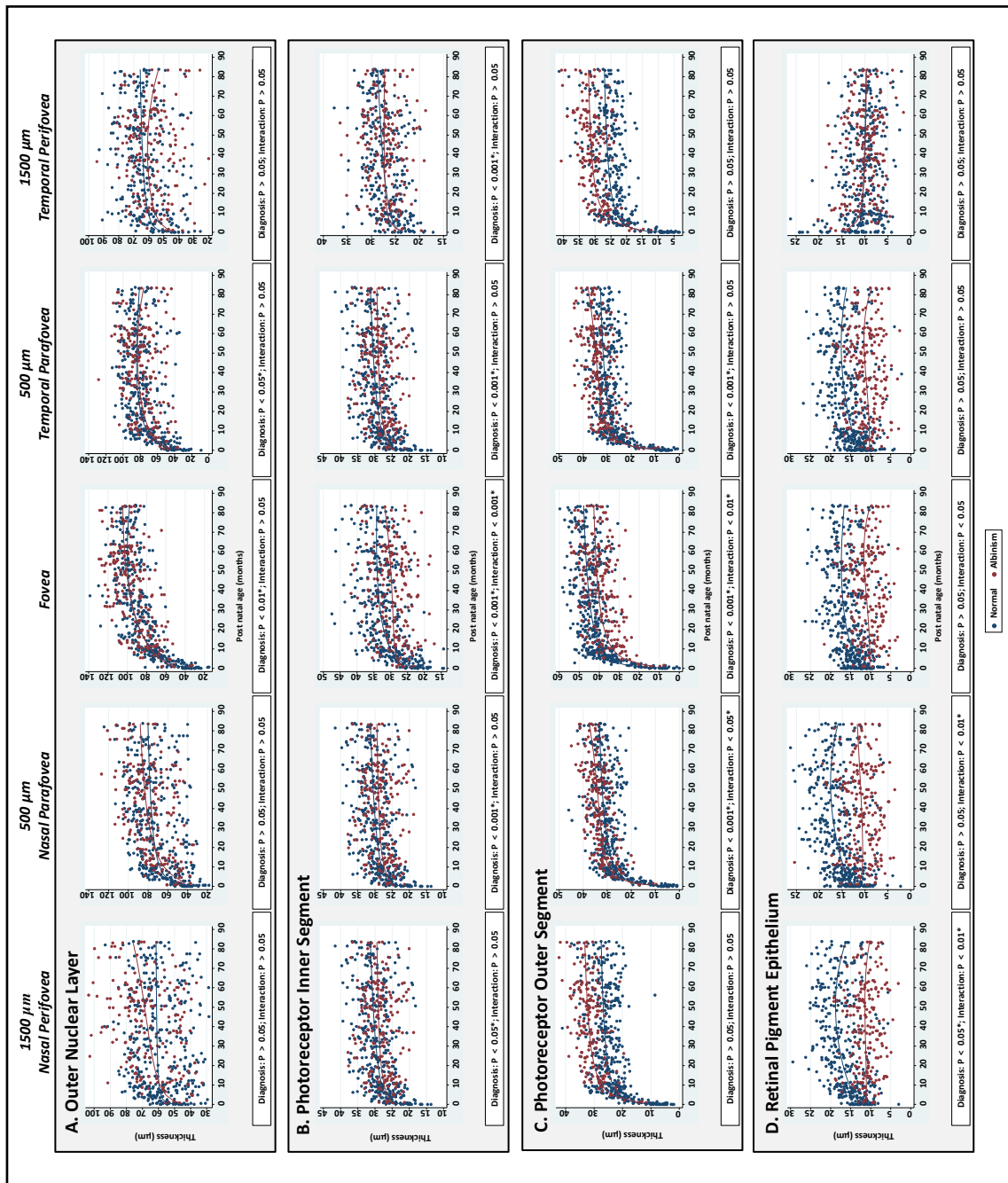


Figure 7.6. Development trajectories for the ONL, OPL, IS, OS and RPE at the fovea, parafovea and periphery.

The trajectories have been plotted over a time period spanning 0 through 90 months post natal age. Each point represents a single value from each OCT examination. The lines of best fit (trend lines) are shown in red and blue for the albinism and control

*groups respectively. P values that were calculated from the generalised linear mixed model analysis are provided with regards to the effects of diagnosis and the diagnosis*age interaction on each measurement.*

ONL = outer nuclear layer; IS = photoreceptor inner segment; OS = photoreceptor outer segment; RPE = retinal pigment epithelium

7.4. Discussion

It is thought that the retinal findings associated with albinism in adults represents arrested retinal development. However, as retinal development is known to continue at least until the age of 4 years, one cannot be certain if development is arrested or continues in an altered spatial and temporal pattern in infants and young children with albinism.

7.41. Inner Retinal Layers in Albinism

This study has demonstrated ongoing regression of the inner retinal layers in albinism, although delayed and incomplete in comparison to normal controls. This results in the presence of the normally absent inner retinal layers at the fovea and a significantly increased central macular thickness. This suggests that L-DOPA or other melanin dependent signalling molecules which are known to be deficient in albinism are necessary for the correct regression of the IRLs away from the fovea. Indeed, previous studies have illustrated the guidance role of both L-DOPA and melanin dependent signalling molecules in directing the correct neuronal projections from the retina to the optic chiasm.^{229-231, 234, 235, 244}

In contrast to the central macular thickness which is increased in albinism, the parafoveal and perifoveal retinal thicknesses are reduced in albinism. This is the result of a reduction in the thicknesses of the parafoveal and perifoveal IRLs, in particular the GCL and IPL. The exact mechanism(s) of how melanin or L-DOPA would cause these developmental alterations is not well understood. A possible explanation for this contrasting pattern of development is suggested in a rat model of albinism.^{232, 245} In this rat model, it has been shown that there is a delay in the normal central to peripheral gradient of maturation of each of the retinal layers in albinism. This affected the GCL, INL and ONL and was associated with significant thinning of the INL and ONL.^{232, 245} An equivalent delay in the central to peripheral maturation of the IRLs in human albinos would result in thicker IRLs at the fovea with corresponding thinning of the parafoveal and perifoveal IRLs as seen in our patients.

7.42. Outer Retinal Layers in Albinism

The photoreceptor outer segments develop in the opposite direction of IRL development in albinism. The foveal OS thickness is significantly decreased, whereas the parafoveal OS thickness is significantly increased. In addition the rate of elongation of the foveal ORLs is reduced in albinism, due mainly to reduction in IS elongation. This suggests that melanin or another signalling molecule such as L-DOPA are required for guiding the normal centripetal migration of the cone photoreceptors into the fovea and the regulation of the growth and differentiation of the photoreceptors. There is supporting evidence in the literature for this, with a correlation demonstrated between the levels of ocular melanin and rod numbers.^{238, 164, 246}

DOPA is known to regulate and alter the normal cell cycle length as well as signal cell cycle exit. As DOPA is deficient in albino eyes, this has implications for retinal development and morphology at the cellular level, with loss of normal regulation of the cell cycle and increased levels of mitosis.^{230, 247, 248} In the albino rat retina this manifests as a transitory retinal thickening followed by an elevated phase of cell death that depletes cell numbers.²³⁰ This peak occurs around birth, when rod production peaks.^{249, 250} It is estimated that approximately 30% of the rod population does not develop in albinism.^{164, 246}

The pattern of OS development that we observed may represent an impaired migration of the cone photoreceptors from the peripheral retina into the fovea as well as altered patterns of mitosis and cell death of the photoreceptors across the albino retina. The decrease in OS thickness that we observe at the central fovea in albinism may represent a reduction in photoreceptor density, while concurrently we may be observing the effects of increased mitosis and transitory thickening of the OS layer in the more peripheral retina. It is possible that a phase of increased cell death involving the peripheral photoreceptors will occur after childhood. It would be interesting to continue to monitor the retinal development of these children into adulthood to confirm if this is the case.

In this study, the rate of maturation of the RPE is significantly reduced in albinism in comparison to the control group, which results in a significant decrease in the thickness of the RPE layer across the retina, suggesting that L-DOPA also has an

important role in the development of the human RPE. Differences in the differentiation of the RPE in comparison to normally pigmented controls have also been shown in a mouse model of albinism.²⁵¹ The reduction in L-DOPA disrupts the normal pattern of RPE development, with an increase in mitosis and a reduction in apoptosis with the overall result of an increase in the total number of RPE cells.

7.43. A Retinal Origin for Chiasmal Misrouting?

It has been hypothesised that the origin of the chiasmal misrouting observed in albinism may arise from perturbations in the development of the neural retina. Evidence for this has been shown in animal models of albinism. Firstly, it has been shown that albino mice have decreased numbers of ganglion cells expressing ipsilateral markers.²⁵² Normally during development of the mouse retina, ganglion cells that would project ipsilaterally through the optic chiasm differentiate earlier than contralaterally projecting ganglion cells.²⁵³ In albinism there may be an alteration in the number of cells produced during each phase of retinal development, resulting in a differentiation bias towards contralaterally projecting ganglion cells.²³³

Secondly, in vitro experiments carried out on albino animals have demonstrated that the retinal ganglion cells from the temporal retina which would normally be expected to project ipsilaterally, tended to behave more like contralaterally projecting axons when confronted with chiasmal cells.^{230, 254, 255} If a similar differentiation pattern is occurring in the human retina, then there may be greater number of ipsilaterally projecting ganglion cells present, causing this asymmetry.

7.44. Residual Plasticity and Potential for Treatment in Albinism

This study has demonstrated multiple abnormalities in the development of the human albino retina, which are likely the result of deficiencies in both melanin and L-DOPA. Melanin and L-DOPA are determining the differentiation, migration and spatial distribution of the neuronal cells within the retina, processes which are disrupted in albinism. The key to understanding how this results in the crossed asymmetry of the chiasm typical of albinism will rely on studies, outlining the effects of melanin dependent signalling molecules produced by the RPE on the differentiating retina.²⁵⁶

Finally, the possibility that melanin and L-DOPA are responsible for the retinal deficits in albinism presents opens the possibility for a number of therapeutic targets, some of which are already being administered on a trial basis.²³⁹⁻²⁴³ This study has demonstrated that development is not arrested but is ongoing in the albino retina after birth, which suggests that potentially administration of therapy in early infancy and childhood, while there is still residual plasticity in the retina may improve retinal development and optimise vision.

Chapter 8

Discussion and Conclusion

Previous histological and molecular studies have illustrated the multiple mechanisms required for normal foveal development. These include several growth factors, guidance molecules¹⁸⁻²⁰ and anti-angiogenic factors^{5, 9-17}; the mechanical effects of intraocular pressure,²³ growth induced stretch of the retina³³ and the presence of a foveal avascular zone^{23, 24} which interact to trigger a cascade of events that leads to formation of the fovea. This manifests as migration of the inner retinal layers away from the fovea, migration of the outer retinal layers into the fovea and elongation of the photoreceptors over time.³⁶ These studies were limited by the small numbers of human histological specimens available. With the development of non-invasive, rapid, high resolution (2.4 μm) paediatric retinal imaging in the form of hand-held spectral domain optical coherence tomography, large scale in vivo studies of both normal and abnormal foveal development in human infants and young children have become possible.

HH-SDOCT has been previously used successfully to image children with several pathologies including ROP, although problems reported specific to paediatric imaging include difficulties with fixation and movement artefacts.^{49, 98-101, 257} Therefore, we investigated whether HH-SDOCT can produce reliable and repeatable measurements. We found that it is very reliable, with ICCs of 0.966 in children with nystagmus and 0.960 in control children for measurements of central retinal thickness, thus validating it as a tool for investigating retinal and foveal development in vivo.¹⁹²

The timing of completion of foveal maturation is debated with a wide range reported in the literature from between 11 months and 5 years of age.^{36, 37, 50, 60} Using the HH-SDOCT we were able to image the retinae of a group of 223 healthy control children aged between birth and 6 years of age and model the complex non-linear individual developmental trajectories for each retinal layer. We found evidence of concurrent retinal layer thickening and migration affecting the inner retinal layers at differing rates, giving rise to unique developmental trajectories for these layers. There was evidence that retinal development continues beyond the age of 5 years, with the OS continuing to increase in size till the age of 12 years. This mimics findings of longitudinal MRI cortical development studies.¹⁹⁷ In addition, we found that

development of each of the outer retinal layers at the fovea, in particular the ONL contributes to the development of visual acuity.

With a clear picture of normal *in vivo* retinal and foveal development on HH-SDOCT, we proceeded to test the diagnostic potential of the HH-SDOCT in identifying the aetiology of infantile nystagmus in infants and young children based on foveal morphology, as several of these aetiologies are associated with arrested retinal development. We found that it was possible to identify the presence of typical and atypical foveal hypoplasia and other abnormalities of retinal structure in these children. As a result, it was possible to formulate an OCT based diagnostic algorithm which has made diagnosing the aetiology of infantile nystagmus more efficient and has now been implemented in clinical practice.⁷

Conditions associated with abnormal or arrested retinal and foveal development offer a unique opportunity to study the contribution of specific components of the foveal developmental pathway on overall development. Achromatopsia, a condition that specifically affects the cone photoreceptors is a prime example of this.¹⁵³ We were able to successfully image 8 infants and young children with achromatopsia longitudinally across several time points using HH-SDOCT and found that the presence of normal functional cone photoreceptors is necessary for the normal development of downstream intraretinal circuitry. This manifests as alterations in inner and outer plexiform layer thickness. In addition, assuming that all other factors (biochemical and mechanical) are similar in the achromatopsia retina as compared to the normal control retina, it appears that elongation of cone photoreceptors contributes to pit formation, perhaps by exerting an upward mechanical force. We have also demonstrated that retinal development is not arrested in children with achromatopsia, but continues at an altered rate and magnitude in comparison to normal controls. Potentially, administering treatment at this stage, while there is residual plasticity in the retina may help to normalise retinal development and optimise vision in achromatopsia. With gene therapy imminent in achromatopsia, this data suggests that the therapy may be more beneficial at an earlier age.²¹⁶

Albinism is typically associated with arrested retinal development.^{138, 147} It is of particular interest, as it offers clues to retinal development at the cellular level. We imaged the retinae of 44 infants and young children with a diagnosis of albinism at

several time points and have demonstrated a multitude of developmental abnormalities, including impaired but ongoing centrifugal migration of the inner retinal layers from the fovea, a reduction in the rate of the normal centre to periphery gradient of maturation, a reduction in the size of the photoreceptor layers, alterations in the rate at which the photoreceptor layers increase in size and a reduction in RPE thickness. This indicates that melanin, L-dopa or perhaps other signalling molecules deficient in albinism play a central role in normal retinal development. They appear to regulate the normal cell cycle, mitosis and migration patterns within the retina.^{124, 230, 232, 233, 236-238, 245} It is possible that the crossed asymmetry of the optic chiasm typically seen in albinism is the result of perturbations in retinal development.²³⁵ The key to understanding the origin of misrouting in albinism may lie in understanding the molecular signalling pathways in albinism and their effects on the developing retina.

This work has demonstrated how hand-held spectral domain optical coherence tomography has revolutionised the investigation of infants and young children with retinal conditions. Normal *in vivo* foveal development has been modelled in detail and this provides a basis with which abnormal retinal development can be identified and compared. The study of conditions associated with abnormal retinal development, such as achromatopsia and albinism, have provided important clues with regards to retinal and foveal development. Future studies may look at other conditions such as idiopathic infantile nystagmus and retinal dystrophies to define what effect these conditions may have on the developing retina.

8.2 Future Research Questions

1. It has been demonstrated in older children that race and gender influences RNFL, macular volume and thickness measurements.^{117, 118, 258} Exploration of the influence of race and gender on normal retinal development in infants and young children would be interesting.
2. It has been suggested that the presence of macular oedema in premature infants may be associated with a possible delay in maturation of the inner retinal layers.⁴⁹ A number of full-term infants were identified in this study where macular oedema was present on their tomograms. The longitudinal effect of the presence of macular oedema in normal full term infants and its effects on retinal development remains to be explored.
3. In addition to foveal tomograms, optic nerve tomograms were also obtained on many of the participants in this study. Recently published work has demonstrated differences in optic nerve development in preterm infants as compared to full term infants.²⁵⁹ We need to investigate the course of normal optic nerve development in our participants and correlate it with retinal development.
4. In chapters 6 and 7 of this thesis, ongoing changes in the morphology of each of the retinal layers in children aged 0-6 years with achromatopsia and albinism was demonstrated. It would be very important to continue with longitudinal OCT assessments of achromatopsia and albinism beyond the age range examined in this thesis in order to identify alterations in retinal development that may only become manifest at an older age.
5. In chapter 4, we showed how measurements of each of the outer retinal layers was correlated with visual acuity. In addition in adults with albinism, it has been demonstrated that measurements of the OS are strongly correlated with visual acuity.¹²⁷ It would be interesting to investigate if retinal layer measurements from tomograms obtained in early childhood in infants and young children affected by retinal diseases can be used to predict their future adult visual acuity. In order to develop OCT-based visual prognostic indicators in retinal disease, we will need to maintain longitudinal follow-up of the infants and young children with retinal disease recruited during this study until they reach visual maturity.

6. In chapters 6 and 7, we showed how specific retinal pathology such as abnormal cone photoreceptors in achromatopsia and melanin and L-DOPA deficiency in albinism affects retinal development in different ways. This suggests that the study of other retinal pathology such as IIN and retinal dystrophies may provide additional insights into retinal development. Further recruitment and analysis of the tomograms obtained from the infants and young children with IIN and retinal dystrophy during this study needs to be carried out in order to investigate how IIN and retinal dystrophies might affect retinal development.
7. As part of this work, saliva samples were also collected for genetic analysis. In the future, it would be important to complete the genotypic and phenotypic correlations of all the participants with nystagmus in this study. Genotype-phenotype correlations would greatly increase our understanding of the molecular mechanisms of the diseases (e.g. achromatopsia, albinism, IIN and retinal dystrophies) that cause nystagmus.

Appendices

Appendix 1

Supplementary Data for Chapter 4

Table 1: Demographics

Race	Number (%)
Caucasian	162 (62.1)
Asian	68 (26.1)
Afro-Caribbean	13 (5.0)
Other	18 (6.9)
Total	261 (100)
Gender	Number (%)
Male	127 (48.7)
Female	134 (51.3)
Total	261 (100)
Eyes Scanned	Number (%)
Right	276 (51.7)
Left	258 (48.3)
Total	534 (100)

Summary of the demographic characteristics of the participants in this study

The participants were classified by ethnicity into one of four categories: Caucasian, Asian, Afro-Caribbean and other (for participants not fitting into any one of the aforementioned categories).

Table 2: Birth Weights & Gestational Ages

Age Group	Variable	Min	Max	Mean	SD
<40 weeks GA n = 19	Birth Weight (Kg)	1.93	3.95	3.0458	0.60822
	Gestational Age (months)	8.41	9.40	9.1153	0.29330
41-46 weeks GA n = 18	Birth Weight (Kg)	3.20	4.26	3.6883	0.29673
	Gestational Age (months)	9.46	10.71	9.8622	0.36531
47-52 weeks GA n = 7	Birth Weight (Kg)	3.20	3.87	3.4529	0.30115
	Gestational Age (months)	11.04	12.19	11.5214	0.47136
12-14 months GA n = 23	Birth Weight (Kg)	1.41	6.70	3.3638	0.99368
	Gestational Age (months)	12.22	15.11	13.4752	0.79678
15-17 months GA n = 24	Birth Weight (Kg)	2.14	4.26	3.2706	0.56635
	Gestational Age (months)	15.37	18.17	16.7583	0.89850
18-20 months GA n = 19	Birth Weight (Kg)	2.49	4.26	3.2831	0.46881
	Gestational Age (months)	18.33	20.86	19.3895	0.75055
21-26 months GA n = 15	Birth Weight (Kg)	2.15	4.82	3.4100	0.62701
	Gestational Age (months)	21.39	27.07	24.4440	1.88727
27-32 months GA n = 18	Birth Weight (Kg)	2.72	4.17	3.3079	0.44461
	Gestational Age (months)	27.43	33.02	30.1806	1.79618

33-38 months GA n = 14	Birth Weight (Kg)	2.77	3.67	3.1567	0.36812
	Gestational Age (months)	33.28	38.75	35.8314	1.99794
39-44 months GA n = 14	Birth Weight (Kg)	2.78	3.84	3.2150	0.41139
	Gestational Age (months)	39.92	45.57	42.1321	1.58114
45-56 months GA n = 24	Birth Weight (Kg)	1.90	5.80	3.4811	0.87330
	Gestational Age (months)	46.19	57.13	50.0483	3.20553
57-68 months GA n = 27	Birth Weight (Kg)	2.00	4.85	3.4764	0.80214
	Gestational Age (months)	58.54	69.02	63.1130	3.32302
69-80 months GA n = 17	Birth Weight (Kg)	2.79	3.67	3.1421	0.26790
	Gestational Age (months)	69.62	80.52	74.1065	3.68149
81-92 months GA n = 23	Birth Weight (Kg)	2.02	4.17	3.4820	0.51217
	Gestational Age (months)	81.97	93.07	87.1278	3.72492
93-213 months GA n = 22	Birth Weight (Kg)	2.99	4.82	3.5879	0.44792
	Gestational Age (months)	94.95	238.98	142.1873	32.30317
214-309 months GA n = 16	Birth Weight (Kg)	2.30	4.00	3.2433	0.86524
	Gestational Age (months)	221.21	333.86	260.2506	31.92608

Summary of the Birth weights and gestational ages of the participants broken up by age group

n = number of participants in each age group; GA = gestational age; SD = standard deviation

Table 3: Presence of Photoreceptor Outer Segments

	Nasal							Fovea	Temporal						
Eccentricity (μm)	1750	1500	1250	1000	750	500	250	0	250	500	750	1000	1250	1500	1750
<40 weeks	0.0	0.0	9.1	23.8	33.3	47.6	50.0	62.1	54.2	50.0	33.3	25.0	16.7	15.0	0.0
41-46 weeks	0.0	0.0	0.0	4.2	8.3	9.1	18.2	34.8	20.0	15.0	14.3	5.0	0.0	0.0	0.0
47-52 weeks	0.0	0.0	0.0	0.0	0.0	0.0	0.0	0.0	0.0	0.0	0.0	0.0	0.0	0.0	0.0

Summary of the percentage of eyes in each group where the outer segment of the photoreceptors is absent

Data for the fovea as well as at 250 μm intervals up to 1750 μm on the nasal and temporal side of the fovea are shown.

Table 4: Contact Cylinder Visibility

Age Group	% Absent
<40 weeks GA	96.97
41-46 weeks GA	96.00
47-52 weeks GA	90.00
12-14 months GA	23.53
15-17 months GA	24.24
18-20 months GA	3.57
21-26 months GA	9.09
27-32 months GA	16.67
33-38 months GA	25.00
39-44 months GA	10.00
45-56 months GA	0.00
57-68 months GA	13.95
69-80 months GA	0.00
81-92 months GA	0.00
93-213 months GA	9.09
214-309 months GA	0.00

Summary of the percentage of eyes in each age group where the contact cylinder is not visible

GA = gestational age

Table 5: Foveal Normative Data

		Fovea				95% Confidence Interval	
Age Group	Retinal Layer	N	Mean Thickness (μm)	Std. Deviation	Std. Error Mean	Lower	Upper
< 40 weeks GA	GCL	33	0.00	NA	NA	NA	NA
	IPL	29	17.70	9.77	1.81	0.00	37.23
	INL	32	20.75	18.03	3.19	0.00	56.81
	OPL	34	9.75	5.72	0.98	0.00	21.20
	ONL	15	34.37	5.84	1.51	22.68	46.06
	IS	14	20.44	3.14	0.84	14.15	26.73
	OS	29	3.06	4.78	0.89	0.00	12.62
	RPE	32	12.34	2.25	0.40	7.84	16.85
	GCC	30	18.13	12.05	2.20	0.00	42.24
	ONL-IS Complex	30	52.24	11.83	2.16	28.57	75.90
	OS-RPE Complex	33	15.37	6.38	1.11	2.61	28.13
	Inner Retinal Layers	32	50.25	25.61	4.53	0.00	101.47
	Outer Retinal Layers	32	67.03	13.87	2.45	39.29	94.77
	RT	35	124.39	43.60	7.37	37.18	211.59
41-46 weeks GA	GCL	28	0.00	NA	NA	NA	NA
	IPL	28	15.78	6.82	1.29	2.15	29.42
	INL	26	10.60	8.59	1.68	0.00	27.78
	OPL	24	9.19	5.91	1.21	0.00	21.01
	ONL	18	39.35	17.01	4.01	5.33	73.37
	IS	16	23.70	2.73	0.68	18.24	29.16
	OS	23	8.31	7.54	1.57	0.00	23.40
	RPE	28	12.06	3.74	0.71	4.58	19.54
	GCC	26	17.01	5.35	1.05	6.30	27.71
	ONL-IS Complex	25	59.23	14.92	2.98	29.40	89.07
	OS-RPE Complex	26	21.25	9.10	1.78	3.06	39.45

	Inner Retinal Layers	26	37.85	15.38	3.02	7.09	68.61
	Outer Retinal Layers	26	85.38	28.48	5.59	28.42	142.33
	RT	28	122.61	24.51	4.63	73.58	171.63
47-52 weeks GA	GCL	12	0.63	1.64	0.47	0.00	3.90
	IPL	12	9.64	7.66	2.21	0.00	24.96
	INL	11	5.12	6.16	1.86	0.00	17.43
	OPL	11	8.20	6.02	1.81	0.00	20.24
	ONL	9	46.81	9.35	3.12	28.11	65.51
	IS	10	25.89	3.54	1.12	18.82	32.96
	OS	11	22.67	4.29	1.29	14.10	31.25
	RPE	10	13.41	2.46	0.78	8.48	18.33
	GCC	12	10.26	8.05	2.32	0.00	26.37
	ONL-IS Complex	10	74.28	8.47	2.68	57.35	91.22
	OS-RPE Complex	12	35.16	8.62	2.49	17.92	52.40
	Inner Retinal Layers	10	22.93	10.21	3.23	2.51	43.35
	Outer Retinal Layers	10	104.24	26.02	8.23	52.20	156.28
	RT	12	131.39	20.57	5.94	90.25	172.53
12-14 months GA	GCL	33	0.00	NA	NA	NA	NA
	IPL	33	7.37	7.29	1.27	0.00	21.94
	INL	32	2.72	4.09	0.72	0.00	10.90
	OPL	33	6.30	5.09	0.89	0.00	16.48
	ONL	28	59.76	10.77	2.04	38.21	81.30
	IS	28	26.32	4.23	0.80	17.85	34.79
	OS	34	19.52	9.77	1.68	0.00	39.06
	RPE	35	13.76	2.12	0.36	9.52	18.00
	GCC	35	6.95	7.28	1.23	0.00	21.51
	ONL-IS Complex	35	86.95	11.58	1.96	63.78	110.11

	OS-RPE Complex	38	46.97	6.62	1.07	33.72	60.22
	Inner Retinal Layers	35	17.88	11.30	1.91	0.00	40.49
	Outer Retinal Layers	35	133.88	17.17	2.90	99.54	168.22
	RT	39	151.51	17.67	2.83	116.16	186.85
15-17 months GA	GCL	37	0.38	1.29	0.21	0.00	2.95
	IPL	37	6.39	7.70	1.27	0.00	21.80
	INL	34	1.87	2.92	0.50	0.00	7.70
	OPL	32	4.99	6.02	1.06	0.00	17.02
	ONL	30	72.02	9.46	1.73	53.10	90.93
	IS	32	28.99	4.10	0.73	20.78	37.19
	OS	33	25.96	7.89	1.37	10.19	41.73
	RPE	35	13.85	3.66	0.62	6.54	21.16
	GCC	36	6.96	8.30	1.38	0.00	23.55
	ONL-IS Complex	31	101.07	9.09	1.63	82.89	119.25
	OS-RPE Complex	40	51.23	6.33	1.00	38.57	63.88
	Inner Retinal Layers	33	13.92	8.61	1.50	0.00	31.14
	Outer Retinal Layers	33	154.11	13.20	2.30	127.71	180.52
	RT	41	169.78	14.12	2.21	141.55	198.02
18-20 months GA	GCL	32	0.00	NA	NA	NA	NA
	IPL	32	2.81	4.07	0.72	0.00	10.96
	INL	32	2.17	3.45	0.61	0.00	9.07
	OPL	32	5.21	4.27	0.76	0.00	13.75
	ONL	30	76.39	9.58	1.75	57.23	95.55
	IS	30	29.94	5.85	1.07	18.23	41.64
	OS	28	23.81	5.82	1.10	12.17	35.45
	RPE	27	15.19	2.68	0.52	9.84	20.55
	GCC	32	2.98	4.28	0.76	0.00	11.54

		ONL-IS Complex	32	106.27	8.80	1.56	88.67	123.86
		OS-RPE Complex	33	53.45	8.22	1.43	37.02	69.89
		Inner Retinal Layers	32	10.51	6.29	1.11	0.00	23.09
		Outer Retinal Layers	32	162.79	8.73	1.54	145.33	180.25
		RT	33	173.68	11.30	1.97	151.08	196.28
21-26 months GA		GCL	26	0.02	0.09	0.02	0.00	0.20
		IPL	26	2.15	3.70	0.73	0.00	9.55
		INL	26	2.03	2.77	0.54	0.00	7.57
		OPL	26	6.08	4.63	0.91	0.00	15.35
		ONL	25	89.57	12.69	2.54	64.19	114.96
		IS	25	31.93	4.01	0.80	23.92	39.94
		OS	22	30.37	7.51	1.60	15.35	45.39
		RPE	22	14.41	3.18	0.68	8.05	20.78
		GCC	26	2.17	3.73	0.73	0.00	9.63
		ONL-IS Complex	26	120.69	14.30	2.80	92.09	149.29
		OS-RPE Complex	27	54.76	8.77	1.69	37.22	72.30
		Inner Retinal Layers	26	12.75	9.33	1.83	0.00	31.41
		Outer Retinal Layers	26	179.86	13.65	2.68	152.57	207.16
		RT	27	192.38	16.58	3.19	159.22	225.55
27-32 months GA		GCL	30	0.19	1.02	0.19	0.00	2.24
		IPL	30	3.43	4.50	0.82	0.00	12.43
		INL	30	2.31	4.31	0.79	0.00	10.94
		OPL	30	5.44	5.38	0.98	0.00	16.19
		ONL	27	85.09	13.94	2.68	57.21	112.97
		IS	27	34.98	4.48	0.86	26.02	43.94
		OS	30	30.81	7.92	1.45	14.97	46.65
		RPE	30	16.44	3.29	0.60	9.87	23.02

		GCC	30	4.56	7.58	1.38	0.00	19.73
		ONL-IS Complex	30	119.06	14.53	2.65	90.00	148.12
		OS-RPE Complex	33	59.04	6.49	1.13	46.06	72.03
		Inner Retinal Layers	30	12.55	8.33	1.52	0.00	29.20
		Outer Retinal Layers	30	178.09	16.07	2.93	145.96	210.22
		RT	33	191.23	17.00	2.96	157.22	225.24
33-38 months GA		GCL	25	0.35	1.77	0.35	0.00	3.90
		IPL	24	3.05	5.73	1.17	0.00	14.52
		INL	25	1.58	2.77	0.55	0.00	7.12
		OPL	25	5.04	4.87	0.97	0.00	14.78
		ONL	23	87.67	8.60	1.79	70.47	104.87
		IS	23	32.04	5.81	1.21	20.41	43.66
		OS	23	30.31	5.19	1.08	19.94	40.68
		RPE	24	17.93	4.14	0.85	9.65	26.21
		GCC	25	3.29	5.92	1.18	0.00	15.13
		ONL-IS Complex	25	119.81	9.54	1.91	100.73	138.90
		OS-RPE Complex	25	57.76	10.53	2.11	36.70	78.82
		Inner Retinal Layers	25	10.56	7.24	1.45	0.00	25.03
		Outer Retinal Layers	25	180.50	8.52	1.70	163.46	197.54
		RT	25	191.06	10.18	2.04	170.70	211.42
39-44 months GA		GCL	24	0.13	0.63	0.13	0.00	1.38
		IPL	22	2.87	3.89	0.83	0.00	10.66
		INL	25	0.99	2.48	0.50	0.00	5.94
		OPL	25	4.80	4.35	0.87	0.00	13.51
		ONL	23	93.41	13.49	2.81	66.43	120.39
		IS	23	33.29	4.27	0.89	24.74	41.84
		OS	18	30.31	4.96	1.17	20.40	40.22

	RPE	22	17.42	2.93	0.63	11.55	23.28
	GCC	25	2.93	3.78	0.76	0.00	10.48
	ONL-IS Complex	25	126.40	13.46	2.69	99.49	153.31
	OS-RPE Complex	25	59.80	8.82	1.76	42.15	77.44
	Inner Retinal Layers	25	9.28	5.99	1.20	0.00	21.26
	Outer Retinal Layers	25	189.96	12.52	2.50	164.93	215.00
	RT	25	199.24	14.20	2.84	170.84	227.64
45-56 months GA	GCL	40	0.12	0.59	0.09	0.00	1.29
	IPL	40	2.93	4.77	0.75	0.00	12.48
	INL	41	2.13	3.58	0.56	0.00	9.28
	OPL	41	4.44	4.11	0.64	0.00	12.67
	ONL	38	99.88	14.21	2.31	71.46	128.30
	IS	37	34.17	4.20	0.69	25.77	42.57
	OS	34	33.27	4.95	0.85	23.37	43.17
	RPE	35	14.91	4.00	0.68	6.90	22.91
	GCC	41	3.11	4.99	0.78	0.00	13.09
	ONL-IS Complex	39	131.95	12.29	1.97	107.37	156.52
	OS-RPE Complex	43	58.11	11.15	1.70	35.81	80.41
	Inner Retinal Layers	42	10.32	9.20	1.42	0.00	28.71
	Outer Retinal Layers	42	194.07	13.71	2.12	166.65	221.50
	RT	43	204.70	15.23	2.32	174.25	235.15
57-68 months GA	GCL	47	0.07	0.46	0.07	0.00	1.00
	IPL	47	4.62	6.66	0.97	0.00	17.94
	INL	51	0.83	2.22	0.31	0.00	5.27
	OPL	51	2.57	3.56	0.50	0.00	9.69
	ONL	46	96.95	10.58	1.56	75.78	118.11
	IS	46	32.25	3.73	0.55	24.78	39.71

		OS	43	32.15	7.40	1.13	17.34	46.96
		RPE	43	18.13	3.76	0.57	10.60	25.65
		GCC	51	4.50	6.91	0.97	0.00	18.32
		ONL-IS Complex	51	128.71	12.58	1.76	103.55	153.87
		OS-RPE Complex	50	59.83	9.73	1.38	40.38	79.28
		Inner Retinal Layers	50	7.93	7.15	1.01	0.00	22.22
		Outer Retinal Layers	50	191.56	12.51	1.77	166.54	216.59
		RT	51	199.57	13.65	1.91	172.26	226.88
	69-80 months GA	GCL	32	0.33	1.37	0.24	0.00	3.06
		IPL	32	1.53	3.22	0.57	0.00	7.98
		INL	32	2.33	3.73	0.66	0.00	9.80
		OPL	32	5.65	5.24	0.93	0.00	16.12
		ONL	30	99.07	11.79	2.15	75.49	122.64
		IS	30	34.63	5.48	1.00	23.68	45.59
		OS	25	31.15	5.93	1.19	19.30	43.00
		RPE	26	17.81	4.27	0.84	9.28	26.34
		GCC	32	2.33	4.43	0.78	0.00	11.20
		ONL-IS Complex	32	133.23	12.19	2.16	108.85	157.62
		OS-RPE Complex	32	58.70	10.49	1.85	37.71	79.68
		Inner Retinal Layers	32	11.17	6.80	1.20	0.00	24.76
		Outer Retinal Layers	32	196.31	11.33	2.00	173.66	218.97
		RT	32	207.48	13.04	2.31	181.40	233.57
	81-92 months GA	GCL	36	0.06	0.35	0.06	0.00	0.76
		IPL	36	4.20	5.26	0.88	0.00	14.72
		INL	37	0.93	1.75	0.29	0.00	4.42
		OPL	37	4.66	4.26	0.70	0.00	13.18
		ONL	34	99.85	10.14	1.74	79.58	120.13

	IS	34	34.73	4.29	0.73	26.16	43.30
	OS	32	33.15	4.38	0.77	24.40	41.91
	RPE	33	16.02	3.52	0.61	8.99	23.05
	GCC	37	4.35	5.30	0.87	0.00	14.95
	ONL-IS Complex	37	135.41	10.36	1.70	114.69	156.12
	OS-RPE Complex	37	62.16	8.72	1.43	44.73	79.59
	Inner Retinal Layers	37	10.27	6.77	1.11	0.00	23.81
	Outer Retinal Layers	37	199.84	10.90	1.79	178.03	221.64
	RT	37	210.10	11.23	1.85	187.64	232.56
93-213 months GA	GCL	37	0.00	NA	NA	NA	NA
	IPL	36	3.03	4.61	0.77	0.00	12.25
	INL	41	0.40	1.23	0.19	0.00	2.86
	OPL	41	5.94	6.28	0.98	0.00	18.50
	ONL	41	102.22	13.81	2.16	74.60	129.83
	IS	41	34.72	3.49	0.55	27.74	41.70
	OS	34	32.95	6.00	1.03	20.94	44.96
	RPE	32	17.18	3.89	0.69	9.41	24.96
	GCC	42	3.20	4.86	0.75	0.00	12.92
	ONL-IS Complex	42	137.04	13.28	2.05	110.48	163.60
	OS-RPE Complex	39	61.05	9.86	1.58	41.33	80.78
	Inner Retinal Layers	42	9.48	7.60	1.17	0.00	24.68
	Outer Retinal Layers	42	202.92	11.35	1.75	180.22	225.62
	RT	42	212.40	14.40	2.22	183.59	241.21
214-309 months GA	GCL	23	0.00	NA	NA	NA	NA
	IPL	22	0.79	1.32	0.28	0.00	3.44
	INL	31	0.74	1.65	0.30	0.00	4.03
	OPL	31	2.55	3.83	0.69	0.00	10.21

ONL	29	100.87	14.27	2.65	72.33	129.40
IS	30	33.74	3.55	0.65	26.65	40.83
OS	27	33.01	5.77	1.11	21.47	44.56
RPE	28	18.07	3.24	0.61	11.58	24.55
GCC	31	0.71	1.29	0.23	0.00	3.29
ONL-IS Complex	31	134.97	14.39	2.58	106.20	163.74
OS-RPE Complex	31	65.63	7.37	1.32	50.89	80.37
Inner Retinal Layers	31	5.77	4.66	0.84	0.00	15.10
Outer Retinal Layers	31	201.04	13.64	2.45	173.75	228.32
RT	31	206.92	13.83	2.48	179.26	234.57

Summary of the mean values, standard deviations and 95% confidence intervals obtained for each of the retinal layers for each age group at the fovea

N = number of examinations where the layer(s) could be reliably segmented; Std = standard; RNFL = retinal nerve fibre layer; GCL = ganglion cell layer; IPL = inner plexiform layer; INL = inner nuclear layer; OPL = outer plexiform layer; ONL = outer nuclear layer; IS = inner segment of the photoreceptor; OS = outer segment of the photoreceptor; RPE = retinal pigment epithelium; GCC = ganglion cell complex; RT = total retinal thickness; GA = gestational age

Table 6: Parafoveal Normative Data

		Nasal Parafovea (1000 μ m from the Fovea)				95% Confidence Interval		Temporal Parafovea (1000 μ m from the Fovea)				95% Confidence Interval	
Age Group	Retinal Layer	N	Mean	SD	SEM	LCI	UCI	N	Mean	SD	SEM	LCI	UCI
<40 weeks GA	RNFL	27	16.42	5.83	1.12	4.77	28.08	29	12.29	4.62	0.86	3.06	21.52
	GCL	26	50.39	10.26	2.01	29.88	70.90	28	42.80	14.72	2.78	13.36	72.23
	IPL	26	54.72	10.83	2.12	33.05	76.38	28	59.09	13.05	2.47	32.99	85.18
	INL	26	66.72	13.18	2.58	40.36	93.08	27	62.62	11.01	2.12	40.60	84.65
	OPL	26	18.55	6.38	1.25	5.80	31.31	28	18.78	6.21	1.17	6.36	31.20
	ONL	14	45.12	7.55	2.02	30.01	60.22	13	39.70	7.89	2.19	23.92	55.47
	IS	13	21.93	2.61	0.72	16.72	27.14	13	20.49	2.87	0.80	14.74	26.23
	OS	21	4.43	3.29	0.72	0.00	11.02	24	5.11	3.71	0.76	0.00	12.53
	RPE	28	12.34	2.21	0.42	7.92	16.77	29	12.07	2.73	0.51	6.61	17.53
	GCC	26	105.1	9.19	1.80	86.72	123.5	28	101.9	13.30	2.51	75.29	128.5
	ONL-IS Complex	24	63.80	8.31	1.70	47.18	80.43	26	56.95	10.64	2.09	35.67	78.23
	OS-RPE Complex	28	15.98	3.77	0.71	8.43	23.52	30	16.40	3.64	0.66	9.12	23.68
	Inner Retinal Layers	25	206.8	14.16	2.83	178.5	235.1	27	196.0	14.97	2.88	166.1	225.9
	Outer Retinal Layers	25	79.29	9.65	1.93	60.00	98.59	27	72.55	11.45	2.20	49.65	95.46
	RT	30	283.6	21.34	3.90	241.0	326.3	30	268.1	21.49	3.92	225.1	311.1
41-46 weeks GA	RNFL	27	15.76	3.83	0.74	8.11	23.42	23	11.51	3.44	0.72	4.63	18.39
	GCL	27	52.47	14.20	2.73	24.08	80.87	23	40.81	10.21	2.13	20.40	61.23
	IPL	27	54.96	12.47	2.40	30.01	79.90	23	57.63	10.64	2.22	36.35	78.91
	INL	25	58.58	11.41	2.28	35.77	81.39	22	57.50	11.60	2.47	34.29	80.70
	OPL	24	26.83	8.21	1.68	10.40	43.25	21	23.90	8.12	1.77	7.65	40.14
	ONL	17	46.87	7.89	1.91	31.09	62.65	14	43.60	8.16	2.18	27.28	59.93
	IS	17	23.94	3.69	0.90	16.56	31.32	14	23.89	4.13	1.10	15.63	32.14
	OS	24	7.71	3.59	0.73	0.53	14.89	20	6.67	3.25	0.73	0.18	13.17
	RPE	27	11.40	3.09	0.59	5.22	17.57	23	11.97	3.05	0.64	5.88	18.06

	GCC	27	107.4	10.80	2.08	85.75	129.0	23	98.44	9.06	1.89	80.31	116.6
	ONL-IS Complex	24	67.56	10.30	2.10	46.97	88.15	20	63.71	12.31	2.75	39.09	88.33
	OS-RPE Complex	27	19.29	5.25	1.01	8.78	29.80	23	18.48	5.12	1.07	8.24	28.73
	Inner Retinal Layers	25	205.5	13.88	2.78	177.7	233.2	23	190.7	9.72	2.03	171.2	210.1
	Outer Retinal Layers	25	91.31	19.94	3.99	51.43	131.2	23	86.69	19.13	3.99	48.43	125.0
	RT	27	295.8	18.42	3.54	258.9	332.6	24	276.9	19.35	3.95	238.2	315.6
47-52 weeks GA	RNFL	11	14.30	2.58	0.78	9.15	19.46	5	9.35	2.42	1.08	4.51	14.19
	GCL	11	49.54	11.88	3.58	25.77	73.31	5	43.70	6.20	2.77	31.30	56.09
	IPL	11	53.10	8.34	2.51	36.43	69.78	5	53.53	14.30	6.40	24.92	82.14
	INL	10	52.51	10.80	3.41	30.91	74.10	5	50.72	5.74	2.57	39.24	62.19
	OPL	10	27.43	12.50	3.95	2.43	52.44	5	24.70	5.91	2.64	12.87	36.53
	ONL	9	52.77	11.47	3.82	29.82	75.72	4	53.83	8.40	4.20	37.03	70.63
	IS	10	26.74	2.83	0.89	21.08	32.39	4	26.44	5.52	2.76	15.40	37.49
	OS	10	14.53	3.11	0.98	8.31	20.75	5	13.93	2.97	1.33	7.98	19.88
	RPE	9	12.70	1.69	0.56	9.32	16.08	4	14.32	3.49	1.75	7.33	21.30
	GCC	11	102.6	12.48	3.76	77.68	127.6	5	97.22	15.31	6.85	66.61	127.8
	ONL-IS Complex	9	76.92	11.09	3.70	54.73	99.10	4	80.27	5.73	2.86	68.81	91.72
	OS-RPE Complex	11	25.39	5.01	1.51	15.38	35.41	6	21.16	13.13	5.36	0.00	47.41
	Inner Retinal Layers	9	195.5	14.40	4.80	166.7	224.3	4	173.5	8.72	4.36	156.1	190.9
	Outer Retinal Layers	9	104.2	14.35	4.78	75.44	132.9	4	102.0	18.99	9.50	63.98	140.0
	RT	11	303.0	18.58	5.60	265.8	340.2	5	279.9	19.02	8.50	241.9	317.9
12-14 months GA	RNFL	36	13.63	4.65	0.77	4.34	22.92	33	9.64	3.27	0.57	3.11	16.17
	GCL	33	49.51	8.21	1.43	33.08	65.93	31	39.13	9.92	1.78	19.29	58.97
	IPL	33	45.27	8.85	1.54	27.58	62.96	30	48.83	11.69	2.13	25.45	72.22
	INL	32	54.53	10.30	1.82	33.92	75.14	29	52.11	8.51	1.58	35.09	69.14
	OPL	32	27.17	11.41	2.02	4.34	49.99	29	27.70	9.49	1.76	8.71	46.68
	ONL	27	64.13	12.27	2.36	39.59	88.67	23	57.02	13.52	2.82	29.99	84.06

	IS	27	25.03	2.95	0.57	19.13	30.93	25	25.76	2.93	0.59	19.89	31.63
	OS	33	11.59	6.90	1.20	0.00	25.39	30	9.99	6.99	1.28	0.00	23.97
	RPE	34	14.51	2.75	0.47	9.01	20.02	31	13.50	2.34	0.42	8.83	18.18
	GCC	33	94.77	6.97	1.21	80.83	108.7	30	88.28	12.33	2.25	63.61	113.0
	ONL-IS Complex	32	88.15	12.46	2.20	63.24	113.1	29	83.22	13.21	2.45	56.80	109.7
	OS-RPE Complex	36	35.73	5.63	0.94	24.47	46.99	34	34.19	5.16	0.88	23.88	44.51
	Inner Retinal Layers	32	191.0	16.02	2.83	159.0	223.1	29	178.3	20.19	3.75	137.9	218.7
	Outer Retinal Layers	32	122.1	15.87	2.80	90.33	153.8	29	117.2	15.84	2.94	85.52	148.9
	RT	36	313.6	16.71	2.78	280.2	347.0	34	294.5	15.20	2.61	264.1	324.9
15-17 months GA	RNFL	40	12.61	3.94	0.62	4.74	20.49	30	8.76	4.77	0.87	0.00	18.30
	GCL	37	48.55	10.47	1.72	27.62	69.49	29	37.17	7.26	1.35	22.65	51.69
	IPL	36	43.34	8.62	1.44	26.09	60.58	29	47.14	9.79	1.82	27.56	66.72
	INL	34	54.39	9.42	1.62	35.54	73.23	27	50.60	5.69	1.10	39.22	61.98
	OPL	31	32.73	13.72	2.46	5.30	60.16	25	28.15	11.74	2.35	4.67	51.64
	ONL	29	61.41	14.60	2.71	32.20	90.61	25	66.56	15.66	3.13	35.24	97.88
	IS	31	26.25	3.25	0.58	19.75	32.76	28	26.02	2.87	0.54	20.29	31.75
	OS	32	13.14	5.64	1.00	1.86	24.42	26	11.92	5.57	1.09	0.78	23.06
	RPE	35	14.37	2.96	0.50	8.44	20.29	27	14.45	3.79	0.73	6.86	22.03
	GCC	36	91.76	9.20	1.53	73.36	110.2	29	84.31	8.80	1.63	66.70	102.0
	ONL-IS Complex	31	86.85	15.00	2.69	56.84	116.8	25	92.47	15.38	3.08	61.70	123.2
	OS-RPE Complex	40	37.55	6.65	1.05	24.25	50.86	31	37.77	5.11	0.92	27.55	47.99
	Inner Retinal Layers	32	194.9	21.36	3.78	152.2	237.7	26	173.1	13.51	2.65	146.0	200.1
	Outer Retinal Layers	32	126.1	14.10	2.49	97.90	154.3	26	134.0	14.51	2.84	105.0	163.0
	RT	41	319.0	16.46	2.57	286.0	351.9	33	301.3	18.10	3.15	265.1	337.5
18-20 months GA	RNFL	33	11.79	3.54	0.62	4.70	18.87	27	7.87	2.81	0.54	2.26	13.49
	GCL	32	46.96	8.45	1.49	30.07	63.85	27	37.16	7.86	1.51	21.43	52.89
	IPL	32	44.89	7.80	1.38	29.29	60.49	27	44.54	8.81	1.69	26.93	62.15

	INL	32	50.88	7.93	1.40	35.01	66.75	27	44.45	7.84	1.51	28.76	60.13
	OPL	32	38.50	17.12	3.03	4.27	72.73	27	30.15	10.55	2.03	9.05	51.25
	ONL	30	59.52	19.56	3.57	20.40	98.64	25	66.88	13.04	2.61	40.81	92.95
	IS	30	25.41	2.67	0.49	20.06	30.75	25	27.63	3.63	0.73	20.37	34.90
	OS	28	11.52	4.44	0.84	2.64	20.40	24	9.73	3.98	0.81	1.78	17.69
	RPE	27	15.03	3.64	0.70	7.74	22.31	23	14.61	3.52	0.73	7.56	21.66
	GCC	32	91.66	8.25	1.46	75.17	108.2	27	81.63	7.14	1.37	67.34	95.91
	ONL-IS Complex	32	85.58	19.89	3.52	45.80	125.4	27	93.81	11.93	2.30	69.95	117.7
	OS-RPE Complex	33	38.30	7.38	1.28	23.54	53.06	27	37.99	6.13	1.18	25.74	50.24
	Inner Retinal Layers	32	191.8	23.42	4.14	145.0	238.6	28	166.6	18.09	3.42	130.4	202.8
	Outer Retinal Layers	32	127.3	20.28	3.59	86.77	167.9	28	133.5	14.10	2.67	105.3	161.7
21-26 months GA	RT	33	319.2	12.29	2.14	294.7	343.8	28	300.1	13.36	2.52	273.4	326.8
	RNFL	26	11.30	3.31	0.65	4.69	17.91	20	6.80	2.83	0.63	1.15	12.45
	GCL	25	51.42	7.73	1.55	35.95	66.89	20	40.87	7.97	1.78	24.94	56.81
	IPL	25	41.69	8.25	1.65	25.20	58.19	20	43.35	11.12	2.49	21.11	65.60
	INL	25	51.70	8.79	1.76	34.12	69.28	20	48.09	7.57	1.69	32.95	63.23
	OPL	25	38.34	16.45	3.29	5.43	71.24	20	30.86	13.16	2.94	4.53	57.19
	ONL	24	65.06	19.97	4.08	25.12	105.0	19	68.67	16.40	3.76	35.87	101.5
	IS	24	27.78	3.05	0.62	21.68	33.89	19	28.62	3.48	0.80	21.66	35.59
	OS	22	14.18	5.69	1.21	2.81	25.55	16	13.06	6.31	1.58	0.45	25.67
	RPE	22	15.44	4.58	0.98	6.28	24.60	16	15.93	5.26	1.32	5.40	26.46
	GCC	25	93.11	7.49	1.50	78.14	108.1	20	84.23	8.95	2.00	66.33	102.1
	ONL-IS Complex	25	92.50	19.63	3.93	53.24	131.8	20	98.32	17.57	3.93	63.18	133.5
	OS-RPE Complex	27	38.98	11.07	2.13	16.84	61.13	21	37.94	8.65	1.89	20.64	55.24
	Inner Retinal Layers	24	191.9	19.69	4.02	152.5	231.3	19	172.0	17.97	4.12	136.1	207.9
	Outer Retinal Layers	24	137.8	18.52	3.78	100.8	174.9	19	137.8	20.68	4.74	96.39	179.1
	RT	25	329.6	11.52	2.30	306.6	352.6	20	309.5	10.54	2.36	288.4	330.6

27-32 months GA	RNFL	32	12.27	3.36	0.59	5.55	18.99	26	7.98	3.21	0.63	1.56	14.39
	GCL	29	49.59	6.78	1.26	36.02	63.15	23	39.38	10.17	2.12	19.03	59.72
	IPL	29	42.81	7.83	1.45	27.16	58.46	24	43.50	9.98	2.04	23.54	63.45
	INL	29	50.09	9.37	1.74	31.35	68.82	25	48.83	7.98	1.60	32.88	64.78
	OPL	29	39.61	14.48	2.69	10.64	68.58	25	27.75	10.07	2.01	7.61	47.90
	ONL	26	57.04	19.96	3.91	17.12	96.96	22	66.52	15.69	3.34	35.15	97.90
	IS	26	28.00	2.59	0.51	22.82	33.18	22	28.40	2.94	0.63	22.52	34.28
	OS	29	15.10	7.10	1.32	0.90	29.31	25	13.51	5.75	1.15	2.01	25.02
	RPE	29	17.34	3.32	0.62	10.70	23.99	25	16.43	3.82	0.76	8.79	24.06
	GCC	29	92.38	8.76	1.63	74.86	109.9	25	83.78	8.68	1.74	66.43	101.1
	ONL-IS Complex	29	86.42	20.94	3.89	44.55	128.3	25	95.19	16.49	3.30	62.21	128.2
	OS-RPE Complex	32	42.70	5.76	1.02	31.18	54.22	28	41.68	6.22	1.18	29.24	54.12
	Inner Retinal Layers	29	190.5	20.59	3.82	149.3	231.7	25	168.5	16.21	3.24	136.1	200.9
	Outer Retinal Layers	29	133.2	19.39	3.60	94.40	172.0	25	137.8	16.77	3.35	104.2	171.3
	RT	32	323.7	13.48	2.38	296.7	350.7	28	306.1	16.27	3.08	273.6	338.6
33-38 months GA	RNFL	25	12.45	4.09	0.82	4.28	20.63	20	8.26	2.42	0.54	3.42	13.09
	GCL	24	51.57	9.98	2.04	31.61	71.54	20	44.08	7.73	1.73	28.63	59.54
	IPL	24	43.10	9.14	1.87	24.81	61.39	20	42.78	7.33	1.64	28.12	57.44
	INL	25	47.16	11.22	2.24	24.73	69.59	20	48.08	8.80	1.97	30.47	65.68
	OPL	25	34.14	16.61	3.32	0.92	67.35	20	25.14	8.02	1.79	9.10	41.18
	ONL	23	67.80	18.83	3.93	30.14	105.5	20	69.86	11.62	2.60	46.63	93.09
	IS	23	28.58	3.42	0.71	21.74	35.41	20	28.53	3.25	0.73	22.02	35.03
	OS	23	14.28	6.78	1.41	0.73	27.84	20	14.62	6.25	1.40	2.11	27.12
	RPE	24	17.69	4.00	0.82	9.70	25.69	21	17.48	4.35	0.95	8.78	26.19
	GCC	25	94.38	10.00	2.00	74.39	114.4	20	86.86	6.27	1.40	74.33	99.40
	ONL-IS Complex	25	95.99	18.72	3.74	58.56	133.4	21	98.90	11.86	2.59	75.19	122.6
	OS-RPE Complex	25	43.45	7.77	1.55	27.92	58.98	22	42.45	6.99	1.49	28.46	56.43
	Inner Retinal Layers	25	191.2	22.32	4.46	146.6	235.9	21	170.8	12.14	2.65	146.5	195.1

	Outer Retinal Layers	25	139.9	19.35	3.87	101.2	178.6	21	142.4	12.34	2.69	117.7	167.0
	RT	25	331.2	11.86	2.37	307.4	354.9	22	313.4	10.01	2.13	293.4	333.4
39-44 months GA	RNFL	24	11.98	2.76	0.56	6.46	17.49	23	7.53	2.68	0.56	2.17	12.89
	GCL	21	53.49	6.13	1.34	41.23	65.74	22	42.54	8.52	1.82	25.49	59.58
	IPL	21	39.69	6.75	1.47	26.18	53.19	22	42.16	9.16	1.95	23.84	60.48
	INL	24	52.54	8.50	1.73	35.54	69.54	24	45.60	9.16	1.87	27.28	63.91
	OPL	24	30.78	14.76	3.01	1.26	60.30	24	31.14	11.98	2.45	7.17	55.11
	ONL	22	69.73	17.81	3.80	34.12	105.4	22	67.76	16.54	3.53	34.68	100.8
	IS	22	27.70	2.73	0.58	22.24	33.15	22	29.24	3.25	0.69	22.74	35.74
	OS	17	14.50	6.62	1.61	1.25	27.74	17	12.89	6.13	1.49	0.64	25.15
	RPE	21	17.07	3.94	0.86	9.20	24.94	21	17.76	3.44	0.75	10.88	24.64
	GCC	24	92.63	7.73	1.58	77.18	108.1	24	86.32	10.74	2.19	64.84	107.8
	ONL-IS Complex	24	95.99	17.34	3.54	61.32	130.7	24	97.72	17.00	3.47	63.72	131.7
	OS-RPE Complex	24	43.84	7.86	1.61	28.11	59.57	24	43.78	7.68	1.57	28.43	59.13
	Inner Retinal Layers	25	189.8	18.16	3.63	153.5	226.2	24	170.5	14.78	3.02	140.9	200.1
	Outer Retinal Layers	25	142.4	19.08	3.82	104.2	180.5	24	144.8	17.79	3.63	109.2	180.4
	RT	25	332.2	15.55	3.11	301.1	363.3	24	315.3	11.73	2.39	291.8	338.8
45-56 months GA	RNFL	41	12.43	3.70	0.58	5.04	19.82	39	8.00	2.80	0.45	2.40	13.60
	GCL	38	55.26	8.68	1.41	37.90	72.62	36	46.72	7.39	1.23	31.95	61.49
	IPL	38	43.81	7.95	1.29	27.91	59.71	36	44.10	8.86	1.48	26.39	61.81
	INL	39	49.91	7.41	1.19	35.09	64.73	36	46.47	7.65	1.28	31.16	61.77
	OPL	39	33.82	16.07	2.57	1.67	65.96	36	27.33	8.94	1.49	9.44	45.22
	ONL	37	69.13	18.30	3.01	32.53	105.7	35	74.61	15.36	2.60	43.90	105.3
	IS	36	27.96	2.88	0.48	22.19	33.73	35	28.81	2.89	0.49	23.03	34.58
	OS	34	14.02	3.10	0.53	7.81	20.22	31	13.31	3.46	0.62	6.39	20.23
	RPE	35	15.93	4.49	0.76	6.95	24.91	32	15.61	4.80	0.85	6.01	25.21
	GCC	39	99.70	8.71	1.39	82.29	117.1	36	90.82	6.54	1.09	77.74	103.9
	ONL-IS Complex	38	96.03	18.87	3.06	58.30	133.8	36	101.5	16.97	2.83	67.53	135.4

	OS-RPE Complex	41	42.57	8.17	1.28	26.24	58.91	40	41.31	8.88	1.40	23.54	59.07
	Inner Retinal Layers	39	195.3	20.63	3.30	154.1	236.6	38	171.0	14.52	2.35	141.9	200.0
	Outer Retinal Layers	39	141.0	17.12	2.74	106.8	175.3	38	146.8	16.60	2.69	113.6	180.0
	RT	40	337.4	16.84	2.66	303.8	371.1	41	318.3	14.34	2.24	289.6	347.0
57-68 months GA	RNFL	50	12.83	3.63	0.51	5.56	20.10	50	6.60	3.23	0.46	0.13	13.06
	GCL	46	54.62	8.49	1.25	37.65	71.59	44	45.30	9.55	1.44	26.19	64.40
	IPL	46	42.74	9.38	1.38	23.98	61.50	44	45.75	10.25	1.55	25.24	66.25
	INL	50	49.38	6.18	0.87	37.02	61.75	50	46.54	6.25	0.88	34.03	59.05
	OPL	50	33.71	14.52	2.05	4.67	62.74	49	25.47	8.34	1.19	8.79	42.15
	ONL	45	67.25	16.72	2.49	33.82	100.7	46	72.93	12.38	1.82	48.18	97.69
	IS	45	27.39	4.09	0.61	19.20	35.58	46	28.44	3.84	0.57	20.77	36.12
	OS	42	14.27	5.44	0.84	3.39	25.14	43	13.48	5.55	0.85	2.39	24.58
	RPE	42	18.60	3.88	0.60	10.85	26.35	43	18.39	3.72	0.57	10.95	25.82
	GCC	50	96.90	7.65	1.08	81.60	112.2	49	90.54	8.41	1.20	73.72	107.4
	ONL-IS Complex	50	94.39	17.01	2.41	60.37	128.4	49	101.9	13.58	1.94	74.74	129.1
	OS-RPE Complex	49	43.31	8.36	1.19	26.59	60.04	49	43.79	7.97	1.14	27.85	59.72
	Inner Retinal Layers	49	191.0	17.09	2.44	156.8	225.1	49	169.2	15.07	2.15	139.1	199.4
	Outer Retinal Layers	49	142.5	16.12	2.30	110.3	174.7	49	148.2	13.99	2.00	120.3	176.2
	RT	50	333.5	14.94	2.11	303.7	363.4	51	317.7	13.71	1.92	290.2	345.1
69-80 months GA	RNFL	32	11.81	3.27	0.58	5.27	18.35	32	5.97	2.91	0.51	0.15	11.79
	GCL	32	53.72	8.40	1.49	36.91	70.53	28	45.66	10.80	2.04	24.07	67.26
	IPL	32	42.30	8.81	1.56	24.68	59.92	28	41.68	11.74	2.22	18.20	65.16
	INL	32	47.41	8.69	1.54	30.04	64.79	32	46.23	5.88	1.04	34.47	57.99
	OPL	32	36.63	16.27	2.88	4.10	69.16	32	31.56	11.37	2.01	8.83	54.30
	ONL	30	64.67	16.80	3.07	31.06	98.27	30	68.90	16.20	2.96	36.49	101.3
	IS	30	27.56	4.60	0.84	18.36	36.75	30	29.39	4.15	0.76	21.09	37.69
	OS	25	12.83	4.22	0.84	4.38	21.27	25	11.39	3.90	0.78	3.60	19.18
	RPE	26	18.75	4.61	0.90	9.52	27.97	26	18.51	4.77	0.94	8.97	28.04

	GCC	32	95.94	8.15	1.44	79.64	112.2	28	87.34	8.05	1.52	71.23	103.5
	ONL-IS Complex	32	93.14	17.07	3.02	58.99	127.3	32	98.27	17.45	3.08	63.37	133.2
	OS-RPE Complex	32	43.35	8.94	1.58	25.47	61.22	32	42.16	8.39	1.48	25.38	58.93
	Inner Retinal Layers	32	194.7	19.37	3.42	156.0	233.4	31	173.9	16.64	2.99	140.6	207.2
	Outer Retinal Layers	32	138.3	18.90	3.34	100.5	176.1	31	143.2	20.93	3.76	101.4	185.1
	RT	32	332.9	16.89	2.99	299.2	366.7	31	317.1	16.38	2.94	284.4	349.9
81-92 months GA	RNFL	37	12.31	3.23	0.53	5.85	18.78	36	6.41	2.36	0.39	1.69	11.12
	GCL	36	54.54	6.62	1.10	41.30	67.77	32	50.68	8.48	1.50	33.71	67.64
	IPL	36	42.88	9.96	1.66	22.96	62.80	32	40.09	7.48	1.32	25.13	55.05
	INL	37	50.49	8.30	1.36	33.89	67.08	36	47.11	6.48	1.08	34.14	60.07
	OPL	37	35.49	15.23	2.50	5.03	65.96	36	29.83	11.06	1.84	7.72	51.95
	ONL	34	64.69	17.63	3.02	29.43	99.95	33	71.28	12.94	2.25	45.41	97.15
	IS	34	29.67	3.59	0.62	22.49	36.86	33	29.91	3.03	0.53	23.85	35.96
	OS	32	13.69	3.26	0.58	7.17	20.21	31	13.36	3.15	0.57	7.07	19.66
	RPE	33	16.09	4.26	0.74	7.58	24.61	32	16.68	3.89	0.69	8.89	24.46
	GCC	37	97.35	8.07	1.33	81.20	113.5	36	90.94	9.66	1.61	71.63	110.3
	ONL-IS Complex	37	94.80	17.13	2.82	60.54	129.1	36	101.1	12.56	2.09	75.94	126.2
	OS-RPE Complex	37	45.09	6.71	1.10	31.68	58.51	36	44.92	6.72	1.12	31.47	58.37
	Inner Retinal Layers	37	197.0	18.26	3.00	160.4	233.5	37	174.2	14.30	2.35	145.6	202.8
	Outer Retinal Layers	37	141.9	18.41	3.03	105.1	178.7	37	149.3	14.12	2.32	121.1	177.5
	RT	37	338.9	13.35	2.20	312.2	365.6	37	323.5	15.48	2.54	292.5	354.5
93-213 months GA	RNFL	41	13.04	3.48	0.54	6.09	20.00	42	6.76	2.37	0.37	2.02	11.49
	GCL	36	52.71	11.28	1.88	30.15	75.26	35	50.52	12.22	2.07	26.08	74.97
	IPL	36	44.59	11.60	1.93	21.40	67.78	35	42.26	10.90	1.84	20.45	64.06
	INL	41	50.48	8.72	1.36	33.04	67.92	42	45.61	6.59	1.02	32.43	58.78
	OPL	41	35.30	17.91	2.80	0.00	71.12	42	28.23	11.86	1.83	4.51	51.96
	ONL	40	71.45	21.36	3.38	28.73	114.2	41	76.25	15.55	2.43	45.15	107.4

	IS	40	28.05	3.50	0.55	21.05	35.04	41	29.64	3.40	0.53	22.83	36.45
	OS	33	15.80	4.30	0.75	7.20	24.40	34	14.91	4.96	0.85	4.99	24.83
	RPE	32	17.96	3.52	0.62	10.92	25.00	32	16.87	3.99	0.71	8.89	24.85
	GCC	41	97.14	9.74	1.52	77.66	116.6	40	92.80	8.44	1.33	75.92	109.7
	ONL-IS Complex	41	98.72	21.40	3.34	55.92	141.5	42	106.2	15.56	2.40	75.04	137.3
	OS-RPE Complex	38	45.19	9.62	1.56	25.95	64.42	39	43.47	9.86	1.58	23.76	63.19
	Inner Retinal Layers	41	195.0	21.14	3.30	152.7	237.3	41	171.5	15.38	2.40	140.7	202.2
	Outer Retinal Layers	41	147.3	22.06	3.45	103.2	191.5	41	154.6	14.32	2.24	126.0	183.3
	RT	41	342.3	14.45	2.26	313.4	371.2	41	326.1	13.87	2.17	298.4	353.8
214-309 months GA	RNFL	31	11.80	3.93	0.71	3.94	19.66	31	7.40	2.49	0.45	2.41	12.39
	GCL	22	57.45	9.80	2.09	37.86	77.05	19	48.98	8.31	1.91	32.36	65.61
	IPL	22	38.23	9.88	2.11	18.47	57.98	19	44.06	9.19	2.11	25.68	62.44
	INL	31	52.59	9.00	1.62	34.59	70.59	31	45.43	7.66	1.38	30.10	60.76
	OPL	31	32.45	13.57	2.44	5.32	59.58	31	23.72	8.53	1.53	6.66	40.79
	ONL	29	68.29	14.62	2.72	39.05	97.53	29	77.92	9.13	1.70	59.67	96.18
	IS	30	28.04	3.43	0.63	21.17	34.90	30	28.72	4.05	0.74	20.61	36.82
	OS	27	15.47	5.10	0.98	5.27	25.66	27	14.76	4.30	0.83	6.17	23.36
	RPE	28	17.28	2.96	0.56	11.35	23.20	28	18.10	3.48	0.66	11.15	25.06
	GCC	29	96.78	10.32	1.92	76.15	117.4	30	90.88	9.03	1.65	72.83	108.9
	ONL-IS Complex	31	96.53	14.13	2.54	68.27	124.8	31	106.2	9.82	1.76	86.59	125.9
	OS-RPE Complex	31	48.52	6.64	1.19	35.25	61.79	31	49.02	7.22	1.30	34.58	63.47
	Inner Retinal Layers	31	192.7	21.09	3.79	150.5	234.9	31	167.3	16.05	2.88	135.2	199.4
	Outer Retinal Layers	31	147.0	15.07	2.71	116.8	177.1	31	157.2	11.18	2.01	134.8	179.5
	RT	31	339.7	18.05	3.24	303.6	375.8	31	324.4	19.47	3.50	285.5	363.4

Summary of the mean values, standard deviations and 95% confidence intervals obtained for each of the retinal layers for each age group at the parafovea

N = number of examinations where the retinal layer(s) could be reliably segmented; SD = standard deviation; SEM = standard error of the mean; LCI = lower confidence interval; UCI = upper confidence interval; RNFL = retinal nerve fibre layer; GCL = ganglion cell layer; IPL = inner plexiform layer; INL = inner nuclear layer; OPL = outer plexiform layer; ONL = outer nuclear layer; IS = inner segment of the photoreceptor; OS = outer segment of the photoreceptor; RPE = retinal pigment epithelium; GCC = ganglion cell complex; GA = gestational age

Table 7: Perifoveal Normative Data

		Nasal Perifovea (2000 μ m from the Fovea)				95% Confidence Interval		Temporal Perifovea (2000 μ m from the Fovea)				95% Confidence Interval	
Age Group	Retinal Layer	N	Mean	SD	SEM	LCI	UCI	N	Mean	SD	SEM	LCI	UCI
<40 weeks GA	RNFL	21	41.95	4.68	1.02	32.58	51.31	15	12.73	6.44	1.66	0.00	25.62
	GCL	21	38.44	8.33	1.82	21.78	55.10	15	33.69	10.48	2.71	12.73	54.64
	IPL	21	51.37	6.29	1.37	38.79	63.95	15	51.17	6.42	1.66	38.32	64.01
	INL	21	46.72	9.51	2.07	27.71	65.74	15	49.31	12.58	3.25	24.15	74.47
	OPL	21	22.91	6.49	1.42	9.93	35.89	15	19.50	6.66	1.72	6.18	32.81
	ONL	12	52.30	5.80	1.67	40.70	63.89	8	46.24	9.29	3.29	27.65	64.83
	IS	11	24.03	3.03	0.91	17.98	30.09	8	24.27	3.86	1.37	16.54	32.00
	OS	20	7.44	2.77	0.62	1.91	12.98	14	8.49	2.97	0.79	2.55	14.43
	RPE	21	12.40	2.71	0.59	6.97	17.83	13	13.25	3.94	1.09	5.37	21.13
	GCC	21	89.81	9.73	2.12	70.34	109.3	15	84.85	10.88	2.81	63.10	106.6
	ONL-IS Complex	21	73.24	7.50	1.64	58.24	88.24	15	68.56	7.14	1.84	54.28	82.85
	OS-RPE Complex	22	20.24	3.56	0.76	13.12	27.37	15	20.29	5.61	1.45	9.07	31.51
	Inner Retinal Layers	20	200.2	14.92	3.34	170.4	230.0	14	164.0	16.38	4.38	131.2	196.8
	Outer Retinal Layers	20	94.18	8.63	1.93	76.92	111.5	14	90.53	10.11	2.70	70.31	110.8
	RT	22	292.5	18.26	3.89	256.0	329.1	14	254.5	19.06	5.10	216.4	292.6
41-46 weeks GA	RNFL	19	43.40	6.96	1.60	29.48	57.32	9	12.01	3.83	1.28	4.35	19.67
	GCL	18	34.10	5.55	1.31	23.00	45.21	9	29.45	11.03	3.68	7.38	51.52
	IPL	19	49.48	7.70	1.77	34.07	64.89	9	54.69	7.18	2.39	40.33	69.04
	INL	18	45.85	6.34	1.49	33.17	58.53	8	48.73	6.62	2.34	35.49	61.96
	OPL	18	21.88	6.79	1.60	8.29	35.46	8	16.67	3.85	1.36	8.97	24.36
	ONL	12	49.70	5.80	1.67	38.11	61.30	7	56.91	9.45	3.57	38.02	75.81
	IS	12	25.62	3.42	0.99	18.77	32.47	7	24.89	2.11	0.80	20.68	29.11
	OS	17	10.56	3.00	0.73	4.55	16.56	8	10.82	3.40	1.20	4.01	17.62
	RPE	19	12.06	3.33	0.76	5.41	18.72	9	12.77	2.87	0.96	7.04	18.50
	GCC	18	83.08	9.26	2.18	64.56	101.6	9	84.13	9.95	3.32	64.24	104.0

	ONL-IS Complex	18	75.06	5.91	1.39	63.25	86.88	8	78.25	6.81	2.41	64.63	91.88
	OS-RPE Complex	19	22.89	3.39	0.78	16.12	29.66	9	24.06	5.39	1.80	13.27	34.84
	Inner Retinal Layers	15	191.0	16.11	4.16	158.8	223.2	8	160.1	13.37	4.73	133.4	186.9
	Outer Retinal Layers	15	99.19	10.25	2.65	78.68	119.7	8	103.5	6.43	2.27	90.69	116.4
	RT	16	289.9	14.85	3.71	260.2	319.6	9	264.7	12.96	4.32	238.8	290.6
47-52 weeks GA	RNFL	10	40.05	5.85	1.85	28.36	51.75	1b	10.19			10.19	10.19
	GCL	10	33.83	6.33	2.00	21.18	46.48	1b	29.52			29.52	29.52
	IPL	10	48.89	10.21	3.23	28.46	69.31	1b	48.06			48.06	48.06
	INL	9	41.57	6.45	2.15	28.67	54.47	1b	39.97			39.97	39.97
	OPL	8	31.24	13.36	4.72	4.52	57.96	2	17.58	6.06	4.29	5.46	29.69
	ONL	8	48.12	10.37	3.67	27.38	68.86	1b	56.99			56.99	56.99
	IS	9	25.20	2.64	0.88	19.93	30.48	1b	21.18			21.18	21.18
	OS	9	16.03	3.81	1.27	8.41	23.64	1b	14.53			14.53	14.53
	RPE	9	12.67	2.23	0.74	8.20	17.14	0b, c				0.00	0.00
	GCC	10	82.72	8.72	2.76	65.27	100.2	1b	77.58			77.58	77.58
	ONL-IS Complex	8	73.44	10.25	3.62	52.94	93.94	1b	78.17			78.17	78.17
	OS-RPE Complex	10	28.30	5.84	1.85	16.62	39.97	1b	14.53			14.53	14.53
	Inner Retinal Layers	9	191.5	15.13	5.04	161.2	221.7	0b, c				0.00	0.00
	Outer Retinal Layers	9	104.3	7.55	2.52	89.20	119.4	0b, c				0.00	0.00
	RT	11	294.8	14.16	4.27	266.5	323.1	0b, c				0.00	0.00
12-14 months GA	RNFL	27	40.37	8.49	1.63	23.39	57.35	9	12.05	3.34	1.11	5.36	18.74
	GCL	25	30.46	7.87	1.57	14.72	46.20	9	23.74	6.16	2.05	11.43	36.06
	IPL	25	45.84	5.65	1.13	34.54	57.13	9	51.91	7.17	2.39	37.57	66.26
	INL	25	36.28	7.06	1.41	22.17	50.40	9	38.32	3.56	1.19	31.20	45.44
	OPL	25	26.93	10.65	2.13	5.64	48.23	9	23.42	5.91	1.97	11.61	35.23
	ONL	20	56.64	7.75	1.73	41.15	72.13	8	58.30	9.54	3.37	39.23	77.37
	IS	20	23.36	3.25	0.73	16.86	29.85	8	23.76	1.13	0.40	21.51	26.01

	OS	25	9.39	6.15	1.23	0.00	21.69	8	8.62	6.87	2.43	0.00	22.36
	RPE	26	14.04	2.86	0.56	8.32	19.75	8	14.97	2.70	0.95	9.57	20.36
	GCC	25	76.30	9.86	1.97	56.59	96.01	9	75.66	9.08	3.03	57.50	93.82
	ONL-IS Complex	25	77.62	9.70	1.94	58.21	97.03	9	81.83	9.33	3.11	63.17	100.5
	OS-RPE Complex	27	33.46	3.78	0.73	25.90	41.01	8	34.36	3.90	1.38	26.56	42.15
	Inner Retinal Layers	26	183.6	22.19	4.35	139.2	227.9	10	152.9	17.76	5.62	117.4	188.4
	Outer Retinal Layers	26	110.4	11.07	2.17	88.27	132.6	10	115.2	10.91	3.45	93.33	137.0
	RT	28	296.0	19.62	3.71	256.7	335.2	10	268.0	14.59	4.62	238.8	297.2
15-17 months GA	RNFL	34	37.30	6.41	1.10	24.48	50.11	10	12.10	3.21	1.02	5.67	18.52
	GCL	32	28.06	7.17	1.27	13.71	42.40	9	26.22	4.90	1.63	16.42	36.02
	IPL	31	40.95	6.78	1.22	27.38	54.52	9	41.34	9.75	3.25	21.83	60.84
	INL	29	37.59	6.64	1.23	24.31	50.86	9	37.25	8.09	2.70	21.07	53.42
	OPL	27	27.97	8.64	1.66	10.69	45.24	8	26.71	10.27	3.63	6.17	47.25
	ONL	25	56.26	10.43	2.09	35.40	77.12	8	57.62	14.34	5.07	28.95	86.30
	IS	26	24.20	2.15	0.42	19.89	28.51	10	26.46	2.96	0.94	20.55	32.38
	OS	27	12.26	5.70	1.10	0.87	23.66	10	10.37	6.39	2.02	0.00	23.14
	RPE	29	14.68	2.96	0.55	8.76	20.59	10	15.81	3.61	1.14	8.58	23.03
	GCC	31	69.39	9.40	1.69	50.58	88.19	9	67.55	8.91	2.97	49.74	85.36
	ONL-IS Complex	26	80.78	10.22	2.00	60.33	101.2	8	83.61	12.08	4.27	59.46	107.8
	OS-RPE Complex	33	36.02	5.47	0.95	25.09	46.96	11	36.68	6.20	1.87	24.28	49.08
	Inner Retinal Layers	28	176.1	17.87	3.38	140.4	211.9	7	140.0	9.94	3.76	120.1	159.9
	Outer Retinal Layers	28	116.4	12.08	2.28	92.21	140.5	7	122.5	14.76	5.58	92.96	152.0
	RT	35	290.5	14.20	2.40	262.1	318.9	8	265.0	18.57	6.57	227.8	302.1
18-20 months GA	RNFL	31	36.80	7.09	1.27	22.61	50.99	10	9.12	2.13	0.67	4.85	13.39
	GCL	30	27.56	6.40	1.17	14.76	40.35	10	21.75	7.89	2.50	5.96	37.53
	IPL	30	41.77	6.94	1.27	27.89	55.64	10	48.78	6.81	2.15	35.15	62.40
	INL	30	36.06	7.39	1.35	21.28	50.84	10	33.91	6.33	2.00	21.25	46.57
	OPL	30	29.68	8.45	1.54	12.79	46.58	10	23.25	8.26	2.61	6.73	39.77

	ONL	28	53.13	9.28	1.75	34.56	71.69	10	59.76	10.82	3.42	38.13	81.39
	IS	28	25.17	2.77	0.52	19.63	30.71	10	25.70	2.24	0.71	21.23	30.18
	OS	26	9.30	4.62	0.91	0.06	18.55	9	9.77	4.89	1.63	0.00	19.55
	RPE	25	14.95	4.44	0.89	6.07	23.83	8	15.11	4.64	1.64	5.83	24.38
	GCC	30	69.56	8.19	1.50	53.18	85.94	10	70.52	9.61	3.04	51.30	89.75
	ONL-IS Complex	30	78.69	9.82	1.79	59.04	98.34	10	85.47	10.11	3.20	65.25	105.7
	OS-RPE Complex	31	35.23	7.14	1.28	20.95	49.51	10	35.37	6.75	2.14	21.86	48.88
	Inner Retinal Layers	30	172.1	16.85	3.08	138.4	205.8	10	136.8	14.43	4.56	108.0	165.7
	Outer Retinal Layers	30	117.5	10.05	1.83	97.39	137.6	10	123.8	9.69	3.06	104.4	143.2
	RT	31	289.3	14.17	2.55	260.9	317.6	10	260.6	15.19	4.81	230.2	291.0
21-26 months GA	RNFL	23	35.73	8.38	1.75	18.97	52.49	11	9.76	3.12	0.94	3.53	16.00
	GCL	23	32.14	8.15	1.70	15.84	48.45	11	22.43	7.21	2.17	8.01	36.86
	IPL	23	41.42	5.46	1.14	30.49	52.35	11	45.81	4.51	1.36	36.78	54.84
	INL	23	37.77	6.97	1.45	23.83	51.71	11	37.60	3.66	1.10	30.27	44.92
	OPL	23	30.27	8.67	1.81	12.92	47.61	11	22.63	6.89	2.08	8.84	36.42
	ONL	22	57.76	12.98	2.77	31.81	83.71	10	63.08	6.80	2.15	49.48	76.68
	IS	22	25.95	2.77	0.59	20.41	31.50	10	27.87	2.71	0.86	22.45	33.29
	OS	21	11.82	5.97	1.30	0.00	23.76	8	10.82	5.18	1.83	0.46	21.19
	RPE	21	15.31	4.37	0.95	6.56	24.05	8	18.11	6.00	2.12	6.11	30.11
	GCC	23	73.56	8.26	1.72	57.04	90.08	11	68.24	5.72	1.72	56.80	79.68
	ONL-IS Complex	23	83.63	13.07	2.72	57.50	109.8	11	91.84	8.65	2.61	74.54	109.1
	OS-RPE Complex	23	38.62	6.87	1.43	24.87	52.36	12	34.68	10.50	3.03	13.67	55.69
	Inner Retinal Layers	21	175.6	11.92	2.60	151.8	199.5	11	139.4	9.58	2.89	120.3	158.6
	Outer Retinal Layers	21	125.5	12.71	2.77	100.0	150.9	11	127.9	12.22	3.69	103.5	152.4
	RT	21	301.1	15.76	3.44	269.6	332.6	12	267.8	10.33	2.98	247.1	288.4
27-32 months GA	RNFL	29	36.43	4.97	0.92	26.50	46.37	19	10.41	2.98	0.68	4.45	16.37
	GCL	26	28.46	6.21	1.22	16.03	40.88	17	24.30	3.25	0.79	17.81	30.79
	IPL	26	40.67	5.90	1.16	28.87	52.48	18	45.14	7.91	1.86	29.31	60.96

	INL	26	36.45	6.82	1.34	22.81	50.09	19	33.86	6.54	1.50	20.78	46.94
	OPL	26	31.22	8.66	1.70	13.91	48.54	19	27.02	9.14	2.10	8.75	45.30
	ONL	23	51.47	12.40	2.58	26.68	76.26	16	53.15	9.63	2.41	33.90	72.40
	IS	23	26.48	3.76	0.78	18.95	34.00	17	26.93	3.49	0.85	19.96	33.91
	OS	26	11.66	6.81	1.33	0.00	25.27	20	10.79	5.94	1.33	0.00	22.66
	RPE	26	18.42	3.32	0.65	11.78	25.07	20	18.24	3.04	0.68	12.16	24.32
	GCC	26	69.13	8.49	1.67	52.14	86.11	19	69.94	7.15	1.64	55.65	84.24
	ONL-IS Complex	26	78.70	13.03	2.56	52.64	104.8	20	76.88	14.58	3.26	47.72	106.1
	OS-RPE Complex	29	40.40	5.30	0.98	29.80	50.99	20	41.68	3.22	0.72	35.24	48.11
	Inner Retinal Layers	25	170.3	15.84	3.17	138.6	202.0	20	140.0	14.06	3.14	111.9	168.2
	Outer Retinal Layers	25	121.3	12.13	2.43	97.07	145.6	20	120.8	11.07	2.47	98.64	142.9
	RT	28	291.2	15.10	2.85	261.0	321.4	21	261.2	16.53	3.61	228.2	294.3
33-38 months GA	RNFL	20	35.79	7.02	1.57	21.74	49.83	18	10.65	3.52	0.83	3.61	17.68
	GCL	19	28.04	7.25	1.66	13.53	42.54	18	21.74	6.32	1.49	9.11	34.37
	IPL	19	41.36	6.71	1.54	27.95	54.78	18	45.04	3.37	0.80	38.29	51.79
	INL	20	35.94	7.03	1.57	21.89	50.00	18	35.13	5.60	1.32	23.93	46.33
	OPL	20	27.80	7.08	1.58	13.63	41.96	18	26.49	9.08	2.14	8.33	44.64
	ONL	18	57.50	10.71	2.52	36.07	78.92	17	55.89	8.76	2.13	38.37	73.42
	IS	18	26.95	3.69	0.87	19.56	34.34	17	25.80	3.66	0.89	18.48	33.12
	OS	18	12.33	7.69	1.81	0.00	27.70	17	10.24	4.87	1.18	0.49	19.98
	RPE	19	18.85	4.13	0.95	10.60	27.10	18	20.53	3.80	0.90	12.93	28.14
	GCC	20	69.50	7.65	1.71	54.20	84.79	18	66.78	5.55	1.31	55.67	77.88
	ONL-IS Complex	20	84.52	9.93	2.22	64.67	104.4	18	82.21	8.38	1.97	65.46	98.97
	OS-RPE Complex	20	40.24	7.68	1.72	24.88	55.60	18	42.01	5.87	1.38	30.27	53.75
	Inner Retinal Layers	21	173.0	14.70	3.21	143.6	202.4	19	140.7	8.85	2.03	123.0	158.4
	Outer Retinal Layers	21	125.8	10.25	2.24	105.3	146.3	19	125.6	9.46	2.17	106.7	144.5
	RT	21	298.8	12.13	2.65	274.5	323.1	19	266.3	10.76	2.47	244.8	287.8
39-44 months	RNFL	20	36.88	4.95	1.11	26.98	46.79	15	11.25	2.16	0.56	6.94	15.57

GA	GCL	19	30.51	7.52	1.73	15.46	45.56	15	27.47	7.81	2.02	11.85	43.09
	IPL	19	40.60	7.94	1.82	24.72	56.49	15	45.73	5.82	1.50	34.10	57.37
	INL	20	36.64	5.98	1.34	24.69	48.59	15	38.21	6.32	1.63	25.56	50.86
	OPL	20	26.57	7.09	1.59	12.38	40.75	15	25.05	7.54	1.95	9.96	40.14
	ONL	19	59.17	6.61	1.52	45.95	72.38	13	58.76	9.31	2.58	40.14	77.37
	IS	19	26.46	2.25	0.52	21.96	30.96	13	28.98	3.42	0.95	22.13	35.83
	OS	14	8.90	4.55	1.22	0.00	18.00	10	8.10	4.57	1.44	0.00	17.24
	RPE	17	18.50	3.64	0.88	11.21	25.78	13	18.58	5.17	1.43	8.24	28.92
	GCC	20	71.06	8.91	1.99	53.24	88.89	15	73.21	7.22	1.86	58.77	87.64
	ONL-IS Complex	20	84.48	8.82	1.97	66.85	102.1	15	87.59	9.66	2.49	68.27	106.9
	OS-RPE Complex	20	40.78	7.94	1.78	24.89	56.67	15	40.45	8.10	2.09	24.24	56.66
	Inner Retinal Layers	22	172.7	12.32	2.63	148.1	197.4	14	149.7	13.74	3.67	122.2	177.2
	Outer Retinal Layers	22	127.2	10.80	2.30	105.6	148.8	14	132.3	11.63	3.11	109.0	155.5
	RT	22	299.9	17.18	3.66	265.5	334.3	14	281.9	11.86	3.17	258.2	305.7
45-56 months GA	RNFL	36	39.38	6.45	1.07	26.48	52.28	33	10.65	4.20	0.73	2.25	19.04
	GCL	33	29.26	7.65	1.33	13.96	44.56	31	26.96	7.98	1.43	11.00	42.92
	IPL	33	40.55	7.16	1.25	26.24	54.86	31	44.92	6.86	1.23	31.19	58.65
	INL	34	37.50	7.25	1.24	23.00	51.99	31	37.79	7.43	1.33	22.93	52.66
	OPL	34	28.07	7.77	1.33	12.54	43.60	31	24.71	5.68	1.02	13.35	36.07
	ONL	32	57.80	12.64	2.24	32.51	83.09	29	58.88	11.55	2.14	35.79	81.98
	IS	31	25.64	2.59	0.46	20.46	30.81	29	27.15	2.46	0.46	22.24	32.06
	OS	30	9.84	2.81	0.51	4.21	15.46	27	9.65	2.64	0.51	4.36	14.93
	RPE	31	17.65	5.02	0.90	7.62	27.68	28	17.18	5.79	1.10	5.59	28.77
	GCC	34	69.68	8.33	1.43	53.03	86.33	31	71.88	8.37	1.50	55.15	88.61
	ONL-IS Complex	33	82.67	11.75	2.05	59.17	106.2	30	84.35	11.05	2.02	62.25	106.5
	OS-RPE Complex	35	40.27	8.20	1.39	23.88	56.66	34	39.67	7.61	1.30	24.46	54.89
	Inner Retinal Layers	33	174.0	14.20	2.47	145.6	202.4	32	144.2	12.84	2.27	118.5	169.9
	Outer Retinal Layers	33	126.1	10.86	1.89	104.4	147.8	32	127.7	10.89	1.93	105.9	149.5

	RT	35	300.8	15.58	2.63	269.6	332.0	35	272.9	12.71	2.15	247.4	298.3
57-68 months GA	RNFL	48	34.68	5.38	0.78	23.92	45.45	38	9.54	3.17	0.51	3.20	15.88
	GCL	44	34.72	6.48	0.98	21.76	47.67	34	27.01	7.00	1.20	13.01	41.02
	IPL	44	41.98	6.89	1.04	28.20	55.76	34	45.56	7.34	1.26	30.88	60.24
	INL	48	39.13	7.62	1.10	23.89	54.38	37	35.52	4.84	0.80	25.84	45.20
	OPL	48	30.92	8.60	1.24	13.73	48.11	37	23.03	5.44	0.89	12.15	33.92
	ONL	43	55.66	10.27	1.57	35.12	76.21	36	63.26	9.70	1.62	43.86	82.66
	IS	43	26.59	3.78	0.58	19.03	34.15	36	26.58	3.12	0.52	20.34	32.82
	OS	40	10.54	5.52	0.87	0.00	21.58	32	10.36	5.57	0.98	0.00	21.49
	RPE	40	20.02	3.81	0.60	12.40	27.64	32	19.86	3.54	0.63	12.79	26.94
	GCC	48	76.55	6.63	0.96	63.28	89.81	37	72.43	6.40	1.05	59.63	85.22
	ONL-IS Complex	48	81.58	11.33	1.64	58.92	104.3	37	89.88	10.35	1.70	69.17	110.6
	OS-RPE Complex	47	40.30	8.06	1.18	24.18	56.42	37	40.87	8.32	1.37	24.24	57.51
	Inner Retinal Layers	48	178.9	14.73	2.13	149.4	208.4	38	141.1	10.07	1.63	121.0	161.2
	Outer Retinal Layers	48	126.0	11.48	1.66	103.0	148.9	38	133.0	11.53	1.87	110.0	156.1
	RT	49	304.9	15.05	2.15	274.8	335.0	39	274.3	14.01	2.24	246.3	302.3
69-80 months GA	RNFL	31	31.99	4.43	0.80	23.12	40.86	30	9.86	2.29	0.42	5.29	14.43
	GCL	31	36.90	6.57	1.18	23.76	50.03	28	26.50	9.53	1.80	7.45	45.56
	IPL	31	42.20	5.56	1.00	31.08	53.32	28	48.50	10.48	1.98	27.54	69.47
	INL	31	39.88	7.67	1.38	24.53	55.22	30	37.09	8.27	1.51	20.56	53.62
	OPL	31	34.18	9.23	1.66	15.71	52.65	30	29.29	7.72	1.41	13.84	44.73
	ONL	29	55.07	10.17	1.89	34.73	75.42	29	56.77	10.91	2.03	34.95	78.59
	IS	29	26.55	3.15	0.59	20.25	32.86	29	28.75	3.10	0.58	22.55	34.96
	OS	25	8.49	3.41	0.68	1.68	15.30	23	7.64	2.90	0.60	1.84	13.43
	RPE	26	19.97	3.31	0.65	13.35	26.59	24	20.10	4.41	0.90	11.29	28.92
	GCC	31	79.33	7.99	1.44	63.35	95.31	28	75.01	6.43	1.22	62.14	87.87
	ONL-IS Complex	31	82.59	10.85	1.95	60.90	104.3	30	85.62	12.06	2.20	61.50	109.8
	OS-RPE Complex	31	40.43	8.46	1.52	23.50	57.35	30	39.72	8.76	1.60	22.21	57.24
	Inner Retinal Layers	30	188.5	13.91	2.54	160.7	216.3	28	150.5	14.85	2.81	120.8	180.2

	Outer Retinal Layers	30	125.0	11.64	2.12	101.7	148.3	28	129.4	14.41	2.72	100.6	158.2
	RT	30	313.5	12.52	2.29	288.4	338.5	28	279.9	16.14	3.05	247.6	312.2
81-92 months GA	RNFL	37	31.75	5.48	0.90	20.79	42.72	34	10.72	2.68	0.46	5.37	16.08
	GCL	36	37.45	7.17	1.20	23.10	51.80	31	30.65	9.39	1.69	11.87	49.44
	IPL	36	43.61	6.74	1.12	30.14	57.09	31	45.71	8.71	1.56	28.30	63.13
	INL	37	40.99	8.68	1.43	23.62	58.36	34	39.02	8.10	1.39	22.83	55.21
	OPL	37	29.77	10.26	1.69	9.24	50.29	34	26.48	6.75	1.16	12.98	39.98
	ONL	34	56.77	10.37	1.78	36.02	77.51	31	59.03	8.15	1.46	42.73	75.33
	IS	34	28.58	2.93	0.50	22.73	34.43	31	28.95	3.01	0.54	22.94	34.96
	OS	32	10.82	2.35	0.42	6.12	15.52	30	10.67	4.44	0.81	1.79	19.55
	RPE	33	16.84	4.03	0.70	8.78	24.90	31	17.85	4.00	0.72	9.84	25.86
	GCC	37	81.17	8.54	1.40	64.09	98.24	34	76.20	8.74	1.50	58.72	93.68
	ONL-IS Complex	37	84.87	10.99	1.81	62.89	106.9	34	87.84	7.48	1.28	72.89	102.8
	OS-RPE Complex	37	41.35	6.32	1.04	28.71	53.99	34	42.74	7.22	1.24	28.30	57.18
	Inner Retinal Layers	37	184.9	12.10	1.99	160.7	209.1	35	152.1	10.11	1.71	131.9	172.4
	Outer Retinal Layers	37	128.4	12.25	2.01	103.9	152.9	35	133.3	9.87	1.67	113.6	153.1
	RT	37	313.3	16.21	2.66	280.8	345.7	35	285.5	14.39	2.43	256.7	314.2
93-213 months GA	RNFL	40	34.04	5.45	0.86	23.15	44.94	37	10.56	3.41	0.56	3.75	17.37
	GCL	35	40.73	8.81	1.49	23.11	58.36	32	32.98	5.70	1.01	21.58	44.38
	IPL	35	42.27	8.97	1.52	24.34	60.21	32	43.80	7.73	1.37	28.33	59.27
	INL	40	40.27	7.39	1.17	25.50	55.04	37	39.02	5.18	0.85	28.66	49.38
	OPL	40	29.73	9.91	1.57	9.92	49.55	37	24.09	6.81	1.12	10.46	37.71
	ONL	39	61.46	11.28	1.81	38.89	84.02	36	63.52	8.94	1.49	45.64	81.39
	IS	39	26.30	3.22	0.52	19.86	32.74	36	28.36	3.54	0.59	21.27	35.44
	OS	32	11.96	4.68	0.83	2.60	21.31	30	11.02	5.81	1.06	0.00	22.65
	RPE	31	18.60	3.52	0.63	11.56	25.63	28	18.45	3.50	0.66	11.44	25.46
	GCC	40	82.53	6.88	1.09	68.77	96.29	36	76.71	7.86	1.31	60.99	92.44
	ONL-IS Complex	40	87.20	11.54	1.82	64.12	110.3	37	91.91	9.11	1.50	73.68	110.1
	OS-RPE Complex	37	41.89	9.66	1.59	22.58	61.21	35	42.05	9.78	1.65	22.50	61.60

	Inner Retinal Layers	40	186.1	12.26	1.94	161.5	210.6	36	149.3	11.55	1.92	126.2	172.4
	Outer Retinal Layers	40	133.2	11.65	1.84	109.9	156.5	36	138.4	9.93	1.66	118.5	158.3
	RT	40	319.2	12.70	2.01	293.8	344.6	36	287.7	14.97	2.50	257.7	317.6
214-309 months GA	RNFL	30	33.81	5.86	1.07	22.09	45.52	30	11.45	4.00	0.73	3.46	19.44
	GCL	22	36.97	9.55	2.04	17.87	56.07	19	31.84	9.04	2.07	13.77	49.91
	IPL	22	41.23	7.20	1.54	26.83	55.63	19	43.66	6.02	1.38	31.62	55.70
	INL	30	38.00	5.92	1.08	26.15	49.84	30	36.15	6.09	1.11	23.97	48.33
	OPL	30	27.18	7.43	1.36	12.33	42.04	30	23.29	5.45	0.99	12.39	34.19
	ONL	28	59.61	10.32	1.95	38.98	80.24	28	64.09	7.90	1.49	48.30	79.89
	IS	29	27.13	3.40	0.63	20.33	33.94	29	27.37	2.95	0.55	21.46	33.27
	OS	26	12.60	4.66	0.91	3.27	21.92	26	12.40	3.79	0.74	4.82	19.97
	RPE	27	17.70	3.45	0.66	10.81	24.59	27	18.97	4.95	0.95	9.06	28.87
	GCC	29	77.75	10.12	1.88	57.52	97.98	29	75.38	6.97	1.29	61.44	89.31
	ONL-IS Complex	30	87.16	10.44	1.91	66.27	108.0	30	91.51	7.63	1.39	76.25	106.8
	OS-RPE Complex	30	45.97	6.68	1.22	32.62	59.33	31	44.99	10.61	1.91	23.78	66.21
	Inner Retinal Layers	30	177.4	14.58	2.66	148.2	206.6	30	146.9	13.72	2.51	119.4	174.3
	Outer Retinal Layers	30	134.1	10.66	1.95	112.7	155.4	30	140.2	8.72	1.59	122.7	157.6
	RT	30	311.3	19.70	3.60	271.9	350.7	30	287.4	16.84	3.07	253.7	321.1

Summary of the mean values, standard deviations and 95% confidence intervals obtained for each of the retinal layers for each age group at the perifovea

N = number of examinations where the retinal layer(s) could be reliably segmented; SD = standard deviation; SEM = standard error of the mean; LCI = lower confidence interval; UCI = upper confidence interval; RNFL = retinal nerve fibre layer; GCL = ganglion cell layer; IPL = inner plexiform layer; INL = inner nuclear layer; OPL = outer plexiform layer; ONL = outer nuclear layer; IS = inner segment of the

photoreceptor; OS = outer segment of the photoreceptor; RPE = retinal pigment epithelium; GCC = ganglion cell complex; GA = gestational age

Table 8: Ages at which Retinal Layer Development reaches Maturity

Position	Nasal		Fovea	Temporal	
	Perifovea	Parafovea		Parafovea	Perifovea
RNFL	31.4 months	16.8 months	NA	17.4 months	12.0 months
GCL	53.5 months	61.9 months	10.6 months	55.3 months	65.5 months
IPL	13.4 months	39.1 months	18.7 months	15.1 months	22.1 months
INL	41.5 months	13.1 months	17.6 months	22.5 months	34.8 months
OPL	10.0 months	11.6 months	17.8 months	<i>No Plateau</i>	11.5 months
ONL	42.7 months	19.4 months	45.3 months	<i>92.9 months*</i>	128.4 months
IS	29.8 months	18.6 months	26.9 months	17.9 months	19.7 months
OS	68.5 months	23.0 months	32.4 months	31.0 months	146 months
RPE	<i>No Plateau</i>	27.4 months	54.4 months	41.0 months	17.3 months

Summary of the gestational ages at which the developmental trajectory for each retinal layer at the fovea, parafovea and perifovea reaches the 95% confidence interval of the mean adult value, as calculated using the fractional polynomial equations generated from the model

These were calculated only if there was evidence of a plateau in the development of each retinal layer.

RNFL= retinal nerve fibre layer; GCL = ganglion cell layer; IPL = inner plexiform layer; GCC = ganglion cell complex; INL = inner nuclear layer; OPL = outer plexiform layer; ONL = outer nuclear layer; IS = inner segment of the photoreceptor; OS = outer segment of the photoreceptor; RPE = retinal pigment epithelium; NA = not applicable

**Could not be solved using the fractional polynomial from the model. A solution was calculated using an alternative 4th order polynomial equation: $(0.42 * (\text{LogGA} - 7)^4) + (17.61 * (\text{LogGA} - 7)^3) + (-80.43 * (\text{LogGA} - 7)^2) + (120.53 * (\text{LogGA} - 7)) + 9.01$*

Supplementary Video 1 Legend: Foveal Development between Birth and Adulthood

There is migration of the inner retinal layers away from the fovea, migration of the photoreceptors into the fovea and thickening of each of the retinal layers over time.

RNFL = retinal nerve fibre layer; GCL = ganglion cell layer; IPL = inner plexiform layer; INL = inner nuclear layer; OPL = outer plexiform layer; ONL = outer nuclear layer; IS = inner segment of the photoreceptor; OS = outer segment of the photoreceptor; RPE = retinal pigment epithelium; GA = gestational age.

Appendix 2

Supplementary Data for Chapter 5

Table 1: Demographics

Category	Nystagmus				Controls			
	No.	Mean Age (months)	Range (months)	SD (months)	No.	Mean Age (months)	Range (months)	SD (months)
1	23	41.8	11-76	21.3	23	41.9	10-77	21.5
2	5	29.2	2-70	26.4	5	28.4	4-69	23.3
3	6	43.3	3-77	24.1	6	43.8	4-74	22.9
4	16	39.4	7-81	24.5	16	39.2	7-83	24.5

Summary of the number of subjects, mean age, age range and standard deviations of both the nystagmus and control groups in each category

No. = number of participants; SD = standard deviation

Table 2: Clinical Characteristics (Typical Foveal Hypoplasia)

Patient ID	Age (months)	Sex	BCVA BE (LogMAR)	Refraction	Iris TID	Other Features 	Genetic Diagnosis	VEP Crossed Asymmetry	ERG	Foveal Hypoplasia Grade
1	37	M	0.70	+4.25/+1.50@180 RE +5.00/+1.00@90 LE	Y	Blonde hair Pale fundus	Non <i>TYR</i>	Y	Normal	3
2	12	M	----	----	Y	Blonde hair Pale fundus	+ Family history albinism Non <i>TYR</i>	Y	Normal	4
7	81	M	0.225	+3.50/+3.00@90 RE +4.50/+3.50@90 LE	N	Ginger hair + TID in both parents	Non <i>TYR</i>	N	Normal	1
8	32	M	0.60	+5.0 RE +5.0 LE	----	+ TID in both parents	----	Unreliable	Unreliable	1
9	15	F	0.60	+1.00/-1.00@10 RE +1.00/-1.25@170 LE	----	Blonde hair Pale fundus + TID in mum	----	----	----	1
10	45	M	0.60	Plano/+1.00@90 RE Plano/+1.00@90 LE	----	Light brown hair	Non <i>TYR</i>	N	Normal	1
12	56	F	0.70	+7.00/-3.50@180 RE +8.50/-2.50@180 LE	Y	Blonde hair Pale fundus	<i>TYR</i>	Y	Normal	2
15	13	F	0.30	-0.25 RE -0.25 LE	----	Blonde hair Pale fundus + TID in both parents	Non <i>TYR</i>	N	Normal	1
16	49	M	0.95	+5.50/-3.00@05 RE +6.00/-3.50@180 LE	Y	Blonde hair Pale fundus + TID in both parents	<i>TYR</i>	Y	Normal	3
22	45	F	0.65	+5.25 RE +5.25 LE	Y	Blonde hair Pale fundus	Non <i>TYR</i>	N	Normal	2
23	50	M	0.40	-2.50/-2.75@180 RE -2.25/-1.50@80 LE	Y	Blonde hair Pale fundus	Non <i>TYR</i>	N	Normal	2
27	70	M	0.75	+4.25/-1.25@155 RE +4.75/-0.50@5 LE	Y	Light brown hair Pale fundus	+ Family history albinism	----	----	4
28	58	M	0.35	+4.50/1.50@20 RE	Y	Blonde hair Pale fundus + TID in both parents	Non <i>TYR</i>	Y	Normal	1
29	24	M	0.92	+6.00/-2.00@160 LE	Y	Blonde hair Pale fundus	<i>TYR</i>	Unreliable	Unreliable	3
30	46	M	0.60	+0.75/+0.75@70 RE +0.75/+0.75@75 LE	Y	Blonde hair Pale fundus + TID in mum	Non <i>TYR</i>	----	----	3
32	14	M	0.30	----	----	Blonde hair Pale fundus + TID in mum	Non <i>TYR</i>	Unreliable	Normal	1
34	27	M	F and F	+2.50/-2.00@20 RE +2.00/-2.00@160 LE	Y	Blonde hair Pale fundus	+ Family history albinism	Abandoned	Normal	4
39	40	F	0.60	+2.00/-1.50@80 RE Plano/-0.50@180 LE	----	Blonde hair Pale fundus	Non <i>TYR</i>	Unreliable	Normal	2

40*	55	F	0.375	+3.25 RE +3.00 LE	Y	Blonde hair Pale fundus	PAX6	N	Normal	1
41*	76	M	0.50	+5.50 RE +5.50 LE	Y	Blonde hair Pale fundus	PAX6	Unreliable	Normal	1
43	11	F	0.70	+3.00/-3.00@180 RE +3.00/-3.00@180 LE	----	Blonde hair Pale fundus + TID in both parents	Non TYR	Y	Normal	4
49	70	M	0.825	+3.50/-2.00@25 RE +4.25/2.50@10 LE	Y	Red hair Pale fundus	Non TYR	Y	----	4
50	36	F	0.20	+0.25/-0.50@180 RE +0.25/-0.50@180 LE	Y	Blonde hair Pale fundus	Non TYR	Y	Normal	2

Clinical characteristics of patients with typical foveal hypoplasia

ID = identification; M = male; F = female; BCVA = best corrected visual acuity; BE = both eyes; LogMAR = Logarithm of the Minimum Angle of Resolution; F and F = fixing and following; RE = right eye; LE = left eye; TID = transillumination defects; Y = yes; N = no; TYR = tyrosinase gene VEP = visual evoked potential; ERG = electroretinogram

△ See table 3 for further details of pigmentary characteristics based on modified Schmitz classification

** indicate sibling pairs. All patients where nystagmus is not described had conjugate horizontal nystagmus*

---- indicates not assessed or could not be performed

Table 3: Pigmentary Characteristics in Albinism

Patient ID	Age (months)	Sex	Skin	Hair	Iris Translucency	Fovea	ONH
1	37	M	1	2	4	3	0
2	12	M	1	2	4	3	0
7	81	M	1	8	0	0	0
8	32	M	1	5	2	3	0
9	15	F	1	8	---	---	---
10	45	M	3	9	0	0	0
12	56	F	1	5	2	3	0
15	13	F	1	5	2	0	0
16	49	M	1	5	2	3	0
22	45	F	1	5	2	3	0
23	50	M	1	5	2	3	0
27	70	M	1	6	2	3	0
28	58	M	1	5	2	3	0
29	24	M	1	4	2	3	0
30	46	M	1	5	2	3	0
32	14	M	1	5	---	3	0
34	27	M	1	4	2	3	0
39	40	F	1	5	---	0	0
43	11	F	1	5	---	3	0
49	70	M	1	8	2	3	0
50	36	F	1	5	2	3	0

Pigmentary characteristics of patients with albinism using a modified Schmitz classification

Pigmentation levels were determined by visual assessment of hair and skin, iris translucency and slit lamp or indirect examination of the fundus and classified on a numeric scale as described by Schmitz et al 2003.²⁶⁰ The scale used is as follows: Skin: 1: white not tanning, 2: white, maybe pigmented nevi, some tanning, 3: pale, some visible tanning, 4: pale, good tanning, 5: normal, good tanning. Hair colour: 1: completely white, 2: silvery white, 3: white with yellowish touch, 4: whitish blonde, 5: pale blonde, 6: medium blonde, 7: dark blonde, 8: red, red-blonde, 9: medium brown, 10: dark brown black. Degree of iris translucency: 1: peripheral punctate iris

translucency (only visible with confocal light slit lamp, 2: diffuse peripheral iris translucency near pupillary border not translucent, 3: diffuse peripheral iris translucency, lens margin clearly visible throughout iris, pupillary margin not translucent, 4: complete iris translucency including the pupillary margin. Degree of hypo-pigmentation of the retinal pigment epithelium and of foveal hypoplasia: 1: peripheral retinal hypo-pigmentation, foveal structures visible, 2: peripheral distinct and centrally visible, foveal reflex not visible, 3: pronounced peripheral and central hypo-pigmentation, foveal and macular hypoplasia. 4: grade 3, plus atypical choroidal vessels crossing the presumed macular region. Degree of morphologic anomaly of optic nerve head: 0: ONH not pathologic, 1: ONH pale, normal size, 2: ONH small, vital colour, 3: ONH small and pale, 4: dysplasia of ONH

ID = identification; M = male; F = female; ONH = optic nerve hypoplasia

---- indicates not assessed or could not be performed

Table 4: Clinical Findings in Albinism

Total no. of patients affected	TID in Child/ Parents	Ocular/Cutaneous Hypopigmentation	Crossed asymmetry on VEP	+ Family History of OCA/ + Genetic mutation of <i>TYR</i>
3	●	●	●	●
5	●	●	●	---
3	●	●	---	●
7	●	●	---	---
2	●	---	---	---
1	---	●	---	---
n = 21	n= 20 positive	n = 19 positive	n = 8 positive	n = 3 positive

Summary of clinical findings in patients with suspected albinism

No = number; TID = transillumination defects; VEP = visual evoked potentials; OCA = oculocutaneous albinism; TYR = tyrosinase gene; n = total number

● *indicates a positive result consistent with albinism*

--- *indicates a negative or unobtainable result*

Table 5: Clinical Characteristics (Atypical Foveal Hypoplasia)

Patient ID	Age (months)	Sex	BCVA BE (LogMar)	Refraction	Iris TID	Other Features Δ	Genetic Diagnosis	VEP Crossed Asymmetry	ERG	Foveal Hypoplasia Grade
3a	12	F	1.62	+7.50/-2.00 @11 RE +4.00/-2.00 @171 LE	----	Photophobia	CNGB3	----	----	Atypical
4a	70	M	1.00	+4.00/-2.00 @14 RE +4.00/-2.00 @171 LE	----	Photophobia	CNGB3	----	----	Atypical
11	25	M	0.92	+6.50/-1.00 @180 RE +6.00/-1.00 @180 LE	----	Photophobia	CNGA3	----	Severe generalized cone dysfunction	Atypical
47b	37	M	0.92	+6.00 RE +6.00/-1.00 @180 LE	----	Photophobia Vertical nystagmus	CNGB3	----	Severe generalized cone dysfunction	Atypical
48b	2	F	----	+2.50/-1.50 @90 RE +2.50/-1.50 @90 LE	----	Vertical nystagmus	CNGB3	----	----	Atypical

Clinical and genetic characteristics of patients with atypical foveal hypoplasia patients

ID = identification; F = female; M = male; BCVA = best corrected visual acuity; BE = both eyes; LogMAR = Logarithm of the Minimum Angle of Resolution; RE = right eye; LE = left eye; TID = transillumination defects; VEP = visual evoked potentials; ERG = electroretinogram

Δ All patients had fine fast nystagmus

a b indicate sibling pairs

---- *indicates not assessed or could not be performed*

Table 6: Clinical Characteristics (Abnormal Macular Morphology)

Patient ID	Age (months)	Sex	BCVA BE (LogMar)	Refraction	Iris TID	Other Features	VEP Crossed Asymmetry	ERG	Macular Morphology
17a	101	M	1.10	+9.50 RE +9.00/-3.00@ 180 LE	----	Microcephaly Lymphoedema Chorioretinal dysplasia	Unreliable	Unreliable	Thinning of the RPE, foveal hypoplasia and abnormal lamination of inner retinal layers
18a	51	F	0.70	+6.50 RE +5.50 LE	----	Microcephaly Lymphoedema Chorioretinal dysplasia	Unreliable	Unreliable	Thinning of the RPE, foveal hypoplasia and abnormal lamination of inner retinal layers
19b	36	M	Poor Coop	-6.00/+1.00@ 125 RE -5.25/+1.50@ 45 LE	----	Speckled fundus Vertical nystagmus	Unreliable	Absent rod and cone response	Thinning of the RPE
20b	48	M	0.80	----	----	Speckled fundus Vertical nystagmus	Unreliable	Absent rod and cone response	Thinning of the RPE
38	2	F	PL	+1.50 RE +1.50 LE	----	Attenuated retinal vasculature	Unreliable	Absent rod and cone response	IS/OS disruption
45	45	M	0.70	-6.25 RE -6.25 LE	----	Microcephaly Developmental delay Hypotonia Optic nerve pallor	N	Abnormal rod and cone response	Thinning of the RPE

Clinical characteristics of patients with abnormal macular morphology patients

ID = identification; F = female; M = male; BCVA, best corrected visual acuity; BE = both eyes; LogMAR = Logarithm of the Minimum Angle of Resolution; Coop = cooperation; PL = perception of light; RE = right eye; LE = left eye; TID, transillumination defects; VEP, visual evoked potential; ERG, electroretinogram; N = no; RPE = retinal pigment epithelium; IS/OS = inner segment/outer segment junction of photoreceptors

a b indicate sibling pairs

---- indicates not assessed or could not be performed

Table 7: Clinical Characteristics (Normal Macular Morphology)

Patient ID	Age (months)	Sex	BCVA BE (LogMar)	Refraction	Iris TID	Other Features Δ	Genetic Diagnosis	VEP Crossed Asymmetry	ERG	Macular Morphology
5	52	M	0.475	+6.00/-1.50@180 RE +6.25/-1.75@180 LE	N		---	N	Normal	Normal
6	7	M	0.30	----	----		----	N	Normal	Normal
13	81	M	0.075	----	N		----	N	Normal	Normal
14	18	F	0.10	+1.00/-1.00@170 RE +0.75/-1.25@10 LE	N		----	Unreliable	Unreliable	Normal
21	26	F	0.30	+1.00 RE +0.75 LE	N		Non-FRMD7	No	Normal	Normal
24	51	M	0.35	----	----		----	----	----	Normal
25	68	M	0.10	+1.75/-0.50@170 RE +2.25/-2.25@10 LE	----		----	----	----	Normal
26	7	M	1.50	+2.75/-0.50@170 RE +3.25/-2.25@10 LE	----		FRMD7	----	----	Normal
31	21	F	0.20	----	----	Latent nystagmus	Non-FRMD7	Unreliable	Normal	Normal
33	11	F	0.40	+4.00 RE +4.00 LE	----		----	No	Normal	Normal
35	67	M	0.20	+5.00/-0.50@180 RE +6.00/-0.75@180 LE	----		----	No	Normal	Normal
36	75	M	0.20	+1.00 RE +2.00 LE	N		Non-FRMD7	No	Normal	Normal
37	41	M	0.175	+6.0/-2.50@160 RE +5.0/-1.0@180 LE	----	Latent nystagmus	----	----	----	Normal
42	44	M	0.50	----	N		----	----	----	Normal
44	36	M	0.175	----	N	Latent nystagmus	----	No	Normal	Normal
46	26	F	0.00	+0.50 RE +1.00 LE	N	Latent nystagmus	----	Unreliable	Normal	Normal

Clinical characteristics of patients with normal macular morphology

ID = identification; F = female; M = male; BCVA = best corrected visual acuity; BE = both eyes; TID = transillumination defects; Y = yes; N = no; VEP = visual evoked potential; ERG = electroretinogram; RE = right eye; LE = left eye

Δ *All patients where nystagmus is not described had conjugate horizontal nystagmus typical for IIN*

---- *indicates not assessed or could not be performed*

Appendix 3

Supplementary Data for Chapter 6

Marginal Effects of Achromatopsia on Retinal Layer Thickness Measurements

Post-hoc estimates of the marginal effects of achromatopsia on retinal layer thickness measurements were calculated for: (A) overall retinal thickness (RT), (B) inner retinal layers (IRLs) and (C) outer retinal layers (ORLs). This analysis gives an estimate of the effect a diagnosis of achromatopsia has on retinal layer thickness measurements in comparison to controls, while controlling for the other covariates (age, eye and the interaction between diagnosis and age) in the model. The estimated marginal effects tables and margins plots are provided below for the fovea, parafovea and perifovea at 13 time points:

Age Group	Age (months)
1	6
2	12
3	18
4	24
5	30
6	36
7	42
8	48
9	54
10	60
11	66
12	72
13	80

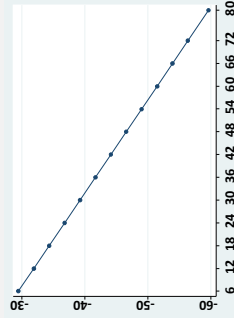
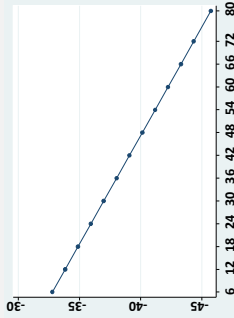
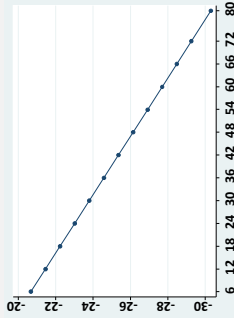
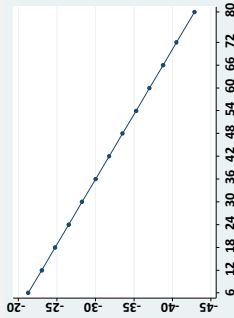
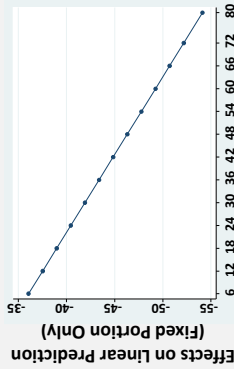
The parafoveal and perifoveal measurements were taken at 500 μm and 1500 μm nasal and temporal to the central fovea, respectively. This legend applies to all subsequent figures and tables in this appendix.

Std. Err. = standard error; C.I. = confidence interval

Average Marginal Effects of Achromatopsia on Retinal Layer Thickness Measurements

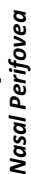
1500 μm Nasal Perifovea 500 μm Nasal Parafovea Fovea 500 μm Temporal Parafovea 1500 μm Temporal Perifovea

A. Retinal Thickness



Age Group	dy/dx (Std.Err.)	z (p > z)	95% C.I.	Age Group	dy/dx (Std.Err.)	z (p > z)	95% C.I.	Age Group	dy/dx (Std.Err.)	z (p > z)	95% C.I.	Age Group	dy/dx (Std.Err.)	z (p > z)	95% C.I.
1	-36.05 (6.91)	-5.22 (p < 0.0001)	-49.59 to -22.51	1	-20.67 (8.64)	-2.39 (p < 0.05)	-37.61 to -3.73	1	-32.77 (8.95)	-3.66 (p < 0.0001)	-50.30 to -15.24	1	-29.46 (8.78)	-3.35 (p < 0.01)	-46.67 to -12.24
2	-37.52 (6.50)	-5.77 (p < 0.0001)	-50.26 to -24.77	2	-23.02 (9.62)	-2.39 (p < 0.05)	-41.88 to -4.17	2	-33.82 (8.33)	-4.06 (p < 0.0001)	-50.15 to -17.50	2	-31.90 (8.22)	-3.88 (p < 0.0001)	-48.01 to -15.79
3	-38.98 (6.15)	-6.34 (p < 0.0001)	-51.04 to -26.93	3	-24.77 (8.94)	-2.77 (p < 0.01)	-42.30 to -7.24	3	-34.88 (7.79)	-4.48 (p < 0.0001)	-50.14 to -19.61	3	-34.35 (7.71)	-4.45 (p < 0.0001)	-49.46 to -19.23
4	-40.45 (5.86)	-6.9 (p < 0.0001)	-51.93 to -28.97	4	-26.52 (8.37)	-3.17 (p < 0.01)	-42.94 to -10.11	4	-35.93 (7.33)	-4.9 (p < 0.0001)	-50.29 to -21.56	4	-36.79 (7.28)	-5.06 (p < 0.0001)	-51.05 to -22.53
5	-41.91 (5.64)	-7.44 (p < 0.0001)	-52.96 to -30.86	5	-28.27 (7.93)	-3.56 (p < 0.0001)	-43.82 to -12.73	5	-36.98 (6.98)	-5.3 (p < 0.0001)	-50.66 to -23.30	5	-39.24 (6.92)	-5.67 (p < 0.0001)	-52.80 to -25.67
6	-43.38 (5.49)	-7.89 (p < 0.0001)	-54.15 to -32.61	6	-30.03 (7.64)	-3.93 (p < 0.0001)	-45.00 to -15.05	6	-38.03 (6.75)	-5.64 (p < 0.0001)	-51.26 to -24.80	6	-41.68 (6.66)	-6.26 (p < 0.0001)	-54.73 to -28.63
7	-44.85 (5.44)	-8.25 (p < 0.0001)	-55.50 to -34.19	7	-31.78 (7.52)	-4.23 (p < 0.0001)	-46.51 to -17.05	7	-39.08 (6.65)	-5.87 (p < 0.0001)	-52.12 to -26.04	7	-44.13 (6.50)	-6.79 (p < 0.0001)	-56.87 to -31.38
8	-46.31 (5.47)	-8.47 (p < 0.0001)	-57.03 to -35.59	8	-33.53 (7.57)	-4.43 (p < 0.0001)	-48.36 to -18.70	8	-40.14 (6.70)	-5.99 (p < 0.0001)	-53.26 to -27.01	8	-46.57 (6.46)	-7.21 (p < 0.0001)	-59.23 to -33.91
9	-47.78 (5.59)	-8.55 (p < 0.0001)	-58.73 to -36.82	9	-35.28 (7.79)	-4.53 (p < 0.0001)	-50.55 to -20.01	9	-41.19 (6.88)	-5.99 (p < 0.0001)	-54.67 to -27.71	9	-49.02 (6.53)	-7.5 (p < 0.0001)	-61.82 to -36.21
10	-49.24 (5.79)	-8.51 (p < 0.0001)	-60.59 to -37.90	10	-37.03 (8.17)	-4.53 (p < 0.0001)	-53.05 to -21.01	10	-42.24 (7.18)	-5.88 (p < 0.0001)	-56.32 to -28.16	10	-51.46 (6.72)	-7.66 (p < 0.0001)	-64.63 to -38.29
11	-50.71 (6.06)	-8.37 (p < 0.0001)	-62.59 to -38.83	11	-38.78 (8.69)	-4.46 (p < 0.0001)	-55.82 to -21.74	11	-43.29 (7.60)	-5.69 (p < 0.0001)	-58.19 to -28.39	11	-53.91 (7.01)	-7.69 (p < 0.0001)	-67.64 to -40.17
12	-52.17 (6.40)	-8.16 (p < 0.0001)	-64.71 to -39.64	12	-40.53 (9.33)	-4.35 (p < 0.0001)	-58.81 to -22.25	12	-44.35 (8.11)	-5.46 (p < 0.0001)	-60.25 to -28.44	12	-56.35 (7.39)	-7.63 (p < 0.0001)	-70.83 to -41.87
13	-54.13 (6.93)	-7.81 (p < 0.0001)	-67.71 to -40.55	13	-42.87 (10.31)	-4.16 (p < 0.0001)	-63.08 to -22.65	13	-45.75 (8.92)	-5.13 (p < 0.0001)	-63.22 to -28.27	13	-59.61 (8.01)	-7.44 (p < 0.0001)	-75.31 to -43.91

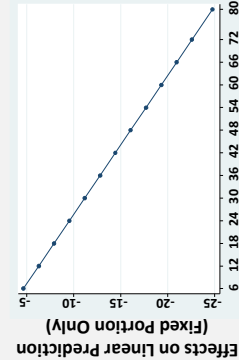
1500 μm
Temporal Perifovea



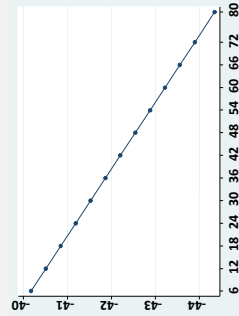
	Age Group	dY/dX (Std.Err.)	z (P > z)	95% C.I.	Age Group	dY/dX (Std.Err.)	z (P > z)	95% C.I.	Age Group	dY/dX (Std.Err.)	z (P > z)	95% C.I.
1	1	-34.87 (7.42)	-4.7 (P < 0.0001)	-49.41 to -20.32	1	17.07 (11.32)	1.51 (P > 0.05)	-5.11 to 39.25	1	54.43 (5.27)	10.34 (P < 0.0001)	44.11 to 64.75
	2	-34.19 (6.73)	-5.08 (P < 0.0001)	-47.39 to -20.99	2	16.12 (10.27)	1.57 (P > 0.05)	-4.01 to 36.24	2	53.00 (4.77)	11.1 (P < 0.0001)	43.65 to 62.36
	3	-33.51 (6.11)	-5.49 (P < 0.0001)	-45.48 to -21.54	3	15.17 (9.31)	1.63 (P > 0.05)	-3.08 to 33.41	3	51.57 (4.32)	11.93 (P < 0.0001)	43.10 to 60.05
	4	-32.83 (5.56)	-5.91 (P < 0.0001)	-43.72 to -21.94	4	14.21 (8.47)	1.68 (P > 0.05)	-2.39 to 30.82	4	50.14 (3.93)	12.77 (P < 0.0001)	42.45 to 57.84
	5	-32.15 (5.11)	-6.29 (P < 0.0001)	-42.16 to -22.14	5	13.26 (7.80)	1.7 (P > 0.05)	-2.02 to 28.54	5	48.72 (3.61)	13.5 (P < 0.0001)	41.65 to 55.79
	6	-31.47 (4.79)	-6.57 (P < 0.0001)	-40.86 to -22.08	6	12.31 (7.32)	1.68 (P > 0.05)	-2.05 to 26.67	6	47.29 (3.38)	13.98 (P < 0.0001)	40.65 to 53.92
	7	-30.79 (4.63)	-6.64 (P < 0.0001)	-39.87 to -21.71	7	11.36 (7.10)	1.6 (P > 0.05)	-2.55 to 25.27	7	45.86 (3.27)	14 (P < 0.0001)	39.44 to 52.27
	8	-30.11 (4.65)	-6.47 (P < 0.0001)	-39.22 to -20.99	8	10.41 (7.14)	1.46 (P > 0.05)	-3.59 to 24.40	8	44.43 (3.29)	13.49 (P < 0.0001)	37.97 to 50.88
	9	-29.43 (4.84)	-6.08 (P < 0.0001)	-38.91 to -19.94	9	9.45 (7.45)	1.27 (P > 0.05)	-5.14 to 24.05	9	43.00 (3.44)	12.51 (P < 0.0001)	36.26 to 49.73
	10	-28.75 (5.18)	-5.55 (P < 0.0001)	-38.90 to -18.59	10	8.50 (7.99)	1.06 (P > 0.05)	-7.15 to 24.16	10	41.57 (3.69)	11.26 (P < 0.0001)	34.33 to 48.80
	11	-28.07 (5.65)	-4.97 (P < 0.0001)	-39.14 to -16.99	11	7.55 (8.72)	0.87 (P > 0.05)	-9.54 to 24.64	11	40.14 (3.81)	9.95 (P < 0.0001)	32.23 to 48.05
	12	-27.39 (6.22)	-4.4 (P < 0.0001)	-39.57 to -15.20	12	6.60 (9.60)	0.69 (P > 0.05)	-12.21 to 25.41	12	38.71 (4.45)	8.7 (P < 0.0001)	29.99 to 47.43
	13	-26.48 (7.08)	-3.74 (P < 0.0001)	-40.37 to -12.60	13	5.33 (10.93)	0.49 (P > 0.05)	-16.10 to 26.76	13	36.80 (5.08)	7.25 (P < 0.0001)	26.86 to 46.75

Average Marginal Effects of Achromatopsia on Retinal Layer Thickness Measurements

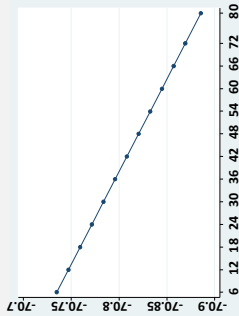
1500 μm
Nasal Perifovea



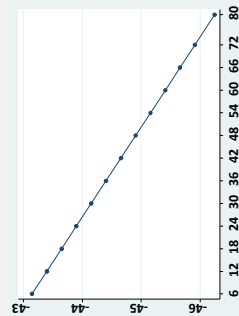
500 μm
Nasal Parafovea



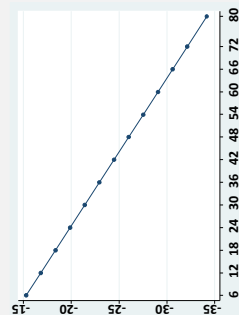
Fovea



500 μm
Temporal Parafovea



1500 μm
Temporal Perifovea



C. Outer Retinal Layers

Effects on Linear Prediction
(Fixed Portion Only)

Age Group	dy/dx (Std.Err.)	z (p > z)	95% C.I.	Age Group	dy/dx (Std.Err.)	z (p > z)	95% C.I.	Age Group	dy/dx (Std.Err.)	z (p > z)	95% C.I.	Age Group	dy/dx (Std.Err.)	z (p > z)	95% C.I.
1	-4.66 (5.60)	-0.83 (p > 0.05)	-15.63 to 6.31	1	-40.17 (8.94)	-4.49 (p < 0.0001)	-57.69 to -22.65	1	-70.73 (7.30)	-9.69 (p < 0.0001)	-85.04 to -56.43	1	-43.14 (8.35)	-5.17 (p < 0.0001)	-59.51 to -26.78
2	-6.29 (5.07)	-1.24 (p > 0.05)	-16.22 to 3.65	2	-40.51 (8.10)	-5 (p < 0.0001)	-56.38 to -24.64	2	-70.75 (6.69)	-10.57 (p < 0.0001)	-83.86 to -57.63	2	-43.40 (7.57)	-5.73 (p < 0.0001)	-58.24 to -28.55
3	-7.92 (4.58)	-1.73 (p > 0.05)	-16.90 to 1.06	3	-40.85 (7.32)	-5.58 (p < 0.0001)	-55.20 to -26.49	3	-70.76 (6.14)	-11.52 (p < 0.0001)	-82.80 to -58.72	3	-43.65 (6.87)	-6.36 (p < 0.0001)	-57.10 to -30.19
4	-9.55 (4.15)	-2.3 (p < 0.05)	-17.69 to -1.41	4	-41.19 (6.65)	-6.2 (p < 0.0001)	-54.21 to -28.16	4	-70.77 (5.67)	-12.48 (p < 0.0001)	-81.89 to -59.66	4	-43.90 (6.25)	-7.03 (p < 0.0001)	-56.14 to -31.66
5	-11.18 (3.80)	-2.94 (p < 0.01)	-18.63 to -3.73	5	-41.53 (6.10)	-6.81 (p < 0.0001)	-53.47 to -29.58	5	-70.78 (5.30)	-13.36 (p < 0.0001)	-81.17 to -60.40	5	-44.15 (5.74)	-7.69 (p < 0.0001)	-55.41 to -32.89
6	-12.81 (3.55)	-3.61 (p < 0.0001)	-19.76 to -5.85	6	-41.86 (5.71)	-7.33 (p < 0.0001)	-53.05 to -30.68	6	-70.80 (5.05)	-14.03 (p < 0.0001)	-80.68 to -60.91	6	-44.40 (5.39)	-8.23 (p < 0.0001)	-54.97 to -33.83
7	-14.44 (3.42)	-4.22 (p < 0.0001)	-21.14 to -7.74	7	-42.20 (5.52)	-7.65 (p < 0.0001)	-53.02 to -31.38	7	-70.81 (4.93)	-14.36 (p < 0.0001)	-80.47 to -61.14	7	-44.65 (5.22)	-8.55 (p < 0.0001)	-54.89 to -34.42
8	-16.07 (3.42)	-4.7 (p < 0.0001)	-22.77 to -9.36	8	-42.54 (5.55)	-7.67 (p < 0.0001)	-53.42 to -31.66	8	-70.82 (4.96)	-14.27 (p < 0.0001)	-80.55 to -61.09	8	-44.91 (5.25)	-8.55 (p < 0.0001)	-55.20 to -34.61
9	-17.70 (3.56)	-4.97 (p < 0.0001)	-24.68 to -10.72	9	-42.88 (5.79)	-7.4 (p < 0.0001)	-54.24 to -31.52	9	-70.83 (5.14)	-13.78 (p < 0.0001)	-80.91 to -60.75	9	-45.16 (5.48)	-8.24 (p < 0.0001)	-55.90 to -34.42
10	-19.33 (3.82)	-5.06 (p < 0.0001)	-26.81 to -11.84	10	-43.22 (6.23)	-6.94 (p < 0.0001)	-55.43 to -31.01	10	-70.84 (5.45)	-13 (p < 0.0001)	-81.53 to -60.16	10	-45.41 (5.88)	-7.72 (p < 0.0001)	-56.93 to -33.89
11	-20.96 (4.18)	-5.02 (p < 0.0001)	-29.14 to -12.77	11	-43.56 (6.82)	-6.39 (p < 0.0001)	-56.92 to -30.19	11	-70.86 (5.87)	-12.07 (p < 0.0001)	-82.36 to -59.35	11	-45.66 (6.42)	-7.11 (p < 0.0001)	-58.24 to -33.08
12	-22.59 (4.61)	-4.9 (p < 0.0001)	-31.62 to -13.55	12	-43.90 (7.52)	-5.83 (p < 0.0001)	-58.64 to -29.15	12	-70.87 (6.38)	-11.11 (p < 0.0001)	-83.37 to -58.37	12	-45.91 (7.07)	-6.49 (p < 0.0001)	-59.77 to -32.06
13	-24.76 (5.27)	-4.7 (p < 0.0001)	-35.09 to -14.43	13	-44.35 (8.60)	-5.16 (p < 0.0001)	-61.20 to -27.50	13	-70.89 (7.16)	-9.9 (p < 0.0001)	-84.92 to -56.85	13	-46.25 (8.06)	-5.74 (p < 0.0001)	-62.04 to -30.45

Appendix 4

Supplementary Data for Chapter 7

Table 1: Demographics

Race	Number (%)
Caucasian	41 (93.2)
Asian	1 (2.3)
Afro-Caribbean	1 (2.3)
Other	1 (2.3)
Total	44 (100)
Gender	Number (%)
Male	30 (68.2)
Female	14 (31.8)
Total	44 (100)
Eyes Scanned	Number (%)
Right	113 (51.6)
Left	106 (48.4)
Total	219 (100)

Summary of the demographic characteristics of the participants in this study

The participants were classified by ethnicity into one of four categories: Caucasian, Asian, Afro-Caribbean and other (for participants not fitting into any one of the aforementioned categories).

Table 2: Clinical Characteristics

			BCVA (LogMAR)		Refraction			
ID	Sex	Age at Each Visit (months)	Right Eye	Left Eye	Right Eye	Left Eye	TID	Cutaneous Hypo- Pigmentation
1	M	29.1	1.2	2.1	+1.20/-1.50@33	+8.50/-1.25@173	Y	Y
2	F	36.2	0.4	0.4	+0.25/-0.50@180	+0.25/-0.50@180	Y	Y
		40.4	0.45	0.4	+0.50/-2.00@10	+0.50/-1.00@180		
		53.3	0.775	0.7	+0.00/-2.25@8	+0.75/-1.25@180		
3	F	13.2	0.4	0.4	+1.00/-2.50@180	+1.00/-2.50@180	Y	Y
		13.3	0.4	0.4	+1.00/-2.50@180	+1.00/-2.50@180		
		31.8	0.75	0.75	-0.75/-1.25@180	-0.50/-1.00@180		
		36.4	0.75	0.75	-0.75/-1.25@180	-0.50/-1.00@180		
4	F	56.2	0.75	0.725	+7.00/-3.00@180	+8.50/-2.50@180	Y	Y
		63.8	0.65	0.65	+7.25/-2.50@180	+8.25/-2.00@180		
		75.6	0.85	0.775	+7.00/-2.00@180	+8.00/-1.75@180		
5	M	36.7	0.7	0.7	+0.00/-2.50@27	-1.00/-1.00@27	N	N
		45.5	0.575	0.55	-0.50/-3.00@30	-1.75/-2.00@175		
6	M	50.5	0.6	0.45	-2.50/-2.25@180	-2.50/-2.25@180	Y	Y
		53.5	0.4	0.35	-2.50/-2.25@180	-2.50/-2.25@180		
		63.2	0.55	0.55	-2.75/-2.50@5	-2.25/-1.75@175		
		69.2	0.525	0.425	-2.00/+2.76@180	-2.00/+1.50@180		
7	F	15.9	0.6	0.6	+1.00/-1.00@10	+1.00/-1.25@170	Y	Y
		26.2	---	---	+1.25/-1.00@5	+1.75/-1.50@170		
8	F	86.6	0.2	0.2	Plano	-0.50	N	N
9	F	8.7	0.8	0.8	+0.25/+0.50@90	+0.25/+0.50@90	Y	Y
		11.4	1.0	1.0	+0.25	+0.25		
		14.4	0.7	0.7	+0.25/+0.50@90	+0.25		
		19.0	---	---	+4.00	+4.00		
		23.9	---	---	+4.00	+4.00		
		28.93	0.8	0.8	+4.50	+4.50		
10	M	4.5	1.6	1.6	No significant Prescription	No significant Prescription	Y	Y
		12.4	0.9	0.9				
		19.8	1.0	1.0				
11	M	46.1	0.5	0.6	+0.75/+0.75@170	+0.75/+0.75@75	Y	Y
		63.1	0.825	0.8	+1.75/-0.50@10	+1.75/-0.50@170		

12	M	81.3	0.35	0.3	+6.25/-2.75@175	+7.00/-3.00@180	N	Y
		86.4	0.325	0.325	+6.25/-2.75@175	+7.00/-3.00@180		
13	M	42.9	1.0	0.95	+0.00/-3.25@16	+0.25/-2.75@167	Y	Y
		48.9	0.9	1.0	+0.00/-3.25@16	+0.00/-2.75@167		
		54.9	0.75	0.75	+0.00/-3.25@16	+0.00/-2.75@167		
14	F	45.0	0.85	0.75	+4.00	+4.00	Y	Y
		47.5	0.7	0.75	+6.00/-0.50@155	+5.50		
		62.2	0.65	0.6	+6.50/-0.75@150	+5.75		
15	M	49.8	1.0	1.0	+5.50/-3.00@5	+6.50/-3.50@100	Y	Y
		55.7	1.0	1.0	+5.50/-3.00@5	+6.50/-3.50@180		
		61.7	1.0	1.0	+6.00/-3.50@5	+6.00/-3.50@175		
		67.7	1.0	1.0	+6.00/-3.50@5	+6.00/-3.50@175		
16	M	26.8	0.9	0.9	No significant Prescription	No significant Prescription	Y	Y
17	M	32.0	0.6	0.5	+3.00/+1.00@90	+3.00/+1.00@90	Y	Y
		37.1	0.8	0.7	+3.00/+1.00@90	+3.00/+1.00@90		
		49.7	0.7	0.65	+5.75/-1.75@51	+4.50/-1.25@177		
18	M	5.5	---	---	+2.00/+0.50@90	+2.00/+0.50@90	Y	Y
		8.2	1.0	1.0	+2.00/+0.50@90	+2.00/+0.50@90		
19	M	57.8	0.7	0.7	No significant Prescription	No significant Prescription	Y	Y
20	M	45.9	0.5	0.5	1.50/-0.50@180	1.50/-0.50@180	N	Y
		50.5	0.375	0.3	1.50/-0.50@180	1.50/-0.50@180		
21	F	60.2	0.5	0.3	+0.25/+2.00@90	+0.75/+1.75@96	Y	N
22	M	59.2		0.75		+4.75/-0.50@5	Y	Y
23	M	0.92	---	---	+1.50	+1.50	Y	Y
		1.1	---	---	+1.50	+1.50		
		1.6	---	---	+1.50	+1.50		
		2.0	---	---	+1.50	+1.50		
		10.5	1	1	+0.50	+0.50		
24	F	40.4	0.6	0.6	+2.00/-1.50@180	+0.00/-0.50@180	N	N
		53.0	0.35	0.35	+2.00/-1.50@180	+0.00/-0.50@180		
		58.8	0.375	0.4	+2.25/-2.50@170	+0.25/-1.75@180		
25	F	11.6	---	---	No significant Prescription	No significant Prescription	Y	Y
		14.4	1.0	1.0	No significant Prescription	No significant Prescription		
26	M	14.7	0.5	0.5	No significant Prescription	No significant Prescription	Y	Y
		21.4	---	---				
		31.4	---	---				

		37.7	0.5	0.5				
27	M	9.2	0.7	0.7	+3.00	+3.00	Y	Y
		11.1	0.9	0.9	3.00	3.00		
		17.1	0.6	0.6	3.00	3.00		
28	M	12.7	---	---	+6.50/+1.00@90	+6.50/+1.00@90	Y	Y
		21.9	0.7	0.7	+7.50/-0.50@180	+7.00		
29	M	54.1	0.5	0.325	+5.50	+6.00	Y	N
30	M	10.2	1.0	1.0	No significant Prescription	No significant Prescription	N	N
31	M	71.0	0.275	0.2	+3.50/-2.00@25	+4.50/-2.00@10	Y	Y
32	M	80.1	0.55	0.55	+1.00/+1.50@100	+0.25/+2.75@85	Y	N
		83.1	0.525	0.575	+1.00/+1.50@100	+0.25/+2.75@85		
33	M	54.5	0.4	1.75	+4.50/-1.50@20	+6.00/-2.00@160	Y	N
		75.8	0.625	0.625	+4.50/-1.50@20	+6.00/-2.00@160		
34	M	37.0	1.2	1.0	-1.75	-1.75	Y	Y
35	M	23.9	---	---	+3.00/-4.00@15	+3.50/-4.00@162	Y	Y
		30.2	---	---	+3.00/-4.00@15	+3.50/-4.00@162		
		36.8	0.95	1.05	+2.50/-3.40@30	+3.00/-3.50@160		
36	F	11.3	---	---	+7.00	+7.00	Y	Y
37*	M	48.1	0.85	0.8	-0.50/+0.75@180	-0.50/+1.00@180	N	Y
		59.4	0.65	0.75	-0.50/+1.00@130	-1.50/+0.75@110		
38	F	43.6	0.7	0.8	+4.00/-3.00@180	+4.50/-3.00@180	Y	Y
39	M	54.2	0.9	0.9	-1.00/-1.50@9	-1.00/-1.50@0	N	N
		58.0	0.45	0.45	-1.00/-3.00@175	-1.25/-2.00@5		
		62.6	0.5	0.5	-1.00/-3.00@175	-1.25/-2.00@5		
40	M	37.0	1.3	1.3	No significant Prescription	No significant Prescription	Y	N
41	F	37.9	1.2	1.2	+2.50/-4.25@179	+3.00/-4.25@2	Y	Y
42	F	6.6	1.3	1.3	+1.50/+1.50@90	+1.50/+1.50@90	Y	Y
43	M	16.2	1.6	1.6	-0.50/+0.50+180	-0.50/+0.50+180	N	N
		24.5	0.6	0.6	-0.50/+0.50+180	-0.50/+0.50+180		
44*	M	48.1	0.126	0.1	-0.25	-0.25	N	Y
		59.4	0.1	0.1	-0.25	-0.25		
45	M	58.55	0.3		+2.00+1.75@90		Y	N
		61.51	0.6		+2.00+1.75@90			
		73.28		0.525		+2.00+1.75@90		
46		24.8	0.9	1.0	+4.00/-6.00@180	+4.00/-6.00@180		
		28.0	1.5	1.5	+4.00/-6.00@180	+4.00/-6.00@180		

40	M	35.6	1.1	1.0	+2.50/-6.00@5	+4.00/-6.00@180	Y	Y
		39.7	1.2	1.2	+3.00/-6.00@180	+4.00/-6.00@180		
47	F	72.3	0.4	0.45	+2.25	+2.50/-0.75@100	Y	Y
		83.6	0.5	0.5	+2.25	+2.75/-0.25@45		
48	M	36.3	0.7	0.7	+4.25/+1.50@85	+5.00/+1.00@90	Y	Y
49	F	4.64	1.5	1.5	+0.25/-1.0@180	+0.25/-1.0@180	Y	Y
		7.63	---	---		+0.25/-1.0@180		
		16.87		0.7		+0.25/-1.0@180		
50	F	11.2	---	---	+4.50/+1.50@90	+4.50/+1.00@90	N	Y
		19.2	0.3	0.3	+7.75/-1.75@180	+7.75/-1.50@180		
		25.4	0.9	0.9	+7.00/-1.75@10	+7.50/-1.75@10		
51	F	83.4	0.6	0.6	+5.50/-2.50@170	+5.25/-2.50@10	Y	Y
52	M	66.5	0.6	0.675	+3.75/-1.00@4	+4.00/-1.00@178	Y	Y
		76.9	0.65	0.5	+3.50/-1.00@175	+4.00/-1.00@175		
53	M	33.4	0.9	---	+1.50	+1.50	Y	N
		38.5	---	0.5	+1.50	+1.50		
		47.3	0.35	0.45	+1.50	+1.50		
54	M	59.7	0.45	0.65	+5.00/-3.00@2	+5.50/-2.50@5	Y	Y
		62.7	0.575	0.7	+5.00/-3.00@2	+5.50/-2.50@5		

ID = identification number; M = male; F = female; BCVA = best corrected visual acuity; LogMAR = Logarithm of the Minimum Angle of Resolution; TID = iris transillumination defects; N = no; Y = yes;

* *indicate sibling pairs*

--- *indicates not assessed or could not be performed*

Table 3: Summary of Foveal Hypoplasia Grading, VEP and Genetic Testing

			Foveal Hypoplasia Grade*			
ID	Sex	Age at Each Visit (months)	Right	Left	VEP	Genetic Testing
1	M	29.1	2	2	Crossed Asymmetry	Awaited
2	F	36.2	1	1	Crossed Asymmetry	<i>OCA1</i> Negative
		40.4	1	1		
		53.3	1	1		
3	F	13.2	1	1	Normal	<i>OCA1</i> Negative
		13.3	1	1		
		31.8	1	1		
		36.4	1	1		
4	F	56.2	1	1	Crossed Asymmetry	<i>OCA1</i> Positive LOC 1: 89017973 C>T LOC 2: 88911734 C>A
		63.8	1	1		
		75.6	1	1		
5	M	36.7	0	0	Crossed Asymmetry	Awaited
		45.5	0	0		
6	M	50.5	1	1	Normal	Awaited
		53.5	1	1		
		63.2	1	1		
		69.2	1	1		
7	F	15.9	1	1	Normal	Awaited
		26.2	1	1		
8	F	86.6	1	1	Awaited	<i>OCA1</i> Negative
9	F	8.7	3	3	Crossed Asymmetry	<i>OCA1</i> Negative
		11.4	3	3		
		14.4	3	3		
		19.0	3	3		
		23.9	3	3		
		28.93	3	3		
10	M	4.5	0	0	Crossed Asymmetry	Awaited
		12.4	0	0		

		19.8	0	0		
11	M	46.1	3	3	Normal	Awaited
		63.1	3	3		
12	M	81.3	1	1	Normal	OCAI Negative
		86.4	1	1		
13	M	42.9	2	2	---	Awaited
		48.9	2	2		
		54.9	2	2		
14	F	45.0	1	1	Normal	Awaited
		47.5	1	1		
		62.2	1	1		
15	M	49.8	3	3	Crossed Asymmetry	Awaited
		55.7	3	3		
		61.7	3	3		
		67.7	3	3		
16	M	26.8	1	1	Crossed Asymmetry	OCAI Positive 88961072 C>A (HOM)
17	M	32.0	1	1	Crossed Asymmetry	Awaited
		37.1	1	1		
		49.7	1	1		
18	M	5.5	1	1	Crossed Asymmetry	Awaited
		8.2	1	1		
19	M	57.8	3	3	Crossed Asymmetry	Awaited
20	M	45.9	1	1	Unreliable	OCAI Negative
		50.5	1	1		
21	F	60.2	1	1	---	Awaited
22	M	59.2		3	---	Awaited
23	M	0.92	4	4	Crossed Asymmetry	Awaited
		1.1	4	4		
		1.6	4	4		
		2.0	4	4		
		10.5	4	4		
24	F	40.4	1	1	Unreliable	Awaited
		53.0	1	1		
		58.8	1	1		
25	F	11.6	3	3	Crossed	Awaited

		14.4	3	3	Asymmetry	
26	M	14.7	1	1	Unreliable	<i>OCAI</i> Negative
		21.4	1	1		
		31.4	1	1		
		37.7	1	1		
27	M	9.2	1	1	Crossed Asymmetry	Awaited
		11.1	1	1		
		17.1	1	1		
28	M	12.7	4	4	Crossed Asymmetry	<i>OCAI</i> Negative
		21.9	4	4		
29	M	54.1	1	1	Normal	Awaited
30	M	10.2	3	3	Crossed Asymmetry	Awaited
31	M	71.0	2	2	Crossed Asymmetry	<i>OCAI</i> Negative
32	M	80.1	1	1	Crossed Asymmetry	Awaited
		83.1	1	1		
33	M	54.5	1	1	Crossed Asymmetry	<i>OCAI</i> Negative
		75.8	1	1		
34	M	37.0	4	4	---	Awaited
35	M	23.9	4	4	Unreliable	Awaited
		30.2	4	4		
		36.8	4	4		
36	F	11.3	1	1	---	Awaited
37a	M	48.1	1	1	Crossed Asymmetry	Awaited
		59.4	1	1		
38	F	43.6	2	2	Crossed Asymmetry	Awaited
39	M	54.2	1	1	Normal	Awaited
		58.0	1	1		
		62.6	1	1		
40	M	37.0	4	4	Unreliable	Awaited
41	F	37.9	4	4	---	Awaited
42	F	6.6	4	4	Crossed Asymmetry	Awaited
43	M	16.2	1	1	Crossed Asymmetry	Awaited
		24.5	1	1		
44a	M	48.1	1	1	Normal	Awaited

		59.4	1	1		
45	M	58.55	1		Increased Latency	Awaited
		61.51	1			
		73.28		1		
46	M	24.8	4	4	Crossed Asymmetry	<i>OCA1</i> Positive 88924382 C>T (HOM)
		28.0	4	4		
		35.6	4	4		
		39.7	4	4		
47	F	72.3	1	1	Crossed Asymmetry	<i>OCA1</i> Negative
		83.6	1	1		
48	M	36.3	4	4	Crossed Asymmetry	<i>OCA1</i> Negative
49	F	4.64	1	1	Crossed Asymmetry	Awaited
		7.63		1		
		16.87		1		
50	F	11.2	1	1	Unreliable	Awaited
		19.2	1	1		
		25.4	1	1		
51	F	83.4	1	1	Crossed Asymmetry	Awaited
52	M	66.5	1	1	Unreliable	Awaited
		76.9	1	1		
53	M	33.4	1	1	Normal	Awaited
		38.5	1	1		
		47.3	1	1		
54	M	59.7	2	2	Crossed Asymmetry	Awaited
		62.7	2	2		

* *Foveal hypoplasia was graded based on the classification system described by Thomas et al. A grade of 0 indicates no evidence of foveal hypoplasia on optical coherence tomography examination*

ID = identification number; M = male; F = female; VEP = visual evoked potential; OCA1 = oculocutaneous albinism 1 gene; LOC = locus

a indicate sibling pairs

Marginal Effects of Albinism on Retinal Layer Thickness Measurements

Post-hoc estimates of the average marginal effects of albinism on retinal layer thickness measurements were calculated for: (A) overall retinal thickness (RT), (B) inner retinal layers (IRLs) and (C) outer retinal layers (ORLs). This analysis gives an estimate of the effect a diagnosis of albinism has on retinal layer thickness measurements in comparison to controls, while controlling for the other covariates (age, eye and the interaction between diagnosis and age) in the model. The estimated average marginal effects tables and margins plots are provided below for the fovea, parafovea and perifovea for 14 age groups:

Age Group	Age Range
1	37-40 weeks GA
2	41-46 weeks GA
3	47-52 weeks GA
4	3-5 PNA
5	6-8 PNA
6	9-11 PNA
7	12-17 PNA
8	18-23 PNA
9	24-29 PNA
10	30-35 PNA
11	36-47 PNA
12	48-59 PNA
13	60-71 PNA
14	72-83 PNA

The parafoveal and perifoveal measurements were taken at 500 μm and 1500 μm nasal and temporal to the central fovea, respectively. This legend applies to all subsequent figures and tables in this appendix.

GA = gestational age; PNA = postnatal age; Std. Err. = standard error; C.I. = confidence interval

Average Marginal Effects of Albinism on Retinal Layer Thickness Measurements

1500 μm
Nasal Perifovea

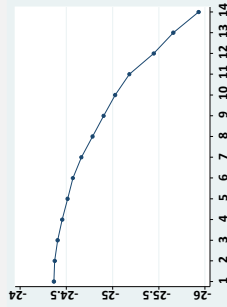
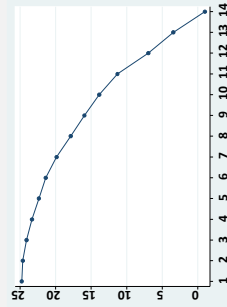
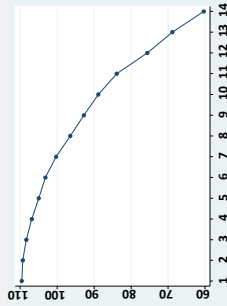
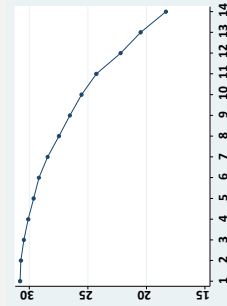
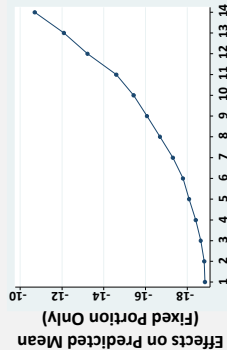
500 μm
Nasal Parafovea

Fovea

500 μm
Temporal Parafovea

1500 μm
Temporal Perifovea

A. Retinal Thickness

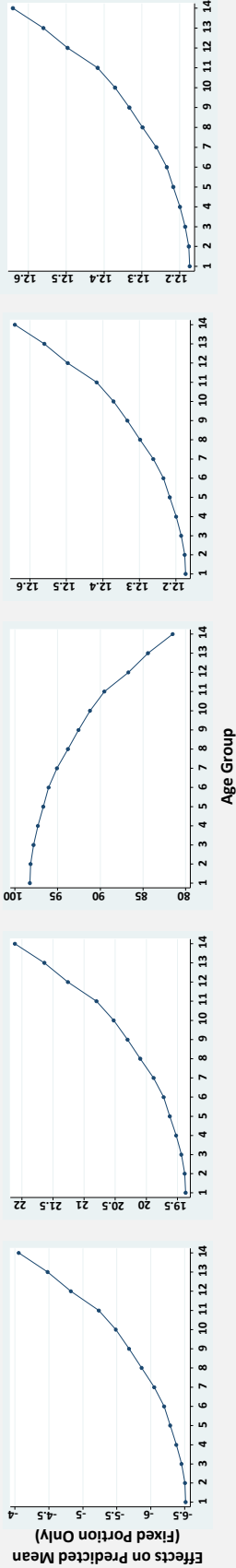


Age Group	dy/dx (Std.Err.)	z (P > z)	95% C.I.	Age Group	dy/dx (Std.Err.)	z (P > z)	95% C.I.	Age Group	dy/dx (Std.Err.)	z (P > z)	95% C.I.
1	-18.85 (3.67)	-5.14 (p<0.0001)	-26.04 to -11.66	1	24.76 (5.15)	4.81 (p<0.0001)	14.67 to 34.85	1	109.56 (5.60)	19.57 (p<0.0001)	98.59 to 120.53
2	-18.82 (3.65)	-5.15 (p<0.0001)	-25.97 to -11.66	2	24.63 (5.12)	4.81 (p<0.0001)	14.60 to 34.66	2	109.30 (5.56)	19.64 (p<0.0001)	98.39 to 120.21
3	-18.65 (3.57)	-5.23 (p<0.0001)	-25.64 to -11.65	3	24.12 (5.01)	4.81 (p<0.0001)	14.30 to 33.93	3	108.32 (5.44)	19.91 (p<0.0001)	97.66 to 118.99
4	-18.41 (3.45)	-5.33 (p<0.0001)	-25.18 to -11.64	4	23.34 (4.85)	4.82 (p<0.0001)	13.84 to 32.84	4	106.86 (5.26)	20.3 (p<0.0001)	96.54 to 117.17
5	-18.09 (3.31)	-5.47 (p<0.0001)	-24.58 to -11.60	5	22.36 (4.65)	4.81 (p<0.0001)	13.24 to 31.47	5	104.96 (5.04)	20.82 (p<0.0001)	95.08 to 114.84
6	-17.80 (3.18)	-5.59 (p<0.0001)	-24.03 to -11.56	6	21.40 (4.47)	4.79 (p<0.0001)	12.64 to 30.16	6	103.17 (4.84)	21.31 (p<0.0001)	93.68 to 112.66
7	-17.31 (2.99)	-5.79 (p<0.0001)	-23.17 to -11.45	7	19.87 (4.21)	4.72 (p<0.0001)	11.62 to 28.11	7	100.26 (4.55)	22.05 (p<0.0001)	91.35 to 109.17
8	-16.69 (2.78)	-6.00 (p<0.0001)	-22.14 to -11.24	8	17.88 (3.92)	4.56 (p<0.0001)	10.20 to 25.56	8	96.43 (4.22)	22.85 (p<0.0001)	88.16 to 104.70
9	-16.07 (2.62)	-6.13 (p<0.0001)	-21.22 to -10.93	9	15.94 (3.71)	4.3 (p<0.0001)	8.67 to 23.21	9	92.78 (3.99)	23.27 (p<0.0001)	84.97 to 100.59
10	-15.43 (2.52)	-6.12 (p<0.0001)	-20.38 to -10.49	10	13.86 (3.58)	3.88 (p<0.0001)	6.85 to 20.87	10	88.82 (3.84)	23.14 (p<0.0001)	81.29 to 96.34
11	-14.60 (2.50)	-5.83 (p<0.0001)	-19.51 to -9.70	11	11.30 (3.56)	3.17 (p<0.01)	4.32 to 18.28	11	83.89 (3.82)	21.95 (p<0.0001)	76.40 to 91.38
12	-13.23 (2.73)	-4.84 (p<0.0001)	-18.59 to -7.87	12	6.95 (3.90)	1.78 (p>0.05)	-0.70 to 14.60	12	75.62 (4.21)	17.97 (p<0.0001)	67.37 to 83.86
13	-12.09 (3.13)	-3.87 (p<0.0001)	-18.22 to -5.96	13	3.42 (4.45)	0.77 (p>0.05)	-5.30 to 12.14	13	68.82 (4.83)	14.25 (p<0.0001)	59.36 to 78.29
14	-10.69 (3.78)	-2.83 (p<0.01)	-18.09 to -3.29	14	-1.03 (5.36)	-0.19 (p>0.05)	-11.54 to 9.48	14	60.34 (5.85)	10.31 (p<0.0001)	48.86 to 71.81

Average Marginal Effects of Albinism on Retinal Layer Thickness Measurements

1500 μm Nasal Perifovea 500 μm Nasal Parafovea Fovea 500 μm Temporal Parafovea 1500 μm Temporal Perifovea

B. Inner Retinal Layers

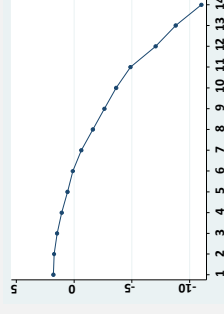
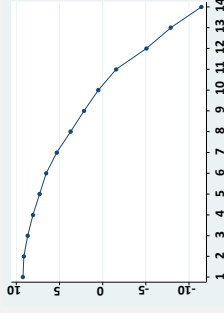
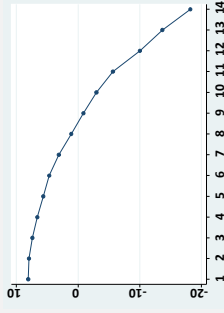
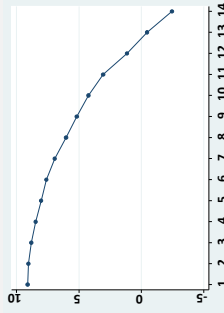
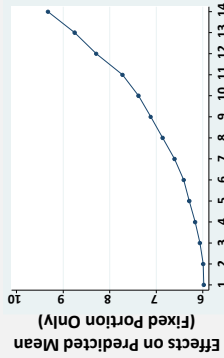


Age Group	dy/dx (Std.Err.)	z (P > z)	95% C.I.	Age Group	dy/dx (Std.Err.)	z (P > z)	95% C.I.	Age Group	dy/dx (Std.Err.)	z (P > z)	95% C.I.	Age Group	dy/dx (Std.Err.)	z (P > z)	95% C.I.
1	-24.34 (3.87)	-6.3 (p<0.0001)	-31.92 to -16.76	1	19.37 (5.43)	3.56 (p<0.0001)	8.72 to 30.02	1	98.25 (5.32)	18.46 (p<0.0001)	87.82 to 108.68	1	12.17 (4.65)	2.62 (p<0.01)	3.06 to 21.28
2	-24.32 (3.84)	-6.33 (p<0.0001)	-31.86 to -16.79	2	19.38 (5.40)	3.59 (p<0.0001)	8.79 to 29.97	2	98.16 (5.29)	18.56 (p<0.0001)	87.80 to 108.52	2	12.18 (4.62)	2.64 (p<0.01)	3.12 to 21.23
3	-24.24 (3.74)	-6.48 (p<0.0001)	-31.57 to -16.92	3	19.44 (5.27)	3.69 (p<0.0001)	9.10 to 29.77	3	97.82 (5.16)	18.97 (p<0.0001)	87.71 to 107.92	3	12.19 (4.50)	2.71 (p<0.01)	3.36 to 21.01
4	-24.13 (3.59)	-6.72 (p<0.0001)	-31.17 to -17.09	4	19.52 (5.08)	3.84 (p<0.0001)	9.56 to 29.48	4	97.32 (4.74)	19.59 (p<0.0001)	87.58 to 107.05	4	12.20 (4.34)	2.81 (p<0.01)	3.70 to 20.70
5	-23.99 (3.42)	-7.02 (p<0.0001)	-30.58 to -17.29	5	19.62 (4.86)	4.04 (p<0.0001)	10.10 to 29.15	5	96.68 (4.74)	20.41 (p<0.0001)	87.40 to 105.96	5	12.22 (4.13)	2.95 (p<0.01)	4.11 to 20.32
6	-23.85 (3.25)	-7.34 (p<0.0001)	-30.22 to -17.48	6	19.72 (4.65)	4.24 (p<0.0001)	10.60 to 28.84	6	96.07 (4.53)	21.23 (p<0.0001)	87.20 to 104.95	6	12.23 (3.94)	3.1 (p<0.01)	4.50 to 19.96
7	-23.62 (3.00)	-7.87 (p<0.0001)	-29.50 to -17.74	7	19.88 (4.34)	4.58 (p<0.0001)	11.37 to 28.40	7	95.09 (4.21)	22.58 (p<0.0001)	86.84 to 103.35	7	12.26 (3.66)	3.35 (p<0.01)	5.08 to 19.44
8	-23.33 (2.72)	-8.58 (p<0.0001)	-28.66 to -18.00	8	20.10 (3.99)	5.03 (p<0.0001)	12.27 to 27.93	8	93.79 (3.85)	24.35 (p<0.0001)	86.24 to 101.34	8	12.30 (3.35)	3.68 (p<0.0001)	5.74 to 18.86
9	-23.04 (2.50)	-9.23 (p<0.0001)	-27.93 to -18.15	9	20.30 (3.74)	5.43 (p<0.0001)	12.97 to 27.63	9	92.55 (3.59)	25.8 (p<0.0001)	85.52 to 99.58	9	12.33 (3.11)	3.97 (p<0.0001)	6.25 to 18.42
10	-22.74 (2.34)	-9.7 (p<0.0001)	-27.34 to -18.15	10	20.52 (3.57)	5.74 (p<0.0001)	13.52 to 27.53	10	91.20 (3.41)	26.75 (p<0.0001)	84.52 to 97.88	10	12.37 (2.94)	4.2 (p<0.0001)	6.60 to 18.14
11	-22.35 (2.30)	-9.73 (p<0.0001)	-26.85 to -17.85	11	20.80 (3.54)	5.87 (p<0.0001)	13.86 to 27.74	11	89.52 (3.37)	26.56 (p<0.0001)	82.91 to 96.13	11	12.42 (2.90)	4.28 (p<0.0001)	6.73 to 18.11
12	-21.71 (2.58)	-8.4 (p<0.0001)	-26.77 to -16.65	12	21.26 (3.92)	5.42 (p<0.0001)	13.57 to 28.95	12	86.72 (3.16)	23.08 (p<0.0001)	79.35 to 94.08	12	12.50 (3.24)	3.86 (p<0.0001)	6.15 to 18.85
13	-21.18 (3.08)	-6.87 (p<0.0001)	-27.22 to -15.14	13	21.64 (4.56)	4.74 (p<0.0001)	12.70 to 30.58	13	84.41 (4.40)	19.18 (p<0.0001)	75.79 to 93.04	13	12.56 (3.80)	3.31 (p<0.01)	5.12 to 20.00
14	-20.52 (3.88)	-5.29 (p<0.0001)	-28.13 to -12.91	14	22.11 (5.60)	3.95 (p<0.0001)	11.13 to 33.09	14	81.53 (5.45)	14.95 (p<0.0001)	70.84 to 92.21	14	12.64 (4.72)	2.68 (p<0.01)	3.39 to 21.89

Average Marginal Effects of Albinism on Retinal Layer Thickness Measurements

1500 μm Nasal Perifovea 500 μm Nasal Parafovea Fovea 500 μm Temporal Parafovea 1500 μm Temporal Perifovea

C. Outer Retinal Layers



Age Group	dy/dx (Std.Err.)	z ($P > z $)	95% C.I.	Age Group	dy/dx (Std.Err.)	z ($P > z $)	95% C.I.	Age Group	dy/dx (Std.Err.)	z ($P > z $)	95% C.I.	Age Group	dy/dx (Std.Err.)	z ($P > z $)	95% C.I.
1	5.98 (3.60)	1.66 ($p < 0.05$)	-1.07 to 13.03	1	9.23 (5.67)	1.63 ($p > 0.05$)	-1.87 to 20.34	1	8.09 (5.99)	1.35 ($p > 0.05$)	-3.66 to 19.83	1	9.23 (5.67)	1.63 ($p > 0.05$)	-1.87 to 20.34
2	6.00 (3.58)	1.68 ($p < 0.05$)	-1.02 to 13.01	2	9.12 (5.63)	1.62 ($p > 0.05$)	-1.92 to 20.16	2	7.95 (5.96)	1.33 ($p > 0.05$)	-3.73 to 19.63	2	9.12 (5.63)	1.62 ($p > 0.05$)	-1.92 to 20.16
3	6.07 (3.48)	1.74 ($p < 0.05$)	-0.76 to 12.89	3	8.82 (5.21)	1.69 ($p < 0.05$)	-1.38 to 19.03	3	7.41 (5.83)	1.27 ($p > 0.05$)	-4.02 to 18.85	3	8.70 (5.50)	1.58 ($p > 0.05$)	-2.08 to 19.49
4	6.17 (3.35)	1.84 ($p < 0.05$)	-0.40 to 12.73	4	8.47 (5.01)	1.69 ($p < 0.05$)	-1.35 to 18.28	4	6.62 (5.66)	1.17 ($p > 0.05$)	-4.46 to 17.71	4	8.08 (5.32)	1.52 ($p > 0.05$)	-2.34 to 18.50
5	6.29 (3.19)	1.97 ($p < 0.05$)	0.04 to 12.54	5	8.04 (4.77)	1.68 ($p < 0.05$)	-1.31 to 17.39	5	5.62 (5.44)	1.03 ($p > 0.05$)	-5.04 to 16.28	5	7.30 (5.09)	1.43 ($p > 0.05$)	-2.67 to 17.28
6	6.41 (3.04)	2.11 ($p < 0.05$)	0.46 to 12.37	6	7.62 (4.55)	1.67 ($p < 0.05$)	-1.30 to 16.54	6	4.67 (5.25)	0.89 ($p > 0.05$)	-5.61 to 14.95	6	6.54 (4.88)	1.34 ($p > 0.05$)	-3.03 to 16.10
7	6.61 (2.81)	2.35 ($p < 0.05$)	1.10 to 12.12	7	6.94 (4.22)	1.64 ($p < 0.05$)	-1.34 to 15.21	7	3.13 (4.96)	0.63 ($p > 0.05$)	-6.59 to 12.85	7	5.31 (4.57)	1.16 ($p > 0.05$)	-3.64 to 14.27
8	6.86 (2.56)	2.68 ($p < 0.01$)	1.85 to 11.88	8	6.04 (3.84)	1.57 ($p < 0.05$)	-1.50 to 13.57	8	1.08 (4.64)	0.23 ($p > 0.05$)	-8.02 to 10.18	8	3.72 (4.23)	0.88 ($p > 0.05$)	-4.57 to 12.00
9	7.12 (2.36)	3.02 ($p < 0.01$)	2.50 to 11.74	9	5.18 (3.57)	1.45 ($p < 0.05$)	-1.81 to 12.16	9	-0.87 (4.42)	-0.2 ($p > 0.05$)	-9.54 to 7.79	9	2.16 (3.97)	0.54 ($p > 0.05$)	-5.62 to 9.94
10	7.38 (2.22)	3.32 ($p < 0.01$)	3.03 to 11.74	10	4.24 (3.38)	1.26 ($p < 0.05$)	-2.38 to 10.87	10	-2.99 (4.28)	-0.7 ($p > 0.05$)	-11.38 to 5.40	10	0.49 (3.80)	0.13 ($p > 0.05$)	-6.97 to 7.94
11	7.73 (2.18)	3.55 ($p < 0.0001$)	3.46 to 11.99	11	3.07 (3.34)	0.92 ($p > 0.05$)	-3.47 to 9.62	11	-5.63 (4.27)	-1.32 ($p > 0.05$)	-14.01 to 2.74	11	-1.56 (3.77)	-0.41 ($p > 0.05$)	-8.95 to 5.83
12	8.29 (2.44)	3.4 ($p < 0.01$)	3.51 to 13.06	12	1.14 (3.75)	0.3 ($p > 0.05$)	-6.21 to 8.50	12	-10.04 (4.65)	-2.16 ($p > 0.05$)	-19.16 to -0.92	12	-5.07 (4.15)	-1.22 ($p > 0.05$)	-13.20 to 3.06
13	8.75 (2.89)	3.03 ($p < 0.01$)	3.09 to 14.41	13	-0.45 (4.43)	-0.1 ($p > 0.05$)	-9.13 to 8.23	13	-13.67 (5.27)	-2.6 ($p > 0.01$)	-23.99 to 3.35	13	-7.89 (4.77)	-1.66 ($p > 0.05$)	-17.24 to 1.45
14	9.33 (3.62)	2.58 ($p < 0.05$)	2.24 to 16.42	14	-2.45 (5.53)	-0.44 ($p > 0.05$)	-13.28 to 8.38	14	-18.20 (6.29)	-2.89 ($p < 0.01$)	-30.52 to -5.88	14	-11.46 (5.81)	-1.97 ($p > 0.05$)	-22.84 to 0.08

Bibliography

Bibliography

Bibliography

Bibliography

1. Rossi EA, Roorda A. The relationship between visual resolution and cone spacing in the human fovea. *Nat Neurosci* 2010;13:156-7.
2. Neveu MM, von dem Hagen E, Morland AB, et al. The fovea regulates symmetrical development of the visual cortex. *J Comp Neurol* 2008;506:791-800.
3. Baseler HA, Brewer AA, Sharpe LT, et al. Reorganization of human cortical maps caused by inherited photoreceptor abnormalities. *Nat Neurosci* 2002;5:364-70.
4. O'Brien KM, Schulte D, Hendrickson AE. Expression of photoreceptor-associated molecules during human fetal eye development. *Mol Vis* 2003;9:401-9.
5. Provis JM, Hendrickson AE. The foveal avascular region of developing human retina. *Arch Ophthalmol* 2008;126:507-11.
6. Curcio CA, Allen KA. Topography of ganglion cells in human retina. *J Comp Neurol* 1990;300:5-25.
7. Lee H, Sheth V, Bibi M, et al. Potential of handheld optical coherence tomography to determine cause of infantile nystagmus in children by using foveal morphology. *Ophthalmology* 2013;120:2714-24.
8. Provis JM, Diaz CM, Dreher B. Ontogeny of the primate fovea: a central issue in retinal development. *Prog Neurobiol* 1998;54:549-80.
9. Kozulin P, Natoli R, O'Brien KM, et al. Differential expression of anti-angiogenic factors and guidance genes in the developing macula. *Mol Vis* 2009;15:45-59.
10. Kozulin P, Provis JM. Differential gene expression in the developing human macula: microarray analysis using rare tissue samples. *J Ocul Biol Dis Infor* 2009;2:176-89.
11. Tombran-Tink J, Barnstable CJ. PEDF: a multifaceted neurotrophic factor. *Nat Rev Neurosci* 2003;4:628-36.
12. Levin ER, Gardner DG, Samson WK. Natriuretic peptides. *N Engl J Med* 1998;339:321-8.
13. Pedram A, Razandi M, Hu RM, et al. Vasoactive peptides modulate vascular endothelial cell growth factor production and endothelial cell proliferation and invasion. *J Biol Chem* 1997;272:17097-103.
14. Pedram A, Razandi M, Levin ER. Natriuretic peptides suppress vascular endothelial cell growth factor signaling to angiogenesis. *Endocrinology* 2001;142:1578-86.

15. Provis JM, Sandercoe T, Hendrickson AE. Astrocytes and blood vessels define the foveal rim during primate retinal development. *Invest Ophthalmol Vis Sci* 2000;41:2827-36.
16. Provis JM. Development of the primate retinal vasculature. *Prog Retin Eye Res* 2001;20:799-821.
17. Chinkers M, Garbers DL, Chang MS, et al. A membrane form of guanylate cyclase is an atrial natriuretic peptide receptor. *Nature* 1989;338:78-83.
18. Tanaka M, Hiroe M, Ito H, et al. Differential localization of atrial natriuretic peptide and skeletal alpha-actin messenger RNAs in left ventricular myocytes of patients with dilated cardiomyopathy. *J Am Coll Cardiol* 1995;26:85-92.
19. Okabe S, Hirokawa N. Actin dynamics in growth cones. *J Neurosci* 1991;11:1918-29.
20. Gelfand MV, Hong S, Gu C. Guidance from above: common cues direct distinct signaling outcomes in vascular and neural patterning. *Trends Cell Biol* 2009;19:99-110.
21. Hendrickson A, Djajadi H, Erickson A, et al. Development of the human retina in the absence of ganglion cells. *Exp Eye Res* 2006;83:920-31.
22. Gariano RF, Iruela-Arispe ML, Hendrickson AE. Vascular development in primate retina: comparison of laminar plexus formation in monkey and human. *Invest Ophthalmol Vis Sci* 1994;35:3442-55.
23. Springer AD. New role for the primate fovea: a retinal excavation determines photoreceptor deployment and shape. *Vis Neurosci* 1999;16:629-36.
24. Springer AD, Hendrickson AE. Development of the primate area of high acuity. 2. Quantitative morphological changes associated with retinal and pars plana growth. *Vis Neurosci* 2004;21:775-90.
25. Dubis AM, Hansen BR, Cooper RF, et al. Relationship between the foveal avascular zone and foveal pit morphology. *Invest Ophthalmol Vis Sci* 2012;53:1628-36.
26. McGuire DE, Weinreb RN, Goldbaum MH. Foveal hypoplasia demonstrated in vivo with optical coherence tomography. *Am J Ophthalmol* 2003;135:112-4.
27. Marmor MF, Choi SS, Zawadzki RJ, et al. Visual insignificance of the foveal pit: reassessment of foveal hypoplasia as fovea plana. *Arch Ophthalmol* 2008;126:907-13.
28. Meyer CH, Lapolice DJ, Freedman SF. Foveal hypoplasia demonstrated in vivo with optical coherence tomography. *Am J Ophthalmol* 2003;136:397; author reply 97-8.

29. Meyer CH, Lapolice DJ, Freedman SF. Foveal hypoplasia in oculocutaneous albinism demonstrated by optical coherence tomography. *Am J Ophthalmol* 2002;133:409-10.
30. Azuma N, Nishina S, Yanagisawa H, et al. PAX6 missense mutation in isolated foveal hypoplasia. *Nat Genet* 1996;13:141-2.
31. Mietz H, Green WR, Wolff SM, et al. Foveal hypoplasia in complete oculocutaneous albinism. A histopathologic study. *Retina* 1992;12:254-60.
32. Wu W, Peters WH, 3rd, Hammer ME. Basic mechanical properties of retina in simple elongation. *J Biomech Eng* 1987;109:65-7.
33. Springer AD, Hendrickson AE. Development of the primate area of high acuity, 3: temporal relationships between pit formation, retinal elongation and cone packing. *Vis Neurosci* 2005;22:171-85.
34. Krebs IP, Krebs W. Discontinuities of the external limiting membrane in the fovea centralis of the primate retina. *Exp Eye Res* 1989;48:295-301.
35. Cornish EE, Natoli RC, Hendrickson A, et al. Differential distribution of fibroblast growth factor receptors (FGFRs) on foveal cones: FGFR-4 is an early marker of cone photoreceptors. *Mol Vis* 2004;10:1-14.
36. Hendrickson AE, Yuodelis C. The morphological development of the human fovea. *Ophthalmology* 1984;91:603-12.
37. Yuodelis C, Hendrickson A. A qualitative and quantitative analysis of the human fovea during development. *Vision Res* 1986;26:847-55.
38. La Vail MM, Rapaport DH, Rakic P. Cytogenesis in the monkey retina. *J Comp Neurol* 1991;309:86-114.
39. Springer AD, Hendrickson AE. Development of the primate area of high acuity. 1. Use of finite element analysis models to identify mechanical variables affecting pit formation. *Vis Neurosci* 2004;21:53-62.
40. Volpert OV, Zaichuk T, Zhou W, et al. Inducer-stimulated Fas targets activated endothelium for destruction by anti-angiogenic thrombospondin-1 and pigment epithelium-derived factor. *Nat Med* 2002;8:349-57.
41. Serini G, Valdembri D, Zanivan S, et al. Class 3 semaphorins control vascular morphogenesis by inhibiting integrin function. *Nature* 2003;424:391-7.
42. Cai J, Jiang WG, Grant MB, et al. Pigment epithelium-derived factor inhibits angiogenesis via regulated intracellular proteolysis of vascular endothelial growth factor receptor 1. *J Biol Chem* 2006;281:3604-13.

43. Dorn EM, Hendrickson L, Hendrickson AE. The appearance of rod opsin during monkey retinal development. *Invest Ophthalmol Vis Sci* 1995;36:2634-51.
44. Hendrickson A, Kupfer C. The histogenesis of the fovea in the macaque monkey. *Invest Ophthalmol Vis Sci* 1976;15:746-56.
45. Hendrickson A. A morphological comparison of foveal development in man and monkey. *Eye (Lond)* 1992;6 (Pt 2):136-44.
46. Linberg KA, Fisher SK. A burst of differentiation in the outer posterior retina of the eleven-week human fetus: an ultrastructural study. *Vis Neurosci* 1990;5:43-60.
47. Diaz-Araya C, Provis JM. Evidence of photoreceptor migration during early foveal development: a quantitative analysis of human fetal retinae. *Vis Neurosci* 1992;8:505-14.
48. van Driel D, Provis JM, Billson FA. Early differentiation of ganglion, amacrine, bipolar, and Muller cells in the developing fovea of human retina. *J Comp Neurol* 1990;291:203-19.
49. Maldonado RS, O'Connell RV, Sarin N, et al. Dynamics of human foveal development after premature birth. *Ophthalmology* 2011;118:2315-25.
50. Abramov I, Gordon J, Hendrickson A, et al. The retina of the newborn human infant. *Science* 1982;217:265-7.
51. Nag TC, Wadhwa S. Differential expression of syntaxin-1 and synaptophysin in the developing and adult human retina. *J Biosci* 2001;26:179-91.
52. Packer O, Hendrickson AE, Curcio CA. Development redistribution of photoreceptors across the *Macaca nemestrina* (pigtail macaque) retina. *J Comp Neurol* 1990;298:472-93.
53. Hendrickson A, Troilo D, Possin D, et al. Development of the neural retina and its vasculature in the marmoset *Callithrix jacchus*. *J Comp Neurol* 2006;497:270-86.
54. Robb RM. Increase in retinal surface area during infancy and childhood. *J Pediatr Ophthalmol Strabismus* 1982;19:16-20.
55. Mintz-Hittner HA, Knight-Nanan DM, Satriano DR, et al. A small foveal avascular zone may be an historic mark of prematurity. *Ophthalmology* 1999;106:1409-13.
56. Mintz-Hittner HA, Miyashiro MJ, Knight-Nanan DM, et al. Vitreoretinal findings similar to retinopathy of prematurity in infants with compound heterozygous protein S deficiency. *Ophthalmology* 1999;106:1525-30.

57. Hughes S, Yang H, Chan-Ling T. Vascularization of the human fetal retina: roles of vasculogenesis and angiogenesis. *Invest Ophthalmol Vis Sci* 2000;41:1217-28.
58. Sandercoe TM, Geller SF, Hendrickson AE, et al. VEGF expression by ganglion cells in central retina before formation of the foveal depression in monkey retina: evidence of developmental hypoxia. *J Comp Neurol* 2003;462:42-54.
59. Hendrickson A, Possin D, Vajzovic L, et al. Histologic Development of the Human Fovea From Midgestation to Maturity. *Am J Ophthalmol* 2012.
60. Dubis AM, Costakos DM, Subramaniam CD, et al. Evaluation of normal human foveal development using optical coherence tomography and histologic examination. *Arch Ophthalmol* 2012;130:1291-300.
61. Teller DY, Regal DM, Videen TO, et al. Development of visual acuity in infant monkeys (*Macaca nemestrina*) during the early postnatal weeks. *Vision Res* 1978;18:561-6.
62. Parodi MB, Visintin F, Della Rupe P, et al. Foveal avascular zone in macular branch retinal vein occlusion. *Int Ophthalmol* 1995;19:25-8.
63. Gabriele ML, Wollstein G, Ishikawa H, et al. Optical coherence tomography: history, current status, and laboratory work. *Invest Ophthalmol Vis Sci* 2011;52:2425-36.
64. Drexler W, Morgner U, Kartner FX, et al. In vivo ultrahigh-resolution optical coherence tomography. *Opt Lett* 1999;24:1221-3.
65. Yun SH, Tearney G, de Boer J, et al. Pulsed-source and swept-source spectral-domain optical coherence tomography with reduced motion artifacts. *Opt Express* 2004;12:5614-24.
66. Wojtkowski M, Leitgeb R, Kowalczyk A, et al. In vivo human retinal imaging by Fourier domain optical coherence tomography. *J Biomed Opt* 2002;7:457-63.
67. de Boer JF, Cense B, Park BH, et al. Improved signal-to-noise ratio in spectral-domain compared with time-domain optical coherence tomography. *Opt Lett* 2003;28:2067-9.
68. Leitgeb R, Wojtkowski M, Kowalczyk A, et al. Spectral measurement of absorption by spectroscopic frequency-domain optical coherence tomography. *Opt Lett* 2000;25:820-2.
69. Wojtkowski M, Srinivasan V, Fujimoto JG, et al. Three-dimensional retinal imaging with high-speed ultrahigh-resolution optical coherence tomography. *Ophthalmology* 2005;112:1734-46.

70. Choma MA, Hsu K, Izatt JA. Swept source optical coherence tomography using an all-fiber 1300-nm ring laser source. *J Biomed Opt* 2005;10:44009.
71. Zhang J, Rao B, Chen Z. Swept source based fourier domain functional optical coherence tomography. *Conf Proc IEEE Eng Med Biol Soc* 2005;7:7230-3.
72. Choma M, Sarunic M, Yang C, et al. Sensitivity advantage of swept source and Fourier domain optical coherence tomography. *Opt Express* 2003;11:2183-9.
73. Ditchburn RW, Foley-Fisher JA. Assembled data in eye movements. *Opt Acta (Lond)* 1967;14:113-8.
74. Ditchburn RW, Ginsborg BL. Involuntary eye movements during fixation. *J Physiol* 1953;119:1-17.
75. Moller F, Laursen ML, Sjolie AK. The contribution of microsaccades and drifts in the maintenance of binocular steady fixation. *Graefes Arch Clin Exp Ophthalmol* 2006;244:465-71.
76. Moller F, Laursen ML, Tygesen J, et al. Binocular quantification and characterization of microsaccades. *Graefes Arch Clin Exp Ophthalmol* 2002;240:765-70.
77. Ratliff F, Riggs LA. Involuntary motions of the eye during monocular fixation. *J Exp Psychol* 1950;40:687-701.
78. Schulz E. Binocular micromovements in normal persons. *Graefes Arch Clin Exp Ophthalmol* 1984;222:95-100.
79. Ferguson RD, Hammer DX, Paunescu LA, et al. Tracking optical coherence tomography. *Opt Lett* 2004;29:2139-41.
80. Hammer DX, Ferguson RD, Magill JC, et al. Active retinal tracker for clinical optical coherence tomography systems. *J Biomed Opt* 2005;10:024038.
81. Ishikawa H, Gabriele ML, Wollstein G, et al. Retinal nerve fiber layer assessment using optical coherence tomography with active optic nerve head tracking. *Invest Ophthalmol Vis Sci* 2006;47:964-7.
82. Hewko M. Optical Coherence Tomography (OCT): National Research Council Canada.
83. Schuman SG, Koreishi AF, Farsiu S, et al. Photoreceptor layer thinning over drusen in eyes with age-related macular degeneration imaged in vivo with spectral-domain optical coherence tomography. *Ophthalmology* 2009;116:488-96 e2.

84. Forooghian F, Cukras C, Meyerle CB, et al. Evaluation of time domain and spectral domain optical coherence tomography in the measurement of diabetic macular edema. *Invest Ophthalmol Vis Sci* 2008;49:4290-6.
85. Han IC, Jaffe GJ. Comparison of spectral- and time-domain optical coherence tomography for retinal thickness measurements in healthy and diseased eyes. *Am J Ophthalmol* 2009;147:847-58, 58 e1.
86. Maldonado RS, Izatt JA, Sarin N, et al. Optimizing hand-held spectral domain optical coherence tomography imaging for neonates, infants, and children. *Invest Ophthalmol Vis Sci* 2010;51:2678-85.
87. Patel PJ, Chen FK, da Cruz L, et al. Segmentation error in Stratus optical coherence tomography for neovascular age-related macular degeneration. *Invest Ophthalmol Vis Sci* 2009;50:399-404.
88. Sadda SR, Wu Z, Walsh AC, et al. Errors in retinal thickness measurements obtained by optical coherence tomography. *Ophthalmology* 2006;113:285-93.
89. Costa RA, Calucci D, Skaf M, et al. Optical coherence tomography 3: Automatic delineation of the outer neural retinal boundary and its influence on retinal thickness measurements. *Invest Ophthalmol Vis Sci* 2004;45:2399-406.
90. Liakopoulos S, Ongchin S, Bansal A, et al. Quantitative optical coherence tomography findings in various subtypes of neovascular age-related macular degeneration. *Invest Ophthalmol Vis Sci* 2008;49:5048-54.
91. Sanchez-Tocino H, Alvarez-Vidal A, Maldonado MJ, et al. Retinal thickness study with optical coherence tomography in patients with diabetes. *Invest Ophthalmol Vis Sci* 2002;43:1588-94.
92. Vajzovic L, Hendrickson AE, O'Connell R V, et al. Maturation of the Human Fovea: Correlation of Spectral-Domain Optical Coherence Tomography Findings With Histology. *Am J Ophthalmol* 2012.
93. Spaide RF, Curcio CA. Anatomical correlates to the bands seen in the outer retina by optical coherence tomography: literature review and model. *Retina* 2011;31:1609-19.
94. Drexler W, Sattmann H, Hermann B, et al. Enhanced visualization of macular pathology with the use of ultrahigh-resolution optical coherence tomography. *Arch Ophthalmol* 2003;121:695-706.
95. Jousseaume F, Spitznas M. The fine structure of the human retina at the ora serrata. *Albrecht Von Graefes Arch Klin Exp Ophthalmol* 1972;185:177-88.
96. Feeney L. Editorial: Intercellular junctions: sites of permeability barriers and cellular communication. *Invest Ophthalmol* 1974;13:811-4.

97. Oishi A, Otani A, Sasahara M, et al. Photoreceptor integrity and visual acuity in cystoid macular oedema associated with retinitis pigmentosa. *Eye (Lond)* 2009;23:1411-6.
98. Gerth C, Zawadzki RJ, Heon E, et al. High-resolution retinal imaging in young children using a handheld scanner and Fourier-domain optical coherence tomography. *J Aapos* 2009;13:72-4.
99. Scott AW, Farsiu S, Enyedi LB, et al. Imaging the infant retina with a handheld spectral-domain optical coherence tomography device. *Am J Ophthalmol* 2009;147:364-73 e2.
100. Chavala SH, Farsiu S, Maldonado R, et al. Insights into advanced retinopathy of prematurity using handheld spectral domain optical coherence tomography imaging. *Ophthalmology* 2009;116:2448-56.
101. Chong GT, Farsiu S, Freedman SF, et al. Abnormal foveal morphology in ocular albinism imaged with spectral-domain optical coherence tomography. *Arch Ophthalmol* 2009;127:37-44.
102. Cook A, White S, Batterbury M, et al. Ocular growth and refractive error development in premature infants with or without retinopathy of prematurity. *Invest Ophthalmol Vis Sci* 2008;49:5199-207.
103. Gordon RA, Donzis PB. Refractive development of the human eye. *Arch Ophthalmol* 1985;103:785-9.
104. Friling R, Weinberger D, Kremer I, et al. Keratometry measurements in preterm and full term newborn infants. *Br J Ophthalmol* 2004;88:8-10.
105. Isenberg SJ, Del Signore M, Chen A, et al. Corneal topography of neonates and infants. *Arch Ophthalmol* 2004;122:1767-71.
106. Inagaki Y. The rapid change of corneal curvature in the neonatal period and infancy. *Arch Ophthalmol* 1986;104:1026-7.
107. Mohindra I, Held R, Gwiazda J, et al. Astigmatism in infants. *Science* 1978;202:329-31.
108. Howland HC, Atkinson J, Braddick O, et al. Infant astigmatism measured by photorefractometry. *Science* 1978;202:331-3.
109. Fulton AB, Hansen RM, Moskowitz A, et al. Multifocal ERG in subjects with a history of retinopathy of prematurity. *Doc Ophthalmol* 2005;111:7-13.
110. Barnaby AM, Hansen RM, Moskowitz A, et al. Development of scotopic visual thresholds in retinopathy of prematurity. *Invest Ophthalmol Vis Sci* 2007;48:4854-60.
111. Akerblom H, Larsson E, Eriksson U, et al. Central macular thickness is correlated with gestational age at birth in prematurely born children. *Br J Ophthalmol* 2011;95:799-803.

112. Ecsedy M, Szamosi A, Karko C, et al. A comparison of macular structure imaged by optical coherence tomography in preterm and full-term children. *Invest Ophthalmol Vis Sci* 2007;48:5207-11.
113. Hammer DX, Iftimia NV, Ferguson RD, et al. Foveal fine structure in retinopathy of prematurity: an adaptive optics Fourier domain optical coherence tomography study. *Invest Ophthalmol Vis Sci* 2008;49:2061-70.
114. Lago A, Matieli L, Gomes M, et al. Stratus optical coherence tomography findings in patients with retinopathy of prematurity. *Arq Bras Oftalmol* 2007;70:19-21.
115. Vinekar A, Avadhani K, Sivakumar M, et al. Understanding clinically undetected macular changes in early retinopathy of prematurity on spectral domain optical coherence tomography. *Invest Ophthalmol Vis Sci* 2011;52:5183-8.
116. El-Dairi MA, Asrani SG, Enyedi LB, et al. Optical coherence tomography in the eyes of normal children. *Arch Ophthalmol* 2009;127:50-8.
117. Gupta G, Donahue JP, You T. Profile of the retina by optical coherence tomography in the pediatric age group. *Am J Ophthalmol* 2007;144:309-10.
118. Huynh SC, Wang XY, Rochtchina E, et al. Distribution of macular thickness by optical coherence tomography: findings from a population-based study of 6-year-old children. *Invest Ophthalmol Vis Sci* 2006;47:2351-7.
119. Sarvananthan N, Surendran M, Roberts EO, et al. The prevalence of nystagmus: the Leicestershire nystagmus survey. *Invest Ophthalmol Vis Sci* 2009;50:5201-6.
120. Gottlob I. Nystagmus. *Curr Opin Ophthalmol* 2000;11:330-5.
121. Proudlock FA, Gottlob I. Nystagmus in Childhood. In: Hoyt CS, Taylor D, editors. *Pediatric Ophthalmology and Strabismus*. 4 ed: Saunders Ltd, 2012:911-16.
122. Kumar AP, Frank A; Gottlob, Irene. Management of Congenital Nystagmus with and without Strabismus. In: Lorenz BB, Michael, editor. *Pediatric Ophthalmology, Neuro-Ophthalmology, Genetics*: Springer Berlin Heidelberg, 2010:153-71.
123. Yang H, Yu T, Sun C, et al. Spectral-domain optical coherence tomography in patients with congenital nystagmus. *Int J Ophthalmol* 2011;4:627-30.
124. Cronin TH, Hertle RW, Ishikawa H, et al. Spectral domain optical coherence tomography for detection of foveal morphology in patients with nystagmus. *J Aapos* 2009;13:563-6.

125. Holmstrom G, Eriksson U, Hellgren K, et al. Optical coherence tomography is helpful in the diagnosis of foveal hypoplasia. *Acta Ophthalmol* 2010;88:439-42.
126. Thomas MG, Kumar A, Kohl S, et al. High-resolution in vivo imaging in achromatopsia. *Ophthalmology* 2011;118:882-7.
127. Mohammad S, Gottlob I, Kumar A, et al. The functional significance of foveal abnormalities in albinism measured using spectral-domain optical coherence tomography. *Ophthalmology* 2011;118:1645-52.
128. Thomas MG, Kumar A, Mohammad S, et al. Structural grading of foveal hypoplasia using spectral-domain optical coherence tomography a predictor of visual acuity? *Ophthalmology* 2011;118:1653-60.
129. Thomas MG, McLean RJ, Kohl S, et al. Early signs of longitudinal progressive cone photoreceptor degeneration in achromatopsia. *Br J Ophthalmol* 2012;96:1232-6.
130. Querques G, Prascina F, Iaculli C, et al. Isolated foveal hypoplasia. *Int Ophthalmol* 2009;29:271-4.
131. Srinivasan VJ, Wojtkowski M, Witkin AJ, et al. High-definition and 3-dimensional imaging of macular pathologies with high-speed ultrahigh-resolution optical coherence tomography. *Ophthalmology* 2006;113:2054 e1-14.
132. Lim JI, Tan O, Fawzi AA, et al. A pilot study of Fourier-domain optical coherence tomography of retinal dystrophy patients. *Am J Ophthalmol* 2008;146:417-26.
133. Hood DC, Zhang X, Ramachandran R, et al. The inner segment/outer segment border seen on optical coherence tomography is less intense in patients with diminished cone function. *Invest Ophthalmol Vis Sci* 2011;52:9703-9.
134. Birch DG, Wen Y, Locke K, et al. Rod sensitivity, cone sensitivity, and photoreceptor layer thickness in retinal degenerative diseases. *Invest Ophthalmol Vis Sci* 2011;52:7141-7.
135. Aleman TS, Cideciyan AV, Sumaroka A, et al. Retinal laminar architecture in human retinitis pigmentosa caused by Rhodopsin gene mutations. *Invest Ophthalmol Vis Sci* 2008;49:1580-90.
136. Jacobson SG, Aleman TS, Sumaroka A, et al. Disease boundaries in the retina of patients with Usher syndrome caused by MYO7A gene mutations. *Invest Ophthalmol Vis Sci* 2009;50:1886-94.
137. Jacobson SG, Cideciyan AV, Aleman TS, et al. RDH12 and RPE65, visual cycle genes causing leber congenital amaurosis, differ in disease expression. *Invest Ophthalmol Vis Sci* 2007;48:332-8.

138. Wilson HR, Mets MB, Nagy SE, et al. Albino spatial vision as an instance of arrested visual development. *Vision Res* 1988;28:979-90.
139. Apkarian P. A practical approach to albino diagnosis. VEP misrouting across the age span. *Ophthalmic Paediatr Genet* 1992;13:77-88.
140. Gronskov K, Ek J, Brondum-Nielsen K. Oculocutaneous albinism. *Orphanet J Rare Dis* 2007;2:43.
141. Kamaraj B, Purohit R. Mutational Analysis of Oculocutaneous Albinism: A Compact Review. *BioMed research international* 2014;2014:905472.
142. Oetting WS. New insights into ocular albinism type 1 (OA1): Mutations and polymorphisms of the OA1 gene. *Hum Mutat* 2002;19:85-92.
143. Gahl WA. Hermansky-Pudlak Syndrome. In: Pagon RA, Adam MP, Ardinger HH, editors. *GeneReviews. Medical Genetics Information Resource (database online): University of Washington, Seattle, 1993-2014.*
144. Introne WJ, Westbroek W, Golas GA, et al. Chediak-Higashi Syndrom. In: Pagon RA, Adam MP, Ardinger HH, editors. *Gene Reviews. GeneTests: Medical Genetics Information Resource [database online]: University of Washington, Seattle, 1993-2014.*
145. Pal SS, Gella L, Sharma T, et al. Spectral domain optical coherence tomography and microperimetry in foveal hypoplasia. *Indian J Ophthalmol* 2011;59:503-5.
146. Gargiulo A, Testa F, Rossi S, et al. Molecular and clinical characterization of albinism in a large cohort of Italian patients. *Invest Ophthalmol Vis Sci* 2011;52:1281-9.
147. McAllister JT, Dubis AM, Tait DM, et al. Arrested development: high-resolution imaging of foveal morphology in albinism. *Vision Res* 2010;50:810-7.
148. Izquierdo NJ, Emanuelli A, Izquierdo JC, et al. Foveal thickness and macular volume in patients with oculocutaneous albinism. *Retina* 2007;27:1227-30.
149. Harvey PS, King RA, Summers CG. Spectrum of foveal development in albinism detected with optical coherence tomography. *J Aapos* 2006;10:237-42.
150. Hingorani M, Williamson KA, Moore AT, et al. Detailed ophthalmologic evaluation of 43 individuals with PAX6 mutations. *Invest Ophthalmol Vis Sci* 2009;50:2581-90.
151. Gregory-Evans K, Cheong-Leen R, George SM, et al. Non-invasive anterior segment and posterior segment optical coherence tomography

- and phenotypic characterization of aniridia. *Can J Ophthalmol* 2011;46:337-44.
152. Querques G, Bux AV, Iaculli C, et al. Isolated foveal hypoplasia. *Retina* 2008;28:1552-3.
153. Michaelides M, Hunt DM, Moore AT. The cone dysfunction syndromes. *Br J Ophthalmol* 2004;88:291-7.
154. Kohl S, Marx T, Giddings I, et al. Total colourblindness is caused by mutations in the gene encoding the alpha-subunit of the cone photoreceptor cGMP-gated cation channel. *Nat Genet* 1998;19:257-9.
155. Kohl S, Baumann B, Broghammer M, et al. Mutations in the CNGB3 gene encoding the beta-subunit of the cone photoreceptor cGMP-gated channel are responsible for achromatopsia (ACHM3) linked to chromosome 8q21. *Hum Mol Genet* 2000;9:2107-16.
156. Kohl S, Baumann B, Rosenberg T, et al. Mutations in the cone photoreceptor G-protein alpha-subunit gene GNAT2 in patients with achromatopsia. *Am J Hum Genet* 2002;71:422-5.
157. Kohl S, Coppieters F, Meire F, et al. A nonsense mutation in PDE6H causes autosomal-recessive incomplete achromatopsia. *Am J Hum Genet* 2012;91:527-32.
158. Barthelmes D, Sutter FK, Kurz-Levin MM, et al. Quantitative analysis of OCT characteristics in patients with achromatopsia and blue-cone monochromatism. *Invest Ophthalmol Vis Sci* 2006;47:1161-6.
159. Varsanyi B, Somfai GM, Lesch B, et al. Optical coherence tomography of the macula in congenital achromatopsia. *Invest Ophthalmol Vis Sci* 2007;48:2249-53.
160. Thiadens AA, Somervuo V, van den Born LI, et al. Progressive loss of cones in achromatopsia: an imaging study using spectral-domain optical coherence tomography. *Invest Ophthalmol Vis Sci* 2010;51:5952-7.
161. Yang P, Michaels KV, Courtney RJ, et al. Retinal morphology of patients with achromatopsia during early childhood: implications for gene therapy. *JAMA ophthalmology* 2014;132:823-31.
162. Thiadens AA, Roosing S, Collin RW, et al. Comprehensive analysis of the achromatopsia genes CNGA3 and CNGB3 in progressive cone dystrophy. *Ophthalmology* 2010;117:825-30 e1.
163. Free SL, Mitchell TN, Williamson KA, et al. Quantitative MR image analysis in subjects with defects in the PAX6 gene. *Neuroimage* 2003;20:2281-90.
164. Jeffery G. The albino retina: an abnormality that provides insight into normal retinal development. *Trends Neurosci* 1997;20:165-9.

165. Hamel C. Retinitis pigmentosa. *Orphanet J Rare Dis* 2006;1:40.
166. Hamel CP. Cone rod dystrophies. *Orphanet J Rare Dis* 2007;2:7.
167. Ehrh O. Infantile and acquired nystagmus in childhood. *Eur J Paediatr Neurol* 2012;16:567-72.
168. Tarpey P, Thomas S, Sarvananthan N, et al. Mutations in FRMD7, a newly identified member of the FERM family, cause X-linked idiopathic congenital nystagmus. *Nat Genet* 2006;38:1242-4.
169. Kerrison JB, Arnould VJ, Barmada MM, et al. A gene for autosomal dominant congenital nystagmus localizes to 6p12. *Genomics* 1996;33:523-6.
170. Klein C, Vieregge P, Heide W, et al. Exclusion of chromosome regions 6p12 and 15q11, but not chromosome region 7p11, in a German family with autosomal dominant congenital nystagmus. *Genomics* 1998;54:176-7.
171. Ragge NK, Hartley C, Dearlove AM, et al. Familial vestibulocerebellar disorder maps to chromosome 13q31-q33: a new nystagmus locus. *J Med Genet* 2003;40:37-41.
172. Abel LA. Infantile nystagmus: current concepts in diagnosis and management. *Clin Exp Optom* 2006;89:57-65.
173. Thomas MG, Crosier M, Lindsay S, et al. Abnormal retinal development associated with FRMD7 mutations. *Hum Mol Genet* 2014;23:4086-93.
174. Chandna A. Natural history of the development of visual acuity in infants. *Eye (Lond)* 1991;5 (Pt 1):20-6.
175. Magoon EH, Robb RM. Development of myelin in human optic nerve and tract. A light and electron microscopic study. *Arch Ophthalmol* 1981;99:655-9.
176. Hickey TL. Postnatal development of the human lateral geniculate nucleus: relationship to a critical period for the visual system. *Science* 1977;198:836-8.
177. Huttenlocher PR, de Courten C, Garey LJ, et al. Synaptogenesis in human visual cortex--evidence for synapse elimination during normal development. *Neurosci Lett* 1982;33:247-52.
178. Teller DY, McDonald MA, Preston K, et al. Assessment of visual acuity in infants and children: the acuity card procedure. *Dev Med Child Neurol* 1986;28:779-89.
179. Birch EE, Hale LA. Criteria for monocular acuity deficit in infancy and early childhood. *Invest Ophthalmol Vis Sci* 1988;29:636-43.

180. van Hof-van Duin J, Mohn G. The development of visual acuity in normal fullterm and preterm infants. *Vision Res* 1986;26:909-16.
181. Dobson V, Schwartz TL, Sandstrom DJ, et al. Binocular visual acuity of neonates: the acuity card procedure. *Dev Med Child Neurol* 1987;29:199-206.
182. McDonald M, Sebris SL, Mohn G, et al. Monocular acuity in normal infants: the acuity card procedure. *Am J Optom Physiol Opt* 1986;63:127-34.
183. Chandna A, Pearson CM, Doran RM. Preferential looking in clinical practice: a year's experience. *Eye (Lond)* 1988;2 (Pt 5):488-95.
184. Hamer RD, Norcia AM, Tyler CW, et al. The development of monocular and binocular VEP acuity. *Vision Res* 1989;29:397-408.
185. Charles SJ, Moore AT, Grant JW, et al. Genetic counselling in X-linked ocular albinism: clinical features of the carrier state. *Eye (Lond)* 1992;6 (Pt 1):75-9.
186. Charles SJ, Moore AT, Zhang Y, et al. Carrier detection in X linked ocular albinism using linked DNA polymorphisms. *Br J Ophthalmol* 1994;78:539-41.
187. Odom JV, Bach M, Brigell M, et al. ISCEV standard for clinical visual evoked potentials (2009 update). *Doc Ophthalmol* 2010;120:111-9.
188. Mayer DL, Beiser AS, Warner AF, et al. Monocular acuity norms for the Teller Acuity Cards between ages one month and four years. *Invest Ophthalmol Vis Sci* 1995;36:671-85.
189. Lambert V, Coad J, Hicks P, et al. Young children's perspectives of ideal physical design features for hospital-built environments. *J Child Health Care* 2013.
190. Sanchez-Cano A, Baraibar B, Pablo LE, et al. Magnification characteristics of the Optical Coherence Tomograph STRATUS OCT 3000. *Ophthalmic Physiol Opt* 2008;28:21-8.
191. Thomas MG, Kumar A, Thompson JR, et al. Is high-resolution spectral domain optical coherence tomography reliable in nystagmus? *Br J Ophthalmol* 2011.
192. Lee H, Proudlock F, Gottlob I. Is handheld optical coherence tomography reliable in infants and young children with and without nystagmus? *Invest Ophthalmol Vis Sci* 2013;54:8152-9.
193. Spong CY. Defining "term" pregnancy: recommendations from the Defining "Term" Pregnancy Workgroup. *JAMA : the journal of the American Medical Association* 2013;309:2445-6.

194. Royston P, Sauerbrei W. A new approach to modelling interactions between treatment and continuous covariates in clinical trials by using fractional polynomials. *Statistics in medicine* 2004;23:2509-25.
195. Vajzovic L, Hendrickson AE, O'Connell RV, et al. Maturation of the human fovea: correlation of spectral-domain optical coherence tomography findings with histology. *Am J Ophthalmol* 2012;154:779-89 e2.
196. Michaelides M, Hunt DM, Moore AT. The genetics of inherited macular dystrophies. *J Med Genet* 2003;40:641-50.
197. Giedd JN, Blumenthal J, Jeffries NO, et al. Brain development during childhood and adolescence: a longitudinal MRI study. *Nat Neurosci* 1999;2:861-3.
198. Wang YZ, Morale SE, Cousins R, et al. Course of development of global hyperacuity over lifespan. *Optom Vis Sci* 2009;86:695-700.
199. Gargiulo A, Bonetti C, Montefusco S, et al. AAV-mediated tyrosinase gene transfer restores melanogenesis and retinal function in a model of oculocutaneous albinism type I (OCA1). *Mol Ther* 2009;17:1347-54.
200. Pang JJ, Deng WT, Dai X, et al. AAV-mediated cone rescue in a naturally occurring mouse model of CNGA3-achromatopsia. *PLoS One* 2012;7:e35250.
201. Carvalho LS, Xu J, Pearson RA, et al. Long-term and age-dependent restoration of visual function in a mouse model of CNGB3-associated achromatopsia following gene therapy. *Hum Mol Genet* 2011;20:3161-75.
202. Kriss A, Russell-Eggitt I, Harris CM, et al. Aspects of albinism. *Ophthalmic Paediatr Genet* 1992;13:89-100.
203. Bouzas EA, Caruso RC, Drews-Bankiewicz MA, et al. Evoked potential analysis of visual pathways in human albinism. *Ophthalmology* 1994;101:309-14.
204. Soong F, Levin AV, Westall CA. Comparison of techniques for detecting visually evoked potential asymmetry in albinism. *J Aapos* 2000;4:302-10.
205. Zuhlke C, Stell A, Kasmann-Kellner B. [Genetics of oculocutaneous albinism]. *Ophthalmologe* 2007;104:674-80.
206. Weiss AH, Kelly JP. Acuity development in infantile nystagmus. *Invest Ophthalmol Vis Sci* 2007;48:4093-9.
207. Fu VL, Bilonick RA, Felius J, et al. Visual acuity development of children with infantile nystagmus syndrome. *Invest Ophthalmol Vis Sci* 2011;52:1404-11.

208. Cuenca N, Pinilla I, Sauve Y, et al. Early changes in synaptic connectivity following progressive photoreceptor degeneration in RCS rats. *The European journal of neuroscience* 2005;22:1057-72.
209. Sundaram V, Wilde C, Aboshiha J, et al. Retinal structure and function in achromatopsia: implications for gene therapy. *Ophthalmology* 2014;121:234-45.
210. Cao LH, Yu YC, Zhao JW, et al. Expression of natriuretic peptides in rat Muller cells. *Neurosci Lett* 2004;365:176-9.
211. Komaromy AM, Alexander JJ, Rowlan JS, et al. Gene therapy rescues cone function in congenital achromatopsia. *Human molecular genetics* 2010;19:2581-93.
212. Michalakis S, Muhlfridel R, Tanimoto N, et al. Restoration of cone vision in the CNGA3^{-/-} mouse model of congenital complete lack of cone photoreceptor function. *Molecular therapy : the journal of the American Society of Gene Therapy* 2010;18:2057-63.
213. Koch S, Sothilingam V, Garcia Garrido M, et al. Gene therapy restores vision and delays degeneration in the CNGB1^(-/-) mouse model of retinitis pigmentosa. *Human molecular genetics* 2012;21:4486-96.
214. Michalakis S, Muhlfridel R, Tanimoto N, et al. Gene therapy restores missing cone-mediated vision in the CNGA3^{-/-} mouse model of achromatopsia. *Advances in experimental medicine and biology* 2012;723:183-9.
215. Schon C, Biel M, Michalakis S. Gene replacement therapy for retinal CNG channelopathies. *Molecular genetics and genomics : MGG* 2013;288:459-67.
216. Pang JJ, Alexander J, Lei B, et al. Achromatopsia as a potential candidate for gene therapy. *Adv Exp Med Biol* 2010;664:639-46.
217. D'Cruz PM, Yasumura D, Weir J, et al. Mutation of the receptor tyrosine kinase gene *Mertk* in the retinal dystrophic RCS rat. *Human molecular genetics* 2000;9:645-51.
218. Nandrot E, Dufour EM, Provost AC, et al. Homozygous deletion in the coding sequence of the *c-mer* gene in RCS rats unravels general mechanisms of physiological cell adhesion and apoptosis. *Neurobiology of disease* 2000;7:586-99.
219. Claes E, Seeliger M, Michalakis S, et al. Morphological characterization of the retina of the CNGA3^(-/-)Rho^(-/-) mutant mouse lacking functional cones and rods. *Invest Ophthalmol Vis Sci* 2004;45:2039-48.
220. Alexander JJ, Umino Y, Everhart D, et al. Restoration of cone vision in a mouse model of achromatopsia. *Nature medicine* 2007;13:685-7.

221. Muhlriedel R, Tanimoto N, Seeliger MW. [Gene replacement therapy in achromatopsia type 2]. *Klinische Monatsblätter für Augenheilkunde* 2014;231:232-40.
222. Beermann F, Ruppert S, Hummler E, et al. Rescue of the albino phenotype by introduction of a functional tyrosinase gene into mice. *Embo J* 1990;9:2819-26.
223. Hearing VJ, Jimenez M. Mammalian tyrosinase--the critical regulatory control point in melanocyte pigmentation. *The International journal of biochemistry* 1987;19:1141-7.
224. Jimenez M, Maloy WL, Hearing VJ. Specific identification of an authentic clone for mammalian tyrosinase. *J Biol Chem* 1989;264:3397-403.
225. Stone J, Rowe MH, Campion JE. Retinal abnormalities in the Siamese cat. *J Comp Neurol* 1978;180:773-82.
226. Choudhury BP. Ganglion cell distribution in the albino rabbit's retina. *Exp Neurol* 1981;72:638-44.
227. Kinnear PE, Jay B, Witkop CJ, Jr. Albinism. *Surv Ophthalmol* 1985;30:75-101.
228. Wenzel A, Grimm C, Samardzija M, et al. Molecular mechanisms of light-induced photoreceptor apoptosis and neuroprotection for retinal degeneration. *Prog Retin Eye Res* 2005;24:275-306.
229. Eisenhofer G, Tian H, Holmes C, et al. Tyrosinase: a developmentally specific major determinant of peripheral dopamine. *FASEB journal : official publication of the Federation of American Societies for Experimental Biology* 2003;17:1248-55.
230. Ilia M, Jeffery G. Retinal mitosis is regulated by dopa, a melanin precursor that may influence the time at which cells exit the cell cycle: analysis of patterns of cell production in pigmented and albino retinae. *J Comp Neurol* 1999;405:394-405.
231. Roffler-Tarlov S, Liu JH, Naumova EN, et al. L-Dopa and the albino riddle: content of L-Dopa in the developing retina of pigmented and albino mice. *PLoS One* 2013;8:e57184.
232. Ilia M, Jeffery G. Retinal cell addition and rod production depend on early stages of ocular melanin synthesis. *J Comp Neurol* 2000;420:437-44.
233. Rachel RA, Dolen G, Hayes NL, et al. Spatiotemporal features of early neurogenesis differ in wild-type and albino mouse retina. *J Neurosci* 2002;22:4249-63.

234. Ray K, Chaki M, Sengupta M. Tyrosinase and ocular diseases: some novel thoughts on the molecular basis of oculocutaneous albinism type 1. *Prog Retin Eye Res* 2007;26:323-58.
235. Creel D, Hendrickson AE, Leventhal AG. Retinal projections in tyrosinase-negative albino cats. *J Neurosci* 1982;2:907-11.
236. Williams MA, Pinon LG, Linden R, et al. The pearl mutation accelerates the schedule of natural cell death in the early postnatal retina. *Experimental brain research* 1990;82:393-400.
237. Martinez-Morales JR, Rodrigo I, Bovolenta P. Eye development: a view from the retina pigmented epithelium. *BioEssays : news and reviews in molecular, cellular and developmental biology* 2004;26:766-77.
238. Donatien P, Jeffery G. Correlation between rod photoreceptor numbers and levels of ocular pigmentation. *Invest Ophthalmol Vis Sci* 2002;43:1198-203.
239. Lock EA, Gaskin P, Ellis MK, et al. Tissue distribution of 2-(2-nitro-4-trifluoromethylbenzoyl)cyclohexane-1-3-dione (NTBC): effect on enzymes involved in tyrosine catabolism and relevance to ocular toxicity in the rat. *Toxicology and applied pharmacology* 1996;141:439-47.
240. Lock EA, Ellis MK, Gaskin P, et al. From toxicological problem to therapeutic use: the discovery of the mode of action of 2-(2-nitro-4-trifluoromethylbenzoyl)-1,3-cyclohexanedione (NTBC), its toxicology and development as a drug. *Journal of inherited metabolic disease* 1998;21:498-506.
241. Lock EA, Gaskin P, Ellis MK, et al. Tissue distribution of 2-(2-nitro-4-trifluoromethylbenzoyl)-cyclohexane-1,3-dione (NTBC) and its effect on enzymes involved in tyrosine catabolism in the mouse. *Toxicology* 2000;144:179-87.
242. Lock EA, Gaskin P, Ellis M, et al. Tyrosinemia produced by 2-(2-nitro-4-trifluoromethylbenzoyl)-cyclohexane-1,3-dione (NTBC) in experimental animals and its relationship to corneal injury. *Toxicology and applied pharmacology* 2006;215:9-16.
243. Onojafe IF, Adams DR, Simeonov DR, et al. Nitisinone improves eye and skin pigmentation defects in a mouse model of oculocutaneous albinism. *J Clin Invest* 2011;121:3914-23.
244. Rachel RA, Mason CA, Beermann F. Influence of tyrosinase levels on pigment accumulation in the retinal pigment epithelium and on the uncrossed retinal projection. *Pigment Cell Res* 2002;15:273-81.
245. Ilia M, Jeffery G. Delayed neurogenesis in the albino retina: evidence of a role for melanin in regulating the pace of cell generation. *Brain research. Developmental brain research* 1996;95:176-83.

246. Jeffery G, Brem G, Montoliu L. Correction of retinal abnormalities found in albinism by introduction of a functional tyrosinase gene in transgenic mice and rabbits. *Brain Res Dev Brain Res* 1997;99:95-102.
247. Wick MM, Byers L, Frei E, 3rd. L-dopa: selective toxicity for melanoma cells in vitro. *Science* 1977;197:468-9.
248. Akeo K, Tanaka Y, Okisaka S. A comparison between melanotic and amelanotic retinal pigment epithelial cells in vitro concerning the effects of L-dopa and oxygen on cell cycle. *Pigment Cell Res* 1994;7:145-51.
249. Young RW. The ninth Frederick H. Verhoeff lecture. The life history of retinal cells. *Transactions of the American Ophthalmological Society* 1983;81:193-228.
250. Alexiades MR, Cepko C. Quantitative analysis of proliferation and cell cycle length during development of the rat retina. *Developmental dynamics : an official publication of the American Association of Anatomists* 1996;205:293-307.
251. Pequignot MO, Provost AC, Salle S, et al. The retinal pigment epithelium undergoes massive apoptosis during early differentiation and pigmentation of the optic cup. *Mol Vis* 2011;17:989-96.
252. Rebsam A, Bhansali P, Mason CA. Eye-specific projections of retinogeniculate axons are altered in albino mice. *J Neurosci* 2012;32:4821-6.
253. Drager UC. Calcium binding in pigmented and albino eyes. *Proc Natl Acad Sci U S A* 1985;82:6716-20.
254. Chan SO, Baker GE, Guillery RW. Differential action of the albino mutation on two components of the rat's uncrossed retinofugal pathway. *J Comp Neurol* 1993;336:362-77.
255. Marcus RC, Wang LC, Mason CA. Retinal axon divergence in the optic chiasm: midline cells are unaffected by the albino mutation. *Development* 1996;122:859-68.
256. Ohnuma S, Philpott A, Harris WA. Cell cycle and cell fate in the nervous system. *Curr Opin Neurobiol* 2001;11:66-73.
257. Lee AC, Maldonado RS, Sarin N, et al. Macular features from spectral-domain optical coherence tomography as an adjunct to indirect ophthalmoscopy in retinopathy of prematurity. *Retina* 2011;31:1470-82.
258. El-Dairi MA, Holgado S, Asrani SG, et al. Correlation between optical coherence tomography and glaucomatous optic nerve head damage in children. *Br J Ophthalmol* 2009;93:1325-30.

259. Tong AY, El-Dairi M, Maldonado RS, et al. Evaluation of optic nerve development in preterm and term infants using handheld spectral-domain optical coherence tomography. *Ophthalmology* 2014;121:1818-26.
260. Schmitz B, Schaefer T, Krick CM, et al. Configuration of the optic chiasm in humans with albinism as revealed by magnetic resonance imaging. *Invest Ophthalmol Vis Sci* 2003;44:16-21.